

ON TIME-FREQUENCY ANALYSIS FOR STRUCTURAL DAMAGE DETECTION

by

Leonardo Cano Saldaña

A thesis submitted in partial fulfillment of the requirements for the degree of

DOCTOR OF PHILOSOPHY

in

CIVIL ENGINEERING

UNIVERSITY OF PUERTO RICO

MAYAGÜEZ CAMPUS

2008

Approved by:

Luís E. Suarez Colche, PhD
Member, Graduate Committee

Date

Ricardo R. López Rodríguez, PhD
Member, Graduate Committee

Date

Ali Saffar, PhD
Member, Graduate Committee

Date

José A. Martínez-Cruzado, PhD
President, Graduate Committee

Date

Ismael Pagán Trinidad, M.S.C.E.
Chairperson of the Department

Date

Genock Portela, PhD
Representative of Graduate Studies

Date

ABSTRACT

An integrated study that explores the capability of Time-Frequency Analysis combined with another technique of signal analysis and system identification for damage detection purposes using only output signals is presented in this work.

The necessary background theory of Time-Frequency Analysis is presented, some definitions of damage and general approach employed in this research is given. The problems associated with the selection of a best-performance Time-Frequency Representation (TFR) for structural damage detection in civil engineering structures are discussed and a new multi-criteria measure for an objective and user-independent selection of Time-Frequency Representation is developed. An evaluation of the proposed multicriteria method to select a TFR from several Linear and Quadratic TFRs is shown using synthetic ambient vibration signals and real strong motion records.

A new methodology for system identification and damage detection using output data from Ambient Vibration records is developed. This methodology is based on direct application of a proposed Mean Time-Frequency Representation (MTFR) and the Frequency Domain Decomposition (FDD), this last technique was developed by Brincker et. al. [124]. The methodology proposed in this work has been tested using synthetic and real ambient vibration signals. Several real case studies using ambient vibration data from structures are shown.

The damage detection using Time-Frequency Representations of output records of strong events are addressed, in this regard a new algorithm for instantaneous frequency tracking from TFR maps is proposed and a mathematical expression to link instantaneous frequency changes with damping and structural stiffness loss is also developed. The expression and

algorithms have been tested for damage analysis of non-linear SDOF and MDOF using numerical data.

A Graphical User Interface (GUI) program named “Time-Frequency Damage Detection Program - TFDDP” has been developed using MatLab@[125] language; the developed algorithm has been published as a GNU – Licensed Open File, and can be downloaded from the Puerto Rico Strong Motion Program web page at the internet site: <http://prsmpr.uprm.edu/> or contacting to author of this research on the e-mail: leocano-s@hotmail.com

RESUMEN

Un estudio integrado que explora la capacidad del análisis en Tiempo-Frecuencia unido con otras técnicas de análisis de señales e identificación de sistemas para propósitos de detección del daño usando solamente las señales de salida es presentado en este trabajo.

Los conceptos teóricos básicos de análisis en Tiempo-Frecuencia son presentados, algunas definiciones de daño y el enfoque general empleado en esta investigación son mostrados. Los problemas asociados con la selección de la Representación en Tiempo-Frecuencia (TFR) con mejor desempeño para la detección de daño en estructuras de ingeniería civil son discutidos y una nueva medida de multi-criterios para una selección objetiva e independiente del usuario de representaciones tiempo-frecuencia es desarrollada. Una evaluación del método de multi-criterios propuesto para seleccionar una TFR desde varias TFRs cuadráticas y lineales es mostrada usando señales sintéticas de vibración ambiental y registros reales de movimiento fuerte.

Se desarrolló una nueva metodología para identificación de sistemas y detección de daño usando datos de salida de registros de vibración ambiental. La metodología está basada en la aplicación directa de una propuesta de representación tiempo-frecuencia promedio (MTFR) y la descomposición en el dominio de la frecuencia (FDD), esta última técnica fué propuesta recientemente por Brincker et. al. [124]. La metodología propuesta en este trabajo ha sido ensayada usando señales sintéticas y reales de vibración ambiental. Varios estudios de casos reales usando datos de vibración ambiental en estructuras son mostrados.

La detección de daño usando Representaciones Tiempo-Frecuencia de registros de salida de eventos fuertes es abordada, en este sentido un nuevo algoritmo para el seguimiento de la frecuencia instantánea desde mapas TFR es propuesta y una expresión matemática que vincula los cambios en la frecuencia instantánea con el amortiguamiento y la pérdida de

rigidez estructural es también desarrollada. La expresión y los algoritmos han sido ensayados para análisis de daño de sistemas no lineales de uno y varios grados de libertad usando datos numéricos.

Un programa de interfaz gráfica (GUI) denominado “Programa de Detección de Daño en Tiempo-Frecuencia – TFDDP” ha sido desarrollado usando el lenguaje MatLab [125], los algoritmos desarrollados han sido publicados como un GNU – Archivo de Licencia Abierta, y pueden ser descargados desde la página del Programa de Movimiento Fuerte de Puerto Rico en el sitio de Internet: : <http://prsmf.uprm.edu/> o contactando al autor de esta investigación en el e-mail: leocano-s@hotmail.com

To my wife María Teresa and my beloved son Alejandro.

A STRUCTURAL REFLECTION



“ You’ll play the music, I’ll give the key. The rest is easy, leave it to me”: Fiorello in Act I from The Barber of Seville (IL Barbiere Di Siviglia) Opera in Three Acts by G. Rossini (Figure adapted from reference [232])

“The most beautiful Time-Frequency Representation that the human kind has conceived is the musical representation. Like music, the Civil Engineering Structures have their own language, there exists a lot of information in the signal which is not evident and the future advancement of Earthquake and Structural Engineering depends upon our capability to extract and understand the information contents of the structural symphony by using its own natural language: The signals.”

Leonardo Cano Saldaña
Mayagüez P.R., USA
October 2008

ACKNOWLEDGEMENTS

I would like to start by expressing my sincere gratitude to my advisor, Professor José A. Martínez-Cruzado for his invaluable help and support throughout this research.

I would also like to express my gratitude to the other members of my advisory committee Professors: Luis Suárez, Ricardo López and Ali Saffar for their conceptual and philosophical discussions.

To my professors in the UPRM: Daniel Wendychansky and Carlos Huerta for their help and direction at different stages of this research.

To my former adviser in the UPRM Professor John Clinton (ETH Zurich, Switzerland),. Professor Clinton introduced me to the fascinating world of Time-Frequency Analysis.

To Case Bradford (NASA Jet Propulsion Laboratory) for his valuable insight on Time-Frequency Analysis and his support during my field trip to Millikan Library at the California Institute of Technology (Caltech) campus at Pasadena (Cal) during 2006.

To Professor Rosario Ceravolo (Politecnico di Torino, Italy) for her discussions and valuable bibliographic references.

To my classmate Mohammad Saffar for his friendship and patience during the grammatical review of this document.

To my professors during my master degree studies in the Universidad de los Andes at Bogota (Colombia): Alberto Sarria, Luís Yamin, Luis Enrique García and Omar D. Cardona. They had given me invaluable advices and concept on Earthquake and Structural Engineering that even many years later has been the basis of my academic and professional works.

To my academic mentor and friend Hugo Monsalve, for his undying support and wise advices, from the time of my undergraduate studies to this day. He has always been a role model for me.

To the Puerto Rico Strong Motion Program for the logistic and economic support of this research and especially to Jaffet Martínez, Erick Santana, Liz Negrón and Emmanuel Romero for their valuable cooperation and friendship.

Partial funds for my doctoral studies have been provided by the University of Quindio (Colombia), under contract # 002-2005, which is also appreciated.

I am indebt eternally to my parents Ismael Cano and Ruby Saldaña and my brother Alexander, for their support and comprehension, and the most important thing the immense love and faith in the lord.

Finally, I dedicate this work with special love to my wife and son for their enormous sacrifices and patience during these academic years.

Table of Contents

ABSTRACT.....	II
RESUMEN	IV
A STRUCTURAL REFLECTION.....	VII
ACKNOWLEDGEMENTS.....	VIII
TABLE OF CONTENTS	XI
LIST OF TABLES.....	XIV
LIST OF FIGURES	XVI
1 INTRODUCTION.....	1
1.1 MOTIVATION.....	2
1.2 THESIS OVERVIEW	2
1.3 LITERATURE REVIEW	3
1.3.1 <i>Time-Domain Research</i>	5
1.3.2 <i>Frequency-Domain Research</i>	8
1.3.3 <i>Time-Frequency Domain Research</i>	10
2 FUNDAMENTAL CONCEPTS	21
2.1 DEFINITIONS AND GENERAL ASPECT OF STRUCTURAL DAMAGE	21
2.1.1 <i>Damage</i>	21
2.1.2 <i>Frequency</i>	23
2.1.3 <i>Overview of Application of Time-Frequency Analysis in System Identification and Structural Damage Detection</i>	27
2.2 TIME-FREQUENCY REPRESENTATIONS	34
2.2.1 <i>Basic Concept</i>	34
2.2.2 <i>Classification of Time-Frequency Representations</i>	37
2.2.3 <i>Desirable Mathematical Properties for Time-Frequency Representations in Signal Analysis of Structures</i>	38
2.2.4 <i>Common Time-Frequency Representations</i>	42
2.2.5 <i>A Survey From Spectrogram To Wavelets Trough Time-Frequency Distributions</i>	44
2.3 INSTANTANEOUS FREQUENCY.....	50
2.3.1 <i>Monocomponent Signals</i>	50
2.3.2 <i>Multicomponent Signals</i>	52
3 OBJETIVE SELECTION OF BEST-PERFORMANCE TIME-FREQUENCY REPRESENTATION FOR STRUCTURAL DAMAGE DETECTION IN CIVIL ENGINEERING STRUCTURES.....	53
3.1 PROBLEMS WITH SELECTION OF TIME-FREQUENCY REPRESENTATIONS.....	53

3.1.1	<i>The Amount of Available TFRs</i>	54
3.1.2	<i>Resolution vs Information Losses</i>	56
3.1.3	<i>Aspects Inherent to Structural Applications</i>	58
3.2	APPROACHES USED TO SELECT TFRS	60
3.2.1	<i>Visual Inspection of TFRs</i>	61
3.2.2	<i>Measure of the TFRs Concentration and Resolution</i>	62
3.3	RELEVANT TOPICS FOR MULTICRITERIA METHOD	63
3.3.1	<i>The Philosophy of Proposed Multicriteria Performance Measure of the TFRs</i>	64
3.4	PROPOSED MULTICRITERIA METHOD	66
3.4.1	<i>Weighting Factors (W_i)</i>	67
3.4.2	<i>Evaluation Factors (E_{Fi})</i>	68
3.5	APPLICATION OF MULTICRITERIA METHOD FOR SELECTION OF BEST-PERFORMANCE TIME-FREQUENCY REPRESENTATIONS WITH FIXED KERNEL	89
3.5.1	<i>Evaluation of Weighting Factors</i>	92
3.5.2	<i>Evaluation of Qualification for Desirable Mathematical Properties (DMP)</i>	92
3.5.3	<i>Evaluation of Structural Performance Indicator (SPI)</i>	93
3.5.4	<i>Evaluation of Resolution and Concentration Measure (RCM)</i>	104
3.5.5	<i>Evaluation of Information Measure (IM)</i>	106
3.5.6	<i>Final Evaluation of Structural Multicriteria Quality Factor (SMQ)</i>	107
4	STRUCTURAL SYSTEM IDENTIFICATION AND DAMAGE DETECTION USING AMBIENT VIBRATION OUTPUT SIGNALS.....	108
4.1	GENERAL PROCEDURE FOR STRUCTURAL DAMAGE DETECTION USING OUTPUT SIGNALS FROM AMBIENT VIBRATION	109
4.1.1	<i>Non Instrumented Structures</i>	110
4.1.2	<i>Instrumented Structures</i>	111
4.2	MAIN CHARACTERISTICS OF AMBIENT VIBRATION EXCITATIONS.....	112
4.3	THE EQUIVALENT STRUCTURAL MODEL (ESM)	114
4.3.1	<i>Main Characteristics of the Equivalent Structural Model</i>	114
4.4	MATHEMATICAL FORMULATION FOR DAMAGE DETECTION USING TIME-FREQUENCY REPRESENTATION OF OUTPUT SIGNALS FROM AMBIENT VIBRATION.....	118
4.4.1	<i>General Considerations</i>	118
4.4.2	<i>Mathematical Formulation for Extraction of System Frequencies using the Mean Time-Frequency Representation</i>	121
4.4.3	<i>Detection of Non-System Frequencies</i>	124
4.4.4	<i>Modal Coupling and Frequency Separation</i>	132
4.4.5	<i>Mass, Stiffness and Damping Matrices Estimation</i>	138
4.5	NUMERICAL SIMULATIONS.....	147
4.5.1	<i>Single Degree of Freedom Model</i>	148
4.5.2	<i>Multiple Degree of Freedom Models</i>	154
4.5.3	<i>The Phase I – IASC-ASCE Structural Health Monitoring Benchmark Problem</i>	158
4.6	VARIABLES DEPENDENCE	165
4.7	CASE STUDIES.....	173
4.7.1	<i>El Castillo Building – Mayagüez, Puerto Rico</i>	173
4.7.2	<i>Robert A. Millikan Library - Caltech</i>	188
4.7.3	<i>Airport Control Tower – Beef Island (British Virgin Islands)</i>	201
4.7.4	<i>Plaza Inmaculada Building – San Juan, Puerto Rico</i>	212
5	DAMAGE DETECTION USING TIME-FREQUENCY ANALYSIS OF STRONG EVENTS OUTPUT SIGNALS	228

5.1	TIME-FREQUENCY FOR STRUCTURAL DAMAGE DETECTION METHOD FROM STRONG EVENTS (TFSDDM)	228
5.1.1	<i>Mathematical Formulation for TFSDM</i>	232
5.1.2	<i>Algorithm for Instantaneous Frequency Tracking Estimation for Quasi-Monocomponent Structural Signals</i>	237
5.1.3	<i>Empirical Mode Decomposition (EMD) with Time-Frequency Bandwidths</i>	243
5.1.4	<i>Improving Random Decrement Technique with a Windowed Scheme Obtained From Time-Frequency Bandwidths (IRDM)</i>	253
5.2	NUMERICAL SIMULATIONS FOR TIME-FREQUENCY STRUCTURAL DAMAGE DETECTION METHOD (TFSDDM)	258
5.2.1	<i>Single Degree of Freedom Models</i>	258
5.2.2	<i>Multiple Degree of Freedom Models</i>	272
6	TIME-FREQUENCY DAMAGE DETECTION PROGRAM – TFDDP: A GRAPHICAL USER INTERFACE (GUI)	281
6.1	SOFTWARE REQUIREMENTS OF TFDDP PROGRAM	281
6.2	GENERAL DESCRIPTION OF TFDDP PROGRAM	282
6.2.1	<i>File Module</i>	283
6.2.2	<i>Ambient Vibration Module</i>	284
6.2.3	<i>Strong Motion Events Module</i>	285
6.2.4	<i>Tools Module</i>	286
6.2.5	<i>About Module</i>	288
7	CONCLUSIONS	289

List of Tables

Tables	Page
TABLE 2.1- Kernel, Expression and Properties for a few Cohens Class of TFRs	43
TABLE 2.2 Expression for Localized Bi-Frequency Distributions.....	48
TABLE 3.1 Parameter values for the Structural Multicriteria Quality Measure of Time- Frequency Representation.....	68
TABLE 3.2 Quality Mathematical Factors.....	70
TABLE 3.3 Mathematical Properties values for some Quadratic TFRs	71
TABLE 3.4 Evaluation of Qualification for Desirable Mathematical Properties (DMP)	93
TABLE 3.5 Mean Ambient Vibration Instantaneous Frequency Error	95
TABLE 3.6 Mean Global Frequency Error for Ambient Vibration Test	97
TABLE 3.7 Mean Global Frequency Error for Strong Event.....	103
TABLE 3.8 Structural Performance Indicator for TFR.....	103
TABLE 3.9 Resolution and Concentration Measure (RCM) for TFRs.....	106
TABLE 3.10 Information Measure (IM) for TFRs.....	107
TABLE 3.11 Structural Multicriteria Quality factor (SMQ) for TFRs.	107
TABLE 4.1 Estimative for undamaged case – Phase I – ASCE Benchmark problem.....	162
TABLE 4.2 Estimative for damage pattern 1 – Phase I – ASCE Benchmark problem.....	163
TABLE 4.3 Estimative for damage pattern 2 – Phase I – ASCE Benchmark problem.....	163
TABLE 4.4 Estimative for damage pattern 3 – Phase I – ASCE Benchmark problem.....	164
TABLE 4.5 Estimative for damage pattern 4 – Phase I – ASCE Benchmark problem.....	164
TABLE 4.6 Estimative for damage pattern 5 – Phase I – ASCE Benchmark problem.....	165
TABLE 4.7 Estimation for a 30 DOFs Model.....	172
TABLE 4.8 Estimative for a 3 DOFs Model from El Castillo Building (Uncorrected).....	180
TABLE 4.9 Stiffness Matrix Estimative for a 3 DOFs Model from El Castillo Building (Corrected).....	180
TABLE 4.10 Modal Matrix Estimative for a 3 DOFs Model from El Castillo Building....	180
TABLE 4.11 Comparison between MTFR-FDD and Finite Element Model for El Castillo Building.....	184
TABLE 4.12 Estimative for a 3 DOFs Model for Millikan Library (Uncorrected)	195
TABLE 4.13 Stiffness Matrix Estimative for a 3 DOFs Model from Millikan Library (Corrected)	195
TABLE 4.14 Modal Matrix Estimative for a 3 DOFs Model for Millikan Library	196
TABLE 4.15 Comparison between MTFR-FDD and Finite Element Model to Millikan Library.....	198
TABLE 4.16 Estimative for a 3 DOFs Model from Airport Control Tower (Uncorrected)	208
TABLE 4.17 Stiffness Matrix Estimative for a 3 DOFs Model from Millikan Library (Corrected)	208

TABLE 4.18 Comparison between MTFR-FDD and Finite Element Model [202] for Airport Control Tower	209
TABLE 4.19 Estimative for a 9 DOFs Model for Plaza Inmaculada Building (Uncorrected)	220
TABLE 4.20 Stiffness Matrix Estimative for a 9 DOFs Model from Plaza Inmaculada Building (Corrected)	220
TABLE 4.21 Modal Matrix Estimative for a 9 DOFs Model from Plaza Inmaculada Building	221
TABLE 4.22 Comparison between MTFR-FDD and Finite Element Model for Plaza Inmaculada Building	225

List of Figures

Figures	Page
Figure 2-1 Ambient Vibration Record taken from a MDOF system	28
Figure 2-2 Power Spectra for signal of Figure (2-1).....	29
Figure 2-3 Mean Time-Frequency Representation for signal of Figure (2-1)	30
Figure 2-4 Time-History of a Simulated Structural Response.....	31
Figure 2-5 Power Spectra for signal of fig. (2-4).....	31
Figure 2-6 Pseudo-Wigner-Ville Distribution for simulated response	32
Figure 2-7 Classification of Time-Frequency Representations	38
Figure 3-1 Comparison of TFRs of two tremors recorded in a Residential Building.....	55
Figure 3-2 Reduced Interference Distribution for a Typical Structural Signal # 1	77
Figure 3-3 Reduced Interference Distribution for a Typical Structural Signal # 2	78
Figure 3-4 Parameters to Measure Concentration and Resolution for TFRs according to Boashash and Sucic [159, 162].....	82
Figure 3-5 Flow Chart to Measure Concentration and Resolution of TFRs According to Boashash and Sucic [160].....	84
Figure 3-6 Acceleration, Velocity, and Displacement Time Histories of San Fernando Earthquake recorded on the Roof of Millikan Library (EW Component).....	90
Figure 3-7 (a) Fourier Spectra (a) and (b) Pseudo-Acceleration Spectra of San Fernando Earthquake recorded on the Roof of Millikan Library (EW Component).....	91
Figure 3-8 (a) Time-History and (b) Fourier Spectra of Ambient Vibration Record for Test of TFR	94
Figure 3-9 Choi-William Representation.....	95
Figure 3-10 TFRs for Ambient Vibration Test Signal.....	96
Figure 3-11 TFRs of San Fernando Earthquake (1971) recorded at Millikan Library (EW- Roof Component).....	98
Figure 3-12 Synthetic Pattern to TFRs of San Fernando Earthquake (1971) recorded at Millikan Library (EW-Roof Component).....	99
Figure 3-13 Synthetic Pattern for TFRs of San Fernando Earthquake (1971) recorded at Millikan Library (EW-Roof Component).....	101
Figure 3-14 Frequency Laws for TFRs Vs Theoretical Frequency Law	102
Figure 3-15 Percent of Instantaneous Frequency Error for TFRs.....	102
Figure 3-16 Optimization Procedure for Choi-Williams Distribution. (a) Functional Operator for several Standard Deviation Values. (b) Optimal Instantaneous Standard Deviation to be use.....	105
Figure 4-1 Schematic Procedure for Structural Damage Detection Using Output Signals from Ambient Vibration	109
Figure 4-2 Typical Equivalent Structural Model	115

Figure 4-3 Detection of Non-Structural Frequencies using frequency stability in TFR plane	125
Figure 4-4 Typical Empirical Probabilistic Density Functions (epdf) for Structural Frequencies and Non-Structural Frequencies	127
Figure 4-5 Determination of Non-Structural frequency from Empirical Probabilistic Function Shapes	129
Figure 4-6 Power Spectra for a Coupling MDOF system.....	133
Figure 4-7 Wigner-Ville Distribution of Closely-Spaced Coupled Structure	134
Figure 4-8 Complex Cepstrum.....	137
Figure 4-9 Partial Frequency Marginal for TFR using the information in the Cepstra	137
Figure 4-10 Typical output signal and its FFT for SDOF model	149
Figure 4-11 Mean Time-Frequency Representation for undamaged SDOF model.....	150
Figure 4-12 Typical output signal and its FFT for SDOF model	151
Figure 4-13 Mean Time-Frequency Representation for damaged SDOF model.....	152
Figure 4-14 Empirical Probabilistic Density Function for damaged SDOF model.....	153
Figure 4-15 Mean Time-Frequency Representation (Undamaged) 3 DOFs model	155
Figure 4-16 Mean Time-Frequency Representation (Damage Stage) 3 DOFs model.....	156
Figure 4-17 ASCE Benchmark model in University of British Columbia	158
Figure 4-18 ASCE Benchmark problem (a) Geometry (b) Damage patterns (taken from reference [107]).....	160
Figure 4-19 Mean Time-Frequency Representation for ASCE Benchmark problem	161
Figure 4-20 Noise effect in stiffness predictions for a 10 DOFs model	166
Figure 4-21 Length of measurement effect in stiffness predictions to a 10 DOFs model	167
Figure 4-22 Number of measurements effect in stiffness predictions for a 10 DOFs model	168
Figure 4-23 Stiffness error for 1000 simulated structures	169
Figure 4-24 Error in damage location predictions for 80 models of 30 DOFs	170
Figure 4-25 Error in location for 80 models of 30 DOFs	171
Figure 4-26 Photo of El Castillo Building in Mayagüez, P.R. (photo by: L. Cano).....	174
Figure 4-27 Elevation and Plan view of El Castillo Building	175
Figure 4-28 Typical acceleration recorded from Ambient Vibration taken in several points of roof floor in El Castillo Building	176
Figure 4-29 Five days of continuous acceleration recorded from Ambient Vibration taken on the roof floor in El Castillo Building	176
Figure 4-30 Time Frequency Representation for 2.5 days of continuous acceleration recorded from Ambient Vibration taken on the roof floor in El Castillo Building	177
Figure 4-31 Mean Time Frequency Representation for El Castillo Building.....	178
Figure 4-32 Empirical Probabilistic Density Functions from MTFR of ambient vibration test in the El Castillo Building.....	179
Figure 4-33 Schematic view of the Finite Element structural model for El Castillo Building	183
Figure 4-34 Acceleration record and Fourier Spectra for Earthquake of Tokachi-Oki (2003), recorded in the Station TKCH11.	185

Figure 4-35 Comparison of output signal to El Castillo Building, from Etabs Model and MTFR-FDD Model for Earthquake of Tokachi-Oki of 2003, recorded in the Station TKCH11.....	186
Figure 4-36 Coherence Function for El Castillo Building, from Etabs Model and MTFR-FDD Model for Earthquake of Tokachi-Oki of 2003, recorded in the Station TKCH11.....	187
Figure 4-37 Photo of Robert Millikan Library Caltech (photo by: L. Cano)	189
Figure 4-38 Elevation and Plan view of Millikan Library (taken from COMET website [113])	190
Figure 4-39 Millikan Library Instrumentation (taken from COMET website [113]).....	190
Figure 4-40 Time History of a continuous 24 hours recording in Millikan Library	191
Figure 4-41 Linear Time-Frequency Representation for 19 days of continuous recording in Millikan Library.....	191
Figure 4-42 Linear 3D Time-Frequency for 19 days of continuous recording in Millikan Library.....	192
Figure 4-43 MTFR to Millikan Library (00:00:00 to 08:20:00 June 12 th /2005)	193
Figure 4-44 Empirical Probabilistic Density Functions from MTFR from ambient vibration for Millikan Library.	194
Figure 4-45 Finite Element Model of the Millikan Library.....	198
Figure 4-46 Time History Comparisons for San Simeon Earthquake recorded in Millikan Library.....	199
Figure 4-47 Fourier Spectra Comparisons for San Simeon Earthquake recorded in Millikan Library.....	200
Figure 4-48 Coherence Function for Millikan Library, from Etabs Model and MTFR-FDD Model for San Simeon Earthquake of 2003, recorded in the MIK Station.....	201
Figure 4-49 Photo of Airport Control Tower of British Virgin Island. (Photo by: J. Martinez-Cruzado).....	202
Figure 4-50 Plan view of Airport Control Tower of British Virgin Island. A) Base B) One to 4 th floor C) 5 th Floor D) 6 th floor (Taken from reference [202]).....	202
Figure 4-51 Elevation view of Airport Control Tower of British Virgin Island. (Taken from reference [202]).....	203
Figure 4-52 Acceleration record of ambient vibration test in the Airport Control Tower of British Virgin Island.	204
Figure 4-53 Fourier spectra of ambient vibration test in the Airport Control Tower of British Virgin Island (Horizontal Channels: 1 and 2, Vertical Channel: 3).	204
Figure 4-54 STFT Spectrum for ambient vibration test in the Airport Control Tower of British Virgin Island.	205
Figure 4-55 Mean Time Frequency Representation of ambient vibration test in the Airport Control Tower of British Virgin Island.	206
Figure 4-56 Empirical Probabilistic Density Functions from MTFR of ambient vibration test in the Airport Control Tower of British Virgin Island.....	207
Figure 4-57 Finite Element Model for the Airport Control Tower of British Virgin Island [202]......	209

Figure 4-58 Horizontal Acceleration record and Fourier Spectra for Earthquake from 11-29-2007, recorded in the Basement of Airport Control Tower of British Virgin Islands..	210
Figure 4-59 Comparison of output signal for Etabs Model, MTFR-FDD Model and Real record for Earthquake from 11-29-2007, recorded in the roof of Airport Control Tower of British Virgin Islands.....	211
Figure 4-60 View of Plaza Inmaculada Building (Photo by: L. Cano).	212
Figure 4-61 Plan, Elevation and Installed Instrumentation view of Plaza Inmaculada Building (Adapted from [120]).....	214
Figure 4-62 Time History of a continuous 15 hours recording in Plaza Inmaculada	214
Figure 4-63 Time History of a continuous 20 days (Channel 9) recording in Plaza Inmaculada	215
Figure 4-64 Linear Time-Frequency Representation for a 5 days of continuous recording in Plaza Inmaculada	215
Figure 4-65 Linear 3D Time-Frequency for a 5 days of continuous recording in Plaza Inmaculada Building.....	216
Figure 4-66 MTFR from DC to 100 Hz for Plaza Inmaculada Building (00:00:00 to 08:20:00 August 11 th /2006) (Left: Linear Scale, Right: Logarithmic Scale)	217
Figure 4-67 MTFR from DC to 10 Hz for Plaza Inmaculada Building (00:00:00 to 08:20:00 August 11 th /2006)	218
Figure 4-68 Empirical Probabilistic Density Functions from MTFR of ambient vibration for Plaza Inmaculada Building.	219
Figure 4-69 Finite Element Model of the Plaza Inmaculada Building, (a) 3D View, (b) Plan View of typical floor.....	224
Figure 4-70 Time History Comparisons for Earthquake recorded in Plaza Inmaculada Building.....	226
Figure 4-71 Fourier Spectra Comparisons for Earthquake recorded in Plaza Inmaculada Building.....	227
Figure 4-72 Coherence Function for Plaza Inmaculada Building, (Etabs Model, MTFR-FDD Model and Real Record for Earthquake of January 13 th -2006 recorded on the roof of the building).....	227
Figure 5-1 Schematic Process of Time Frequency Structural Damage Detection Method (TFSDM) for a MDOF system.	231
Figure 5-2 Remanent Stiffness vs Unitary Frequency for a SDOF system	242
Figure 5-3 Schematic Empirical Mode Decomposition procedure (adapted from Flandrin [216]).....	246
Figure 5-4 Evaluation of the Intrinsic Mode Function (IMF) (adapted from Flandrin [216]).	246
Figure 5-5 Sifting Process (adapted from Flandrin [216]).....	247
Figure 5-6 Final results of EMD applied to an original signal of Fig. 5-2 (Taken from Flandrin [216])......	248
Figure 5-7 Time History and Fourier Spectra for a 2 DOFs with stiffness softening	250
Figure 5-8 Time History and Fourier Spectra for a 2 DOFs with stiffness softening	250

Figure 5-9 Frequency Constrained Buffer Zones from TFR to use in EMD algorithm.	251
Figure 5-10 EMD result of a signal from Figure 5-7	252
Figure 5-11 Damping vs Frequency Changes.....	253
Figure 5-12 Pseudo Vibration Damped Curve (PVDC) for Millikan Library: (a) San Simeon Earthquake. (b) Segments and SVDC.....	255
Figure 5-13 Schematic procedure to obtain the Estimation damage for SDOFs	259
Figure 5-14 Time intervals obtained from TFR-RID to apply the Random Decrement Method	260
Figure 5-15 Pseudo Vibration Damped Curves for each time intervals obtained from TFR- RID.....	261
Figure 5-16 Estimate structural damping time history and Theoretical damping time history	262
Figure 5-17 Instantaneous Frequency (IF) evaluated from Phase time derivative.	263
Figure 5-18 Spectrogram using 100 Hamming windows (50% overlap)	264
Figure 5-19 Reduced Interference Distribution for Output Signal	265
Figure 5-20 Reduced Interference Distribution for Output Signal	266
Figure 5-21 Reduced Interference Distribution for Output Signal	267
Figure 5-22 Comparative time history Stiffness Loss between theoretical and stiffness loss from TFSDDM.....	268
Figure 5-23 Theoretical and Predicted Damaged Comparisons (Note: Connecting lines are only for viewing purposes).	269
Figure 5-24 Probability of Occurrence of Relative Error in Stiffness Loss Predictions.	270
Figure 5-25 Excedence Probability for Relative Error in Stiffness Loss Predictions.....	271
Figure 5-26 Two story steel frame used for MDOFs testing (Taken from reference [231])	272
Figure 5-27 Acceleration records obtained in the building	273
Figure 5-28 Displacement records obtained in the building.....	274
Figure 5-29 Linear and Nonlinear Displacement Records obtained at the Roof.....	274
Figure 5-30 Schematic Process of Time Frequency Structural Damage Detection Method (TFSDDM) for a the FEDEASLab example 8 [231].....	275
Figure 5-31 Buffer Zones for Acceleration Record from Sensor 1 (Level 1).	276
Figure 5-32 Buffer Zones for Acceleration Record from Sensor 2 (Roof Level).	276
Figure 5-33 Empirical Mode Functions Extracted using the Buffer Zones of TFR maps...	277
Figure 5-34 TFR for Empirical Mode Functions – Level 1 – Mode 1.	278
Figure 5-35 TFR for Empirical Mode Functions – Level 1 – Mode 2	279
Figure 5-36 TFR for Empirical Mode Functions – Roof Level – Mode 1	279
Figure 5-37 TFR for Empirical Mode Functions – Roof Level – Mode 2	280
Figure 5-38 Predicted Damage for a MDOF model	280
Figure 6-1 Initial Screen of Time-Frequency Damage Detection Program - TFDDP	283
Figure 6-2 Sub-Menu File.....	284
Figure 6-3 Sub-Menu Ambient Vibration.....	285
Figure 6-4 Sub-Menu Strong Motion Events.....	286
Figure 6-5 Sub-Menu Tools.....	287

Figure 6-6 Sub-Menu Help 288

1 INTRODUCTION

For a long time, structural engineers have tried to detect damage through instrumentation. Several techniques have been used, among them changes in modal frequencies and in mode shapes, and matrix updating (stiffness, mass, and damping).

Because the building earthquake structural response depends upon the dynamic properties and the signal itself, changes in the dynamic properties are associated with stiffness and damping changes, and may associated to damage. In low or moderate vibration (ambient vibration and small tremors) such changes may be associated to nonlinear elastic response and non-structural elements response, and not necessarily to damage. In moderate or large events such changes may be associated to soil-structure inelastic response, nonlinear elastic and inelastic response and building permanent structural damage. Damage in the structure will be reflected by a permanent shift of the pre-event natural frequency. Therefore, the establishment of pre-event, event and post-event frequencies and other modal parameters such as mode shapes of the structure is very useful for damage detection. Furthermore, it shall be possible to determine the time of occurrence and the magnitude of the structural dynamic properties changes, and hence the time associated of occurrence, location, and intensity of the damage. For real cases of damage detection in almost all cases, structural identification begins by taking geometrical and materials properties of structural “as built” drawings or other available field information. Also several assumptions regarding supports and boundary conditions are inevitable, thus introducing errors in the mathematical models.

In recent times new techniques of signal analysis have been proposed in others fields such as speech recognition, radar applications, image digital processing and others. Among others techniques, methods using Wavelets Analysis in qualitative and quantitative sense and Time-Frequency Distributions in qualitative sense has been used in damage detection.

1.1 Motivation

An integrated study that explores the capability of Time-Frequency Distributions joint with another technique of signal analysis and system identification for damage proposes has not been proposed yet. It is the goal of the present research to deal with the use of Time-Frequency Analysis for damage detection in civil structures, using only output records of the structure.

The main objective is to research the Time-Frequency Analysis together with other techniques of signal analysis and system identification for structural damage detection using only output data.

1.2 Thesis Overview

An introduction to the thesis is presented in Chapter 1, the motivation and comprehensive bibliography review is given.

In Chapter 2, the necessary background theory of Time-Frequency Analysis is presented, some definitions of damage and general approach employed in this research is shown.

Chapter 3 deals with the problem of selection of a best-performance Time-Frequency Representation for structural damage detection in civil engineering structures. A new multi-criteria measure for an objective and user-independent selection of Time-Frequency Representation is developed and tested with typical signals.

A new methodology to system identification and damage detection using output data from Ambient Vibration records is developed in Chapter 4. The proposed methodology is based on direct application of a proposed Mean Time-Frequency Analysis and the Frequency Domain Decomposition (FDD) technique which was recently proposed by Brincker et. al.

[124]. The methodology proposed in this work has been tested using synthetic and real ambient vibration signals.

In the Chapter 5, the damage detection using Time-Frequency Representations of output records of strong events are addressed, in this regard an algorithm for instantaneous frequency tracking is proposed and a new mathematical expression to link instantaneous frequency changes with structural stiffness loss is also developed. The expression and algorithms has been tested for damage analysis of non-linear SDOF and MDOF using numerical data.

An Graphical User Interface (GUI) program named “Time-Frequency Damage Detection Program - TFDDP” has been developed using MatLab@[125] language, the principal modules and program characteristics are given in Chapter 6.

Finally the conclusion and future scopes are given in Chapter 7.

1.3 Literature Review

Damage detection of structures contributes to large amount of field research in civil engineering, many methods using several approaches have been proposed. In the references [1-6] a detailed analysis and classification of general and specific methodologies that use changes in dynamic characteristics for damage detection is given. In reference [7] it has been mentioned that the first attempt for damage detection using changes in dynamic properties in concrete structures was done by E. Bock in 1942.

In general in accordance with reference [2], methods that use vibration properties can be classified into: Resonant Frequencies, Frequency Response Functions, Mode Shapes (MAC and COMAC), Mode Shape Curvatures, Modal Strain Energy, Dynamic Flexibility,

Damping, Antiresonance, Ritz Vectors, ARMA Family Models, Canonical Variate Analysis (CVA), Nonlinear Features, Time-Frequency Analysis, Empirical Mode Decomposition, Hilbert Transform, Principal Component Analysis or Singular Value Decomposition, Finite Model Updating, Wave Propagation, Autocorrelation Functions, and other Features Methodologies.

Regarding to the methods that do not directly use signal analysis process, Alvandi and Cremona [5] have assessed the most usual vibration-based techniques in damage identification and concluded that the strain energy methods are the most stable methods. However like to others, they had difficulties when the damage was far from the excitation source. The scientific information on Vibration-Based Damage Detection (VBDD) is extensive and a comprehensive review of this can in fact constitute a complete research project (e.g. see ref. [1-6]).

Since long time ago, the scientific community has used structural vibration measurements for damage detection, for example in reference [8] free oscillation tests in Switzerland between 1922 and 1945 has been cited for this purpose.

Salawu[9], using a comprehensive literature review, established some conclusion about damage detection through changes in frequency. In general frequency changes alone do not necessarily imply the damage existence. Also because damage is a local characteristic the changes in global stiffness and mode shapes are not very pronounced except in severe damage stage. The models assumption, such as material properties, boundary conditions, stiffness and structural damping are the main source of errors in damage detection using mathematical models and the use of experimental and field test methods for updating the analytical models are strongly recommended. Salawu concludes that “*Methods that rely only on measured data without any prior theoretical assumptions would be more appropriate to civil engineering structures.*”

Traditionally, standard methodologies of signal analysis have been used for interpretation. The most common of these methods are:

- Analysis in Time-Domain (Time History Analysis)
- Analysis in Frequency-Domain (Fourier Analysis)

Recently other methods of signal analysis have been developed and although their basic principles have been established many years ago, only the evolutions of personal computers allow its current use. These methods are:

- Analysis in Time-Frequency Domain
- Analysis in Time-Scale Domain (mainly wavelets analysis)

In the following the works of traditional signal analysis (Time and Frequency Domains) for system identification and damage detection are related briefly and later with more detail works in Time-Frequency Domain are also reviewed.

1.3.1 Time-Domain Research

In the Time-Domain, an early work by Giberson [10] compiled and described the most important works developed by pioneers Structural Engineers from 1920 to 1967, among those mentioned by Giberson are: Biot, Freeman, Kanai, Hudson, Housner, Caughey, Penzien, Iwan, Jennings, Newmark, Clough, Rosenblueth, Umemura, Shibata, E. L. Wilson. The 1960's decade is considered the beginning of vibration induced studies in civil engineering. Kuroiwa [11] using a shake actuator placed on the roof of Millikan Library (Caltech) determined the dynamic properties of the Building. In the same work [11], one can find the most important research regarding Vibration-Based Identification and Damage Detection development between 1960-1967.

Distefano et. al. [12] presents one method for structural identification for damage detection using a filtering approach and iterative approximation through a Gauss-Newton procedure. Several numerical models using nonlinear viscous damping models have been

developed using Volterra integral equations and nonlinear differential equations, nonlinear damping and bilinear hysteretic models are also treated but in minor scales.

In 1978, Beck [13] presents his Modal Minimization Method, this approach, considered a novel method in structural identification and damage detection, can be applied to the whole record or in a short time window. Furthermore the Modal Minimization Method and other variants have actually been used extensively in structural health monitoring.

Carydis and Mouzakis [14] demonstrated that using vibration experimental data from undamaged, damaged and repaired building through time analysis, it is possible to evaluate the main dynamics characteristic of buildings. They showed that one major problem between experimental and model results are the erroneous assumption used in the mathematical models. On the other hand, they showed a notorious increase in vibration period of building with damage and rigid body modes appear above the damage level.

In 1986, Beck and Beck [15] showed a comparison between transfer function and modal minimization methods for system identification and damage detection, they concluded that for linear models the modal minimization is a better technique for structural identification and damage detection.

Loh and Tsuar [16] in 1987, presented two improved methods of identification, the sequential regression analysis and the Kalman filtering algorithm. They concluded that the Kalman and extended Kalman filtering techniques are more powerful than general methods and it is suitable for non-linear applications and damage detection problems.

In 1991, Beck [17], presented a comprehensive dissertation of fundamental problems in the application of structural identification procedures to damage detection, and he concluded

that: “ .. *the modeling error is the most serious issue in structural identification and damage detection..*”.

Li and Jirsa [18], using data from an instrumented building damaged during the 1994 Northridge Earthquake showed the incapability of time analysis and Non-Linear dynamic analysis of reliably prognosticating the damage occurrence without “a priori” estimation of stiffness and other non-credible assumptions. These assumptions are used frequently in design offices and research projects, in general the results obtained by time history analysis and non-linear analysis are very sensitive of these assumptions.

Yang [19] in 1996 applied the statistical methods for system identification. The importance of Yang’s pioneer work was according with reference[2]: “...*almost none of the hundreds of studies summarized in Doebling et al. (1996, 1998) (reference [3]) make use of any statistical methods to assess if the changes in the selected features used to identify damaged systems are statistically significant...*”, on the contrary the Yang’s research applied rigorous statistical methods in this regard.

In 1997, Goel and Chopra [20] presented the most complete and extensive work in systematic system identification available. The main goal of the study was the comparison of the code empirical formulas to estimate the fundamental vibration period of building with obtained period using record of instrumented buildings. They have been evaluating the performance comparison of the three most popular procedures in system identification and damage detection: Transfer Function, Modal Minimization Method and Auto-Regressive Modeling Adaptative Method (ARMA). In this study Goel and Chopra concluded that the Transfer Function based method is less reliable because when this method is applied in non-steady-state response the variability of the peak rises.

De la Llera et. al. [21] using a multi-input-multi-output scheme and eigensystem realization algorithm in time domain, identified the building response and damage in a time-varying linear model approach. They concluded that for case study (a seven story reinforced concrete structure in Van Nuys) the damage to the building was the main consequence of inelastic torsional behavior. This conclusion is absolutely opposite to the report in reference [31] which uses a frequency domain approach.

In recent times, studies for damage detection in time domain have been the main focus in updating techniques (FEM). These methods can be classified in supervised learning and unsupervised learning. In this sense applications in Neural Networks are very common. The interested reader can review references [2, 5, 22]. Another important issue in time domain in recent times is the Empirical Modal Decomposition (EMD), but this approach will be mentioned in detail in the Chapter 5.

1.3.2 Frequency-Domain Research

Although it is not a procedure for structural system identification, the work by Haskell [23] maybe is the first attempt for the identification in the frequency domain, and has the beginning of the soil dynamics and the propagation of waves in layered media.

Previous to 1971 the existing data for frequency domain research was fairly limited. A few data like those recorded in San Fernando 1957 Earthquake allowed Hudson [24] to present the first scientific paper with the use of real data employed in structural identification of buildings using a frequency domain approach.

In 1974, Distefano et. al. [12] showed the application of frequency domain identification of building to a non-linear model of a two stories building. In the same work, they presented a time-domain method which was previously discussed.

For system identification and damage detection in frequency domain the research by McVerry [25] is the great importance. He showed that identification of single linear models is possible through modal parameters which produce match in a least squares algorithm in frequency bandwidths. McVerry also showed that selecting short-time segments structural parameters identification is possible when structural damage is present.

Using identification in frequency domain Luco and Trifunac [26] showed that the model using structure only do not have enough precision and it is therefore necessary to involucrate soil-structure interaction in structural and damage identification.

Using Nonparametric methods based on Fourier amplitude spectra, transfer function and cross-correlation, Boroschek and Yañez [27] showed that for system identification and damage detection the common structural analytical models have an error between 40% to 80% in structural response prediction if it is compared with real records obtained from the buildings.

Using FFT analysis and Wavelet analysis Melhem and Kim [28], showed that damage detection in Frequency Domain is less reliable than analysis in Time-Scale Domain (Wavelets Analysis).

In a recent work by Bisht and Singh [29], the performances of Wavelet Analysis, Empirical Model Decomposition (EMD), and Parametric Models and Peak-Picking Method (PPM) for structural identification are assessed. They concluded that PPM (an method based in direct interpretation of Fourier Transform) is a simple, easy and reliable method for system identification and damage detection.

An improved method for frequency domain identification has been proposed by Hong and Yun [30], they used an exponential weighting function to improve the frequency response

function (FRF) and using this FRF they could predict the natural frequencies, damping ratios and modes of the structure.

Trifunac et al [31] proposed the use of Fourier Spectrum of average building angle for system identification and damage detection. They used time history angles obtained by relations of horizontal relative motion between the top and ground level divided by building height and its respective Fourier spectra. Contrary to reference [21] (a time domain approach), Trifunac et. al. [31] concluded that building damage (the same building of references [18, 21, 31]) is caused by nonlinearities in the soil.

1.3.3 Time-Frequency Domain Research

Except for Time-Scale Analysis (e.g. Wavelets) the number of investigations on time-frequency analysis application in civil engineering is fairly limited, for example extensive papers review, cited in references [1, 2, 3, 9] do not included any information about of time-frequency analysis for structural damage detection in civil engineering structures. Only in two very recent state of the art publications [80], the Time-Frequency based methods are reviewed. The Empirical Mode Decomposition (EMD) and Hilbert-Huang Transforms (another time-frequency methodology) have been mentioned [81].

This research is focused on time-frequency analysis and not time-scale analysis (like wavelets). For this reason, detailed information analysis about wavelets application for damage detection is omitted in this bibliography review. However, the link between Time-Frequency analysis and Time-Scale analysis will be shown in the chapter 2, some references should be given in this regard. Beginner readers interested in wavelets analysis should refer to “The World According to Wavelets: the story of a mathematical technique in the making” [32], an excellent non mathematic introductory book. In contrast the intermediate and advanced readers may found the mathematical approach to wavelet analysis of great interest [230]. The reference [33] has an excellent, comprehensive and update bibliography review of

“state of the art” on wavelets analysis applied to structural health monitoring. For advanced readers, the select references [34-47] show some recent and interesting applications of wavelets analysis for damage detection in civil engineering structures. Finally reference [48] presents a comprehensive use of continuous wavelet transform for estimation of instantaneous frequency of signal, one topic very close to the focus of this research.

The main idea of time-frequency distributions is to provide a distribution that shows the energy of a signal in time and frequency domain simultaneously [49]. It is well known that damage is a direct consequence of energy balance in the structure [50, 51, 52]. Therefore, if it is possible to calculate the energy distribution of a signal in time and frequency domain then it would be possible to correlate its distribution with damage intensity, location, and time of occurrence. The problem is that the energy distribution is not positive for all the time-frequency intervals. Therefore, the correlation between the energy distribution and damage is difficult. Another approach for damage detection may use the identification of time-varying properties of structures from a time-frequency analysis and correlate these changes with damages into structure.

Time-Frequency energy distribution has its origin in the early work of Wigner [53]. This work does not look like a direct consequence of a spectrogram improvement but as a quantum mechanics problem joining momentum with position (like time and frequency in signal analysis). From basic signal analysis principles it is known that the instantaneous energy for a signal $x(t)$ and the energy density spectrum of its Fourier transform $S(\omega)$ are:

$$\begin{aligned} |x(t)|^2 &: \text{Instantaneous Energy (intensity per unit time at time } t) \\ |S(\omega)|^2 &: \text{Intensity per unit frequency at frequency } \omega \end{aligned} \tag{1-1}$$

Therefore, for a Time-Frequency Energy Distribution (TFED) $P(\omega, t)$, the instantaneous energy and energy density spectrum are:

$$\begin{aligned}
|x(t)|^2 &= \int_{-\infty}^{+\infty} P(t, \omega) d\omega \\
|S(\omega)|^2 &= \int_{-\infty}^{+\infty} P(t, \omega) dt
\end{aligned}
\tag{1-2}$$

Then if the marginal conditions are satisfied, the total energy of the signal is [49]:

$$E = \int_{-\infty}^{+\infty} P(t, \omega) d\omega dt
\tag{1-3}$$

An infinite number of distributions satisfy the equation (1-2, 1-3). Unfortunately the Wigner Distribution had been lost in scientific community until 1948 when Ville [54] applied this distribution to signal analysis and introduced the analytical signal concept. In 1960 Cohen [55] rediscovered its applicability for quantum mechanics, statistical mechanics and signal processing of light waves. In this work, Cohen [55] also showed that the joint-phase-space distribution like time-frequency distribution can take negatives values.

In 1989, Cohen [56] proposed in a classical paper the following general form for these representations, actually known as Cohen's Class:

$$P(t, \omega) = \frac{1}{4\pi^2} \int_{-\infty}^{+\infty} \int_{-\infty}^{+\infty} \int_{-\infty}^{+\infty} e^{-j\theta t - j\tau\omega + j\theta u} \phi(\theta, \tau) x^* \left(u - \frac{1}{2}\tau \right) x \left(u + \frac{1}{2}\tau \right) du d\tau d\theta
\tag{1-4}$$

where $\phi(\theta, \tau)$ is the kernel, which for Cohen's Class Distributions is independent of time and frequency. According to equation (5), the Cohen's Class Distributions satisfy time and frequency shift invariance [56]. If the kernel is independent of time then the TFED is time-shift invariant. On the other hand, if the kernel is frequency independent then the TFED is frequency-shift invariant [49].

Since Cohen's classification [56], a large number of TFEDs has been proposed, theoretically, it is possible to construct infinite TFED by selecting different independent time and frequency kernels.

Hlawatsch and Boudreaux-Bartels [57] present a complete study and classification of Time-Frequency Representations (TFR). According to this reference, TFRs are classified as:

a) Linear TFRs: Garbor Expansion (GE), Short Time Fourier Transform (STFT), Wavelet Transform (WT) .

b) Quadratic TFRs: Active Unterberger Distribution (AUD), Ambiguity Function (AF), Bertrand Distribution (BED), Bon-Jordan Distribution (BJD), Butterworth Distribution (BUD), Choi-Williams Distribution (or exponential distribution) (CWD), Cone-Kernel Distribution (CKD), Generalized Exponential Distribution (GED), Generalized Wigner Distribution (GWD), Levin Distribution (LD), Page Distribution (PD), Passive Unterberger Distribution (PUD), Pseudo Wigner Distribution (PWD), Real-Valued Generalized Wigner Distribution (EGWD), Reduced Interference Distribution (RID), Rihaczek Distribution (RD), Scalogram (or quadratic Wavelet Distribution), Smoothed Pseudo Wigner Distribution (SPWD), Spectrogram (or quadratic STFT), Wigner-Ville Distribution (WVD).

c) Nonlinear, Nonquadratic TFRs: Signal-Adaptative Radially-Gaussian Kernel Distribution (RGD), Cohen's Nonnegative Distribution (CND).

From civil engineering point of view the early work by Udwardia and Trifunac [58] is one of first attempts for joint time and frequency analysis in system identification and damage detection. Although they do not use strictly a time-frequency distribution, in their work Udwardia and Trifunac obtained the sequence and frequency shift of two buildings during Lytle Creek (1970) and San Fernando Earthquake (1971). They used transfer function calculated for 8 sec windows and overlap 2 sec between each sliding window. They also noticed partial or completed recovery of frequency changes during the following months after strong motion.

Udwardia and Marmarelis [59, 60] using Short Time Fourier Transform (STFT) and Weiner method showed the use of STFT in system identification and damage detection in

linear and non-linear range. They also proposed the use of a time-time representation. A similar technique has been recently proposed in references [61, 62].

Until mid 90's, the use of Short Time Fourier Transform (STFT) is almost the only method cited for damage detection in civil engineering structures. For more details consult the recent compilation of these works cited in reference [6, 63].

One of the first technical references in damage detection for civil structures using Wigner distribution has been reported on 1992 by Robin et. al. [64], using acoustic monitoring of hammer impact in metallic beams they concluded that time-frequency representation are more suitable for damage detection than traditional stationary analysis.

In 1996, Hammond and White [65], showed a comparison between several signal analysis techniques including STFT, Wavelets, Evolutionary Spectrum, and quadratic time-frequency methods (Wigner-Ville Distribution and others). They applied several methods to a cantilever beam.

Bonato et. al. [66], using a beam structure, compared the performance of six different time-frequency bilinear transform: Spectrogram, Wigner-Ville(WV), Pseudo Wigner-Ville (PSWV), Choi-Williams (CW), Cone-Kernel and Reduced Interference Distribution(RID) and conclude respect to resolution CW and RID have the best resolutions. They also showed that variations in single frequencies alone do not allow the damage localization.

Staszewski et. al. [67], using a weighted WVD, reduced the interference terms for fault detection and proposed an automatic fault detection method based on image processing techniques and pattern recognition using neural networks.

Olivito and Surace [68], using nondestructive ultrasonic techniques and time-frequency distribution of the cross-ambiguity functions determined the damage in concrete cubes specimens. Perhaps this is one of the few works in which an attempt, to correlate the damage with wave energy and volume of cross-ambiguity function has been made.

A method using instantaneous cross-correlation, ambiguity function, WVD and CWD to identify dynamics properties of structures has been proposed by Bonato et. al. [69]. The authors found that cross-terms present in time-frequency representations can be suppressed most efficiently in the ambiguity function domain. On the other hand they also found that using channels located in nodal positions and cross-correlation the time frequency distributions becomes more clear. The methodology has been tested using record obtained from a bridge in Vancouver.

Using only the recorded data and without introducing strong model assumptions, De la Llera and Chopra [70], applied a time-dependent Fourier transform (spectrogram) to study the dynamic characteristics of eight buildings and they compared this result with UBC-97 code provisions and standard procedures of design. They found that code and standard theoretical models predicted dynamic properties with error between 40% and 100% compared with analysis of the recorded data. For steel building the predicted error has been less than concrete buildings.

In two complementary papers, in 1998 and 1999, Bonato et. al. [71, 72], proposed a new method based on time-frequency and cross-time-frequency techniques for structural identification. In the proposed methodology, using the Choi-William Distribution(CWD) modal and external components are extracted. For system frequencies identification a Phase Ratio Estimation was proposed using cross-time-frequency distribution between two channels. When the identified frequency correspond to system frequency, the phase

difference standard deviation diagram depicted a minima. An analytical three-story shear-type frame has been used for methodology testing.

In 1999, Huang et. al. [73], showed a powerful approach for system identification of dynamic systems, based primarily on empirical mode decomposition and Hilbert transform. This method is known today as Hilbert-Huang Transform (HHT). Actually HHT is one of the most promising modern signal analysis tools available. Huang proved that any real signal could be disintegrated into n-empirical modes and a residue such:

$$x(t) = \sum_{i=1}^n c_i(t) + r_n(t) \quad 1-5$$

where $x(t)$: Original signal

$C_i(t)$: component

$r_n(t)$: residue after sifting process.

After empirical mode decomposition has been made, the Hilbert transform is applied to each component resulting in a Hilbert Spectrum.

For linear signals, Bonato et. al. [74, 75] showed an improved parameter estimator based on earlier works (see references [71, 72]), the improvement has the advantage that no filter in time domain is necessary. For nonlinear systems, the technique was also shown to provide good results for a numerical model of a three story frame building [74]. Using ambient-vibration data, the technique has been used in system identification of an old masonry bell tower in Italy with the Wigner-Ville Distribution [75].

Trifunac et. al. [76] used relative rocking response data (see complementary papers in the reference[31]) from an instrumented building(see other papers from the same building in the references [18, 21]) and two different signals analysis techniques (time-frequency windowed Fourier analysis and zero-crossing analysis). The authors found that the predominant

frequency changes in soil-building response is detectable by time-frequency analysis and that nonlinearities of building response for this particular case is due mainly to the response of the foundation soil.

Using an output only scheme in time-frequency domain, De Stefano et. al. [77] and Ceravolo et. al. [78], proposed a method for structural damping identification. They show that damping obtained using time-frequency methodologies is by far a better estimate compared with other three methods (Direct System Parameter Identification, Eigensystem Realisation Algorithm, Polyreference Time Domain).

In 2002 Cohen et. al. [79] showed that time-frequency distribution can be used for obtaining reliability variable stiffness and damping of a single degree of freedom fault model.

Neild et. al. [80] using accelerometer data from a concrete beam and windowed fourier transform concluded that this time-frequency methodology is suitable for early stages of damage.

In a recent state of the art paper [81], the authors compared the performance in structural vibration analysis of the moving window discrete Fourier transform, the moving window auto-regressive (AR) model, the harmonic wavelet transform, and Wigner-Ville distribution. Using synthetic signals and experimental data they concluded discrete Fourier transform and AR models have similar resolutions. Windowed Wigner-Ville distribution has similar time-frequency estimations compared with wavelet transform. In high modes no method was capable of giving correct estimation.

Yan et. al. [82], presents a very recent state of the art review paper on vibration-based damage detection, they compared traditional-type vibration-based structural damage detection method (TTDD) versus modern-type vibration based structural damage detection

(MTDD). In the last category only time-frequency (Hilbert-Huang Transform and Empirical Mode Decomposition) and time-scale (Wavelet), Neural Network and GA method is included. The authors believe that future of damage detection is in MTDD.

Similar to aforementioned Empirical Mode Decomposition (see ref. [73]), Zhang et. al. [83], proposed a modal parameter identification based on Gabor expansion. They used simulated data of a simply supported beam of three DOF, the method can decompose each signal into uncoupled responses and extracted for each one of the structural modal parameters. The authors mentioned that results are very sensitive to signal noise ratios (SNR) and that damage estimation is less accurate.

Zhou [84] presented the application of time-frequency distribution analysis method to determine the damage of a reinforced concrete high-rise (38 floors) scaled model (1:20) building under white noise and four level of earthquake excitations. Although he has problems during super-strong level earthquake acquisition data, Zhou can evaluate the damage using structural frequency response functions (FRFs), neural networks, joint time-frequency analysis and autoregressive and moving average model (ARMA). Regarding the time-frequency methods, he concluded that Choi-Williams distribution and adaptive spectrogram has the best performance in time-frequency resolution and suggested that damage detection using time-frequency methodologies should be the focus in instantaneous properties rather than energy approach.

In 2004, Mucciarelli et. al. [85] reported that for the first time in Europe, nonlinearitie building response was recorded. Using four analysis methodologies (Short-Time Fourier Transform, Wavelet Transform, Horizontal to Vertical Spectral Ratio and Horizontal to Vertical Moving Window Ratio), they showed that the frequencies estimated by four techniques are consistent. An exception was given for Wavelet Transform where frequencies were underestimated. Therefore WT become less suitable for damage assessment. The

authors proposed, as comparison factor between several techniques, the use of percentage frequency shift.

Zou and Chen [86] using numerical simulations of rotors found in a comparative study that Wavelet Transform is most useful for detect stiffness variation and damage detection than Wigner-Ville distribution.

The use of instantaneous estimators obtained from time-frequency analysis for structural damping evaluation has been proposed in reference [87]. The author using vibration measurements of a Hospital compared the results obtained with a classic identification method (Eigensystem Realization Algorithm – ERA) and thus obtained with Short Time Fourier Transform. She found an excellent agreement between results of both methods.

Politis [88] on 2005, compared the use of adaptive decomposition and empirical mode decomposition using time-frequency and wavelets analysis for system identification and concluded that adaptive methods are most effective. On the other hand empirical mode decomposition required most user supervision when the modes are coupled.

An improved method of Hilbert-Huang transform has been presented by Peng et. al. [89] in 2005. The method is based in application of wavelet packed transform to decompose the signal into a set of narrow band signals and after the empirical mode decomposition is applied.

Bradford [90] and Bradford et. al.[91] worked extensively work on the use of time-frequency analysis for system identification of structures with changing dynamics properties. The authors compared, in qualitative sense, the performance of some time-frequency distributions for chirp functions analysis and three instrumented buildings in California. In general the building response was shown in a qualitative sense with direct user interpretation

of Reduced Interferenced Distribution (RID) results. The authors concluded that wavelet transform and spectrograms are diffuse for this type of analysis and time-frequency representation are most suitable for this purposes.

Roshan-Ghias et. al. [92], presented a method for extract vibration modes using the Smoothed Pseudo Wigner-Ville distribution, the authors showed numerical results obtained with his algorithm for a two DOF's uncoupled system.

Using measurements data from San Fernando earthquake (1971) recorded in the basement of Alhambra Building, Ceravolo et. al. [93] showed the results of a parametric method of instantaneous system identification based on Short Time Fourier Analysis. The identified parameters are affected by external noise and system behavior.

Todorovska and Trifunac[94], used the ridge of Gabor transform for determining the instantaneous system frequency and damage detection of Imperial County services building for Imperial Valley earthquake (1979). The authors mentioned that time-frequency representation offers better control of frequency resolution rather than wavelet transform.

2 FUNDAMENTAL CONCEPTS

The structural language is too extensive, and in general some technical words have been used in different context and usually it does not have the same meaning for all persons involved. A similar situation occurs in signal processing analysis, for this reason this chapter starts with a few but very important definitions that are used in this work and claim to explain their meaning in the context of this thesis.

The second part of the Chapter is a briefly visual and graphical demonstration of some abilities of time-frequency analysis (TFA) to system identification and damage detection. Because the objective of this part is to show TFA in an intuitive sense, in depth mathematical formulations is avoided.

The last part of the chapter is dedicated to time-frequency analysis theory. The main focus is on the mathematical concept useful for analysis of signals from Civil Engineering structures.

2.1 Definitions and General Aspect of Structural Damage

2.1.1 *Damage*

Damage is one of most controversial words in the structural health monitoring field. In many cases it refers to a subjective scale of comparison or acceptable performance according to several levels of exposition. In general, it refers to changes (almost always permanent) of structural properties like stiffness, strength, dynamic properties, or loss of acceptable structural performance according to a pre-established behavior criteria. For buildings it is

frequently associated with inter-story drift and behavior of structural and nonstructural components [126].

Because we attempt to identify damage using only output signals therefore no additional structural information is allowed, for the purposes of this research we define damage like permanent changes in structural frequency (associated with stiffness losses).

Obviously the above definition of “damage” is not absolute, mainly because a “permanent” change in frequency or a permanent displacement does not necessarily imply damage according to several scales or criteria. In general, damage in a scale for one scenario is not necessarily damage for another scenario. For example, in common buildings you can accept a 1.0% of drift during a strong event (and its damage probability associated with it), but in a nano-technological laboratory facilities or nuclear plants a 0.1% of drift may be unacceptable.

According to the literature review there are several other approaches to damage detection like mode-shape-based and modal strain energy, but all of these methods depend on mathematical models of the structure (so one needs structural data like geometry, material properties etc.) and frequency identification. If one can only use the output signal (like in this research), the natural way will be to associate damage to the instantaneous frequency identification or any parameter evaluated from record. One selects frequency because any other structural characteristic that one attempts to get directly is dependent of the signal-based frequency estimation.

Another important issue with previous “damage” definition is the damage severity or danger of the damage. Thus a small frequency change does not necessarily imply no severe damage or non-danger in the structure [2, 9, 147]. The contrary is also true but is less common.

For example, if you have a single span frame and you decrease the stiffness of a column in one corner or reduce its capacity to a very low value, the overall changes in frequency may be very low. An erroneous conclusion in this case will be that no important damage has happened but it is obvious that from structural point of view the damage is severe and the structure is in danger. In this case an additional small demand on a column may cause its failure and the global stability of the structure can be compromised.

This research does not attempt to establish the global stability of the structure or the danger of the damage, because it requires additional structural information (not allowable according to the research objectives of an output-only scheme). Here only the presence of the damage, the damage localization and damage quantity can be evaluated. The resolutions of this information (when, where and how much the damage is?) is obviously limited by the extend of instrumentation in the structure.

The discussion about the damage and its infinite evaluation approaches is currently open. Anybody can argue divine and the human on the matter, but in fact it is necessary to know that at this time the structural engineer does not have a simple and straightforward approach for damage detection and a correct prediction of the damage severity and collapse stages are very far from the actual structural knowledge even in laboratory controlled tests [148].

According to the previously description of the damage in this work, it is evaluated from the analysis of output signal only and one does not use any other structural information. This definition is acceptable and it has been used widely by many research groups [1-8, 14, 29, 37, 47, 66-69, 74-76, 80-82, 84, 90, 93, 94, 118, 121, 147, 168, 190, 223].

2.1.2 Frequency

Frequency is defined as the number of complete cycles of a periodic process occurring per unit time [127].

From structural point of view one can evaluate the undamped frequency of a SDOF using :

$$f = \frac{1}{2\pi} \sqrt{\frac{k}{m}} \quad 2-1$$

where:

f : frequency (Hz),

k : system stiffness, and

m : system mass.

Structural system with one DOF have only one frequency and the output signals are monocomponent mainly (the other signal frequencies are noise or from external sources).

The word “frequency” in this thesis is referring to signal frequency associated directly to structural frequency.

In a MDOF system the frequencies are associated to modal responses and the signals obtained from these types of systems have several frequencies. These signals are namely multicomponent signals. The system frequencies and a lot of other frequencies from noise and external forces are present in the output signal of MDOF systems. In this sense, the system frequencies are referred as signal frequencies. Because the noise or external frequencies have been already separated (or isolated or minimized).

From equation (2-1) it is evident that any change in frequency is due to changes in stiffness or mass or both. It is frequently assumed that mass does not change and it stays constant. Therefore, if there is a change in frequency, it is due to the change in stiffness. In damped systems changes in frequency may result as a consequence of changes in damping and it is common that both (stiffness and damping) change.

In this research it is assumed that changes in frequency are due to changes in stiffness. Thus mass is considered to be constant at all times and damping plays a secondary role in the frequency changes. These assumptions are in accordance with a large number of scientific publications, as it can be seen in the following references [1-10, 14, 17, 18, 20, 21, 25, 26, 31, 69, 70, 81-85, 90, 94, 106-112, 118, 119, 121, 147, 150, 151].

The main reason for taking the damping role as secondary is based on the mathematical relation between damped and undamped frequency:

$$\omega_d = \omega_n \sqrt{1 - \xi^2}$$

where:

ω_d : Damped circular frequency (rad/sec),

ω_n : Undamped circular frequency (rad/sec), and

ξ : Percent of critical damping (in decimal form).

Therefore it is necessary to use an excessive damping factor in order to produce a significant change in frequency (i.e. a damping factor of 30%, only produces a 5% of frequency change).

Like damage definition the previous definition of frequency and structural frequency has some inconveniences, first signal frequency associated directly with structural frequency and it is not absolutely true. One important thing is that in the output signal exists the apparent structural frequency and not the real structural frequency, due to soil-interaction [17, 31], non-structural components response and other signal perturbations (i.e. instrument response, measurements errors) and finally numerical errors and approximations during signal processing.

Therefore, it may be necessary to point out that in this research the input signals are not used and hence is not possible to have a reliable extraction of the soil-structure interaction effect [152]. In fact, even in a controlled laboratory test (like shake table) one can not extract reliably the table-structure interaction if one does not have the input signal or the system properties [84, 151], in this research we do not have neither of them.

It is assumed that external signal perturbations like instrument response, measurements error, quantization error, frequency drift [174], instrument tilt, localization and instrument setup errors and errors during signal processing are small and therefore it can be neglected. Study of these effects is out of scope of this work, the readers can find in the references [116, 206] excellent documents about these topics.

It is important to point out that small changes in frequency of the structure not necessarily imply permanent damage in the structure. In the case of Millikan Library in Caltech, for example, several recent researches [114 - 116] have demonstrated the correlation between the changes in building frequencies and weather conditions, windstorms, daily temperature, and rainfall. A similar behavior has been reported on bridges [8, 150], when weather conditions have directly influenced the mass (concrete absorption of water) and therefore the structural frequencies. However, it has been shown in the same study that these changes are small when compared with frequency changes produced during earthquakes.

Another aspect is that some times, the total changes in frequency is not permanent, it has been reported that structures have a little frequency recovery through time and it is dependent on several factors [26, 76, 94, 114]. Therefore, it may be necessary to detect permanent damage based on frequency changes when analyzing these frequency changes through time.

Other research has proven the existence of a rare but mathematically possible case, when the damage is severe but it does not produce any changes in the system frequencies, because the damage has happened only at exact node points of the modes and no other place is affected [186].

Fortunately this case has an extreme low probability of occurrence, and if this occurs any damage detection method based on dynamic response will fail.

Finally remembering a few very recently words of one of the most famous world research group in damage detection: *“It was particularly interesting to note that the loss of natural frequencies reached about 10% and still the cracks could not visually be observed. This result is rather promising for the future applications of the non-destructive damage estimations of structures from their natural frequencies, **since we can detect damage from vibrations before we could note it from ordinary inspections**”*[151], remarked is by the author of this dissertation.

2.1.3 Overview of Application of Time-Frequency Analysis in System Identification and Structural Damage Detection

As previously discussed in section 1.3.3, the main idea of time-frequency distributions is to provide a distribution that shows the energy of a signal in time and frequency domain simultaneously [49]. In this research a tracking of instantaneous characteristic of signal using Time-Frequency Analysis (TFA) has been done and these values are associated with the dynamic changes in the structure and therefore with damage success according to the damage definition.

TFA has been employed in a diverse field, like radar applications, image processing, biomedical-engineering studies, geophysics, quantum mechanics, signal processing, economics analysis, mechanical, electronic among them [49].

Before giving the mathematical background of time-frequency analysis, in this section the time-frequency ability for system identification and damage detection are shown briefly and graphically.

Suppose that for an instrumented structure of MDOF, the output signals from “n” channels are given. A typical time-history output from ambient vibration (or in-operation conditions) of any channel is shown in the Figure (2-1):

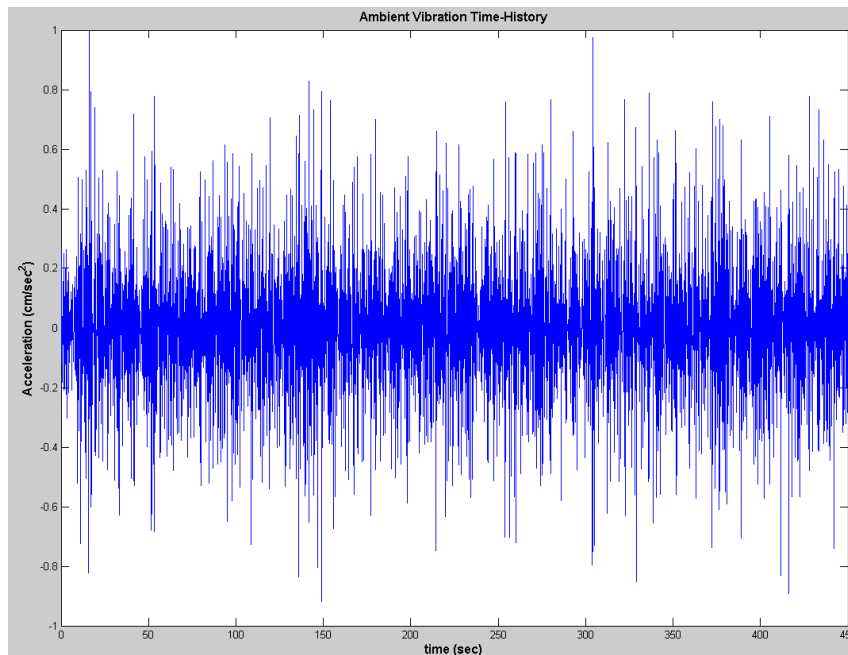


Figure 2-1 Ambient Vibration Record taken from a MDOF system

From the Figure (2-1) it is evident that the system is submitted to random vibration force and obviously in accordance with random vibration theory, its response is random also. Practically one can not say anything about the structure using this time-domain signal, except may be the excitation is small and do not exist evidences of high damping.

If one is asked about the main frequencies (or periods) of a particular structure, an obvious response would be to use Fourier transform theory. In Figure (2-2) the Power Spectra (square magnitude of Fourier transform) is shown to ten time series of this signal.

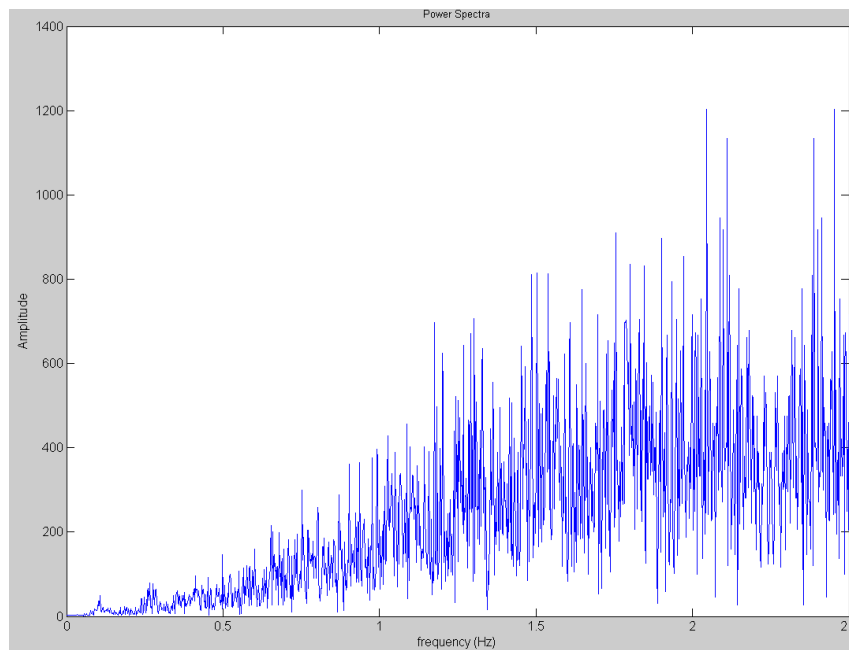


Figure 2-2 Power Spectra for signal of Figure (2-1)

In this case, the Fourier theory is not useful, because in ambient vibration conditions the signal to noise ratio (SNR) is very low (thus signifying that the noise presents in the signal is very high). A filter operation can be used in order to remove this noise, but it will require the knowledge about the range of frequencies. Specifically, in Figure (2-1), what frequencies one should remove? Again if one does not know anything about the structure, one end up removing the noise but also the system frequencies.

One can use other ways, like stochastic subspace system identification [128], or other useful approach, but in many of them one will need additional information of structural system and in remaining the information about input forces are required.

In the Figure (2-3) using a technique proposed in this research, a Normalized Mean Time-Frequency Representation of the ten time series of this signal is shown (see details on section 4.4.2). Trying to answer the original question: what is the main frequencies (or periods) of this structure?

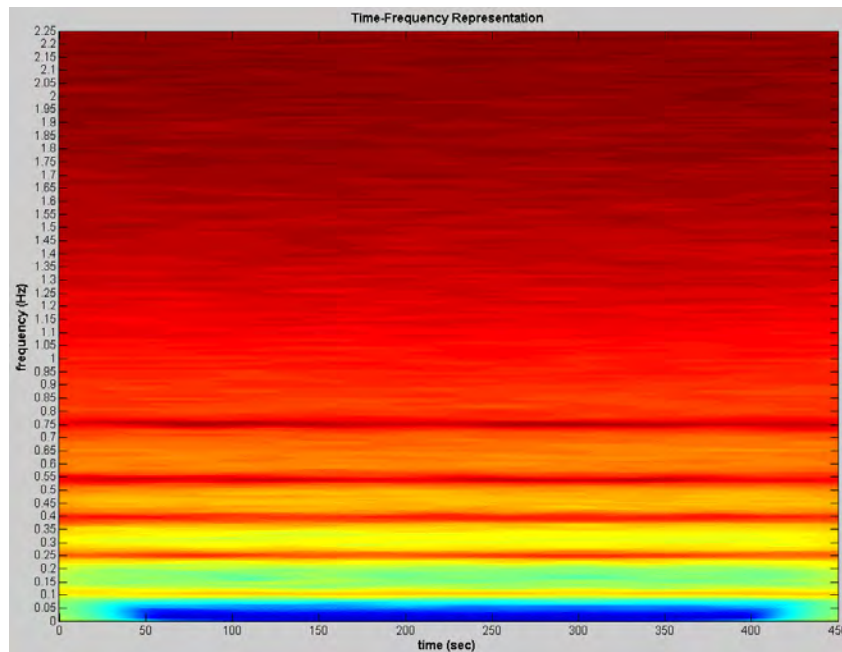


Figure 2-3 Mean Time-Frequency Representation for signal of Figure (2-1)

Now, it becomes clear that by using this powerful theory of signal processing, which is the possible structural frequencies of this structure are determined (may be: 0.12, 0.25 0.4, 0.54 and 0.76 Hz do you agree?). We say “possible” because it is probable that some of these identified frequencies (or may be all of them) are not from the structure and are from the external forces. Fortunately, it is possible to know what are system and not system frequencies using random vibration theory.

Once the main frequencies of the structural system are identified the time-frequency analysis, frequency domain decomposition [124] and singular value decomposition [149] can be used to reconstruct an equivalent mass, stiffness and damping matrices that represent the

dynamic model of the structure. In this particular case a 5 by 5 matrix for each case can be reconstructed, as will be seen in Chapter 4.

For damage detection the time-frequency analysis is very useful also, take for example the following output signal of a numerical simulation system submitted to an earthquake or another strong event:

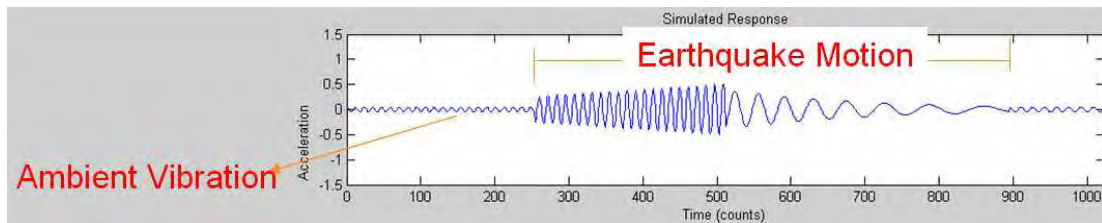


Figure 2-4 Time-History of a Simulated Structural Response

The response shown here is similar to a sine wave before a strong motion, the strong motion was taken as an amplitude modulated sine wave and at 500 counts (any time scale) the system fails. After 900 counts, the external force disappears and the system is back to initial excitation.

All this can be deduced from the Figure (2-4) except may be the failure, because the change in the time-history signal can be due to external force change and not necessarily for damage in the structure. If one uses traditional signal analysis (like fourier analysis) one can get another useful information, see the following graph:

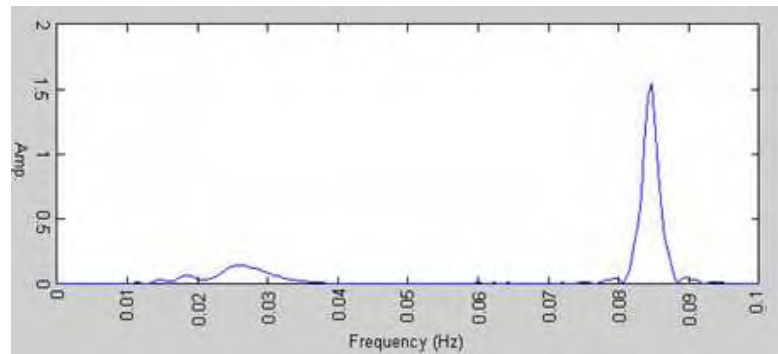


Figure 2-5 Power Spectra for signal of fig. (2-4)

Using Fourier analysis, two frequencies can be seen in Figure (2-5), 0.025 and 0.085 Hz. The additional information although important is not useful for damage detection, because in frequency domain, the information about temporal evolution of the frequency is lost. Theoretically it is possible to extract temporal information of Fourier Spectra using the phase of the transform [49, 57, 146], but it is not practical.

In the following graph a time-frequency of the signal using Pseudo-Wigner-Ville Distribution is shown:

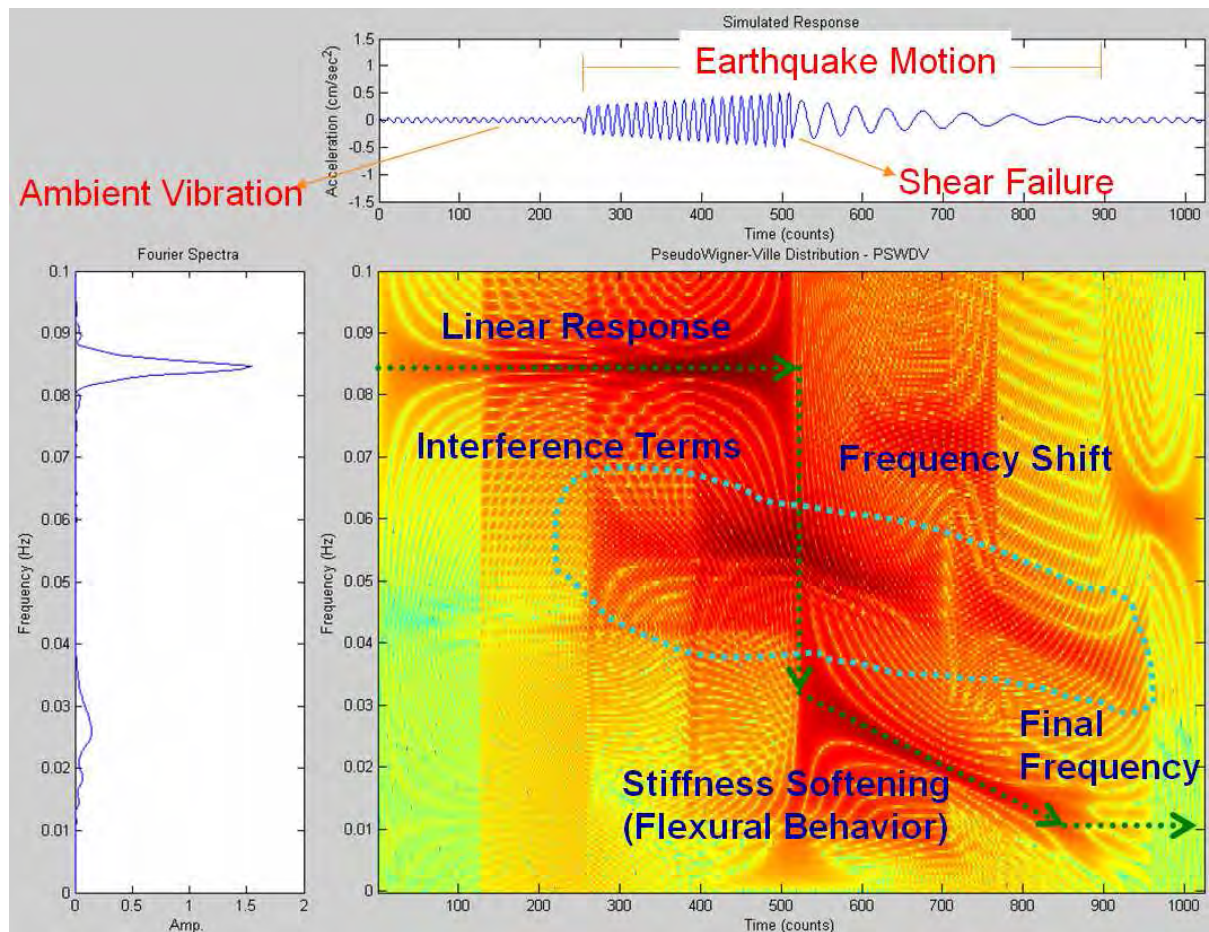


Figure 2-6 Pseudo-Wigner-Ville Distribution for simulated response

From analysis of Figure (2-6), it is possible to have a frequency history evolution. Tracking the damage evolution in the structure, for example, it is easy to see that the frequency starting at 0.085 Hz (the same value of maximum power spectra) will remain constant for up to 500 counts (any time scale) and at this moment the frequency drop instantaneously to 0.033 Hz (loss of stiffness according to the damage definition). Afterward the system has a stiffness softening between 500 and 850 time instants, with the system frequency at 0.01 Hz at the end not return to initial value. Therefore, it is reasonable to assume that a permanent damage has occurred.

A particular zone appear in the time-frequency plane of Figure (2-6), this zone is called interference terms and its presence is in general due to the quadratic terms of the transform, these terms are a numerical artifact and it is not true terms (autoterms), thus the signal do not have frequencies at these time-frequency zones. The interference terms are considered a serious drawback to apply time-frequency methodologies, because similar to the noise case if one does not have information about the structure how one will be able to identify them?

Although many research groups had been dedicated to remove the interference terms and several methodologies had been proposed in the last two decades [96, 100, 129-138, 225-228], the interference terms are not an exclusive problem of time-frequency representations but it is also present in time-scale representations like wavelets analysis, see references [57, 100, 132]. The main problem with many of these methodologies is in the smoothing process the autocomponents terms will disappear together with cross terms.

A new method to search frequencies in zones of the time-frequency plane where interference terms appear is proposed in this research for Civil Engineering structures.

2.2 Time-Frequency Representations

2.2.1 Basic Concept

Definition 2.2.1 :

“Time-Frequency Representation (TFRs) of signals map a one-dimensional signal of time, $x(t)$, into a two-dimensional function of time and frequency, $T_x(t,f)$ ” [57]

Definition 2.2.2:

Any time-frequency representation that fulfill the equations (2-2) is considered a Time-Frequency Energy Distribution (TFED) $P(t,f)$ [49],

$$\begin{aligned} |x(t)|^2 &= \int_{-\infty}^{+\infty} P(t, f) df \\ |S(f)|^2 &= \int_{-\infty}^{+\infty} P(t, f) dt \end{aligned} \quad 2-2$$

If the marginal conditions are satisfied then the total energy of the signal is [49]:

$$E = \int_{-\infty}^{+\infty} P(t, f) df dt \quad 2-3$$

Cohen [56] proved that any time-frequency representation that fulfills equations (2-2, 2-3) can be represented using the following equation:

$$C_x(t, f) = P(t, f) = \frac{1}{4\pi^2} \int_{-\infty}^{+\infty} \int_{-\infty}^{+\infty} \int_{-\infty}^{+\infty} e^{-j\theta t - j\tau f + j\theta u} \phi(\theta, \tau) x^* \left(u - \frac{1}{2} \tau \right) x \left(u + \frac{1}{2} \tau \right) du d\tau d\theta \quad 2-4$$

Where $\phi(\theta, \tau)$ is the kernel, which for Cohen’s Class Distributions is independent of time and frequency. According to equation (2-4) the Cohen’s Class Distributions satisfy time and frequency shift invariance [56]. If the kernel is independent of time then the TFED is time-

shift invariant. On the other hand, if the kernel is frequency independent then the TFED is frequency-shift invariant [49].

In equation (2-4), it is important to note that $x(t)$ is the complex associate analytical signal of the real signal $x_r(t)$. The analytical signal is defined as [49]:

$$x(t) = x_r(t) + jHT(x_r(t)) \quad 2-5$$

where:

$HT(x(t))$: Hilbert Transform of $x(t)$.

The use of analytical signal instead of real signal has its advantages, for computational time and memory computation purposes the Fourier Transform of analytical signal are single sided [123]. For mathematical and symbolic process, the use of analytical signal is also better.

Another good reason for using complex analytical signal instead of real signal is to satisfy the Shanon's sampling theorem and avoid aliasing problems in the time-frequency plane. If the real signal is used then it is necessary to take a sampling rate equal to twice of sampling used in Fourier Analysis. On the other hand, if complex analytical signal is used to evaluate the time-frequency distribution the sampling rate can be taken simply equal to double of Nyquist frequency.

From equation (2-4) it is clear that the only representation that will fulfill equations (2-2, 2-3) is really ***Time-Frequency Energy Distributions (TFED)***, otherwise it is only a time-frequency representation (TFR). Frequently this point is not very clear in scientific literature, and is very common to read indistinctly TFR or TFED or Time-Frequency Distribution (TFD).

In this dissertation when Time-Frequency Representations (TFRs) or Time-Frequency Distributions (TFDs) are used, it refers to Time-Frequency Representations that *not*

necessarily fulfill the equations (2-2) and (2-3). The words Time-Frequency Energy Distribution (TFED) are used for Time Frequency Representations that fulfill the equations (2-2) and (2-3).

This concept is important for structural damage detection if one wishes to use an energy approach, because only time-frequency energy distributions (TFED) can show a real and complete energy flux in the time-frequency plane.

In general time-frequency energy distributions have the drawback that in some places of the time-frequency plane it has negative values, neglecting any physical direct interpretation (relative to energy) [49, 56, 57, 65, 84, 88, 90], and therefore an approach to structural damage detection using the volume (energy) of the distribution is not set yet.

In this regard some authors proposed methodologies to achieve truly positives TFEDs[139-141, 144,] and others have believed that positive TFEDs only can be achieved using smoothing Wigner-Ville Distributions and therefore it is not a truly TFED and it is only TFRs. In reference [142], one attempt for analytical demonstration has been proposed.

Negative local energy values can appear in some places of the time-frequency plane. However it has been demonstrated in the reference [170] that even if negative energy values are present, the local integration over an elliptic domain never exceed the total energy in the system. This will keep the door open for future research of joint structural energy approach with time-frequency analysis.

In this research, an energy approach is not used and the use of direct energy values (equation 2-3) from the TFDs is avoided. Therefore, possible punctual negative energy values from the distributions do not affect ours estimation. The approach for this research is to evaluate instantaneous frequency values from the TFRs and link these values with

instantaneous structural response. When the use of energy is required, a cumulative time-dependent energy flux is evaluated by using integration of TFRs along the frequency axis; therefore we do not deal with negative energy values.

2.2.2 Classification of Time-Frequency Representations

Since Cohen's [56] classification; a large number of TFRs have been proposed. Theoretically, it is possible to construct infinite TFRs by selecting different independent time and frequency kernels. Dozens of TFRs are available and construction of new TFRs is an important part of research in signal analysis field.

An attempt is not made to show and describe hundreds of TFRs actually available. In this work it is preferable to show the main branches of grouping and the desirable mathematical properties that a TFRs must have in order to do the signal analysis for civil engineering structures.

Interested reader on this topic can find additional information about some TFRs application specifically for structural engineering in the references [81, 84, 90]. The applications in soil dynamics, earthquake engineering and seismology can be found in references [143, 153-155, 172, 221]. A brief application of spectrogram to soil liquefaction can be found in the reference [116].

According to reference [57], TFRs can be classified as linear, quadratic and non-linear. At this time it is necessary to add a new class of TFRs, because recently others types of TFRs have begun to appear [73, 97, 145]. In this work the TFRs classification has been enhanced and it is shown in the Figure 2.7. In the same Figure a few typical TFRs are included. As previously mentioned the number of TFRs is extensive. For example regarding Figure. 2-7, in the Adaptive Optimal Kernel type you can get 15 or more TFRs. In Reassigned type you can get 20 or more and so on, for this reason particular description of TFRs is avoided here.

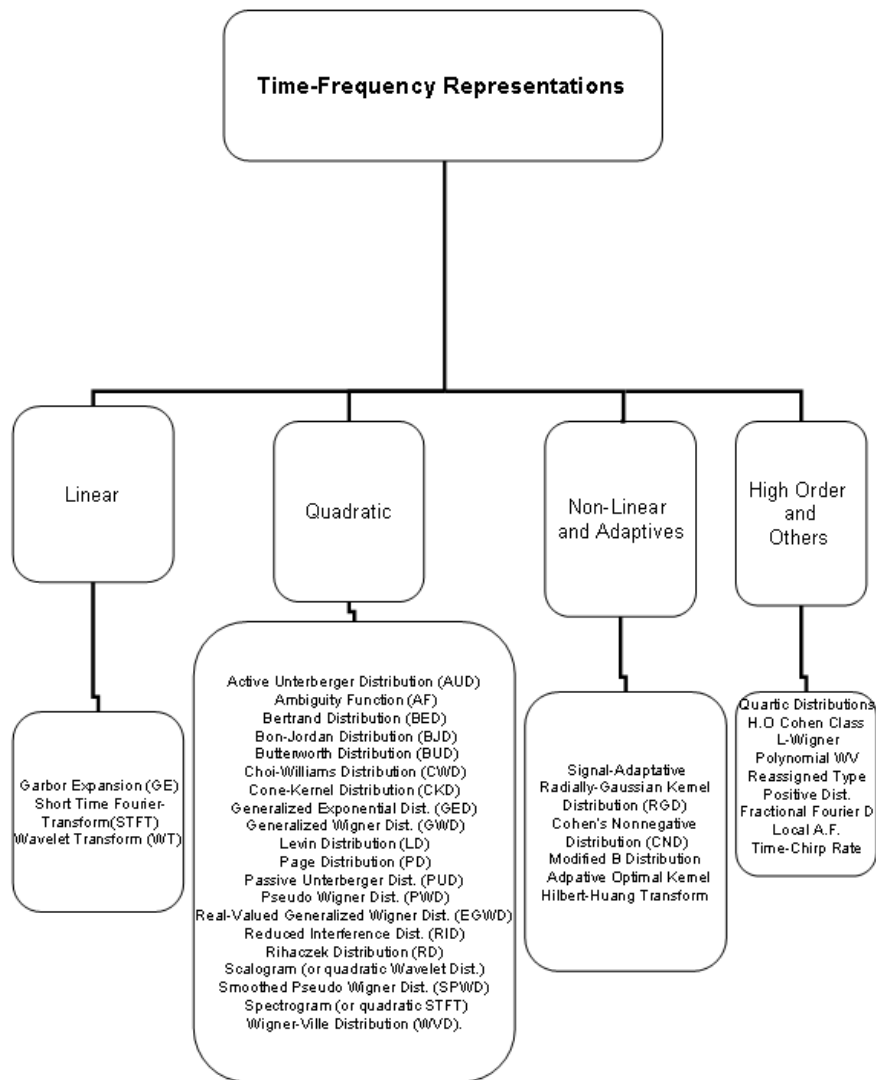


Figure 2-7 Classification of Time-Frequency Representations

2.2.3 Desirable Mathematical Properties for Time-Frequency Representations in Signal Analysis of Structures

There is not an unique criteria to establish mathematical properties of TFRs. Many of them has been shown in the literature, and frequently with different names for the same properties.

The mathematical properties presented here was collected mainly from references [49, 56, 57, 66, 90, 102, 224], and only those with some structural engineering interest were selected.

In what follows, we will explain the principal mathematical properties that TFRs should have in order to have a complete use in structural damage analysis.

The function $P(t,f)$ must be calculated using equation (2-4). For example in the multiplication property:

$$x(t) = x_1(t)x_2(t) \Rightarrow P_x(t, f) = \int_{-\infty}^{+\infty} P_{x_1}(t, f - f')P_{x_2}(t, f')df' \quad 2-6$$

One needs to evaluate the following expressions:

$$x(t) = x_1(t)x_2(t) \Rightarrow P_x(t, f) = \frac{1}{16\pi^4} \int_{-\infty}^{+\infty} \left[\left(\int_{-\infty}^{+\infty} \int_{-\infty}^{+\infty} \int_{-\infty}^{+\infty} e^{-j\theta t - j\tau(f-f') + j\theta u} \phi(\theta, \tau) x_1^* \left(u - \frac{1}{2}\tau \right) x_1 \left(u + \frac{1}{2}\tau \right) dud\tau d\theta \right)^* \right. \\ \left. \left(\int_{-\infty}^{+\infty} \int_{-\infty}^{+\infty} \int_{-\infty}^{+\infty} e^{-j\theta t - j\tau f' + j\theta u} \phi(\theta, \tau) x_2^* \left(u - \frac{1}{2}\tau \right) x_2 \left(u + \frac{1}{2}\tau \right) dud\tau d\theta \right) \right] df' \quad 2-7$$

Always the simple asterisk sign (*) imply multiplication and the superscript asterisk sign (*) imply complex conjugation, the signal $x(t)$ refers to analytical signal (eq. 2-5 using the complex Hilbert transform) instead of the real signal. When uppercase is used $X(f)$, it is refer to Fourier Transform of $x(t)$.

The Kernel function will be taken according to Table (2-1), if one uses a Levin Distribution for example, the kernel is defined by:

$$\phi(\theta, \tau) = e^{j\pi|\tau|\theta} \quad 2-8$$

Substituting equation (2-7) into equation (2-6) we obtained:

$$x(t) = x_1(t)x_2(t) \Rightarrow$$

$$P_x(t, f) = \frac{1}{16\pi^4} \int_{-\infty}^{+\infty} \left[\left(\int_{-\infty}^{+\infty} \int_{-\infty}^{+\infty} \int_{-\infty}^{+\infty} e^{-j\theta t - j\tau(f-f') + j\theta u} e^{j\pi|\tau|\theta} x_1^* \left(u - \frac{1}{2}\tau \right) x_1 \left(u + \frac{1}{2}\tau \right) dud\tau d\theta \right)^* \right. \\ \left. \left(\int_{-\infty}^{+\infty} \int_{-\infty}^{+\infty} \int_{-\infty}^{+\infty} e^{-j\theta t - j\tau f' + j\theta u} e^{j\pi|\tau|\theta} x_2^* \left(u - \frac{1}{2}\tau \right) x_2 \left(u + \frac{1}{2}\tau \right) dud\tau d\theta \right) \right] df', \quad 2-9$$

Simplifying the preceding equation, finally the valid expression (2-10) for multiplication using Levin Distribution is obtained:

$$x(t) = x_1(t)x_2(t) \Rightarrow$$

$$P_x(t, f) = \frac{1}{16\pi^4} \int_{-\infty}^{+\infty} \left[\left(\int_{-\infty}^{+\infty} \int_{-\infty}^{+\infty} \int_{-\infty}^{+\infty} e^{-j\theta t - j\tau(f-f') + j\theta u + j\pi|\tau|\theta} x_1^* \left(u - \frac{1}{2}\tau \right) x_1 \left(u + \frac{1}{2}\tau \right) dud\tau d\theta \right)^* \right. \\ \left. \left(\int_{-\infty}^{+\infty} \int_{-\infty}^{+\infty} \int_{-\infty}^{+\infty} e^{-j\theta t - j\tau f' + j\theta u + j\pi|\tau|\theta} x_2^* \left(u - \frac{1}{2}\tau \right) x_2 \left(u + \frac{1}{2}\tau \right) dud\tau d\theta \right) \right] df', \quad 2-10$$

2.2.3.1 Linearity (P1)

If a signal is a linear combination of two or more components, the TFR is the linear combination of individual TFRs.

$$x(t) = \sum_{i=1}^n (k_i x_i(t)) \Rightarrow P_x(t, f) = \sum_{i=1}^n (k_i P_{x_i}(t, f)) \quad 2-11$$

Only linear TFRs (see fig. 2-7) fulfill the equation (2-6), therefore only Garbor Expansion, Short Time Fourier Transform (STFT) and Wavelet Transform in its time-frequency version (WT) have this good property.

2.2.3.2 Multiplication (P2)

If a signal is a product of two signals, its TFRs can be obtained using:

$$x(t) = x_1(t)x_2(t) \Rightarrow P_x(t, f) = \int_{-\infty}^{+\infty} P_{x_1}(t, f - f')P_{x_2}(t, f')df' \quad 2-12$$

2.2.3.3 Convolution (P3)

If a signal is a convolution of two signals, its TFRs can be obtained using:

$$x(t) = \int_{-\infty}^{\infty} x_1(t - t')x_2(t')dt' \Rightarrow P_x(t, f) = \int_{-\infty}^{+\infty} P_{x_1}(t - t', f)P_{x_2}(t', f)dt' \quad 2-13$$

2.2.3.4 Real Valued (P4)

If a signal $x(t)$ has $P(t, f)$, the TFRs is real valued if:

$$P_x^*(t, f) = P_x(t, f) \quad 2-14$$

2.2.3.5 Time Shift (P5)

Any time shift in the signal, imply the same time shift in its TFR, thus:

$$x_1(t) = x(t - t_0) \Rightarrow P_{x_1}(t, f) = P_x(t - t_0, f) \quad 2-15$$

2.2.3.6 Frequency Shift (P6)

Any frequency shift in the signal, imply the same frequency shift in its TFR, thus:

$$x_1(t) = x(t)e^{j2\pi f_0 t} \Rightarrow P_{x_1}(t, f) = P_x(t, f - f_0) \quad 2-16$$

2.2.3.7 Time Marginal (P7)

The instantaneous energy of the signal $x(t)$, can be obtained:

$$\int_{-\infty}^{+\infty} P_x(t, f) df = |x(t)|^2 \quad 2-17$$

2.2.3.8 Frequency Marginal (P8)

The total power spectrum of the signal $x(t)$, can be obtained:

$$\int_{-\infty}^{+\infty} P_x(t, f) dt = |X(f)|^2 \quad 2-18$$

2.2.3.9 Instantaneous Frequency (P9)

The instantaneous frequency of the signal $x(t)$, can be obtained using the equation 2-19:

$$IF_x(t) = f_x(t) = \frac{\int_{-\infty}^{+\infty} f P_x(t, f) df}{\int_{-\infty}^{+\infty} P_x(t, f) df} \quad 2-19$$

2.2.3.10 Group Delay (P10)

The first derivate of the phase with respect to frequency is called group delay:

$$GD_x(f) = t_x(f) = \frac{\int_{-\infty}^{+\infty} t P_x(t, f) dt}{\int_{-\infty}^{+\infty} P_x(t, f) dt} \quad 2-20$$

2.2.4 Common Time-Frequency Representations

If you take several forms to the kernel function of equation (2-4) you can get theoretically infinite possible TFRs, as has been mentioned earlier, there may exist dozens of TFRs in the literature and its description require a large volume book, therefore for the sake of simplicity in this section we will show only some common Quadratic TFRs and its kernel function. The properties of TFRs aforementioned in the section 2.2.3 that it fulfill.

In the Table (2-1) the common Quadratic TFRs are shown, these types of TFRs are included in Cohen's Class. In the references [49, 56, 57, 123] similar and equivalent expression can be found.

TABLE 2.1- Kernel, Expression and Properties for a few Cohens Class of TFRs

Time-Frequency Representation	Kernel	TFR	Properties
	$\phi_x(\theta, \tau)$	$P_x(t, f)$	
Born-Jordan	$\frac{\sin(\pi\theta\tau)}{\pi\theta\tau}$	$\int_{-\infty}^{+\infty} \frac{1}{ \tau } \int_{t-\frac{ \tau }{2}}^{t+\frac{ \tau }{2}} x\left(u+\frac{\tau}{2}\right)x^*\left(u-\frac{\tau}{2}\right) du e^{-j2\pi f\tau} d\tau$	4-10
Zhao-Atlas-Marks (Cone-Shape Kernel)	$h(\tau) \frac{\sin(\pi\theta\tau)}{\pi\theta\tau}$	$\int_{-\infty}^{+\infty} h(\tau) \int_{t-\frac{ \tau }{2}}^{t+\frac{ \tau }{2}} x\left(u+\frac{\tau}{2}\right)x^*\left(u-\frac{\tau}{2}\right) du e^{-j2\pi f\tau} d\tau$	4-10
Choi-Williams	$e^{-\frac{\theta^2\tau^2}{\sigma}}$	$\frac{1}{4\pi^{3/2}} \int_{-\infty}^{+\infty} \int_{-\infty}^{+\infty} \sqrt{\frac{\sigma}{\tau^2}} e^{-\frac{\sigma(u-t)^2}{4\tau^2} - j\pi f} x\left(u-\frac{1}{2}\tau\right)x\left(u+\frac{1}{2}\tau\right) dud\tau$	4-10
Margenau-Hill	$\cos(\pi\theta\tau)$	$\text{Re} \left\{ \frac{1}{\sqrt{2\pi}} x(t) e^{-j\pi f} X^*(f) \right\}$	1,3 5-8
Rihaczek	$e^{j\pi\theta\tau}$	$x(t)X^*(f)e^{-2j\pi f}$	1,3, 5-8
Levin	$e^{j\pi \tau \theta}$	$x(t)X^*(f)e^{-j\pi f}$	2,4-8
Wigner-Ville Distribution (WVD)	1	$\frac{1}{2\pi} \int_{-\infty}^{+\infty} x\left(t+\frac{1}{2}\tau\right)x^*\left(t-\frac{1}{2}\tau\right) e^{-j\pi f\tau} d\tau$	2-10
Page	$e^{\frac{j \tau \theta}{2}}$	$\frac{\partial}{\partial t} \left \frac{1}{\sqrt{2\pi}} \int_{-\infty}^t x(t') e^{-j\pi f} dt' \right ^2$	2,4-8
Pseudo-Wigner-Ville	$h(\tau)$	$\int_{-\infty}^{+\infty} h(\tau) x\left(t+\frac{1}{2}\tau\right)x^*\left(t-\frac{1}{2}\tau\right) e^{-2j\pi f\tau} d\tau$	2-6,9-10
Spectrogram	$\int_{-\infty}^{+\infty} h\left(u-\frac{1}{2}\tau\right)h\left(u+\frac{1}{2}\tau\right) e^{-j\pi u} du$	$\left \frac{1}{\sqrt{2\pi}} \int_{-\infty}^{+\infty} x(\tau)h(\tau-t) e^{-j\pi f\tau} d\tau \right ^2$	4-6
sinc	$\frac{\sin(a\theta\tau)}{a\theta\tau}$	$\frac{1}{4\pi a} \int_{-\infty}^{+\infty} \left[\frac{1}{\tau} e^{-j\pi f\tau} \int_{t-a\tau}^{t+a\tau} x\left(u+\frac{1}{2}\tau\right)x^*\left(u-\frac{1}{2}\tau\right) du \right] d\tau$	2,4-8

2.2.5 A Survey From Spectrogram To Wavelets Trough Time-Frequency Distributions

Another useful and big group of TFRs is the Affine Class of representation.

In general any TFRs of affine class can be represented by a Wigner-Ville Distribution with a smoothing function, where the Wigner-Ville Distribution (WVD) is defined by [53, 54]:

$$WVD_x(t, f) = \frac{1}{2\pi} \int_{-\infty}^{+\infty} x\left(t + \frac{1}{2}\tau\right) x^*\left(t - \frac{1}{2}\tau\right) e^{-j\tau f} d\tau \quad 2-21$$

Thus imply that the kernel of WVD according to general Cohen's class has the following form [56]:

$$\phi(\theta, \tau) = 1 \quad 2-22$$

The importance of Affine Class of distribution is that it is the joint between time-frequency analysis and time-scale analysis, so the most prominent group of affine class is the Wigner-Ville Distribution and the scalogram (square magnitude of wavelets).

If an arbitrary frequency scale is defined as equal to:

$$a = \frac{f_0}{f} \quad 2-23$$

Then a distribution in the new time- scale domain (t,a) will fulfill covariance by translation in time and dilatation. It can be obtained using [123]:

$$\Omega_x(t, a; \Pi) = \frac{1}{|a|} \int_{-\infty}^{+\infty} \int_{-\infty}^{+\infty} \Psi(f, \omega) X\left(\frac{\omega - \frac{f}{2}}{a}\right) X^*\left(\frac{\omega + \frac{f}{2}}{a}\right) e^{-\frac{j2\pi f t}{a}} df d\omega \quad 2-24$$

Where a bi-frequency kernel is defined by:

$$\Psi(f, \omega) = \int_{-\infty}^{+\infty} \Pi(t, f) e^{-j2\pi f t} dt \quad 2-25$$

Like before, X in uppercase is the Fourier transform of $x(t)$, and superscript $(^*)$ is the complex conjugation.

In general any Cohen's class or affine class of distribution can be obtained as function of another using the following equation, this equation joint time-frequency with time-scale analysis, equations (2-4) and (2-24) [123]:

$$C_x\left(t, \frac{f_0}{a}; \Pi\right) = \Omega_x(t, a; \Pi) \quad 2-26$$

Because all Cohen's class [56] time-frequency representations can be expressed as a smoothing Wigner-Ville Distribution using the following expression [123]:

$$C_x(t, f; \Pi) = \int_{-\infty}^{+\infty} \int_{-\infty}^{+\infty} \Pi(u - t, \theta - f) WVD(u, \theta) du d\theta \quad 2-27$$

where:

$$\Pi(t, f) = \int_{-\infty}^{+\infty} \int_{-\infty}^{+\infty} \phi(\theta, \tau) e^{-j2\pi(f\tau + \theta t)} dt df \quad 2-28$$

$$WVD(u, \theta) = \frac{1}{2\pi} \int_{-\infty}^{+\infty} x\left(u + \frac{1}{2}\tau\right) x^*\left(u - \frac{1}{2}\tau\right) e^{-j\tau\theta} d\tau \quad 2-29$$

Therefore one can get a time-scale distribution like wavelets using a time-frequency distribution or one can get a time-frequency distribution like Wigner-Ville using a time-scale distribution such as scalograms (square magnitude of wavelet transform).

In this sense WVD can be used to obtain all Cohen's time-frequency bilinear distribution such as spectrogram or Choi-Williams and on the other hand WVD can be used to obtain time-scale representation.

In this regard it is important to point out that the procedure for obtaining any Cohen's class and time-scale representation using WVD is valid for all continuous cases, but in the discrete case there is some Cohen's class distribution that can not be obtained using the discrete formulation of WVD, this has been demonstrated in the references [164, 165].

To show the dependence or interconnection between TFRs, for example, it is not difficult to prove [49, 123] that the spectrogram can be obtained by smoothing of Wigner-Ville Distribution using:

$$S_x(t, f) = \int_{-\infty}^{+\infty} \int_{-\infty}^{+\infty} WVD_w(\tau - t, \theta - f) WVD_x(\tau, \theta) d\tau d\theta \quad 2-30$$

where:

$WVD_w(\tau - t, \theta - f)$: Is the Wigner-Ville Distribution of the window h ,

$WVD_x(\tau, \theta)$: Is the Wigner-Ville Distribution of the signal $x(t)$ using lag variables.

In the same way, in the reference [65] it has been proved that using affine smoothing, the scalogram (square magnitude of wavelet transform) can be obtained from Wigner-Ville Distribution using the following expression:

$$\left|CWT(a, \tau)_x\right|^2 = \int_{-\infty}^{+\infty} \int_{-\infty}^{+\infty} WVD_w(\tau, \theta) WVD_{Mw}\left(\frac{\tau-t}{a}, a\theta\right) d\tau d\theta \quad 2-31$$

where:

WVD_{Mw} : Is the Wigner Distribution of the mother wavelet.

$$CWT(a, \tau)_x = \frac{1}{\sqrt{a}} \int_{-\infty}^{+\infty} x(t) \psi\left(\frac{t-\tau}{a}\right) dt \quad 2-32$$

CWT is the continuous wavelet transform of the a signal $x(t)$ [33], and the second term within integral is named the mother wavelet.

$$WVD_w(\tau, \theta) = \int_{-\infty}^{+\infty} x^*\left(\tau - \frac{\nu}{2}\right) x\left(\tau + \frac{\nu}{2}\right) e^{-j\theta\nu} d\nu \quad 2-33$$

In fact by using TFRs members of Cohen's class is possible to get the scalogram, this has been proved mathematically in the reference [173].

Finally an alternative method that link wavelet transform to time-frequency using constant Q-short-time spectral analysis in the time domain has been reported in the reference [156].

2.2.5.1 Bi-Frequency Kernel Distributions

Another good way to express the equation (2-24) is [123]:

$$\Omega_x(t, a; \Pi) = \frac{1}{|a|} \int_{-\infty}^{+\infty} G(f) X\left(\frac{H(f) - \frac{f}{2}}{a}\right) X^*\left(\frac{H(f) + \frac{f}{2}}{a}\right) e^{-\frac{j2\pi ft}{a}} df \quad 2-34$$

where: G, H are any independent functions.

The equation (2-34) represent a new group of affine class namely the localized bi-frequency distributions. By selecting several G, H functions we can get many interesting TFRs, some of these TFRs are shown in the Table below [123]:

TABLE 2.2 Expression for Localized Bi-Frequency Distributions

Time-Frequency Representation	G(f)	H(f)	TFR $\Omega_x(t, a; \Pi)$
Bertrand	$\frac{\frac{f}{2}}{\sinh\left(\frac{f}{2}\right)}$	$\frac{f}{2} \coth\left(\frac{f}{2}\right)$	$\frac{1}{ a } \int_{-\infty}^{+\infty} \frac{\frac{f}{2}}{\sinh\left(\frac{f}{2}\right)} X\left(\frac{fe^{-\frac{f}{2}}}{2a \sinh\left(\frac{f}{2}\right)}\right) X^*\left(\frac{fe^{\frac{f}{2}}}{2a \sinh\left(\frac{f}{2}\right)}\right) e^{-\frac{j2\pi ft}{a}} df$
D-Flandrin	$1 - \left(\frac{f}{4}\right)^2$	$1 + \left(\frac{f}{4}\right)^2$	$\frac{1}{ a } \int_{-\infty}^{+\infty} \left(1 - \left(\frac{f}{4}\right)^2\right) X\left(1 - \left(\frac{f}{4}\right)^2 / a\right) X^*\left(1 + \left(\frac{f}{4}\right)^2 / a\right) e^{-\frac{j2\pi ft}{a}} df$
Active Unterberger	1	$\sqrt{1 + \left(\frac{f}{2}\right)^2}$	$\frac{1}{ a } \int_0^{+\infty} \left(1 + \frac{1}{\alpha^2}\right) X\left(\frac{\alpha}{a}\right) X^*\left(\frac{1}{\alpha a}\right) e^{\frac{j2\pi t\left(\alpha - \frac{1}{\alpha}\right)}{a}} df$
Passive Unterberger	$\frac{1}{\sqrt{1 + \left(\frac{f}{2}\right)^2}}$	$\sqrt{1 + \left(\frac{f}{2}\right)^2}$	$\frac{1}{ a } \int_0^{+\infty} \frac{2}{\alpha} X\left(\frac{\alpha}{a}\right) X^*\left(\frac{1}{\alpha a}\right) e^{\frac{j2\pi t\left(\alpha - \frac{1}{\alpha}\right)}{a}} df$

2.2.5.2 High Order and Polynomial TFRs

Finally it is important to discuss the possibility of defining a high order or polynomial HO-WVDs using [145]:

$$WVD_{kx}(t, f) = \int_{-\infty}^{+\infty} \prod_{i=1}^q \left[x(t + c_i \tau)^{b_i} x^*(t + c_{-i} \tau)^{b_{-i}} \right] e^{-j2\pi f \tau} d\tau \quad 2-35$$

Changing values of the parameters b_i , b_{-i} , c_i , c_{-i} , the polynomial WVD of several k^{th} orders are obtained, for example by taking the following values into equation (2-35):

$$\begin{aligned} q &= 1 \\ b_1 &= b_{-1} = 1 \\ k &= 2 \\ c_1 &= c_{-1} = 0.5 \end{aligned}$$

The equation (2-21) is obtained, therefore WVD is a particular case of polynomial TFRs [145].

In general any type of High-Order Cohen's class TFRs can be obtained using multidimensional kernels, a list of the High-Order generalized Cohen's class and its mathematical properties is given in the reference [166].

Therefore it is possible to define also a great group of High-Order Time-Scales representations, such as High Order Scalograms (square magnitude of wavelet transform), using the High Order Polynomial TFRs, this has been demonstrated in the reference [167].

Another way to obtain time-scale representation from TFRs is to take the time-frequency kernel's second order derivatives to generate symmetrical wavelets like Mexican-Hat, Laplacian or Gaussian wavelets, as has been demonstrated in the reference [168].

2.3 Instantaneous Frequency

2.3.1 Monocomponent Signals

As it has been mentioned before, structural damage will be reflected by a permanent shift of the pre-event frequency [1-10, 84, 90]. For this reason it is important to precisely establish the pre-event, event, and post-event frequencies of the structure. When the analysis of a signal shows just one frequency per each time interval (monocomponent signal), like a constant chirp function, the instantaneous frequency is equal to the first derivative of the phase [49, 123, 127]:

$$IF(t) = \frac{d\phi(t)}{dt} = \frac{x(t)d \frac{HT(x(t))}{dt} - d \frac{x(t)}{dt} HT(x(t))}{x^2(t) + HT^2(t)} = \frac{d}{dt} \tan^{-1} \left(\frac{HT(x(t))}{x(t)} \right) \quad 2-36$$

where:

$x(t)$: Real signal,

$\phi(t)$: Phase of signal, and

$HT(x(t))$: Hilbert Transform of $x(t)$.

If you have the TFRs of a signal, you can evaluate the time variability of the frequency using the equation (2-19). As repeated here, this expression is valid for even high order polynomial TFRs as has been demonstrated in the reference [145] :

$$IF_x(t) = f_x(t) = \frac{\int_{-\infty}^{+\infty} fP_x(t, f)df}{\int_{-\infty}^{+\infty} P_x(t, f)df} \quad 2-37$$

Although the equation (2-36) or (2-37) is useful, the instantaneous frequency is a very controversial term. That is because if instantaneous frequency exist, then the uncertainty principle is violated.

The demonstration of uncertainty principle or Heisenberg principle of quantum mechanics can be found in the literature, and its equivalent to signal analysis as defined by [49, 56]:

$$\Delta t * \Delta f \geq \frac{1}{2} \quad 2-38$$

From equation (2-38), it is absolutely clear that one can not determine time and frequency simultaneously with a desirable precision. In other words if one wishes to have a very good resolution in frequency, one will have a poor time resolution. Conversely if one have an excellent time resolution, it will result in a poor frequency resolution.

Therefore, really the “instantaneous frequency” will not exist because one can not evaluate the exact frequency at an exact time.

The consequences of aforementioned discussion are that the absolute instantaneous time of damage of the structure can not be evaluated. Because we can not preclude the uncertainty principle. This applies for any structure and all structural damage methods. Only the time-window when the damage appears can be estimated.

In this sense when we refer to instantaneous frequency (or instantaneous frequency shift) we are referring to a frequency evaluated in a short time window (but not infinitesimal time window). In the same way, when we refer to an instant time of damage occurrence, we are referring to a short frequency bandwidth when this frequency-shift (damage) happened.

Theoretically, using the instantaneous frequency evaluated by equations (2-19) or (2-36), (2-37), we can estimate the damage and its time of occurrence in all structural system that can be modeled like a SDOF, because the output signal of these structures are

monocomponent mainly. However the noise presence and instability in the IF estimation becomes a difficult procedure, as will be seen in the Chapter 5.

2.3.2 Multicomponent Signals

For multicomponent signals, like output signal of structures with MDOFs, the instantaneous frequency of the signal has a bandwidth. For this reason, the weighted average of the instantaneous frequency is evaluated rather than the instantaneous frequency itself.

The mean instantaneous frequency is defined as [49, 90, 121]:

$$IF(t) = \int_{-\infty}^{+\infty} \left(\frac{d\phi(t)}{dt} \frac{|x(t)|^2}{\int_{-\infty}^{+\infty} |x(t)|^2 dt} \right) dt \quad 2-39$$

The problem with the equation (2-39) is that it refers to a frequency bandwidth, therefore its direct application is limited to structural system with only one dominant mode.

When a MDOFs system have high modal participation factors for secondary modes, the expression (2-39) is useless. In this case we can attempt to isolate individual frequencies, using several approaches such as Frequency Domain Decomposition (FDD) [124] or Empirical Mode Decomposition (EMD) [73], or Instantaneous Frequency Estimators (IFE) [74, 75, 77].

3 OBJECTIVE SELECTION OF BEST-PERFORMANCE TIME-FREQUENCY REPRESENTATION FOR STRUCTURAL DAMAGE DETECTION IN CIVIL ENGINEERING STRUCTURES

In the first part of this Chapter the principal problems with the selection of TFRs is addressed, then a brief review of different approaches for selecting the TFRs is mentioned.

The second part is dedicated to develop a new multi-criteria method for specific selection of TFRs for structural damage detection in civil engineering structures. Finally an example of application of new proposed selector method is presented.

3.1 Problems with Selection of Time-Frequency Representations

The selection of a TFRs is not an easy task, many aspect have to be considered. In addition, the amount of available TFRs in the technical literature is extensive; hundreds of TFRs has been proposed.

The problems associated with selection of a TFRs can be classified in three branches:

- Amount of TFRs already allowed
- Resolution vs Information Loss
- Aspect inherent to structural applications

3.1.1 The Amount of Available TFRs

There are many TFRs available in the technical literature; on a daily base a new type of “theoretically perfect” TFRs is being published.

In addition to this, new techniques for smoothing TFRs being introduced by new sub-groups of “advanced”, “improvement” or “enhanced” TFRs. In wavelets for example frequently new wavelets families are proposed and the dictionaries of waveletes increases constantly.

The structural engineer will be confronted by an immense problem, due to the performance of his system identification or damage detection. At first it is necessary to decide which of the hundreds of TFRs is optimal or adequate for analysis of structure signal output.

In the Figure 3.1, the result of six TFRs of two small tremors recorded in a residential building has been shown.

According to Figure (3-1), which of these TFRs have the best-performance?

As it can be seen, the answer to the previous question begins with subjective criteria, and it is not easy to get a unified and common or unique criteria.

Only a very few TFRs is used, actually the number of available TFRs is greater than one hundred.

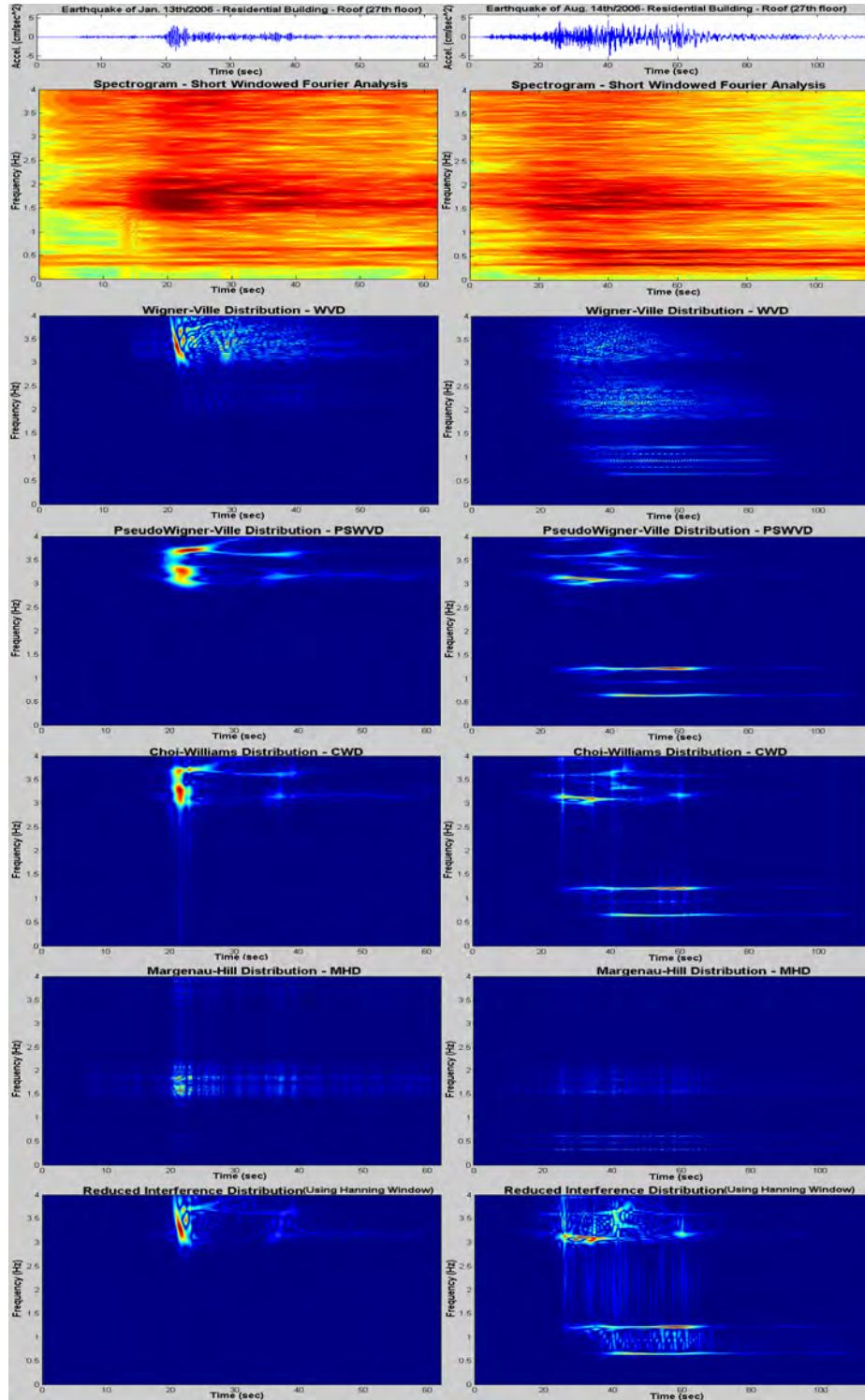


Figure 3-1 Comparison of TFRs of two tremors recorded in a Residential Building

3.1.2 Resolution vs Information Losses

As it has been shown in Chapter 2, the TFRs have the shortcoming due to uncertainty principle, one can not obtain perfect resolution in time and frequency simultaneously, thus if one increases the time resolution the frequency resolution is worst and viceverse.

On the other hand a lot of TFRs, like bilinear or quadratic TFRs, have the presence of so called interference terms.

To remove these interference terms many techniques has been proposed, but in general all of them attempt to smooth the TFRs at the expense of loss information, because when one remove the interference terms (cross-term) one may be removing the signal terms (auto-terms).

Another problem with smoothing process is that detection of small frequency changes or non-stationary events becomes less accurate [67].

New adaptive and optimal kernel design and other techniques of removal interference terms has been proposed [129-135, 137, 138, 145, 170, 178], but at this time, it is not possible to have free interference quadratic distribution without information loss, and the techniques in many cases are signal dependent and do not work in a general sense.

If one sees the previous Figure (3-1) one can see that some of the TFRs appear to have a better performance than others, but their appearance may be deceptive, because important information will be lost in the smoothing process.

In fact, when a specific TFR is selected, for example a subjective visual criteria selection, the problem is far from being over because one will have a new problem: The parameters of

the selected TFR will be taken multiples values, so again one can obtain another group of TFRs.

Let us explain this last problem, by using Fourier inversion in the reference [56], it has been proved that the kernel of the Cohen's general class (equation 2-4) can be obtained by:

$$\phi(\theta, \tau) = \frac{1}{4\pi^2} \frac{\int_{-\infty}^{+\infty} \left[\int_{-\infty}^{+\infty} \left(e^{j\theta t + j\tau f} \int_{-\infty}^{+\infty} \int_{-\infty}^{+\infty} \int_{-\infty}^{+\infty} e^{-j\theta t - j\tau f + j\theta u} x^* \left(u - \frac{1}{2} \tau \right) x \left(u + \frac{1}{2} \tau \right) dud\tau d\theta \right) dt \right] df}{\int_{-\infty}^{+\infty} e^{j\theta u} x^* \left(u - \frac{1}{2} \tau \right) x \left(u + \frac{1}{2} \tau \right) du} \quad 3-1$$

If the kernel function is set to an exponential form such as:

$$\phi(\theta, \tau) = e^{-\frac{\theta^2 \tau^2}{\sigma}} \quad 3-2$$

Replacing the equation (3-2) into general bilinear Cohen's class form (equation 2-4), the Choi-Williams Distribution (CWD) can be obtained [129]:

$$CWD_x(t, f) = \frac{1}{4\pi^{3/2}} \int_{-\infty}^{+\infty} \int_{-\infty}^{+\infty} \sqrt{\frac{\sigma}{\tau^2}} e^{-\frac{\sigma(u-t)^2}{4\tau^2} - j\tau f} x^* \left(u - \frac{1}{2} \tau \right) x \left(u + \frac{1}{2} \tau \right) dud\tau \quad 3-3$$

From equation (3-2) is clear that the smoothing function is dependent of standard deviation coefficient, so if this coefficient changes the distribution will change.

If the value of standard deviation coefficient in equation (3-2) is big the kernel function tends to be one, therefore the CWD of equation (3-3) becomes like the WVD of (equation 2-21), and otherwise the distribution is a WVD with a filtering effect [66, 69].

Therefore which is the optimal CWD ?, The answer is logically signal dependent.

For example in structural engineering applications, the reference [69] suggest that $0.1 \leq \sigma \leq 1.0$ can be taken when low values are recommended for structural linear range and large values are recommended for nonlinear response range. But any way between 0.1 and 1.0 there are infinites values, so there are theoretically infinites CWDs.

In the same way the result obtained using different σ values present great differences in the attenuation of interference terms, and similar results can be obtained for cone-kernel representation, where result are absolutely window length-dependent [171]

As can be seen, there are many TFRs available and for each one of them, a new set of possible TFRs can be obtained.

3.1.3 Aspects Inherent to Structural Applications

The structural responses of civil engineering structures have some particular aspect that is important to take into account.

The definition of structure is too broad, because in the civil engineering field, for example there are micro-structures such as beams or elements in composite studies and huge structures such as dams or similar.

In this work we are referring to typical medium-large civil structures such as buildings, trusses, metallic tower, bridges, tanks, oil platforms, dams and soil instrumented profile (we refer to borehole instrumentation and not to dynamic soil tests in laboratory specimens).

For these typical structures, their vibration signatures have very interesting characteristics, in general the frequency bandwidth is too short, because the principal modes are in the range between 0.1 sec to a few seconds (maybe 5-10 sec for very large buildings or 3-5 sec for very

soft clay soil deposits), therefore the frequency range of interest is between 0.05 and 10-20 Hz.

Note that the frequency bandwidth of response for civil engineering structures is really narrow (10^{-1} Hz to 10^1 Hz) if one compares it with other signal applications, for example in radio the bandwidth is between 3 KHz (3000 Hz) and 300 GHz (300.000.000 Hz), therefore the radio frequency bandwidth is 10^3 Hz to 10^8 Hz.

The short frequency bandwidth imply that may be in structural engineering application the use of logarithmic TFRs is not adequate or at least not strictly necessary and linear frequency scales are enough for many applications.

Another important aspect is the duration of the signal itself, in operation conditions (ambient vibration) the signal is in general very long (from hours to weeks, months and some cases years).

In strong events the duration is relatively short lie from a few minutes or hours in strong wind events, a few dozens of seconds in earthquake strong motions and a few milliseconds in blast, explosions and terrorist attack.

In this way you can separate Time Frequency Analysis (TFA) for civil engineering applications in two main applications:

- a) Applications when the frequencies are semi-constant or its variability in the time is slow (like ambient vibration).
- b) Applications when the frequency change occurring very fast (like strong events)

Using the precedent philosophy, this dissertation separates the applicability of (TFA), because the requirements in one or another case are different. In the first case one generally have a lot of information for system identification and in the second case one have few data for damage detection problem.

On the other hand, the range of the changes in frequency in civil engineering is relatively short, according to several previous studies in ambient vibration conditions a frequency range variation between 0 to 5% is common and for strong motion events and severe damage the change is expected to be no more of 2.5 times the original frequency [114-119].

3.2 Approaches Used to Select TFRs

In Civil Engineering applications to the author best knowledge no work has yet been reported on systematic and objective selection of TFRs. In general, selection of specific TFR has been based on visual criteria or trial-error parameters adjusted to some specific TFR [66, 69, 143, 153].

Even in time-scale analysis (like wavelets) is common in civil engineering applications and damage detection to select the wavelets using general criteria [44].

In other fields, such as speech analysis, imaging process, radar application, radio, automatic face identification, bio-engineering, medical applications, some authors report procedures for selection of TFRs, in the following these approaches will be briefly discussed.

3.2.1 Visual Inspection of TFRs

It is the most common criteria of selections TFRs in all fields. For civil engineering applications, it is almost the only used criteria, some times complemented with optimization iterations of parameters to get a “best-look” TFRs [66, 69].

The visual inspections consist of human inspection (visually comparing plots of the TFRs), in essence are an absolutely subjective criteria, is user-dependent and require the expertise of the person in charge [160].

In visual inspection a common criteria is that the TFRs have a “clean-look”, thus that it does not have much interference terms.

One can try to do a visual inspection procedure, by looking at the previous Figure 3-1, which of these TFRs have the “best-look”?

As it can be seen the answer is personal-dependent, for example regarding the same Figure (3-1) the following observations using visual inspection has been reported in the reference [121], comparing these discussion with your personal observations:

- *“Traditional Signal Analysis TSA (STFT – Spectrogram), has the worst resolution for identification of frequency changes in time.*
- *Wigner-Ville Distribution has good resolution, but the presence of interference terms makes the interpretation difficult. The reassignment version of the Wigner-Ville Distribution has fairly better resolution, and less interference terms.*
- *The Choi-Williams Distribution shows an excellent resolution in time-frequency plane, and shows interference terms only in the frequency band represented by the vertical lines.*
- *Among the distributions studied for damage detection the Margenau-Hill Distribution has the worst resolution. The presence of many interference terms in frequency and time is evident.*

- *The Reduced Interference Distribution has a good time-frequency resolution, but some interference terms appear in both, time and frequency.*
- *For all distributions it is noticeable that when the signal is more disperse then the presence of interference terms in time-frequency distribution increase.” [121]*

3.2.2 Measure of the TFRs Concentration and Resolution

In general, the measures of the TFRs concentration attempt to give a numerical estimate value of the quality TFR based on energy concentration around the frequency signal.

This type of measure can be divided into norm-base and non-norm-base measures, several measures norm-based has been proposed in the literature [95-102], here only we will refer to an interesting measure proposed in the reference [157], because its optimization procedure is taken into account the proposed multicriteria selection procedure.

According to reference [157] to obtain an optimal and adaptive TFR, it is necessary to maximize the following measure:

$$C_x(t, p) = \frac{\int_{-\infty}^{+\infty} \int_{-\infty}^{+\infty} |D_p(\tau, \Omega) w(\tau - t)|^4 d\tau d\Omega}{\left(\int_{-\infty}^{+\infty} \int_{-\infty}^{+\infty} |D_p(\tau, \Omega) w(\tau - t)|^2 d\tau d\Omega \right)^2} \quad 3-4$$

Where:

D_p : Is a TFR with a single parameter p select (i.e. in Choi-Williams Distribution (equation 3-3), the standard deviation value is optimized.

w : Is an one dimensional window function.

Therefore C_x can be taken like a measure for a TFR and one single parameter p , this decisive factor is employed in reference [157] for optimization of several TFRs like STFT, CWD, WVD and wavelets representation.

In a set of recently published papers Sucic and Boashash [159-163], have developed a measure of concentration and resolution for TFRs. The proposed normalized instantaneous resolution measure is evaluated using [159, 162]:

$$P_i(t) = 1 - \frac{1}{3} \left(\frac{A_s(t)}{A_M(t)} + \frac{1}{2} \frac{A_x(t)}{A_M(t)} + (1 - D(t)) \right) \quad 3-5$$

$$0 < P_i(t) < 1$$

where:

$P_i(t)$: Resolution Performance Measure,

$A_s(t), A_x(t)$: Is the magnitudes of sidelobe of auto and cross-term respectively,

$A_m(t)$: Magnitude of the mainlobe, and

$D(t)$: Component separation measure.

This resolution measure proposed by Sucic and Boashash [162] is incorporated in our multicriteria measure proposal and we will refer in detail to it in the next section.

3.3 Relevant Topics for Multicriteria Method

In the previous sections the special characteristics of signal obtained from Civil Engineering structures has been discussed. The main problems in selecting a TFRs has also been pointed out and it has been mentioned that for a specific case of civil engineering applications do not exist a precedent in a systematic and objective procedure for selection of TFRs.

In order to get an objective multicriteria measure of the best TFRs performance, any visual inspection can not be used; therefore its use in the proposed method is avoided.

In this section a new scheme for objective selection of TFRs for structural applications will be proposed. The proposal is based on the special characteristic of structural signals, strengths, and weakness of general measurements reviewed in section 3.2.

3.3.1 The Philosophy of Proposed Multicriteria Performance Measure of the TFRs

3.3.1.1 Desirable Mathematical Properties

Although the methods of the previous section have many strengths, none have taken into account the desirable mathematical properties that an ideal TFR should have and that has been discussed in the section 2.2.3. These properties are important in civil engineering applications.

In order to do this, here for each TFR according to the desirable mathematical properties that it satisfies a qualification is assigned.

3.3.1.2 Structural Behavior Performance

The frequency laws of signal obtained from structures submitted to strong event have particular behavior. In general notorious frequency shift (almost always for low frequency side) is noted and reported, as it has been mentioned in previous chapters. In cases when one have additional device (like in semi-controlled or controlled structures) one can get notorious shift for high values.

On the other hand, the characteristics damage that impulsive waves cause in the structures (like damage for shear, flexural, or shear-flexural behavior), produce in general like-pulse (shear damage) or like exponential frequency laws (flexural damage).

The damping in vibration process of civil structures is important, over all when it is submitted to strong event, in which case the damping increases, for this reason during and when the external excitation disappear or becomes less, the structure is in free vibration and the response signal have a decay exponential form, this is especially true for earthquake motions.

For this reason, TFRs that perform best under the cone-shape signals and have good performances under short like pulse and exponential decay frequency laws will be selected for civil engineering applications. Therefore, a namely TFR structural behavior performance criteria to the multicriteria TFRs measure has been added.

3.3.1.3 Resolution and Concentration Measure

The resolution and concentration of TFRs is strongly important, therefore it is proposed to incorporate in the multicriteria measure the method proposed by Boashash and Sucic [162]. It was modified in the optimization procedure according to equation (3-4) proposed in the reference [157].

3.3.1.4 Information and Complexity Measure

It has been mentioned that there is a compromise between a free-interference term TFRs and the loss of the information.

Also it has been mentioned that one of the most popular method for selecting a TFR is a visual inspection, there exist a strong link between Renyi entropy measure and visually based

on notion of complexity [175]. Thus it is possible to have an objective selection of TFR using a measure of information and complexity.

For this reason and in order to have into account that important information of the signal is not lost forever in the smoothing process, the Renyi information measure proposed in the references [95] will be used as another useful criteria.

3.4 Proposed Multicriteria Method

According to previous section a weighting multicriteria performace measure for structural civil engineering applications using the following expression will be proposed:

$$\begin{aligned}
 SMQ &= \sum_{i=1}^n W_i EF_i \\
 0 < SMQ &\leq 1 \\
 \sum_{i=1}^n W_i &= 1 \\
 W_i &\geq 0 \\
 EF_i &\leq 1
 \end{aligned}
 \tag{3-6}$$

where:

SMQ : Structural Multicriteria Quality factor for the TFR,

W_i : Weighting factor,

EF_i : Evaluation Factor, and

As it has been described the Evaluation factors (EF_i) are:

- Desirable Mathematical Properties (DMP)
- Performance in typical signal analysis for structures, namely here Structural Performance Indicator (SPI).
- Resolution and Concentration Measure (RCM) [162]
- Information Measure (IM) [95]

Therefore the Structural Multicriteria Quality factor for a TFR can be evaluated using:

$$SMQ = \sum_{i=1}^n W_i EF_i \quad 3-7$$
$$SMQ = W_1 * DMP + W_2 * SPI + W_3 * RCM + W_4 * IM$$

The best-performance TFR is those that have the largest SMQ value.

In the following sections the procedure for obtaining the require parameters for evaluating equation 3-7 will be explained.

3.4.1 Weighting Factors (W_i)

There is not a unique way for determining the importance of the several EF_i , so there is not a consensus about of weighting factors, because it is not mathematically obtainable.

But in fact due to a free-user decision in an objective sense, all factors are taken equal to 0.25. This means a 25% of importance of the factor in the selection procedure of TFRs.

However the engineer can argue that for a particular case the values of W_i will change, regardless of any arguments or selected values for W_i , the sum of weigthing factor always is equal to one, according to equation 3-6.

In the Table 3.1, the recommended weighting factors are shown:

TABLE 3.1 Parameter values for the Structural Multicriteria Quality Measure of Time-Frequency Representation

Evaluation Factor (EF _i)	W _i (Recommended Range)
Mathematical Desirable Properties	0 - 0.25
Structural Performance Indicator (SPI)	0 - 0.4
Resolution and Concentration Measure [162, 157] (RCM)	0 - 0.4
Information Loss Information Measure [95] (IM)	0 - 0.25
	$\sum_{i=1}^4 W_i = 1.0 \quad ; \quad W_i \geq 0$

3.4.2 Evaluation Factors (EF_i)

As it can be seen, the proposed multicriteria method for objective selection of TFRs for Earthquake Engineering and Civil Engineering (EE-CE) applications consider four criteria. The first two are specifically oriented to EE-CE, while the last two has been proposed previously in the literature for general applications.

The first criteria identify and quantify the desirable mathematical properties of TFRs relevant to EE-CE applications.

The second criteria namely Structural Performance Indicator is taking into an account the impulsive waves from strong motion records from structures that produce a signal that have a combination of pulse like (shear damage) and exponential frequency laws like characteristics flexural damage, and also the damping of the structure produces a decay exponential form of the signal.

In addition, two qualifications previously proposed for general applications has been taken into account. The first one is the Resolution Measure Criteria proposed by Boashash and Sucic [162] with an adaptive optimization scheme based on the proposal of Jones and Barakiuk [157].

The Renyi-norm proposed by Sang and William [95] is included in the multicriteria method as the fourth criteria; it takes into account the information loss during smoothing process.

3.4.2.1 Desirable Mathematical Properties

As it has been explained in the section 2.2.3 there exist a few mathematical properties that a best-performance TFR have to comply with, and it has been explained in detail in the aforementioned section.

Therefore it was proposed to assign high EF to those TFR that fulfill the mathematical properties described in section 2.2.3

In a specific case the analyst may be required to change the weighting EF factors proposed here, but in an objective sense an equal factor for all properties will be used.

In the Table 3.1, the recommended weighting factors for each mathematical property are shown:

TABLE 3.2 Quality Mathematical Factors

Mathematical Property that TFR fulfill	Simplify Expression	Quality factor
Linearity (P ₁)	$x(t) = (k_i x_i(t))$ $\Rightarrow P_x(t, f) = \sum_{i=1}^n (k_i P_{x_i}(t, f))$	0.1-0.3
Multiplication (P ₂)	$x(t) = x_1(t)x_2(t)$ $\Rightarrow P_x(t, f) = \int_{-\infty}^{+\infty} P_{x_1}(t, f-f')P_{x_2}(t, f')df'$	0.05-0.2
Convolution (P ₃)	$x(t) = \int_{-\infty}^{\infty} x_1(t-t')x_2(t')dt'$ $\Rightarrow P_x(t, f) = \int_{-\infty}^{+\infty} P_{x_1}(t-t', f)P_{x_2}(t', f)dt'$	0.1-0.3
Real Valued (P ₄)	$P_x^*(t, f) = P_x(t, f)$	0.1-0.3
Time-Shift (P ₅)	$x_1(t) = x(t-t_0)$ $\Rightarrow P_{x_1}(t, f) = P_x(t-t_0, f)$	0.1-0.2
Frequency-Shift (P ₆)	$x_1(t) = x(t)e^{j2\pi f_0 t}$ $\Rightarrow P_{x_1}(t, f) = P_x(t, f-f_0)$	0.1-0.2
Time-Marginal (P ₇)	$\int_{-\infty}^{+\infty} P_x(t, f)df = x(t) ^2$	0.1-0.3
Frequency Marginal (P ₈)	$\int_{-\infty}^{+\infty} P_x(t, f)dt = X(f) ^2$	0.1-0.3
Instantaneous Frequency (P ₉)	$IF_x(t) = f_x(t) = \frac{\int_{-\infty}^{+\infty} fP_x(t, f)df}{\int_{-\infty}^{+\infty} P_x(t, f)df}$	0.1-0.35
Group Delay (P ₁₀)	$GD_x(f) = t_x(f) = \frac{\int_{-\infty}^{+\infty} tP_x(t, f)dt}{\int_{-\infty}^{+\infty} P_x(t, f)dt}$	0.1-0.2
		$\sum_{i=1}^{10} Q_i = 1.0$ $Q_i \geq 0$

Therefore, to qualify a specific TFR with respect to desirable mathematical properties is necessary to identify which of these properties it will fulfill. The quality factor can be assigned according to a specific application; in order to have a user-free assignment an equal value of 0.1 can be applied.

Again, regardless of any argument or selected values for quality factor (Q_{fi}), the sum of weighting factor always is equal to one, according to equation 3-6.

In the following Table, the mathematical property values for some quadratic TFRs are shown, in this case a quality factor of 0.1 are assigned for all properties presented in Table (3.2).

TABLE 3.3 Mathematical Properties values for some Quadratic TFRs

TFR	Mathematical Property										$\sum_{i=1}^{10}$
	P ₁	P ₂	P ₃	P ₄	P ₅	P ₆	P ₇	P ₈	P ₉	P ₁₀	
Born-Jordan	×	×	×	✓	✓	✓	✓	✓	✓	✓	0.7
Zhao-Atlas-Marks	×	×	×	✓	✓	✓	✓	✓	✓	✓	0.7
Choi-Williams	×	×	×	✓	✓	✓	✓	✓	✓	✓	0.7
Margenau-Hill	✓	×	✓	×	✓	✓	✓	✓	×	×	0.6
Rihaczek	✓	×	✓	×	✓	✓	✓	✓	×	×	0.6
Levin	×	✓	×	✓	✓	✓	✓	✓	×	×	0.6
Wigner-Ville Distribution	×	✓	✓	✓	✓	✓	✓	✓	✓	✓	0.9
Pseudo-Wigner-Ville	×	✓	✓	✓	✓	✓	×	×	✓	✓	0.7
Spectrogram	×	×	×	✓	✓	✓	×	×	×	×	0.3
sinc	×	✓	×	✓	✓	✓	✓	✓	×	×	0.6

The specific mathematical properties of other TFRs can be found in the technical literature, the interested reader can review the following references [49, 55-57, 65, 66, 96-98, 100, 102, 129-132, 139, 141, 145, 166, 167, 171, 185, 224].

3.4.2.2 Structural Performance Indicator

In order to take into account the specific-signal characteristics of signal obtained from structures, the structural performance indicator evaluates the behavior of each TFR for two types of signal:

- Ambient Vibration
- Strong Event.

The Structural Performance Indicator for a TFR is obtained using:

$$SPI_{TFR} = 1 - (c_1 * AVP_{TFR} + c_2 * SEP_{TFR}) \quad 3-8$$

where:

AVP_{TFR} : Ambient Vibration Performance of TFR

SEP_{TFR} : Strong Event Performance of TFR

c_1, c_2 : Weighting factors for AVP and SEP , suggest values $c_1 = 0.3, c_2 = 0.7$

In ambient vibration conditions the frequency changes in general and becomes smooth (very smooth in sense), the SNR is low and the duration is long.

In this context, the best qualification is obtained for those TFRs that identified better the structural frequencies in a high noise signal, using only the principal values of the time-frequency map.

To evaluate the ambient vibration performance (AVP) of one particular TFR, we select multicomponent synthetical signals contained k number of frequencies using:

$$x(t) = \sum_{i=1}^k (A_i \cos(2\pi f_i t)) + n(t) \quad 3-9$$

where:

A_i : Constant amplitude for frequency f_i

f_i : Frequency (Hz)

$n(t)$: Gaussian noise added

k : Number of the frequencies in the signal

In each signal test k frequencies are included, and the constant amplitude is controlled to have a $\text{SNR} \lll 1$.

The *AVP* qualification procedure starts by applying a sort to the time-frequency map and selecting the first k th maximum values (of the time-frequency map).

Because the theoretical frequency values are constant in time, it can evaluate a time qualify factor for each k^{th} frequency value using:

$$f_{TFRke}(t) = \frac{|f_T - f_{TFR}(t)|}{f_T} \quad 3-10$$

Where:

$f_{TFRke}(t)$: Instantaneous frequency error in decimal form

f_T : Theoretical frequency

$f_{TFR}(t)$: Frequency value for time instant 't' obtained from TFR map

It is known that $f_e(t)$ can get extreme variations therefore it is not desirable to qualify a TFR according to these extreme values (min or max) and we attempt to obtain a medium performance of TFRs for each frequency using:

$$f_{i_{mAVTFR_e}} = \frac{\sum_{i=1}^N f_{TFR_{ke}}(t)}{N} \quad 3-11$$

Where:

$f_{i_{mAVTFR_e}}$: Mean Ambient Vibration instantaneous frequency error in decimal form for frequency i

N : Number of signals samplings

Finally, the mean global frequency error detection for a specific TFR in Ambient Vibration conditions is evaluated using:

$$\bar{f}_{TFR_{AV_e}} = \frac{\sum_{i=1}^k f_{i_{mAVTFR_e}}}{k} \quad 3-12$$

Where:

$\bar{f}_{TFR_{AV_e}}$: Mean global frequency error detection for a specific TFR in Ambient Vibration conditions

The TFR qualification to ambient vibration conditions is then evaluated using:

$$AVP_{TFR} = \bar{f}_{TFR_{AV_e}} \quad 3-13$$

The second part of Structural Performance Indicator, is the assessments of the TFR performance to deal with strong event, this is called:

SEP_{TFR} : Strong Event Performance of TFR

For strong event, the signals obtained from earthquake and wind response of structures are chosen, for this a real base data signal for the response of structures to several events is

selected and used in order to classify the signals in the following groups according to frequency laws obtained from its TFRs:

- Linear Response (without frequency changes)
- Linear Response and then linear stiffness degradation
- Linear Response and then exponential stiffness degradation
- Linear Response, instantaneous stiffness loss and then linear stiffness degradation
- Linear Response, instantaneous stiffness loss and then exponential stiffness degradation
- Linear Response, and then exponential stiffness degradation and instantaneous stiffness loss and then exponential stiffness degradation or linear degradation
- Any precedent behavior and some frequency recovery until the end of signal

Because the first type of signals (Linear response without frequency changes) is included in all types (in its initial segment) and evaluated in the ambient vibration conditions, only the other types of signal are considered for typical structural response.

For modeling these types of signals piecewise monocomponent signals with the following characteristics is chosen:

- The first interval with variable amplitude (increase), and constant frequency
- The second interval with randomly variable amplitude and frequency decreasing according to a linear or exponential frequency law
- The final interval with constant frequency and decreasing amplitude, in some cases to simulate a system stiffness recovery we can use a linear increasing frequency law.
- A combination of any previous behavior and sudden stiffness loss at any time

These types of signals are not only presented in mechanical or structural system, but a lot of natural phenomena's like biological signals can be represented by similar models [169].

Some signals with similar characteristic have been defined in the references [79, 169] using a similar notation as the references for the signals. It can be defined as the following general form:

$$x(t) = \left\{ \begin{array}{ll} A(t) \cos(2\pi f_0 t) & \text{if } 0 \leq t < t_1 \quad ; \quad A(t) = A_0 e^{\frac{a_1 t}{2}} \\ A(t) \cos(2\pi f_0 e^{-b_1 t}) & \text{if } t_1 \leq t < t_2 \quad ; \quad A(t) \text{ with } p(A(t)) = \frac{1}{\sqrt{2\pi}} \int_{-\infty}^{A(t)} e^{-\frac{\xi^2}{2}} d\xi \\ A(t) \cos(2\pi f_0 e^{-b_2 t}) & \text{if } t_2 \leq t \quad ; \quad A(t) = A_0 e^{-\frac{a_2 t}{2}} \end{array} \right\} \quad 3-14$$

$$x(t) = x(t) + n(t)$$

Where:

$x(t)$: Time history (Acceleration, velocity or displacement)

$A(t)$: Amplitude like time function

f_0 : Initial structural frequency (Hz)

a_i, b_i : Parameters greater than zero to control the time variable rate of amplitude or frequency, respectively

t_i : Time instant when a change in amplitude and/or frequency begin or end

$n(t)$: Gaussian noise added.

Therefore, by changing the parameters it is possible to find many signals with desirable structural response appearance. In fact, it is possible to obtain an approximate spectrum form (i.e. for example the spectrum form proposed in the reference [143]), only by adjusting the parameters of the equation 3-14. The amplitude and frequency can be controlled.

In the following plots, typical examples of aforementioned structural signals and the approximate general frequency law obtained from its TFRs are shown, using a Reduced Interference Distribution with Bessel Window [123].

In the graphs the amplitude of time history are any acceleration, velocity or displacement units and for facility interpretation the sampling rate is set to 1 Hz, and the time scale is set to counts units (one can use sec, millisecond or any time unit).

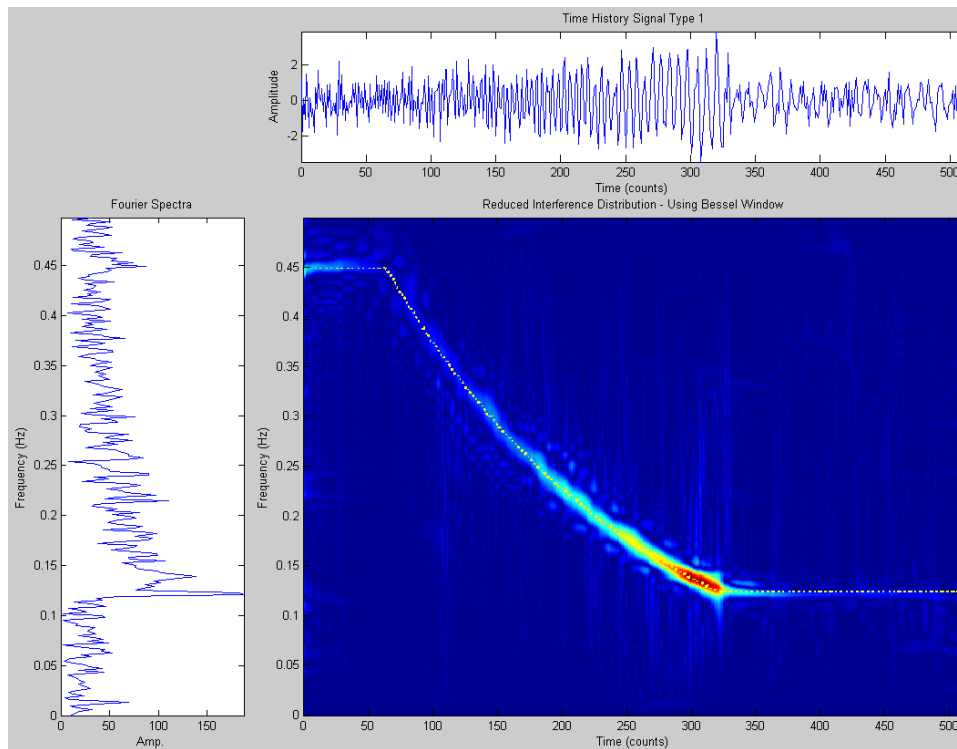


Figure 3-2 Reduced Interference Distribution for a Typical Structural Signal # 1

In the Figure 3-2 a linear response interval, between 0-64 counts with a constant frequency of 0.45 Hz can be seen. The system have a stiffness loss between 64 and 330 counts and in the same interval a shifting in frequency has happened with an exponentially decay frequency. At the end of the signal the structural frequency becomes constant to 0.12 Hz.

The next example is a structure with an instantaneous shift in frequency (may be associated with shear damage):

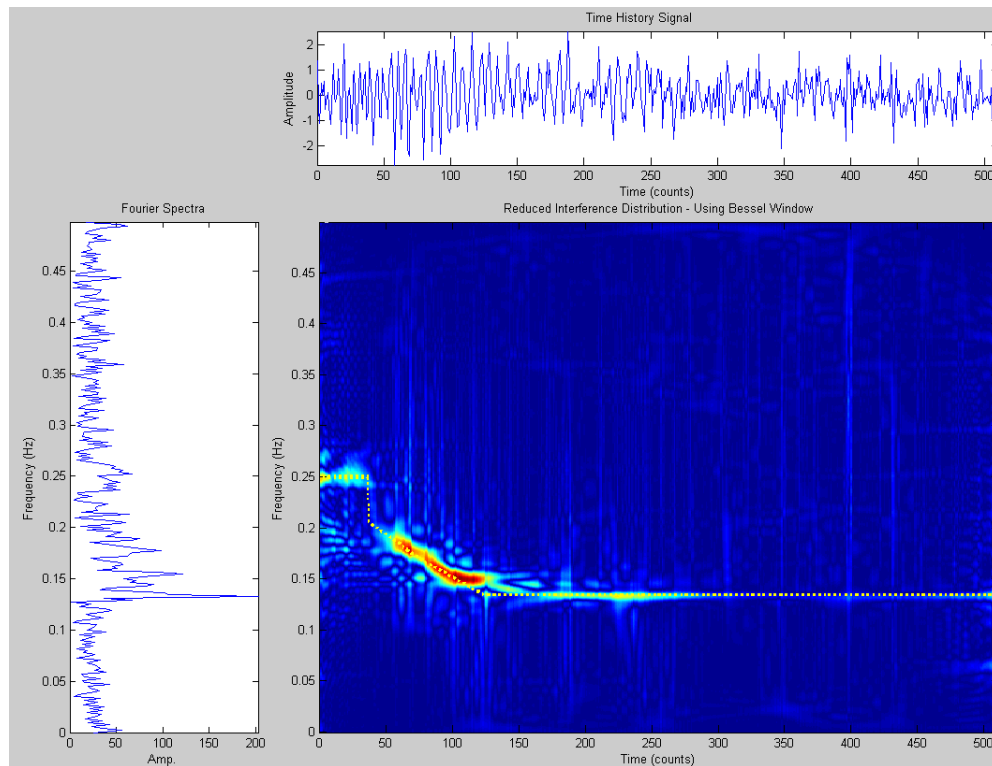


Figure 3-3 Reduced Interference Distribution for a Typical Structural Signal # 2

Analyzing the TFR plot, it is possible to deduce that the initial structural frequency is 0.25 Hz and at a time of 40 counts the structure have a sudden frequency shift (stiffness loss) to 0.2 Hz and then have a linear constant frequency shift to 0.13 Hz (linear stiffness loss), the final frequency of the system is 0.13 Hz.

From the figures 3-2, 3-3, note that by using only time analysis (upside of the plots) or traditional Fourier Analysis (left side of the plots) is practically impossible to get behavior of the structure along the time, and for a system with dynamic properties changing with time the natural choice is to analyze it using joint time-frequency.

According to the previous signal form, several general syntectic signals can be designed and use for testing the structural performance of TFRs. The basic criteria are evaluating each specific signal in the following form:

$$f_e(t) = \frac{|f_T(t) - f_{TFR}(t)|}{f_T(t)} \quad 3-15$$

Where:

$f_e(t)$: Instantaneous frequency error

$f_T(t)$: Theoretical frequency obtained the instantaneous frequency law from eq. 3-13

$f_{TFR}(t)$: Frequency value obtained from TFR map

As before, in ambient vibration case, $f_e(t)$ can get extreme variations and it is not desirable to qualify a TFR according to this extreme values (min or max) and we attempt to obtain a medium performance of TFRs using:

$$f_{i_{mTFRSEe}} = \frac{\sum_{i=1}^N f_e(t)}{N} \quad 3-16$$

Where:

$f_{i_{mTFRSEe}}$: Mean instantaneous frequency error for a signal type of Strong Event in decimal form for each frequency

N : Number of signal samplings

The procedure is to repeat for each of type signals for Strong Event and finally the mean global frequency error detection for a specific TFR is evaluated using all typical signals :

$$\bar{f}_{TFRSE_e} = \frac{\sum_{i=1}^k f_{i_{mTFRSE_e}}}{k} \quad 3-17$$

Where:

$f_{i_{mTFRSE_e}}$: Mean instantaneous frequency error in decimal form to frequency i

k : Number of Strong Event typical signals

The TFR qualification for Strong Events is then evaluated for a specific TFR using:

$$SEP_{TFR} = \bar{f}_{TFRSE_e} \quad 3-18$$

Once the qualification factor for Ambient Vibration Performance (*AVP*) and Strong Events Performance (*SEP*) has been obtained, the Structural Performance Indicator for a TFR is evaluated using the equation 3-8

3.4.2.3 Resolution and Concentration

According to the philosophy (see 3.3.1), it is necessary to evaluate the resolution of TFRs, in a sense that qualificator factor is signal dependent.

Note that the previous two criterias are of specific structural application and in general it means that it is necessary to apply once for all types of TFRs, because the results are not signal dependent.

On the contrary the present criteria is signal dependent, it means that if you have a new signal is necessary to perform the qualification process again and it might be a time-consuming procedure.

The method proposed by Boashash and Susic [159, 162] is used here to evaluate signal dependent criteria for resolution and concentration.

The theoretical background of the method and its practical applications have been presented by the original authors in several technical publications (see references [158-163]). Therefore only the general methodology necessary to obtain the resolution performance measure is shown.

For clarity the equation (3-5) is repeated :

$$P_i(t) = 1 - \frac{1}{3} \left(\frac{A_s(t)}{A_M(t)} + \frac{1}{2} \frac{A_x(t)}{A_M(t)} + (1 - D(t)) \right) \quad 3-19$$

$$0 < P_i(t) < 1$$

Where:

$P_i(t)$: Resolution Performance Measure

$A_s(t), A_x(t)$: Is the magnitudes of sidelobe of auto and cross-term respectively.

$A_M(t)$: Magnitude of the mainlobe.

$D(t)$: Component separation measure.

According to Boashash and Susic [159, 162], for each instant 't' the parameters of the equation 3-19 are obtained from the following graph:

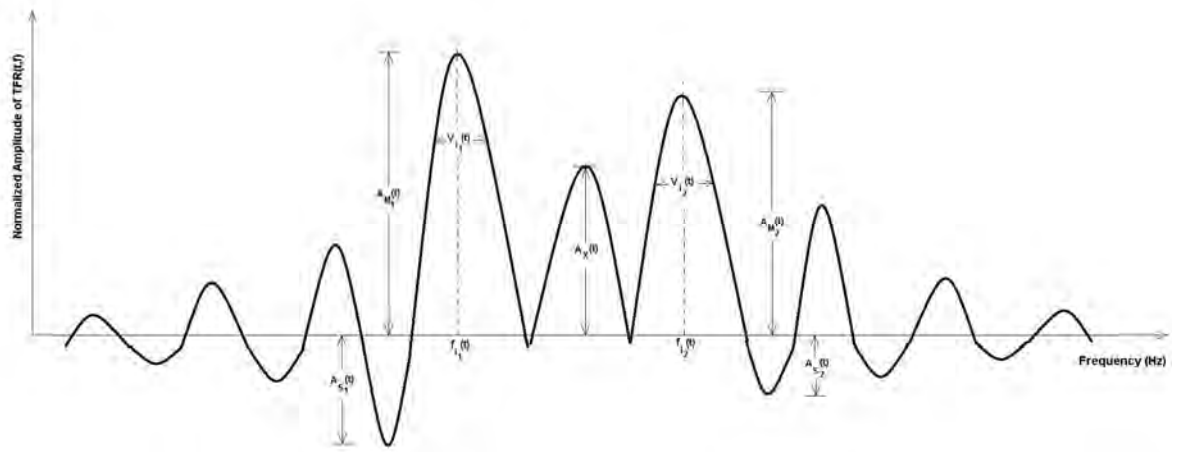


Figure 3-4 Parameters to Measure Concentration and Resolution for TFRs according to Boashash and Susic [159, 162]

From the geometry of Figure 3-4 and using the following expression the parameters to evaluate the Resolution Performance Measure by means of equation 3-19 can be obtained:

$$\begin{aligned}
 A_s(t) &= \frac{A_{s_1}(t) + A_{s_2}(t)}{2} \\
 A_M(t) &= \frac{A_{M_1}(t) + A_{M_2}(t)}{2} \\
 D(t) &= \frac{\left(f_{i_2}(t) - \frac{V_{i_2}(t)}{2} \right) - \left(f_{i_1}(t) - \frac{V_{i_1}(t)}{2} \right)}{2}
 \end{aligned} \tag{3-20}$$

Where:

$A_s(t), A_x(t)$: Is the magnitudes of sidelobe of auto and cross-term respectively.

$A_M(t)$: Magnitude of the mainlobe.

$D(t)$: Component separation measure.

$V_{i_1}(t), V_{i_2}(t)$: bandwidth of the mainlobes, taken to a high of $\frac{\sqrt{2}}{2} A_{M_1}$ and

$\frac{\sqrt{2}}{2} A_{M_2}$ respectively.

A systematic procedure to perform the evaluation of parameters of equation 3-20 has been reported in the reference [160].

Although the expression (3-20) is derived for two main frequencies only, in the reference [161] has been reported the procedure to extend the same principle for a signal with more than two frequencies.

According to reference cited for each TFR a α parameter (i.e. σ value for Choi-William Distribution) can be selected for evaluating the $P_i(t)$ resolution measure. Then the $P_i(t)$ overall (mean of $P_i(t)$ for all times) for this parameter can be evaluated. The precedent procedure is repeated for all possible parameters. Therefore, the optimum α value for this TFR can be obtained.

The above procedure is shown in Figure 3-5, finally the TFR with best resolution is the one that have the maximum $P_i(t)$ overall.

The previous procedure requires a lot of computations because the α 's optimization is very slow. Furthermore, the optimal value for α is not constant in general, and it is time-dependent. For this reason a time-dependent scheme for optimization of TFR is been proposed. This scheme is called in signal analysis a time-frequency adaptive representation.

There are many ways to get an adaptive TFR, according to Figure 2-7, the signal adaptive TFR proposed by Jones and Baraniuk [157] is chosen, because it is powerful and its implementation is not computing demanding.

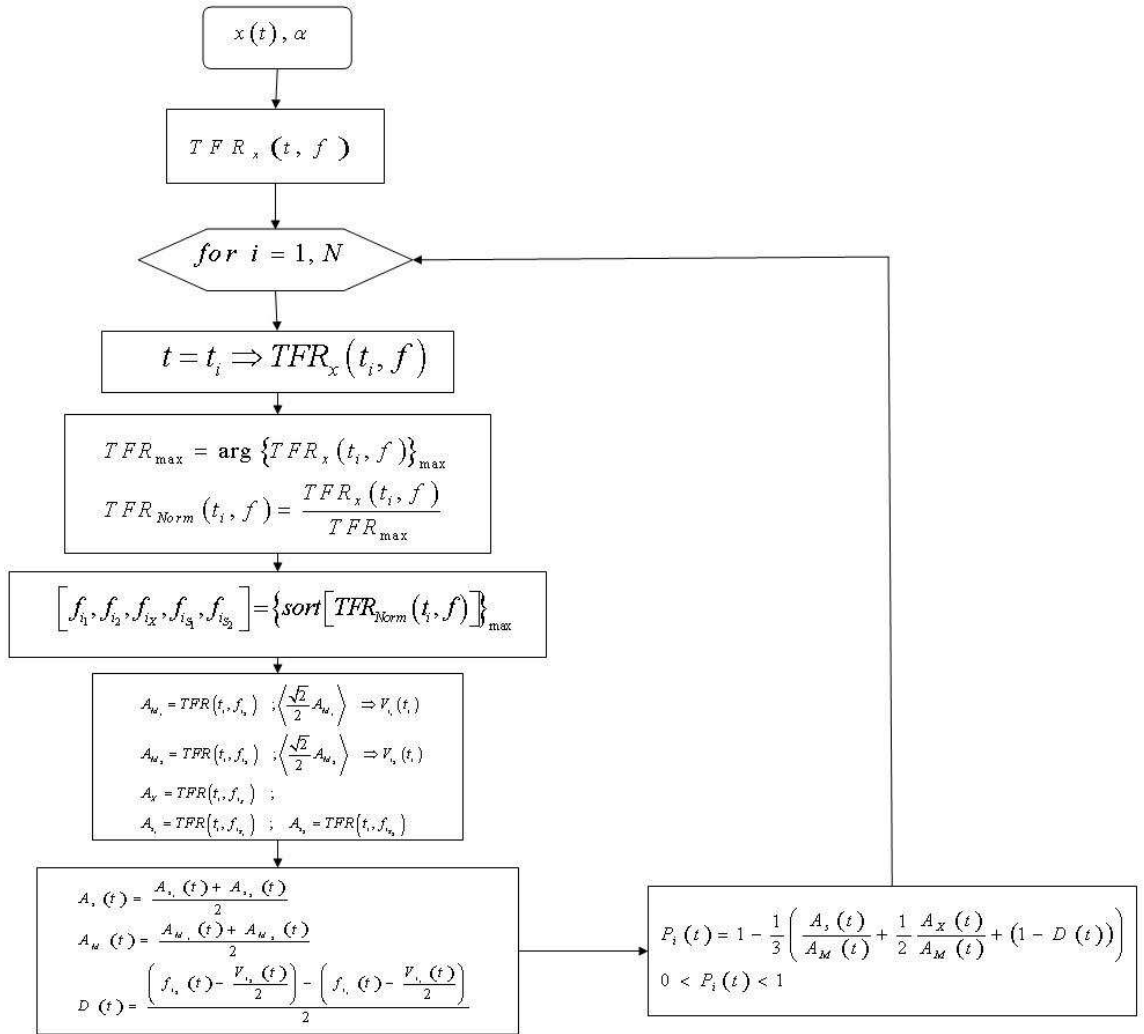


Figure 3-5 Flow Chart to Measure Concentration and Resolution of TFRs According to Boashash and Sucic [160]

As it has been mentioned earlier, according to reference [157] to obtain an optimal and adaptive TFR, it is necessary to maximize the following measure:

$$C_x(t, p) = \frac{\int_{-\infty}^{+\infty} \int_{-\infty}^{+\infty} |D_p(\tau, \Omega) w(\tau - t)|^4 d\tau d\Omega}{\left(\int_{-\infty}^{+\infty} \int_{-\infty}^{+\infty} |D_p(\tau, \Omega) w(\tau - t)|^2 d\tau d\Omega \right)^2}$$

3-21

where:

Dp : Is a TFR with a single parameter p selected (i.e. in Choi-Williams Distribution (equation 3-3), The standard deviation value σ is optimized. w : Is one dimensional window function.

Therefore, to apply the procedure shown in Figure 3-5 first the optimization procedure (thus calculated the adaptive TFR using Jones and Baraniuk[157]) is done for evaluating to “N” instant time the $P_i(t)$ value, and then evaluate the $P_i(t)$ overall for each TFR using:

$$P_{TFR_{overall}} = \frac{\sum_{i=1}^N P_i(t_i)}{N} \quad 3-22$$

The Resolution and Concentration Measure (RCM) is evaluated for each TFR using the equation 3-22, consequently the RCM for equation 3-7 is obtained for each TFR using:

$$RCM = P_{TFR_{overall}} \quad 3-23$$

3.4.2.4 Information Measure (IM):

An important thing in the selection of a best-performance TFR is to take into account the complexity of the TFR and its information content.

In this regard and in a rough sense complexity is linked with the diffuse or visual clarity of a TFR and the capacity of the TFR to concentrate the energy around the fundamental frequencies. As a result an optimal TFR would be less complex (i.e. a best look-like).

In this way traditionally a user-dependent procedure has been applied, because this criteria in general is indirectly accomplished using visual inspection.

In order to avoid the subjective user intervention in the process, some researchers have proposed a few measure of the information content and complexity based mainly on information theory techniques like entropy measures (i.e. Shannon entropy and Renyi entropy) and divergence techniques like Kullback-Leibler divergence, Renyi divergence, Jensen-Shannon divergence and Jensen-Renyi divergence, adapted to time-frequency analysis [176].

A measure the joint information content and complexity simultaneously is the entropy, according to literature the entropy is: “A *measure of the absence of information about a situation, or, equivalently, the uncertainty associate with the nature of a situation*” [174]

In information theory a classical functional to express the entropy is the Shannon entropy, this functional can be represented to time-frequency analysis using [177] :

$$H(P_x) = - \int_{-\infty}^{+\infty} \int_{-\infty}^{+\infty} P_x(t, f) \log_2(P_x(t, f)) dt df \quad 3-24$$

where:

$H(P_x)$: Shannon Entropy to P_x

$P(t, f)$: Time-Frequency Representation of signal $x(t)$

As it has been mentioned earlier, the negative values can appear inside the time-frequency plane, for this reason the Shannon entropy measure (eq. 3-24) can not be used directly, unless that strictly positive TFR is used, like reported in the references [139-141, 144]

To avoid this limitation, the Renyi entropy has been proposed by several researchers like a measure of complexity and information of the TFRs [95, 175-178], a complete description and analytic derivation of Renyi entropy for information theory and probability theory can be found in the appendix of the reference [179].

In time-frequency analysis, the Renyi k^{th} order entropy can be defined by [176]

$$R_{\alpha}(P_x) = \frac{1}{1-\alpha} \log_2 \int_{-\infty}^{+\infty} \int_{-\infty}^{+\infty} P_{N_x}^{\alpha}(t, f) dt df \quad 3-25$$

Where:

$R_{\alpha}(P_x)$: Renyi k^{th} order entropy

α : Order of Renyi entropy, $\alpha \geq 1$

$P_{N_x}(t, f)$: Normalized time frequency representation of $x(t)$ evaluated using:

$$P_{N_x}(t, f) = \frac{P(t, f)}{\int_{-\infty}^{+\infty} \int_{-\infty}^{+\infty} P(t, f) dt df} \quad 3-26$$

Considering a low value for Renyi entropy is indicative of TFR good performance and vice versa, because all Renyi values for each type of TFR has been normalized and it is comparable with each other.

An important aspect to be defined is, what is the k^{th} order of the Renyi to be used ?, In this sense $\alpha = 1$ produced the Shannon entropy measure [178, 180] and it can not be used.

Although some researchers have used the quadratic Renyi entropy (i.e. $\alpha = 2$) [178, 181, 182], it has been demonstrated that the minimum optimal value for well-defined yield for information measure is $\alpha = 3$ [175, 178], so in the proposed method the third order Renyi entropy (\mathbf{R}_3) will be used .

For discrete case the Renyi third order entropy defined by Sang and Williams [95] is adopted:

$$R_3(P_x(t, f)) = \frac{1}{2} \log_2 \left(\sum_{l=-L}^L \sum_{k=-K}^K (P_{N_x}(l, k))^3 \right) \quad 3-27$$

The normalized P_{N_x} distribution can be obtained with respect to energy of TFR [95]:

$$P_{N_x}(t, f) = \frac{P_x(t, f)}{\sum_{l=-L}^L \sum_{k=-K}^K (P_{N_x}(l, k))} \quad 3-28$$

Or with respect to volume of TFR, using [95]:

$$P_{N_x}(t, f) = \frac{P_x(t, f)}{\sum_{l=-L}^L \sum_{k=-K}^K |(P_{N_x}(l, k))|} \quad 3-29$$

The information bounds for discrete random signals of the Renyi entropy (R_3) can be obtained by means of:

Upper Bound [183]:

$$E[R_3(P_x(t, f))] < \log_2((2N+1)(2K+1)) \quad 3-30$$

Lower Bound [183]:

$$E[R_3(P_x(t, f))] \geq \frac{1}{2} \log_2 \left(\frac{4\pi^2 (2K+1)^2 (2N+1)^2}{3 \sum_n \sum_{\tau=-2N}^N |\Psi(n, \tau)|^2 + 4\pi^2 (2N+1)^2 + 2} - \frac{3}{2(\ln 2)(2N+1)} - \frac{1}{2(\ln 2)(2N+1)^2} \right) \quad 3-31$$

where in the equations 3-30 and 3-31 :

$E[\cdot]$: Expectation for R_3

$2N+1$: Number of time points

$2K+1$: Number of frequency points

$\Psi(n, \tau)$: Kernel in the time-lag domain

Using the equation 3-27 (with TFR normalized using eq. 3-28 or 3-29) a useful and objective measure of complexity and information content of TFR can be obtained. This measure can get any value between the maximum and minimum limits obtained by equations 3-30 and 3-31, respectively.

Finally, the information factor to the multicriteria method is evaluated using:

$$IM(P_x(t, f)) = 1 - R_3(P_x(t, f)) \quad 3-32$$

This factor of qualification play a role similar to visual inspection traditionally used, with the advantage that is not user dependent and it is a totally objective criteria.

3.5 Application of Multicriteria Method for Selection of Best-Performance Time-Frequency Representations with Fixed Kernel

In the following section an application for a real case of the multicriteria method developed to select a best-performance TFR will be shown.

The signal to be used is the East-West acceleration record obtained on the roof of the Robert Millikan Library of the California Institute of Technology, during the earthquake of San Fernando on February 9 of 1971, with the following general characteristics [184]:

- $M_L=6.4$
- Epicenter: $34^\circ 24.7' N, 118^\circ 24' W$

- Depth = 13 km
- Distance to Millikan Library = 30 km.

The San Fernando Earthquake, produced a peak ground acceleration of 0.20g and a peak acceleration on the roof of 0.35g, according to reference [25] the building has a nonlinear response during the event, additional information about this specific record in Millikan Library can be found in the references [16, 25, 26, 58, 59, 90, 121].

In the following figures the time histories of acceleration, velocity and displacement for this record and the Fourier and Pseudo-Acceleration spectra evaluate for a 5% critical damping are shown:

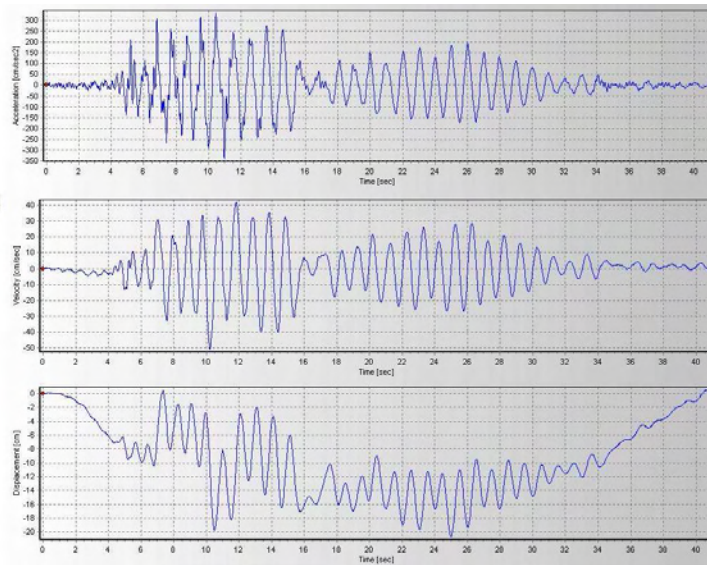


Figure 3-6 Acceleration, Velocity, and Displacement Time Histories of San Fernando Earthquake recorded on the Roof of Millikan Library (EW Component)

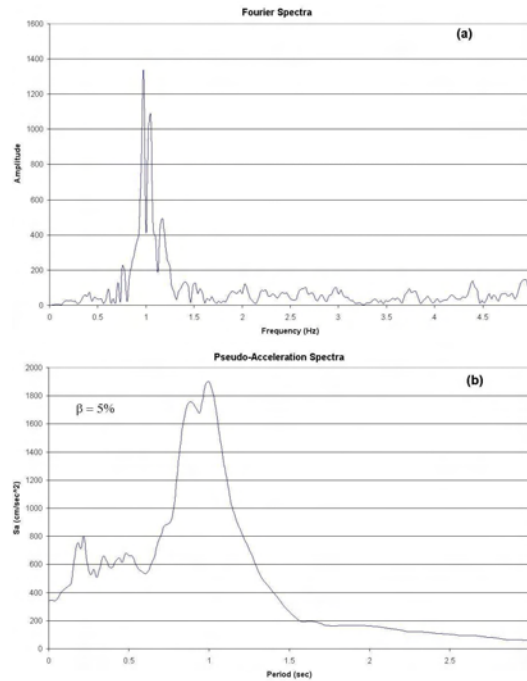


Figure 3-7 (a) Fourier Spectra (a) and (b) Pseudo-Acceleration Spectra of San Fernando Earthquake recorded on the Roof of Millikan Library (EW Component)

The best-performance TFR for this signal between the following TFRs will be selected:

- Spectrogram
- Wigner-Ville Distribution
- Smoothed Pseudo-Wigner Ville Distribution
- Choi-Williams
- Margenau-Hill
- Reduced Interference Distribution

Recalling the multicriteria method (equation 3.7)

$$SMQ = \sum_{i=1}^n W_i EF_i$$

$$SMQ = W_1 * DMP + W_2 * SPI + W_3 * RCM + W_4 * IM$$

And remember that:

W_i : Weight factor

DMP: Qualification for Desirable Mathematical Properties

SPI: Structural Performance Indicator

RCM: Resolution and Concentration Measure [159, 162]

IM: Information Measure [95]

3.5.1 Evaluation of Weighting Factors

In order to avoid any subjective decision all factors are set to an equal value, therefore the weight factor is set to:

$$W_i = 0.25 \qquad 3-33$$

3.5.2 Evaluation of Qualification for Desirable Mathematical Properties (*DMP*)

The first qualification factor is the desirable mathematical properties that each TFRs has, in this case the values suggested in the Table 3.3 can be used. For the Reduced Interference Distribution (thus TFR do not appear in Table 3.3) the properties reported in the reference [185] can be obtained.

TABLE 3.4 Evaluation of Qualification for Desirable Mathematical Properties (DMP)

TFR	Mathematical Property (see table 3.2)										DMP
	P ₁	P ₂	P ₃	P ₄	P ₅	P ₆	P ₇	P ₈	P ₉	P ₁₀	
Spectrogram	×	×	×	✓	✓	✓	×	×	×	×	0.3
Wigner-Ville Distribution	×	✓	✓	✓	✓	✓	✓	✓	✓	✓	0.9
Smoothed Pseudo-Wigner-Ville	×	✓	✓	✓	✓	✓	×	×	✓	✓	0.7
Choi-Williams	×	×	×	✓	✓	✓	✓	✓	✓	✓	0.7
Margenau-Hill	✓	×	✓	×	✓	✓	✓	✓	×	×	0.6
Reduced Interference Distribution	×	✓	✓	✓	✓	✓	✓	✓	✓	✓	0.9

3.5.3 Evaluation of Structural Performance Indicator (SPI)

According to the section 3.4.2.2 the Structural Performance Indicator (SPI) for each TFR takes into account the performance for Ambient Vibration conditions and Strong Event, and it can be obtained by means of the equation (3.8):

$$SPI_{TFR} = 1 - (c_1 * AVP_{TFR} + c_2 * SEP_{TFR})$$

Where:

AVP_{TFR} : Ambient Vibration Performance of TFR

SEP_{TFR} : Strong Event Performance of TFR

c_1, c_2 : Weighting factors for AVP and SEP , suggest values $c_1 = 0.3, c_2 = 0.7$

For ambient vibration conditions the global mean error in the detection of “k” frequencies from a severe noisy signal need to be calculated. This signal is multicomponent and frequency modulated and it is obtained through equation 3-9:

$$x(t) = \sum_{i=1}^k (A_i \cos(2\pi f_i t)) + n(t)$$

For this particular case, the following parameters are selected:

Number of frequencies $k=5$; Sampling rate = 10 sps, Number of samplings: 1024, $t=102.3$ sec, Structural frequencies: $f_i = 0.1$ Hz, 0.3 Hz, 0.5 Hz, 1.0 Hz, and 2 Hz, A_i : Equal to all frequencies, $x(t)$ max = +/- 2 gals ($2 \text{ cm/sec}^2=0.002g$), $n(t)$: Gaussian noise added, with a SNR maximum of 1/16

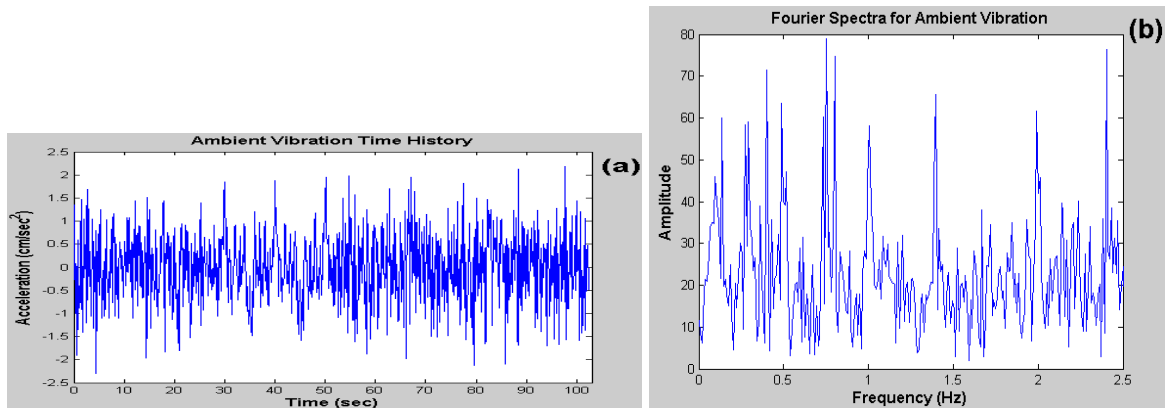


Figure 3-8 (a) Time-History and (b) Fourier Spectra of Ambient Vibration Record for Test of TFR

For this severally contaminated signal is evident that neither the time-history nor the Fourier spectra allow to extract reliably the structural fundamental frequencies (0.1, 0.3, 0.5, 1, 2 Hz), because it is clear from Figure 3-8 that other frequencies with equal or most high energy exist in the signal also.

Only for a comparative purpose in the Figure 3-9 a TFR of this noise signal is shown:

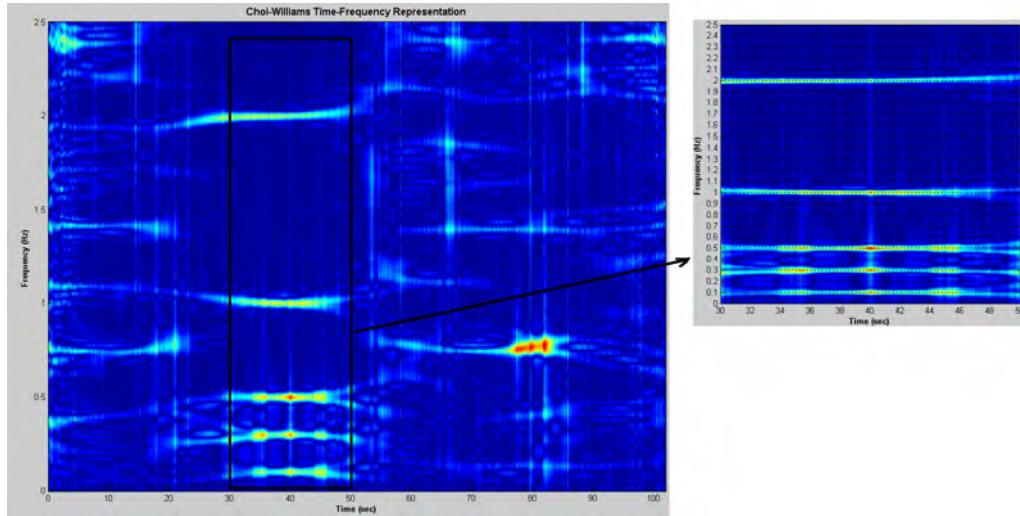


Figure 3-9 Choi-William Representation

From the right side of the previous graph is obvious that the fundamental frequencies of the structure emerge close to : $f_1=0.1$, $f_2=0.3$, $f_3=0.5$, $f_4=1.0$, and $f_5=2$ Hz.

Taking a particular TFR for each time instant and each frequency, the instantaneous frequency error for this TFR can be evaluated by using equation 3-10. Then for each frequency, the mean ambient vibration instantaneous frequency error for each TFR can be evaluated by using equation 3-11.

$$f_{i_{mAVTFRe}} = \frac{\sum_{i=1}^N f_{TFRke}(t)}{N}$$

The result of application of the precedent equation for the TFRs of Figure 3-10 is shown in the following Table:

TABLE 3.5 Mean Ambient Vibration Instantaneous Frequency Error

TFR	$f_1 = 0.1$	$f_{1_{mAVTFRe}}$	$f_2 = 0.3$	$f_{2_{mAVTFRe}}$	$f_3 = 0.5$	$f_{3_{mAVTFRe}}$	$f_4 = 1.0$	$f_{4_{mAVTFRe}}$	$f_5 = 2.0$	$f_{5_{mAVTFRe}}$
		(%)		(%)		(%)		(%)		(%)
Spectrogram	0.1341	34.1	0.2112	29.6	0.6069	21.4	1.3218	32.2	2.0558	2.8
Wigner-Ville	0.0851	14.9	0.2807	6.4	0.4886	2.3	1.2252	22.5	2.0854	4.3
Smoothed Pseudo-Wigner-Ville	0.1123	12.3	0.2276	24.1	0.4406	11.9	0.9457	5.4	1.9377	3.1
Choi-Williams	0.1221	22.1	0.1929	35.7	0.4441	11.2	0.9445	5.6	1.9394	3.0
Margenau-Hill	0.0879	12.1	0.3481	16.0	0.5696	13.9	0.9906	0.9	1.5453	22.7
Reduced Interference	0.1174	17.4	0.2809	6.4	0.5606	12.1	1.0068	0.7	1.9228	3.9

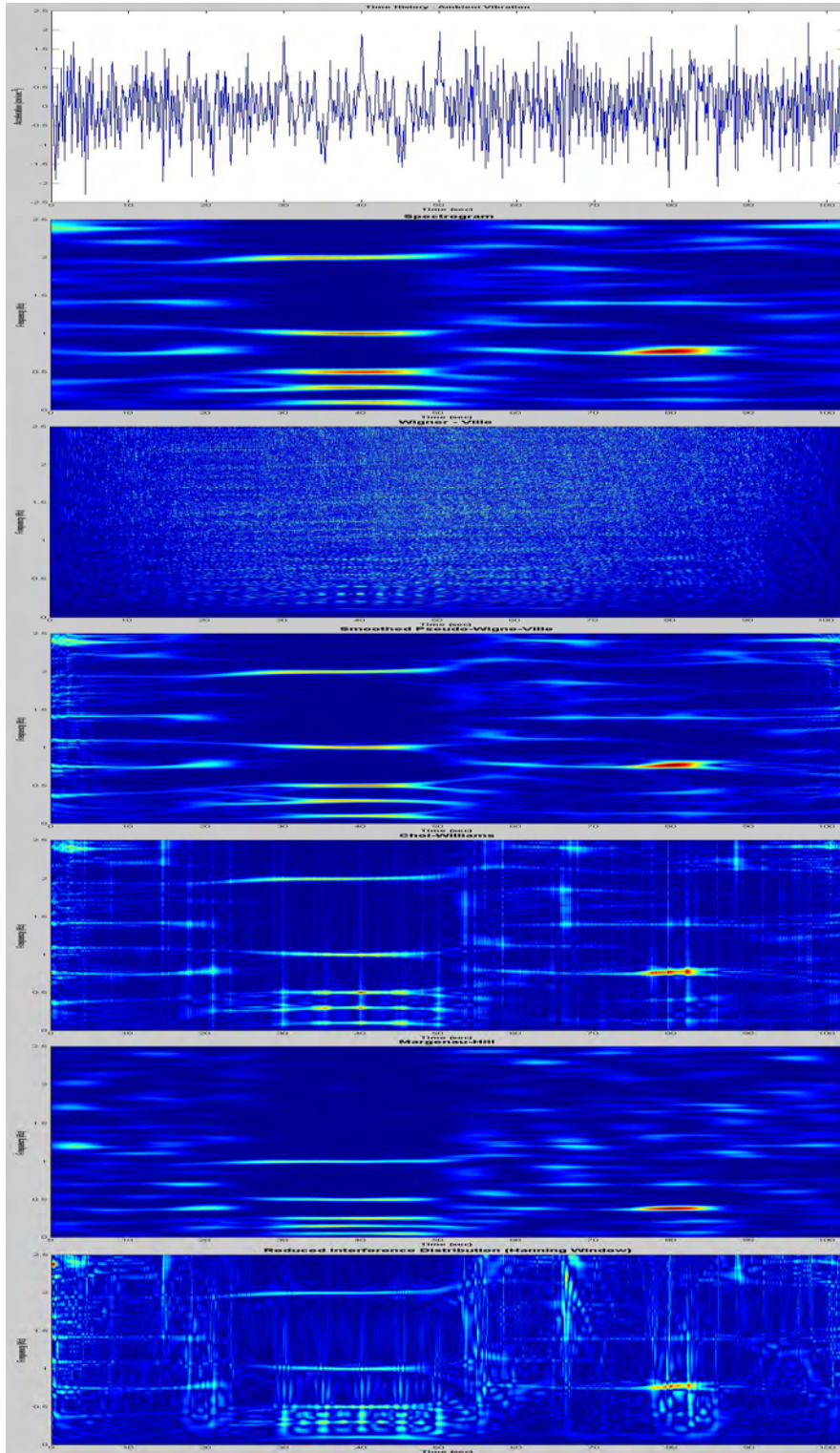


Figure 3-10 TFRs for Ambient Vibration Test Signal

Finally, the mean global frequency error detection for a specific TFR in Ambient Vibration conditions is evaluated using the equation 3-12 and it is shown in the Table 3-6:

TABLE 3.6 Mean Global Frequency Error for Ambient Vibration Test

TFR	$AVP_{TFR} = \bar{f}_{TFRAV_e}$ (%)
Spectrogram	24.0
Wigner-Ville	10.1
Smoothed Pseudo-Wigner-Ville	11.4
Choi-Williams	15.5
Margenau-Hill	13.1
Reduced Interference	8.1

Remembering the equation 3-13, from the above Table, the qualification factor for ambient vibration condition of each TFR is obtained.

Note: In the expression 3-13 the qualification factor AVP is expressed in decimal.

It is important to recall some aspects about the values from Table 3.6:

- These errors are means and in a particular time instant it can take other values
- The large values of error is due to the nature of time-history, because it is a very noise signal, in fact far than normal case really (SNR=1/16)
- The duration of the signal is very short (t=102.3 secs), and most exactly the number of the samplings are very few (only 1024 samplings).
- In a real case, we deal with signals of several minutes and even hours or days. For example as it has been reported in references [90, 114, 116, 121] and the chapter 4 of this research, therefore the mean frequencies become more stable.
- This type of signal (extremely noise and very short) was selected because it is the worst case.

The next step is the assessments of the TFR performance for dealing with strong event, this is called:

SEP_{TFR} : Strong Event Performance of TFR.

The Figure 3-11 shows a TFR of San Fernando Earthquake, to select a typical signal according to this record:

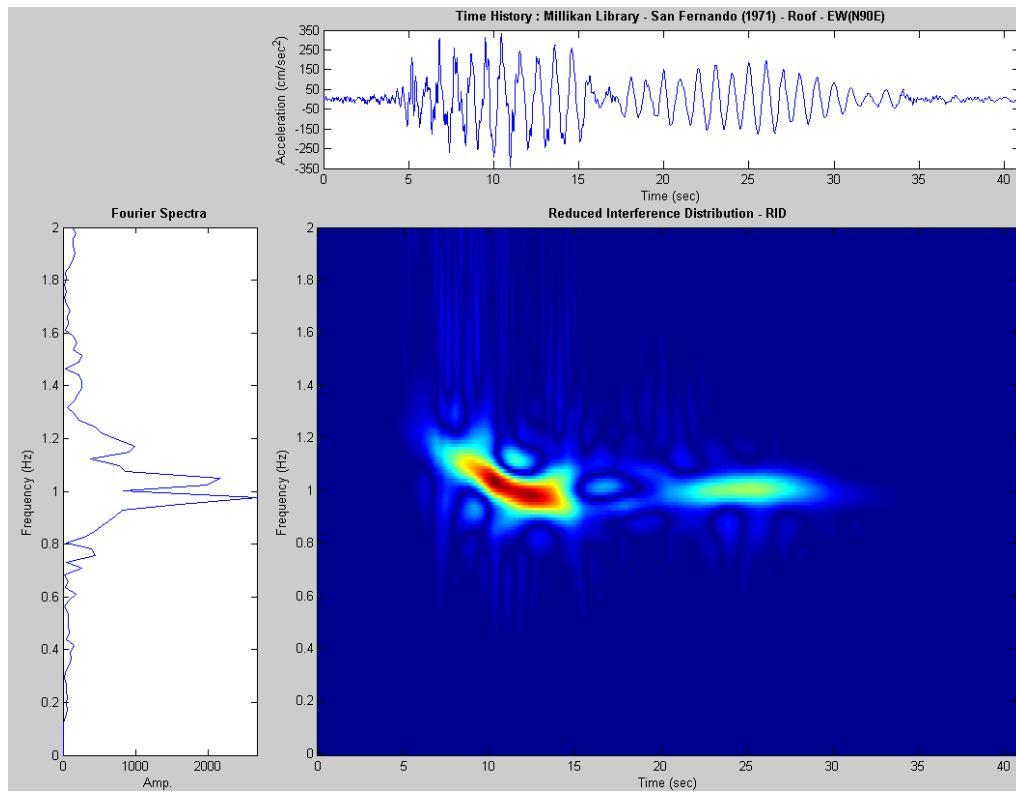


Figure 3-11 TFRs of San Fernando Earthquake (1971) recorded at Millikan Library (EW-Roof Component)

If we see a TFR of the San Fernando Earthquake (shown in the Figure 3-11), we can see that the pattern of the time-frequency plane is like typical signal #1 of section 3.4.2.2., (linear, then exponential decay and finally linear again with a permanent frequency shift), so we select this typical signal in the following test procedure, this synthetic pattern is shown in the Figure 3-12

Therefore in this case $k=1$ in the equation 3-17, if there is any doubt about the pattern, we can select other similar signal-patterns and perform an evaluation using these signals, in those cases $k>1$ in the equation 3-17.

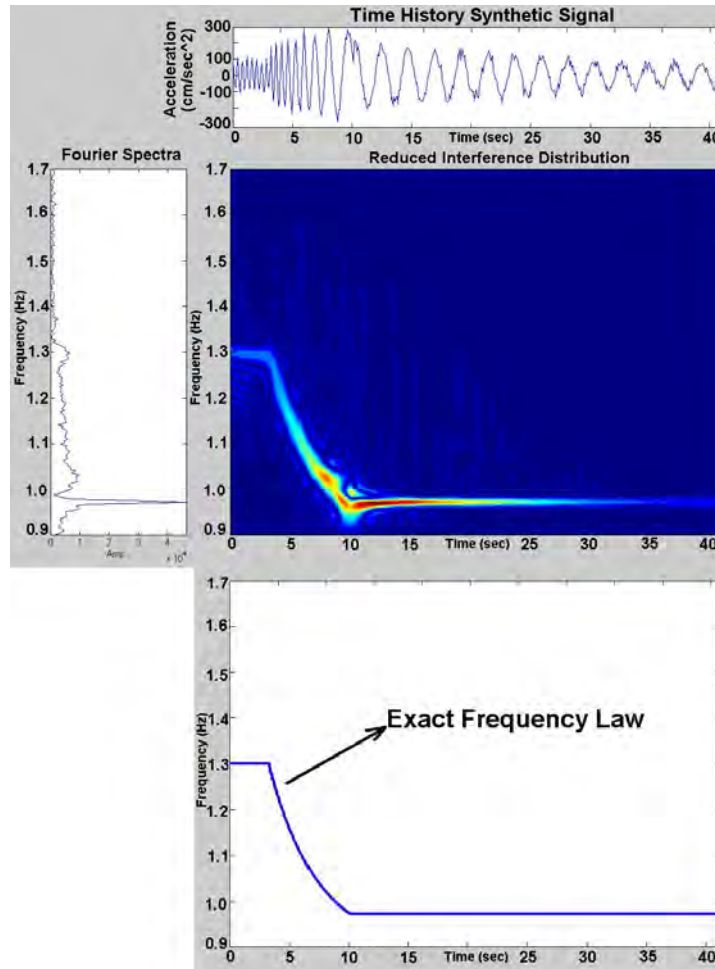


Figure 3-12 Synthetic Pattern to TFRs of San Fernando Earthquake (1971) recorded at Millikan Library (EW-Roof Component)

To acquire the previous synthetic signal, the following values are set into equation 3-14:

$$x(t) = \left\{ \begin{array}{ll} A(t) \cos(2\pi * 1.3t) & \text{if } 0 \leq t < 40 \quad ; \quad A(t) = 0.5 * e^{\frac{0.001t}{2}} \\ A(t) \cos(2\pi * 1.3e^{-0.02t}) & \text{if } 40 \leq t < 128 \quad ; \quad A(t) \text{ with } p(A(t)) = \frac{1}{\sqrt{2\pi}} \int_{-\infty}^{A(t)} e^{-\frac{\xi^2}{2}} d\xi \\ A(t) \cos(2\pi * 1.3e^{-0.006t}) & \text{if } 128 \leq t \quad ; \quad A(t) = e^{\frac{0.001t}{2}} \end{array} \right\}$$

$$x(t) = 200 * (x(t) + n(t))$$

- Duration: 42 sec
- Noise Level : 10%
- The factor scale of 200 is only to get an acceleration close to real signal

From figures 3-11 and 3-12 it is evident that to perform an evaluation using an approximate (or synthetic) pattern is a very valuable tool to select the best performance TFR, because the exact frequency law of the signal is known.

With this theoretical frequency law the ability of any TFR can be evaluated in order to adjust or track at each instant for this type of frequency law. This pattern should be associated with a typical mechanism of structural damage as can be seen in chapter 5.

The next step is the evaluation of all the TFRs for this synthetic signal; it is shown in the next graph:

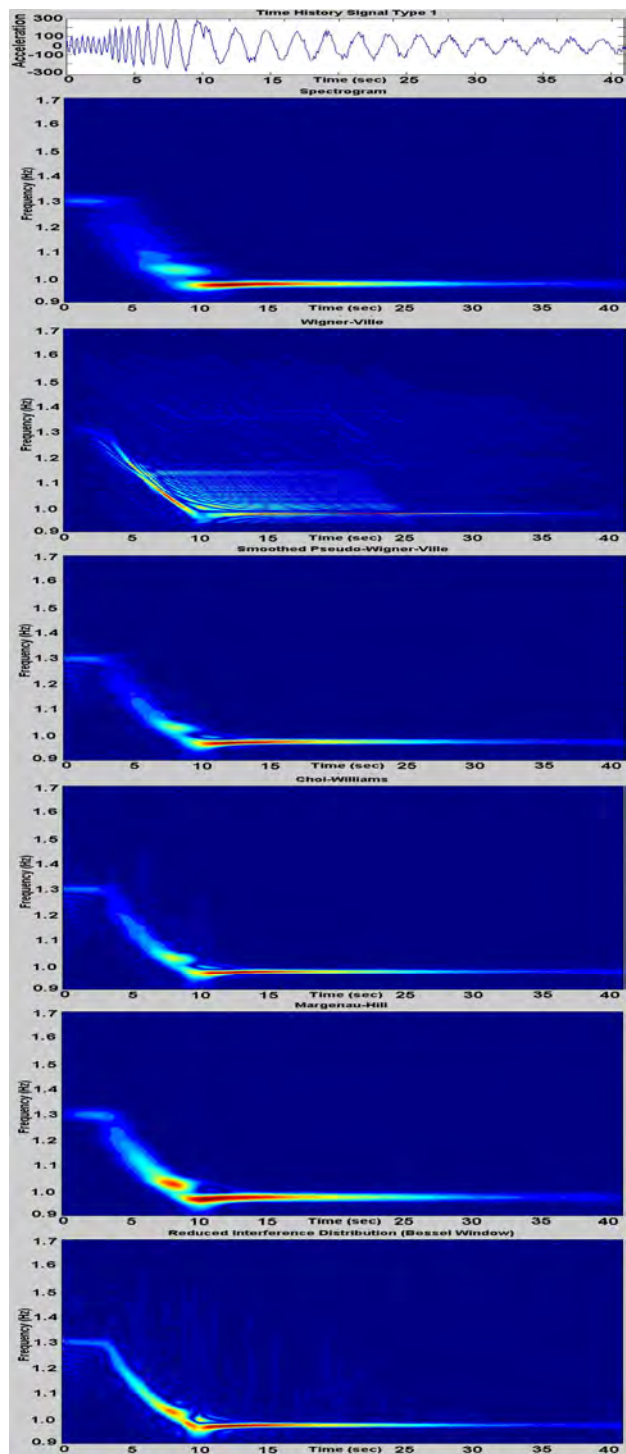


Figure 3-13 Synthetic Pattern for TFRs of San Fernando Earthquake (1971) recorded at Millikan Library (EW-Roof Component)

From the Figure 3-13, the empirical instantaneous frequency law for each one of TFRs can be evaluated, as it is shown in the following graph:

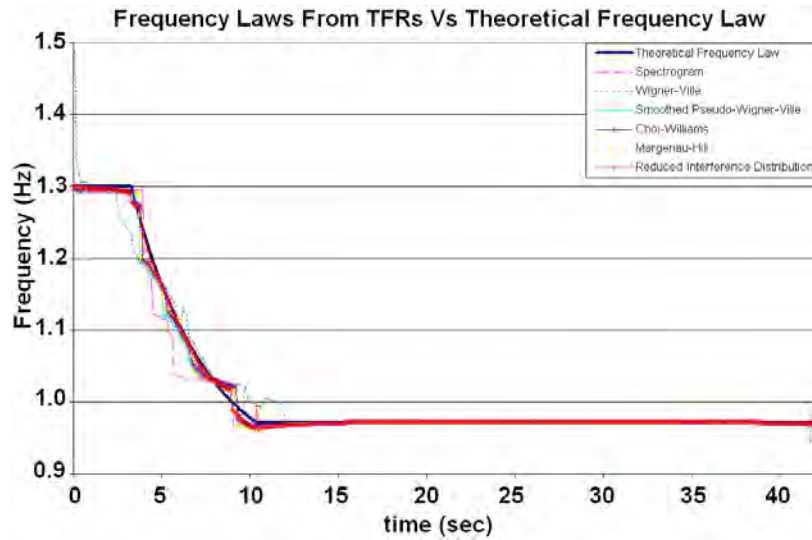


Figure 3-14 Frequency Laws for TFRs Vs Theoretical Frequency Law

For each TFR in each time instants an instantaneous frequency error using the equation 3-15 can be evaluated, as it is shown in the following Figure:

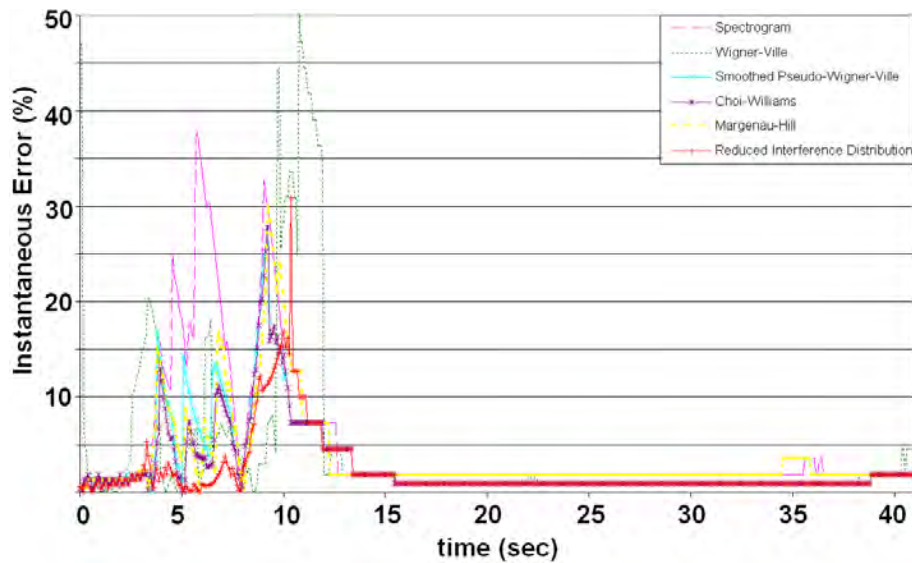


Figure 3-15 Percent of Instantaneous Frequency Error for TFRs

Using the equation 3-16 the mean global frequency error for each TFR can be evaluated, as it is shown in the next Table:

TABLE 3.7 Mean Global Frequency Error for Strong Event

TFR	$f_{i_{mTFRSEe}} = \frac{\sum_{i=1}^N f_e(t)}{N}$ (%)
Spectrogram	4.8
Wigner-Ville	4.7
Smoothed Pseudo-Wigner-Ville	2.9
Choi-Williams	2.6
Margenau-Hill	3.5
Reduced Interference	2.1

Therefore the TFR qualification for Strong Events is the values from Table 3.7, but in decimal form, thus for this case :

$$SEP_{TFR} = \frac{f_{i_{mTFRSEe}}}{100}$$

Finally the Structural Performance Indicator is evaluated replacing the values from tables 3.6 and 3.7 into equation 3.8, it is calculated in the next Table, and for this case $c_1=0.3$ and $c_2=0.7$ are taken according to general suggestion:

TABLE 3.8 Structural Performance Indicator for TFR

TFR	$SPI_{TFR} = 1 - (c_1 * AVP_{TFR} + c_2 * SEP_{TFR})$
Spectrogram	0.8947
Wigner-Ville	0.9369
Smoothed Pseudo-Wigner-Ville	0.9455
Choi-Williams	0.9351
Margenau-Hill	0.9358
Reduced Interference	0.9607

TFRs with higher values represent a well-structural performance.

3.5.4 Evaluation of Resolution and Concentration Measure (RCM)

Prior to systematic application of equation 3-19 it is necessary to optimize each available parameter in each single TFR, as have mentioned earlier for a minimization procedure using the equation 3-21 [157]. For example for Choi-Williams Distribution it is necessary to minimize the following function:

$$C_x(t, p) = \frac{\int_{-\infty}^{+\infty} \int_{-\infty}^{+\infty} \left(\frac{1}{4\pi^{3/2}} \int_{-\infty}^{+\infty} \int_{-\infty}^{+\infty} \sqrt{\frac{\sigma_p}{\tau^2}} e^{\frac{-\sigma_p(u-t)^2}{4\tau^2} - j\tau f} x^* \left(u - \frac{1}{2}\tau \right) x \left(u + \frac{1}{2}\tau \right) dud\tau \right) w(\tau-t) \left| d\tau d\Omega \right|^4}{\left(\int_{-\infty}^{+\infty} \int_{-\infty}^{+\infty} \left(\frac{1}{4\pi^{3/2}} \int_{-\infty}^{+\infty} \int_{-\infty}^{+\infty} \sqrt{\frac{\sigma_p}{\tau^2}} e^{\frac{-\sigma_p(u-t)^2}{4\tau^2} - j\tau f} x^* \left(u - \frac{1}{2}\tau \right) x \left(u + \frac{1}{2}\tau \right) dud\tau \right) w(\tau-t) \left| d\tau d\Omega \right|^2 \right)^2}$$

In Figure 3-16 the systematic application of the previous equation is shown for four values of standard deviation. On the bottom side of the same Figure the optimal standard deviation values that should be used in order to get a signal-adaptive optimal Choi-Williams Distribution is shown. The standard deviation values that minimize the equation 3-21 through time are shown in part (b) of the Figure 3-16:

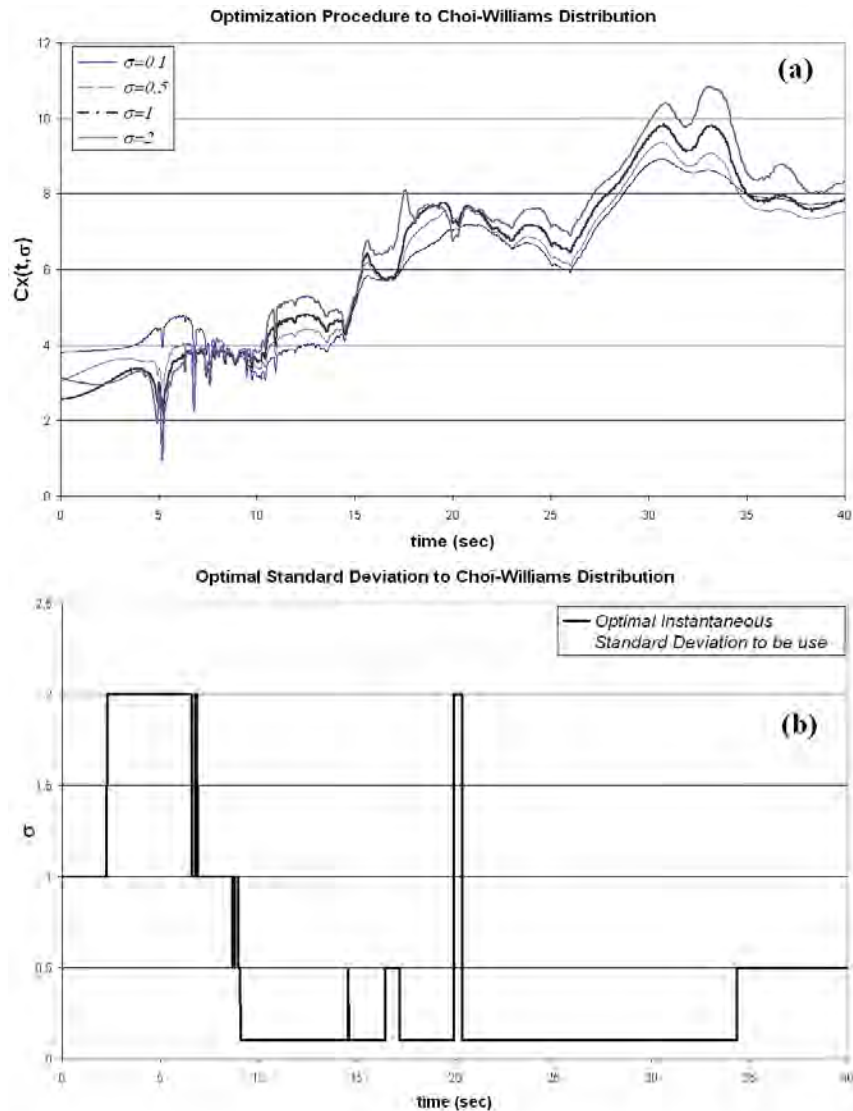


Figure 3-16 Optimization Procedure for Choi-Williams Distribution. (a) Functional Operator for several Standard Deviation Values. (b) Optimal Instantaneous Standard Deviation to be use.

Once the optimization procedure is performed for each TFR, the procedure of the flow chart from Figure 3-5 can be applied and the P_{overall} of the equation 3-23 is then evaluated. The results are presented in Table 3.9:

TABLE 3.9 Resolution and Concentration Measure (RCM) for TFRs

TFR	Resolution and Concentration Measure (RCM)
	P_{overall} (According to Sucic and Boashash [160])
Spectrogram	0.7608
Wigner-Ville	0.7115
Smoothed Pseudo-Wigner-Ville	0.8011
Choi-Williams	0.7457
Margenau-Hill	0.8363
Reduced Interference	0.7707

3.5.5 Evaluation of Information Measure (IM)

As it has been discussed in the literal 3.4.2.4, the Order Three Renyi Entropy Measure has been chosen in the multicriteria method such as a non-user depend criteria to link the best-look TFR appearance.

For discrete case the Renyi third order entropy defined by Sang and Williams [95] was adopted and it was normalized with respect to the energy, thus are:

$$R_3(P_x(t, f)) = \frac{1}{2} \log_2 \left(\sum_{l=-L}^L \sum_{k=-K}^K \left(\frac{P_x(t, f)}{\sum_{l=-L}^L \sum_{k=-K}^K (P_{N_x}(l, k))} \right)^3 \right)$$

Finally the information factor for the multicriteria method is evaluated using the equation 3-32:

$$IM(P_x(t, f)) = 1 - R_3(P_x(t, f))$$

In Table 3-10, the results of the application of equations 3-27, 3-28 and 3-32 for each TFR are shown:

TABLE 3.10 Information Measure (IM) for TFRs

TFR	Information Measure
	$IM=1-R_3$ (According to Sang and Williams [95])
Spectrogram	0.8658
Wigner-Ville	0.8701
Smoothed Pseudo-Wigner-Ville	0.8618
Choi-Williams	0.8619
Margenau-Hill	0.8649
Reduced Interference	0.8627

3.5.6 Final Evaluation of Structural Multicriteria Quality Factor (SMQ)

Finally using the information from tables 3.4, 3.8, 3.9, and 3.10, the Structural Multicriteria Quality factor can be obtained. The values for each TFR are shown in Table 3-11:

TABLE 3.11 Structural Multicriteria Quality factor (SMQ) for TFRs.

TFR	Desiderable Mathematical Properties	Structural Performance Indicator	Resolution and Concentration	Information Measure	Structural Multicriteria Quality Factor
	DMP	SPI	RCM	IM	SMQ
Spectrogram	0.3000	0.8947	0.7608	0.8658	0.7053
Wigner-Ville	0.9000	0.9369	0.7115	0.8701	0.8546
Smoothed Pseudo-Wigner-Ville	0.7000	0.9455	0.8011	0.8618	0.8271
Choi-Williams	0.7000	0.9351	0.7457	0.8619	0.8107
Margenau-Hill	0.6000	0.9358	0.8363	0.8649	0.8092
Reduced Interference	0.9000	0.9607	0.7707	0.8627	0.8735

The values on the Table 3.11 are evaluated using the equation 3-7:

From Table 3.11 the best perform TFR of the selected TFRs is the Reduced Interference Distribution, the traditional Wigner-Ville Distribution closely follows.

4 STRUCTURAL SYSTEM IDENTIFICATION AND DAMAGE DETECTION USING AMBIENT VIBRATION OUTPUT SIGNALS

In this chapter, the system identification and damage detection of structures using only ambient vibration output signals and time-frequency analysis combined with other system identification procedures will be shown.

A method for system identification and damage detection based on information extracted from a Mean Time-frequency Representation (MTFR) plane is proposed. Using this information in the Frequency Domain Decomposition (FDD) system identification technique the damage can be evaluated. This last technique was previously proposed by Brinker et. al. [124]. The main factors of incidence in system identification procedure are also investigated.

Several test using data obtained for MDOFs from simulated structures are shown, including a comparison of the results obtained by applying the methodology for Phase I of IASC-ASCE Structural Health Monitoring Benchmark Problem with previous benchmark result reports [41, 106-112].

Finally the proposed methodology is applied to output signals from finite element models and real ambient vibration records obtained from four real structures.

The studied structures are: Millikan Library of Caltech (in Pasadena, California) a Residential Building in Mayagüez, Puerto Rico, the Airport Control Tower at British Virgin Islands, and a Residential Building, in San Juan, Puerto Rico.

4.1 General Procedure for Structural Damage Detection Using Output Signals From Ambient Vibration

Before presenting the theoretical formulation of the problem, let us show the general approach for system identification and damage detection used here. Basically, the procedure for damage detection using only output signal from ambient vibration proposed here consists of a comparative analysis of the system identification results before and after the event (like earthquake, explosions, blasting, hurricanes). Thus, the structural properties before an event and after the event were identified. By comparing the two the damage can be evaluated. This is shown schematically in Figure 4-1:

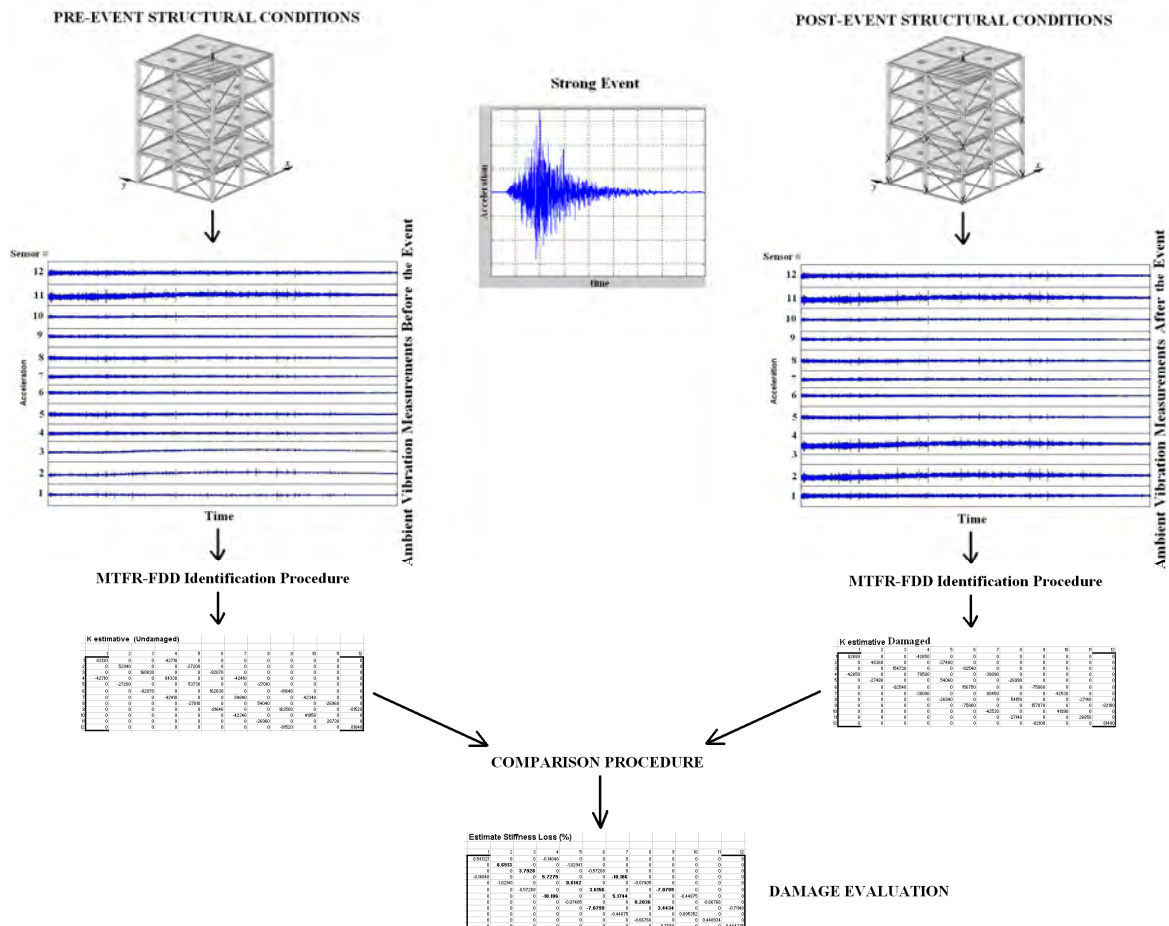


Figure 4-1 Schematic Procedure for Structural Damage Detection Using Output Signals from Ambient Vibration

Some important cases are possible:

- Non instrumented structures (the most common case)
- Instrumented structure in not continuous recording
- Instrumented structure in continuous data acquisition.

4.1.1 Non Instrumented Structures

For non instrumented structures, it is necessary to do a previously and posteriori field record recollection. It is recommended that the signals will be acquired simultaneously in several structural DOF's, for this purpose a wireless acquisition equipment is a good option.

In this case, the damage detection procedure can not get any information about the damage sequence and we only attempt to identify the amount of damage and its location.

It is not commonly possible to trigger at the same time all instruments (i.e. In a building the sensor connection in different floors is not as easy as in the field). In such cases, we can trigger each sensor at different times.

In the case that all sensors have common time from GPS, it is easy to take a particular time like starting time for the records. In the case when GPS information is not available, we can search for a single common peak in all channels and then align the wave forms in time and phase using, for example, the high-resolution alignment procedure proposed in the reference [189]

It is equally important to take the output signals in places where most of the building damage can be acquired. In this sense, valuable information previously reported about the sensor optimal location for damage detection can be viewed in the references [187, 188].

It is obvious but important to take into account the location of places for taking signals before the event and we must use the same location to take measurements after the event, otherwise a reliable comparison would not be possible.

Finally, it is assumed that structural mass does not change before and after the event, therefore if there is any change in structural mass or stiffness, it is absolutely necessary to take additional vibration measurements and make the system identification procedure prior to any strong event.

In fact the same procedure for stiffness changes detection can be applied to mass changes detection, thus if we know that no changes in stiffness happened then any frequency variation imply a mass change. This is useful for evaluation of changes in structural dynamic properties produced by architectural modifications by adding or removing masses.

4.1.2 Instrumented Structures

When a permanent array of sensors has been installed in the structure, there are two possible cases:

- The acquisition is not continuous
- Acquisition is continuous

The former case is very common and requires complete system identification prior to the event. It is highly probable that the record for the strong event is available. In this case the damage sequence can be evaluated using the proposed procedure of chapter 5. On the contrary we could make a previous and posteriori system identification and extract the damage by comparing the two.

An instrumented structure with continuous acquisition is the ideal case. Unfortunately, this is also the least common case. In this case, we will have a complete sequence about structural performance before, during and after the event.

For structures with continuous recording, an on-line or real-time structural damage detection algorithm should be developed using the methodologies proposed in this work. This is not proposed here because it is out of the scope of this research.

4.2 Main Characteristics of Ambient Vibration Excitations

In structural health monitoring technical literature, there exist an extensive amount of references about the ambient vibration, its applications, limitations, and theoretical background. See references [1, 4, 5, 6, 8, 11, 14, 29, 74, 77, 81-84, 89, 90, 113, 114, 119, 121, 150] among them.

Some aspects regarding to origin, nature, amplitude, signal to noise ratio and structural response according to the applications will be briefly mentioned.

Regarding the origin of ambient vibration the source of ambient vibrations are internal and external to the structure.

Within internal source, the strain produced by changes in temperature and humidity, degree of saturation of the soil beneath and around the foundations of the structure can be mentioned.

External sources include wind, soil microtremors, rain, traffic, waves of the sea, machinery, human and animal movements, operational use, trains, and others sources.

Because the time of occurrence, type, amplitude and distance to the structure are variable, all of aforementioned sources, produce in general low intensity waves. These combinations of waves generate a permanent random vibration process.

This type of vibration produces in the structure a multicomponent input signal that have particular characteristic such as a large frequency band-width and low amplitude, in general both amplitude and frequency are random in any particular instant.

Because the excitation is random, the structural response is also random according to random vibration theory [127]. Therefore, the system identification results are absolutely probabilistic and not a closed form solution can be found regardless the analysis method used.

A frequent probabilistic density function in random vibration is the Gaussian distribution [2, 3, 7-9, 74, 124, 127] and this kind of distribution was selected for the analysis.

The amplitude of ambient vibration may be taken from very low values to high values, but in general according to literature reports [3, 5, 8] it is low if compared with strong events, therefore the signal to noise ratio (SNR) is expected to have very low values, thus the noise is a key factor in ambient vibration analysis.

It is obvious that the input signal can not be measured, because it is from unknown sources. This is an important reason to avoid the use of support input signal in this research, because it contribute only a little to the ambient vibration input for the whole structure.

Therefore an estimative of probabilistic structural response using only the output signals will be generated.

Finally, it is important to point out that the duration of ambient vibration records are generally very long, lasting from a few minutes to days, weeks, and months. This will produce problems with the process and computational capabilities.

4.3 The Equivalent Structural Model (ESM)

4.3.1 Main Characteristics of the Equivalent Structural Model

As it has been mentioned earlier, there are a number of system identification procedures such as ARMA models, stochastic methods, or updating models [1-5, 17, 22]. All of these procedures, use input signals and structural information (i.e. material properties, geometry). In the approach we do not use neither.

Since a damage procedure without the use of any structural information has been proposed, an equivalent structural model (ESM) will be obtained that represents the behavior in the linear range of the real structure. The ESM have the following characteristics:

- a) The ESM, represent a reduced equivalent structural system of the real structure. Therefore, the ESM is equivalent to a scale version of the real system modeled to the instrumented DOFs.
- b) The response of the real system and equivalent system are equal for static and dynamic loading in the linear range of response.
- c) The response of the real structure before and after damage is linear, thus after the damage the real structure have a linear response with a modified stiffness parameters.
- d) The damping values are very low, and therefore it does not have significant influence in the identification procedure.
- e) A classical damping is assumed, thus we only have one damping ratio for each mode.

- f) The real and ESM structure have classical normal modes of vibration and it can be modeled using the traditional chains of spring and masses.
- g) The mass and stiffness matrix can be normalized by the modes.
- h) The mass matrix of any ESM can be normalized.

Figure 4-2 demonstrates a typical equivalent structural model procedure, showing the real structure (a), reduced common structural model (b) and our equivalent model for a 3 channel setup (c).



Figure 4-2 Typical Equivalent Structural Model

In the system identification procedure the structural properties (i.e. mass, stiffness, and damping matrix) for an equivalent structural system that have the same static and dynamic linear response as the real structure will be evaluated.

It is necessary to introduce the ESM concept because it is impossible to reconstruct the exact matrixes of the structure using only the output signals from a very few sensors.

For example in Figure 4-2, there is a finite element model of the structure with 6488 DOF and for this structure there are only 3 sensors (the traditional ground sensor does not count, because we do not use input signal). Therefore it is necessary to reduce the model to a 3 DOF.

In this regard the reader must remember that the 6488 DOFs model of Figure 4-2 is not necessarily more precise. In the reference [27], it has been proven that the typical error in the predictions of this type of model for linear response is between 40% to 80%.

Since the structural engineer does not know exactly the important factors such as real support conditions, real material properties, real geometry, real mass distributions, non-structural components interaction, soil-structure interaction, the predictions of its large and “perfect” finite element models differ significantly, There are reported difference of 40% to 120% of the measurements obtained in laboratory and field test. [5, 8, 9, 11, 14, 17, 18, 20, 21, 24, 26, 27, 70, 84].

It will be demonstrated that the error predictions in the linear range are below 5%, possibly because the procedure does not use the strong typical assumptions and only use real structural measurement outputs.

The other important things to point out here are the following aspects:

- The amount of DOFs of the ESM is not necessarily equal to the number of sensor in the structure; in the majority of cases a model equal or bigger than the number of sensors available can be used.
- The size of the ESM is limited to the amount of structural frequencies that can be identified from signals.

- Because we are dealing with linear response, it is possible to obtain probable response for non instrumented DOFs using interpolation algorithms. By using this it is possible to expand the ESM for many additional non instrumented DOFs.
- In general the identified mass, damping and stiffness values do not have any physical meaning and is only a representative of scale values from real values. Since no structural information or input signal was used, therefore the scale factor can not be obtained.
- If there are additional information about the structure (i.e. geometry, mass) or input signals, the real stiffness values can be obtained using traditional updating models of system identification. But the use of any structural information or input signal is prohibited for the goal of this research.
- For a particular structure with constant properties, the identification procedure using TFRs and FDD always converges to the same ESM, thus equivalent mass, stiffness and damping matrices obtained from signals are unique.
- The abovementioned is the key for the damage detection procedure, because it is possible to extract the damage for comparison between damage and undamaged identification results.
- The identified damage of the ESM is in absolute proportion to the real structure. Therefore the percentage of stiffness loss in the ESM is equal to stiffness loss percentage in the real structure. It will be demonstrated by using numerical models and real cases.

4.4 Mathematical Formulation for Damage Detection Using Time-Frequency Representation of Output Signals From Ambient Vibration

4.4.1 General Considerations

For a MDOF with external forces, the classical movement equation in matricial form can be written as [127]:

$$[M]\{\ddot{x}(t)\} + [C]\{\dot{x}(t)\} + [K]\{x(t)\} = \{F(t)\} \quad 4-1$$

Where:

[M]: Mass matrix, defined, positive

[C]: Damping matrix

[K]: Stiffness Matrix

{x(t)}: Displacement time history vectors (superscript dot represent time derivative)

{F(t)}: Force time history vectors

In linear range the structure values of mass, damping and stiffness matrices are independent of the external force f(t), therefore the matrix values do not alter if the system is in free vibration conditions:

$$[M]\{\ddot{x}(t)\} + [C]\{\dot{x}(t)\} + [K]\{x(t)\} = \{0\} \quad 4-2$$

For the equations 4-1 and 4-2, the solutions become a matrix eigenvalue problem [127]:

$$[[K] - \lambda_i [M]]\{\phi\}_i = \{0\} \quad 4-3$$

Where:

$\{\lambda\}$: eigenvalues

$\{\phi\}$: eigenvector

The eigenvalue vector defines the circular frequencies of the system as:

$$\{\lambda_i\} = \{\omega_i^2\} \quad 4-4$$

And the eigenvector matrix defines the structural modes shapes as:

$$[\Phi] = \left[\begin{array}{c|c|c|c} \left\{ \begin{array}{c} \phi_{1,1} \\ \phi_{1,2} \\ \vdots \\ \phi_{1,n} \end{array} \right\} & \left\{ \begin{array}{c} \phi_{2,1} \\ \phi_{2,2} \\ \vdots \\ \phi_{2,n} \end{array} \right\} & \dots & \left\{ \begin{array}{c} \phi_{n,1} \\ \phi_{n,2} \\ \vdots \\ \phi_{n,n} \end{array} \right\} \end{array} \right] \quad 4-5$$

Assuming that the structure has classical damping and the modes are orthogonal, the equations of motion can be uncoupled; and the damping matrix can be evaluated using [127]:

$$[C] = \left[\begin{array}{ccc} \ddots & & \\ & 2\xi_j\omega_j & \\ & & \ddots \end{array} \right] \quad 4-6$$

Where:

ξ_j : Critical damping coefficient to mode 'j'

The structural frequencies and mode shapes can be obtained from experimental measurements, then by using the equations 4-5, 4-4 and 4-3 the mass and stiffness matrices are obtained.

An important field of structural dynamic is known as Operational Modal Analysis or Empirical Modal Analysis have developed several methods for obtaining frequencies and mode shapes from real signals, the number of methods available to obtain frequencies and modes are extensive.

When the structure of the stiffness matrix is known, it is possible to obtain efficient algorithm to estimate mass and stiffness values from experimental measurements. A solution for the shear-building which is of major interest in civil engineering has been recently proposed by Udawadia [190], fo noise free vibration the estimation of k can be evaluated using [190]:

$$\{k\} = \lambda_i^m [\Phi_i^m]^{-1} \{\phi_i^m\} \quad 4-7$$

Where the vector {k} is the stiffness estimative values for a matrix with the following form:

$$[K] = \begin{bmatrix} k_1 + k_2 & -k_2 & & & \\ -k_2 & k_2 + k_3 & -k_3 & & \\ & \cdot & \cdot & \cdot & \\ & & \cdot & \cdot & \cdot \\ & & & -k_n & k_n \end{bmatrix} \quad 4-8$$

And the inverse of measure modal matrix can be obtained for this particular case as [190]:

$$[\Phi_i^m]^{-1} = \begin{bmatrix} \frac{1}{\phi_i^1} & \frac{1}{\phi_i^1} & \frac{1}{\phi_i^1} & \dots & \dots & \frac{1}{\phi_i^1} \\ & \frac{1}{\phi_i^{2,1}} & \frac{1}{\phi_i^{2,1}} & \dots & \dots & \frac{1}{\phi_i^{2,1}} \\ & & \vdots & \vdots & \vdots & \vdots \\ & & & \vdots & \vdots & \vdots \\ & & & & \frac{1}{\phi_i^{n-1,n-2}} & \frac{1}{\phi_i^{n-1,n-2}} \\ & & & & & \frac{1}{\phi_i^{n,n-1}} \end{bmatrix} \quad 4-9$$

When the noise is present the author of reference [190] proposed an iterative algorithm.

Although the equations 4-7, 4-8 and 4-9 are very useful, the procedure has the problem that it is necessary to know the form of the stiffness matrix beforehand and it is only useful for the shear building models.

4.4.2 *Mathematical Formulation for Extraction of System Frequencies using the Mean Time-Frequency Representation*

For a general model-free method, it is proposed here to use the information available in the time-frequency representations of the output signals.

Based on the premise that in a random process with statistical regularity the response has also statistical regularity, we have the mean value at an arbitrary fixed time [127, 206]:

$$\mu_x(t_1) = \lim_{n \rightarrow \infty} \frac{1}{n} \sum_{k=1}^n x_k(t) \quad 4-10$$

Where:

$\mu_x(t_1)$: Mean value at time t_1

$x_k(t)$: Time history

For an ergodic process such as random vibration the mean value is constant and it is assumed to be zero mean.

The implication of the ergodic process is that any sample function is representative of the complete random process [127, 205, 206], so the temporal mean value can be obtained by:

$$\mu_x(k) = \lim_{T \rightarrow \infty} \frac{1}{T} \int_{-T/2}^{T/2} x_k(t) dt \quad 4-11$$

Therefore, it is possible to obtain a time-lag lattice of a Mean Time-Frequency Representation for the process by taking a time-lag variable and evaluating:

$$P_\mu(\tau_k, f) = \frac{1}{N} \sum P_{Norm}(\tau_k, f) \quad 4-12$$

where:

$P_\mu(\tau_k, f)$: Time lattice of Mean time-frequency representation in the time-lag domain

$P_{Norm}(\tau_k, f)$: Normalized time-frequency lattice at time lag τ_k

The normalized time-frequency representation can be obtained using [180]:

$$P_{Norm}(t, f) = \frac{P(t, f)}{\int_{-\infty}^{+\infty} \int_{-\infty}^{+\infty} P(t, f) dt df} \quad 4-13$$

As before, the time-frequency distribution can be obtained using the classical quadratic Cohen class form (see equation 2-4):

$$P(t, f) = \frac{1}{4\pi^2} \int_{-\infty}^{+\infty} \int_{-\infty}^{+\infty} \int_{-\infty}^{+\infty} e^{-j\theta t - j\tau f + j\theta u} \phi(\theta, \tau) x^* \left(u - \frac{1}{2}\tau \right) x \left(u + \frac{1}{2}\tau \right) du d\tau d\theta$$

In an instrumented structure with “n” sensors we have “n” time histories and the equation 4-12 can be expanded in matricial form:

$$P_{\mu}(\tau_k, f) = \frac{2}{n(n+1)} \sum \begin{bmatrix} P_{Norm_{1,1}}(\tau_k, f) & P_{Norm_{1,2}}(\tau_k, f) & \cdots & P_{Norm_{1,n}}(\tau_k, f) \\ 0 & P_{Norm_{2,2}}(\tau_k, f) & \cdots & P_{Norm_{2,n}}(\tau_k, f) \\ \vdots & \vdots & \vdots & \\ 0 & 0 & \cdots & P_{Norm_{n,n}}(\tau_k, f) \end{bmatrix} \quad 4-14$$

In the equation 4-14 the sum is for all possible time-frequency and cross time-frequency representations obtained from all channels, the subscripts imply single time-frequency when $i=j$ and cross time-frequency when $i \neq j$

Note that in the expression 4-14 the matrix form is triangular, and we only evaluate $n(n+1)/2$ terms of TFRs because the cross time-frequency representations are the same when we interchange “i” and “j” subscripts (i.e. “i” and “j” channels).

Finally, collect in a plane the $P_{\mu}(\tau_k, f)$ for all time-lag instants we get the Mean Time-Frequency Representation (MTFR) in the time-lag domain.

The vector with structural frequencies can be obtained from this Mean Time-Frequency Representation using:

$$\{f\} = \arg\{P_{\mu}(\tau, f)\}_{\max} \quad 4-15$$

The resolution of the frequencies obtained using the equation 4-15 is quite remarkable, and for the high capacity of time-frequency analysis it is very stable, even for high noise levels.

It can be shown that almost all structural frequencies present in the signal can be reliably extracted using the equation 4-15, even in the common case of having only few sensors. Further more, the performance can be evaluated by using equation 4-15.

The MTFR proposed here can be used not only for structural frequency estimation, but also the technique is useful in the identification of site response of soil, as it has been shown in a recent published research [221].

4.4.3 *Detection of Non-System Frequencies*

The frequencies extracted using the equation 4-15 may have two uncertainties:

- The first one is: what is the manner of ensuring that the frequency is really from the structure and not from an external source?
- The second one is: if you have two structural frequencies very close to each other, does the structure really have these two frequencies or may be one frequency that wanders?

The solution of the problem can be obtained using one of these three methods (in some cases a combination of them):

- Frequency stability in the time-frequency plane
- Using the form of the probabilistic density function
- Using the excess coefficient evaluated in time-frequency domain

For the former case we can obtain a TFR of the signal and then study the time of occurrence of its frequency. Thus frequencies that appear temporarily in the record have a high probability that its origin is from external sources (i.e. temporary noise produced by machines).

However the previous identification method is not absolute. In a sense that if the frequency is always present in the signals, it is not a uniquely indicator that this is a system frequency, because it can be produced by a permanent equipment.

In the next graph we show a typical TFR plane with these cases:

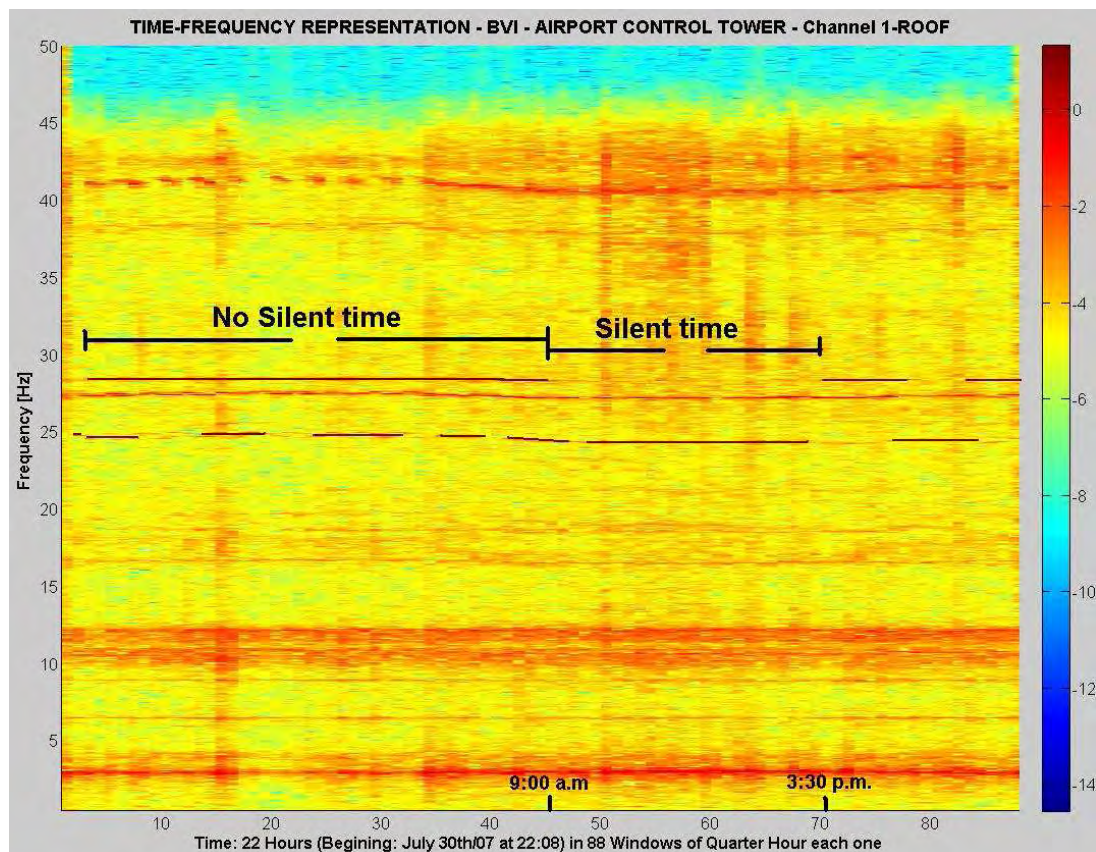


Figure 4-3 Detection of Non-Structural Frequencies using frequency stability in TFR plane

With respect to Figure 4-3, we can see a frequency near to 28 Hz, is practically constant between the 10:00 p.m. (i.e. Beginning of the record) and 9:30 a.m. and disappears between 9:30 a.m. and 3:30 p.m. approximately. It is highly probable that this frequency corresponds to an equipment or machine installed in the building and not from the structural response.

Although this evaluation was based on visual inspection of TFR plane, it is a powerful tool for understanding the structural behavior and it is strongly recommended to begin the signal study with this type of analysis.

A second method to address this problem is the use of random vibration theory. Based on the fact that if we have a random input the structural response is also random (i.e. Gaussian response), but if we have a non-random input (i.e. a systematic vibration produced by a machine), the structural response is not random (i.e. non-gaussian response).

This method has been mentioned theoretically as a direct consequence of the central limit theorem in the references [127, 190, 193, 205, 206], and has been proved experimentally as an excellent indicator for separation of structural and harmonics modes in the reference [192].

Therefore, for a true structural frequency we have a probabilistic density distribution normal or Gaussian (only one peak or a bell form) and for a systematic response (i.e. an external machine frequency) we will have a non-Gaussian probabilistic density function (flat or with two or more peaks), it is shown schematically in the next Figure:

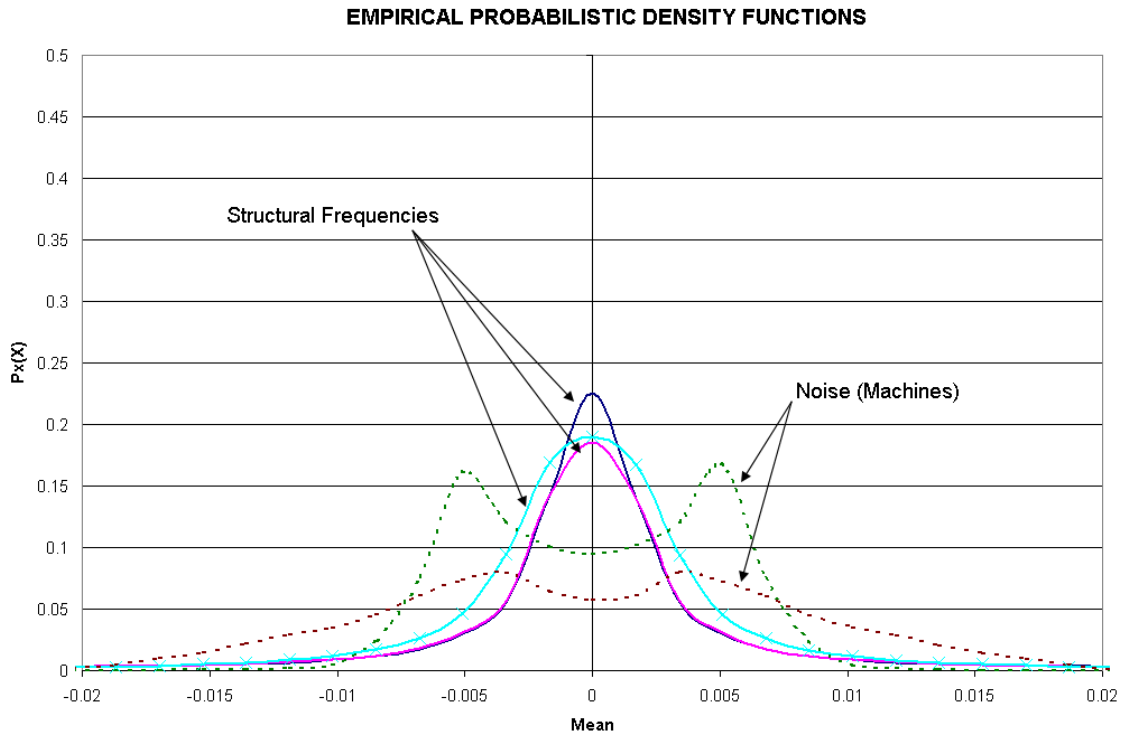


Figure 4-4 Typical Empirical Probabilistic Density Functions (epdf) for Structural Frequencies and Non-Structural Frequencies

For a continuous random variable X (i.e. acceleration, velocity or structural displacement), the probability density function (pdf) is:

$$p_X(x) = d \frac{\text{Prob}\{X \leq x\}}{dx} \quad 4-16$$

If the process is Gaussian the equation 4-16 becomes:

$$p_X(x) = \frac{e^{\left(\frac{-(x-\mu_X)^2}{2\sigma_X^2}\right)}}{\left(\sigma_X \sqrt{2\pi}\right)} \quad 4-17$$

Where:

$p_X(x)$: Probabilistic Density Function (pdf) for normal or Gaussian random variable.

μ_X : Mean

σ_X^2 : Variance

By attempting to identify the true real frequencies using only the output signals, the real pdf cannot be obtained. Therefore an approximately shape scale version of pdf or an empirical scale probabilistic density function is used.

For this reason it is assumed that “the TFR can be treated as a joint two-dimensional probability density function” [98]. In this way, only the truly positive TFRs and its normalized version by applying the expression 4-13 is used.

The negative values in most of the TFRs really limit its application like pdf. For overcoming this limitation we proposed here to use an empirical-shape probabilistic density function based mainly on the concept that the frequency distribution in a bandwidth has approximately the shape of a scale version of pdf.

With this concept in mind, a normalized frequency distribution (histogram) around any frequency of interest can be constructed, since only the shape of the pdf is important and not its real values. This approach is extremely useful and practical.

Therefore, for each frequency of interest the following procedure is proposed:

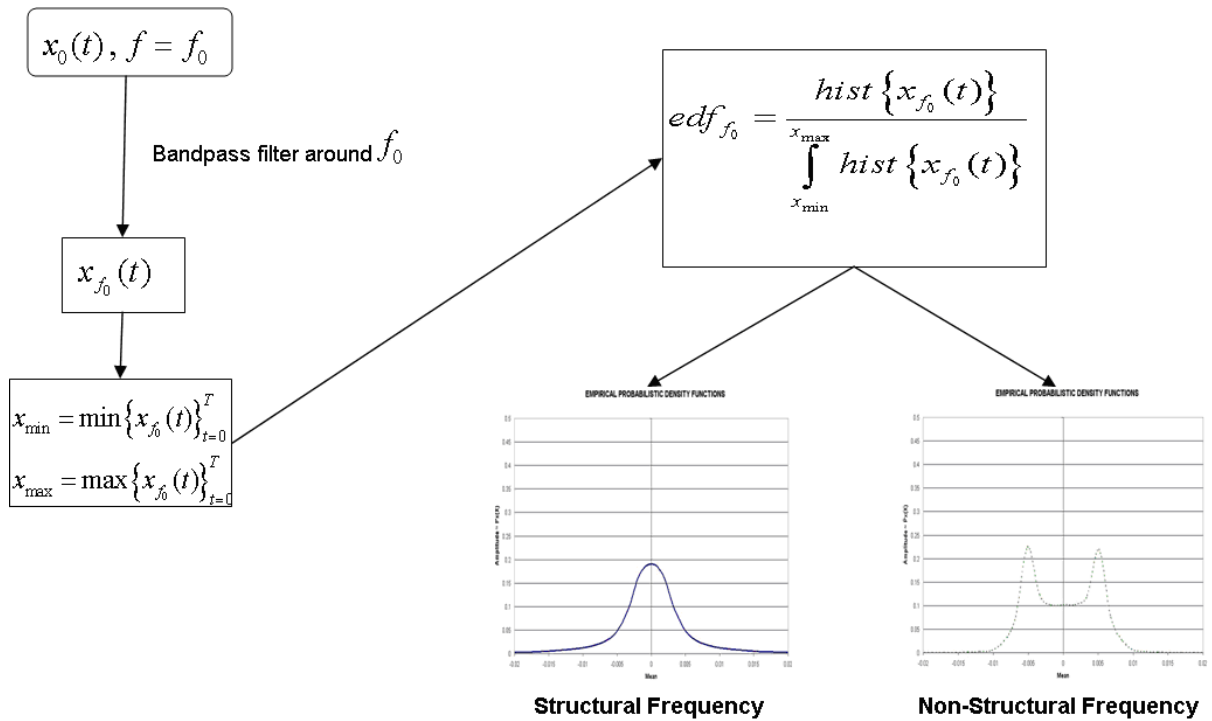


Figure 4-5 Determination of Non-Structural frequency from Empirical Probabilistic Function Shapes

Here it is important to point out that the marginal properties of the TFR can be used in order to acquire a near to real pdf, but because the final result do not improve significantly the method by using the direct time history is preferred.

As it can be seen, a priori a Gaussian distribution is assumed for the precedent procedure. This distribution has been accepted for many years. It has been demonstrated theoretically and experimentally that it has a good performance for random vibration of structures [193]. However, other types (i.e. shapes) of the probability density functions of common use in signal analysis or random vibration can be used [191] (i.e. for wind response non-Gaussian models are frequently used [207], because Gaussian models can underestimate the response [208]).

In signal processing and noise reduction, the other probability density functions such as [191, 206] Multivariate Gaussian Probability Distribution, Mixture Gaussian, Poisson Probability Distribution, Gamma Distribution, Rayleigh Probability Distribution, Laplacian Probability Distribution are frequently used.

The important thing to remember is that regardless of the probability density function chosen, the output signal shall have a shape similar to the original probability density function for any particular frequency, when this frequency is a real structural frequency and have a non-original probability density shape for external frequencies (i.e. non-structural frequencies). Thus the major strength of this “shape” method may be in the fact that, according to random vibration theory, the probability density function of the output signal, for any system is the same as the probability density function of the input signal [191, 205, 206].

If the probability distribution is unknown for the input signals, then probability distribution for our output signals is also unknown. The inaccuracy theory can be used in order to get the unknown probability distribution shape, this theme is not considered here and interested readers can find further information in the references [179, 181].

When the two previous methods fail to determine which of the identified frequencies corresponds to the true system frequencies, one alternative would be the use of coefficient of excess. Values closer to zero for this coefficient indicate that the frequency is a structural response mode, values greater than zero is obtained for non-structural frequencies [193]

It is proposed to evaluate the excess coefficient for TFR by using a lattice frequency of the TFR plane :

$$\gamma(f_0) = \frac{\frac{1}{k} \sum_{i=1}^k \left(P(t_i, f_0) - \frac{1}{k} \sum_{j=1}^k P(t_j, f_0) \right)^2}{\sigma_{P(t, f_0)}^2} - 3 \quad 4-18$$

Where:

$\gamma(f_0)$: Excess coefficient for TFR at the frequency f_0 .

$P(t, f_0)$: Lattice at frequency f_0 for the Time-Frequency Representation

$\sigma_{P(t, f_0)}$: Standard deviation of the Lattice at frequency f_0 for the Time-Frequency Representation.

Using the equation 4-18, a graph can be plotted with all excess coefficients for each frequency of TFR and from this graph evaluate which of these frequencies are or not truly system frequencies.

Finally, discharging the non-structural frequencies from the vector obtained using the Mean Time-Frequency Representation (equation 4-15), eigenvalues matrix can be found by using:

$$[\Lambda] = \begin{bmatrix} \cdot & & & \\ & \cdot & & \\ & & \lambda_i & \\ & & & \cdot & \cdot & \cdot \end{bmatrix} \quad 4-19$$

Where:

$[\Lambda]$: Diagonal matrix with the structural eigenvalues

$$\lambda_i = \omega_i^2 = (2\pi f_i)^2$$

4.4.4 Modal Coupling and Frequency Separation

Although the previous procedures can reliably extract the non-structural frequencies of the system, a last threat that will obscure the identification is the close modes or similar frequencies.

The main problem of close frequencies is the fact that it may or may not be truly system frequencies. There is a high probability that we can identify all close frequencies as system frequencies and the prediction will fail because of that.

If structure or the input signals is known, the close frequencies separation is possible, because any simple information is useful. For example, for input-output systems a robust method for closely-spaced modes separation based on Singular Value Decomposition (SVD) and Signal Subspace Correlation (SSC) has been proposed in the reference [196].

Unfortunately, for this case the structural information or the input signals are not known. Therefore, it can not be mathematically demonstrated if two very close frequencies that appear like structural frequencies correspond to two separate modes or only to one mode with a wander frequency. Similar cases are presented in echo separation in radar and speech signals [206].

For example what would be the answer about the number of frequencies in the Power Spectra of the output signal of the MDOF in Figure 4-6.

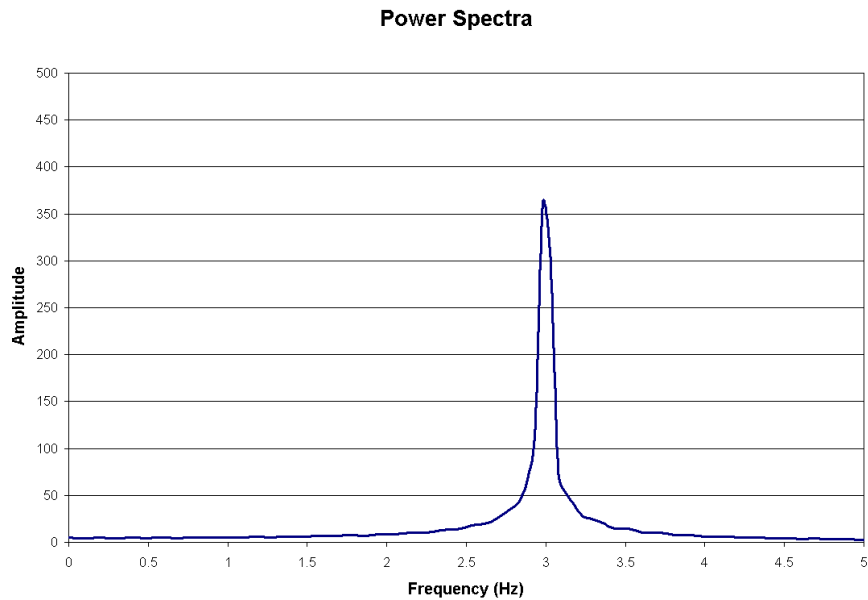


Figure 4-6 Power Spectra for a Coupling MDOF system

The answer is may be one frequency: 3 Hz., although it is true, the system is MDOFs and it has another close-space mode or coupled mode.

Usually, coupled modes are coupled in frequency but not in time (at least not coupled at all time instants), thus in the time-frequency plane the frequency changes in a coupled system.

When these changes are medium or large, it is easy to do the system identification and separation using time-frequency methodologies, because as can be seen in the previous chapters the time-frequency analysis is a useful methodology to deal with this.

However, when the changes are very small the problem of modes separation arise. Figure 4-7 shows, the time-frequency representation of the same structure. A highly coupled frequency system has been adopted intentionally.

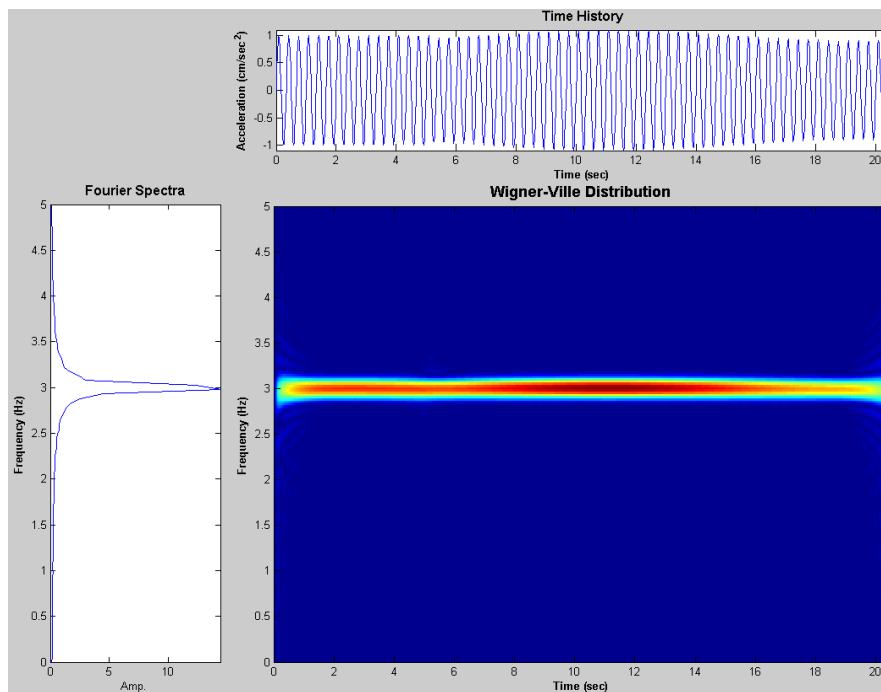


Figure 4-7 Wigner-Ville Distribution of Closely-Spaced Coupled Structure

From the Figure 4-7, it is clear that time-frequency analysis do not append any additional information about the system.

In order to deal with this problem, an interesting alternative is the use of adaptive kernels in the TFRs [130-132, 137, 157, 178]. Other approaches based on time-scale analysis (wavelets) has been also proposed.

A method based on mode separation using warping techniques in the time-frequency plane has been recently proposed in the reference [197]. The method is similar to empirical mode decomposition (EMD) proposed by Huang et. al. [73] in the time domain, and performs satisfactory when the modes are not very close or the structural properties are known.

In this research, a simple but very practical procedure based on the results of Cepstrum analysis [198] and the evaluation of the partial marginals of time-frequency distribution has been proposed.

Because it is very often that the structure has coupling in the frequency domain but not in the time domain (or at least not in all time instants), close modes are coupled in frequency but not necessarily in all time instants. Thus a method that allow separation of modes in time can be used.

A widely used method in radar, sonar, speech separation and seismology is the Cepstrum Analysis [198], the basic idea is to perform an inverse Fourier transformation of the natural logarithm of the Fourier transform of the signal. Therefore, the complex Cepstrum is defined by [122, 198]:

$$y_{cc}(\tau) = \frac{1}{2\pi} \int_{-\pi}^{\pi} \ln \left(\int_{-\infty}^{\infty} x(t) e^{-2\pi j\omega t} dt \right) e^{j\omega\tau} d\omega \quad 4-20$$

The complex Cepstrum provides a transformation in a new domain defined by a horizontal axis namely “quefrequency” and amplitude Cepstra, namely “gamnitude”.

In the literature of Cepstrum analysis other terms like “rahmonics”, “lifter”, saphe” are often used, (i.e. frequency = quefrequency, harmonics=rahmonics, filter= lifter) “*obtained basically by reversing the phoneme of the first syllable of the normal word*” [193].

The advantages of the Cepstrum is that it is possible to detect the separations of very close “rahmonics” in the signal and with this information the close mode in the structural system will be discriminated, using the partial marginals of time-frequency plane evaluated between rahmonics.

The above characteristic of Cepstrum Analysis has been used widely. For example, in seismology, to detect the time arrivals for compress waves and its reflect waves [199], in structures for detection of damage using ultrasonic reflection [200], in speech and radar to pitch and echo detection, respectively [198]

Once the quefreny for each rahmonic has been detected, the partial marginal to the time-frequency representation can be applied in order to get the “hidden” structural frequencies using:

$$\int_{-\infty}^{+\infty} P_x(t, f) dt = |X(f)|^2 \quad 4-21$$

For example, by taking the signal from figures 4-6 and 4.7, and applying the equation 4-20 the Cepstra plot is obtained as shown in the Figure 4.8.

From the Figure 4-8, it is clear that the cepstrum analysis can be used to detect a clear disturbance in the signal produced by uncoupling the structure in the time domain.

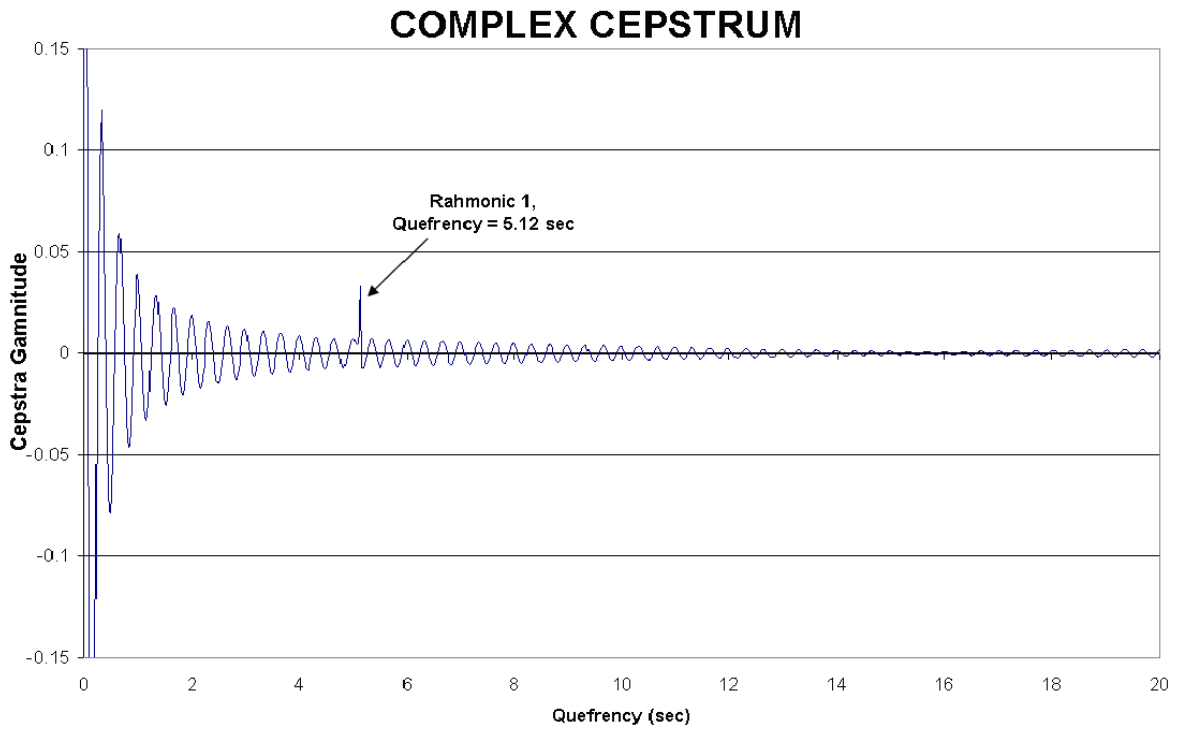


Figure 4-8 Complex Cepstrum

Therefore, the partial frequency marginal for Wigner-Ville Distribution can be evaluated by using the Cepstra information as shown in Figure 4-7, thus the marginal is evaluated from 0 to 5.12 secs and the marginal from the 5.12 sec to the end of signal, as shown in the Figure 4-9:

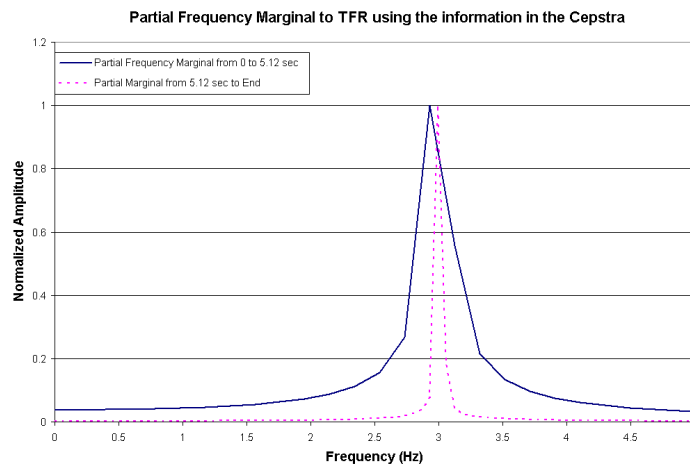


Figure 4-9 Partial Frequency Marginal for TFR using the information in the Cepstra

Now it is clear that the structure has two frequencies. From Figure 4-9 the values at 2.95 Hz and 3 Hz can be obtained.

The additional frequencies obtained with this method can be added to previously identified frequencies (eigenvalues defined in equation 4-19).

It is important to point out that the additional frequencies detected using Cepstrum analysis and TFR do not support the test procedures from the section 4.4.3. Thus if the dominant frequency (3 Hz in this case) is reported as a true structural frequency, it is highly possible that the close-spaced frequency will be identified as a structural frequency also, although it is not necessarily certain.

In order to have the most reliable identification, any information regarding the structure or the input signal will be very useful, but according to the objectives it is prohibited in this research.

4.4.5 Mass, Stiffness and Damping Matrices Estimation

Once the system frequencies have been evaluated, the next step would be the estimation of mass, stiffness, and damping matrices of the structure.

As it was mentioned previously there are a number of methods that do this. However the most of them use input signals and models updating [103-105].

A method based on the Frequency Domain Decomposition (FDD) proposed by Brincker et. al [124] has been selected and this method has been improved by using the information content in the Time-Frequency plane.

The complete theoretical background of FDD has been presented in the reference [124]. It is pointed out that, according to Brincker, the Singular Value Decomposition (SVD) of the spectral matrix is decomposed into auto spectral density functions for each DOF.

The decomposition of the spectral matrix into auto spectral density functions for each DOF has also been reported in the works by Chern [196]. As previously discussed, one can use the SVD to closely-spaced mode separation in the time-domain.

The Singular Value Decomposition (SVD) is actually a routine procedure and many numerical programs have the algorithm to do this. For example, in MatLab [122, 125] the procedure is performed using the single `svd()` command. It is because the algorithms of the LAPACK group are included in MatLab computer program.

The estimative of the power spectral density matrix can be obtained using the Fourier transform of the correlation function or approximately using the product of the Fourier transforms of the signal and the complex conjugation of the signal Fourier transform. However, this simplification do not fulfill the periodic constraint of Fourier Transform as has been mentioned in the reference [194]:

$$\left[G_{yy}(j\omega) \right] = \{ X(\omega) \} \{ X^*(\omega) \}^T \quad 4-22$$

Where:

$\left[G_{yy}(j\omega) \right]$: Estimate of power spectral density matrix

$\{ X(\omega) \}$: Fourier transform of $x(t)$, superscript asterisk implies complex conjugation.

Using the Brincker's notation, the power spectral density matrix can be decomposed using the SVD in the form [124] :

$$[G_{yy}(j\omega_i)] = [U_i][S_i][U_i]^H \quad 4-23$$

Where:

$[U_i]$: Unit matrix with singular vectors, (H) denotes complex transpose conjugation.

$[S_i]$: Diagonal matrix with scalar singular values:

Expand [U]:

$$[U_i] : [\{u_{i1}\} \{u_{i2}\} \dots \{u_{im}\}] \quad 4-24$$

Where:

$\{u_{i1}\}$: Singular vector.

It has been proven by Brincker [124] that an estimation of the scale mode shape corresponding to any structural frequency can be obtained from the first singular vector, so:

$$\{\phi_i\} = \{u_{i1}\} \quad 4-25$$

By taking the system frequency values that have been identified using MTFR, and applying the equations 4-19, and 4-22 to 4-25, an estimation of the scale eigenvector matrix or modal matrix can be constructed for the structure with the following form:

$$[\Phi] : [\{u_{11}\} \{u_{21}\} \dots \{u_{m1}\}] \quad 4-26$$

It has been pointed out that the quality of the estimation of the scale modal matrix is strongly dependent of the resolution in the estimation of the structural frequencies [194, 195].

Since the direct information of MTFR plane is been used, an excellent time-frequency resolution and therefore an excellent modal shape resolution is assured.

It is assumed normal modes with classical damping and using the orthogonal properties of the mass and stiffness matrix [127]:

$$\begin{aligned} [\Phi][M][\Phi]^T &= [I] \\ [\Phi][K][\Phi]^T &= [\Lambda] \end{aligned} \quad 4-27$$

Because up to this point the estimative eigenvalue matrix (equation 4-19) and the estimation of the eigenvector matrix (equation 4-26) are available, from the precedent equation the estimation of the mass and stiffness matrix become:

$$\begin{aligned} [M] &= [\Phi]^{-1} [I] \left[[\Phi]^T \right]^{-1} \\ [K] &= [\Phi]^{-1} [\Lambda] \left[[\Phi]^T \right]^{-1} \end{aligned} \quad 4-28$$

Although the equation 4-28 is useful to predict the stiffness and mass matrix, it has the problem that is data-dependent and, in general, produce matrices with the following characteristics:

- Mass and Stiffness matrix are symmetric
- It is real value matrices
- Mass and stiffness values do not have any physical meaning.
- Mass can take negative values, corroborating that it does not have any physical meaning.

- Mass and stiffness values estimated from different time histories are not equal, even if the structures do not have any changes (i.e. damage or mass changes), so they are data-dependant.

A short explanation of the previously controversial characteristics is been given.

Because by using MTFR-FDD only one of the infinite possible solutions for the eigenvalue problem defined by equation 4-3 has been found:

$$[[K] - \lambda_i [M]] \{\phi\}_i = \{0\}$$

Any pairs of the stiffness and mass matrix that satisfies the equation 4-3 are the solution of the problem. Because the estimative are signal-dependent, it changes when the signal changes.

In fact, when the structural engineers defined the material properties (i.e. Young modulus, shear strength, poisson ratio, mass), geometry properties (i.e. inertia, area), they constructed a particular stiffness and mass matrix for their structure, and with this they found a pair of eigenvalues (frequency) and eigenvector (modes) using the above expression (equation 4-3), so they have pre-defined a particular solution to the problem.

Therefore, again it is clear that the particular mass and stiffness matrices used by structural engineers are only one of the infinite possible solutions, and any other pairs of mass and stiffness matrices that fulfill the equation 4-3 are equivalent systems, consequently the “perfect” finite element model is only one of the infinite equivalent structures that satisfys the eigenvalue problem.

But then, which of these infinite possible domain solutions are the correct one? Mathematically the answer is easy: All of them!

Remember, the “perfect” and largely extensive finite element model is also an estimation of a real structure, and very often (almost always) a very poor estimative [13, 14, 17, 18, 26, 27, 70, 104, 119, 148]. Note that the structural engineers only have an approximate idea of the real values of material properties, geometry, mass, load distribution and structure boundary conditions.

The key for damage detection using ambient vibration signals with MTFR-FDD is whatever the solution; all of them differ in a scale or proportional factors (i.e. the scale factor between model or “real” modes and any particular solution).

Therefore, if the mass is unchanged, any possible change in the frequencies and modes shapes is due to stiffness change. Note that the damping factors are very small and it does not contribute to frequency changes in the ambient vibration conditions.

The mass and stiffness matrices estimated by using the equation 4-28 in two different time histories are different because the power spectral density matrices are similar but not equals, it is a scale version of one to another.

If the mass is unchanged an approximate scale or transformation matrix can be defined in order to relate the two different identification results for real signals cases.

Here a simple but very consistent scale matrix is proposed:

$$\left[\widetilde{SM} \right] = \left[M_0 \right] / \left[M_1 \right] \quad 4-29$$

Where:

$[\widetilde{SM}]$: Scale matrix between two different system identification results.

$[M_0]$: Mass matrix estimated using the data set zero (i.e. before of damage)

$[M_1]$: Mass matrix estimated using the data set one (i.e. after of damage)

$\overline{[M_0]/[M_1]}$: Scalar division (term by term) between mass matrices $[M_0]$ and $[M_1]$

Therefore, any particular term of the matrix $[SM]$ will be obtained by scalar division:

$$\widetilde{sm}_{i,j} = \frac{m_{0,i,j}}{m_{1,i,j}} \quad 4-30$$

Once the scale matrix has been evaluated, a corrected stiffness matrix will be obtained using:

$$[Kc_1] \cong \overline{[K_1]/[SM]} \quad 4-31$$

Where:

$[\widetilde{SM}]$: Scale matrix between two different system identification results.

$[K_1]$: Stiffness matrix estimated using the data set one (i.e. After of damage)

$[Kc_1]$: Stiffness matrix included correction for data set differences

$\overline{[K_1]/[\widetilde{SM}]}$: Scalar division (term by term)

Again, the corrected particular values of the matrix $[Kc_1]$ can be obtained by scalar division:

$$kc_{1,j} = \frac{k_{1,j}}{\widetilde{sm}_{i,j}} \quad 4-32$$

Finally, any damage in the structure will be detected by using:

$$\Delta k_{i,j} = \frac{|k_{0,i,j} - kc_{1,j}|}{k_{0,i,j}} \quad 4-33$$

According to the numerical and experimental tests, the approximate correction for scale (equation 4-29) produced errors between 0% to 2%. Therefore, the minimum damage detection threshold for events that produce changes in the stiffness is at 2%.

Practical recommendation about record length and field measurements is given in order to improve the reliability of this damage detection procedure.

The final aspect in identification is the damping estimation. Since dealing with ambient vibration signals, it is expected that damping will take very low values, for this reason it was not taken into account for the MTFR-FDD method of damage detection using ambient vibration signals.

However, if there is any interest in damping factor for ambient vibration conditions, any method previously proposed in the literature or the damping estimative based on MTFR that is proposed in this research can be used.

Using FDD, Brincker [124] has proposed an estimation of damping using the logarithm decrement method of a time lag-history obtained by inverse Fourier transform of SDOF bells

estimated from mean power spectral density. In the reference [195] numerical results for this method has been presented.

A method for damping estimation using time-frequency information has been reported by one of the most active research group in time-frequency theory for civil engineer applications; the method is based mainly on the instantaneous amplitude ratio and phase ratio estimation. The theoretical background including numerical and real cases studies, for these types of time-frequency based estimators can be found in the references [69, 71, 72, 74, 75, 77, 78, 87, 93]

A method based on the detection of time intervals is proposed when one modal component is dominating. A similar approach has been proposed recently by Ceravolo [87] using instantaneous estimators.

The method for damping estimation can be synthesized in the following steps:

- Determine the structural frequencies using MTFR (section 4.4.2)
- Extract any non-structural frequencies (section 4.4.3)
- Filter the output signals using band-pass between system frequencies with an bandwidth less than $0.2f$
- Using a reduced interference time-frequency distribution, obtain the time intervals when this frequency component is dominating in the whole TFR plane (i.e. maximum TFR amplitude).
- Use random logarithm decrement techniques to obtain an estimation of the damping for each time interval.

In the chapter 5, some study-cases for this method is presented.

4.5 Numerical Simulations

In the following the results for damage detection method using numerical models with known properties are shown and some possible error sources and capability of this method is also studied.

It is assumed that ambient vibration data has been obtained before and after of strong event. Records during the event are not available (because this type of analysis is shown in the chapter 5).

It is compulsory that the records before and after the event has been taken at the same places (the same DOFs measurements points in both case is assumed). This assumption is one of the most important aspect of this method. Otherwise, the comparison scheme is not applicable.

Theoretically it is possible to do an interpolation procedure in order to estimate the outputs for unmeasured points (for the case when the measurements places change unintentionally).

First a structural model with known properties is defined and then this model is submitted to random vibration excitations at all DOFs and also at the supports.

In an attempt to simulate real conditions, the output signals are contaminated with Gaussian noise added with very low signal to noise ratio (SNR) (in fact, frequently less than normal conditions).

Using structural dynamic theory, the output signals of the model are evaluated. Using only these output signals (i.e. the initial set of measurements) and applying the method developed in this chapter, the structural parameter for the “unknown” undamaged model are estimated.

Next, damage to the mathematical model is generated (i.e. modifying the stiffness matrix) and submitting the modified model again to random vibration excitations. Then another set of output signals (i.e. the second set of measurements) is obtained and finally noise for these output signals is added.

The damage identification method is applied for estimating the structural parameters for the “unknown” damage model by using the second set of output signals.

It can be determined where and how much is the structural damage by comparing the undamaged stage identification with damaged stage identification.

The performance of this method and the possible error sources can be evaluated by comparing the results from the calculation damage of the method with the previous known damage.

4.5.1 Single Degree of Freedom Model

SDOF model is the most basic case. However, it has important practical applications for identifying damage in towers or inverted pendulum structures.

For this particular case, only the results obtained directly from the time-frequency plane can be applied. Noise effects and other sources of error are not considered here. It will be shown in the section 4.5.3.

The following structural values (in a compatible free unit system) are assumed:

M=1

K=100

Damping = 3% of the critical

Noise=10%

Sampling rate: 5 Hz

Sampling Length: 6.83 minutes

Number of Records:12

$$\omega = \sqrt{\frac{k}{m}}$$

$$\omega = 2\pi f$$

$$f = 1.5915 \text{ Hz}$$

$$SNR = 10\%$$

In the Figure 4-10 a typical 6.83 minutes record and its Fourier Transform is shown. The maximum value is obtained at 1.61 Hz, the difference between real frequency and frequency from the FFT is due to noise in the signal.

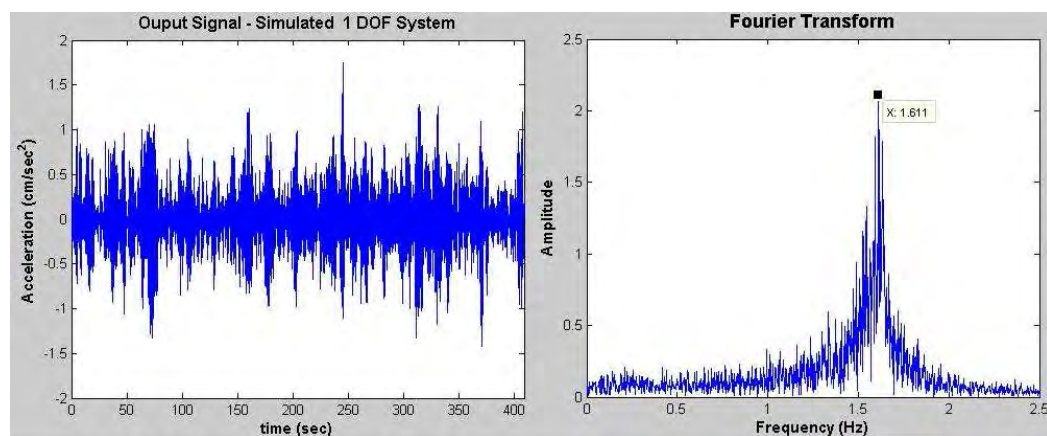


Figure 4-10 Typical output signal and its FFT for SDOF model

In the Figure 4-11 the Mean Time-Frequency Representation (MTFR) obtained for the first set of measurements (12 Records) using the equation 4-14 is shown

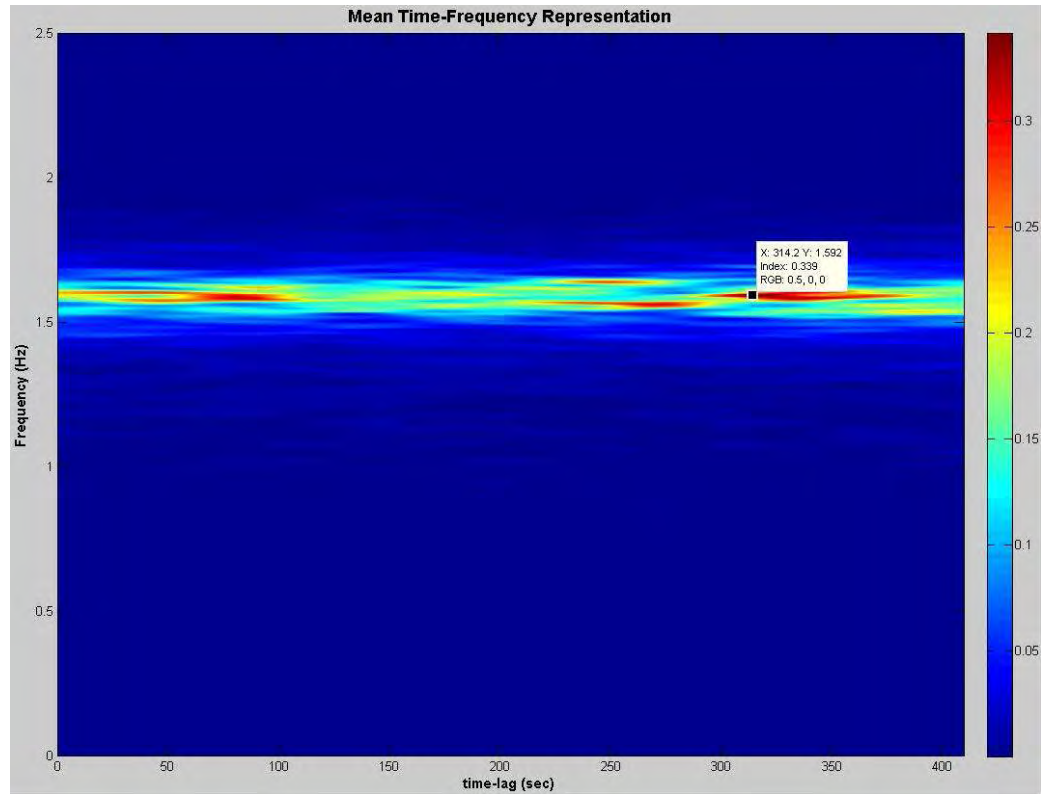


Figure 4-11 Mean Time-Frequency Representation for undamaged SDOF model

Using the equation 4-15, the maximum amplitude of MTFR can be evaluated and with it the corresponding frequency at $f = 1.592$ Hz which is practically the same as theoretical frequency.

If a mass unitary value is assumed, then the scale stiffness value can be obtained. Note that any value for the mass can be assumed. The important thing is that the assumed mass value is unchanged before and after damage:

$$f_0 = 1.592 \text{ Hz}$$

$$\omega_0 = 2\pi f_0 = 10.0028$$

$$\omega_0 = \sqrt{\frac{k_0}{m_0}} \Rightarrow k_0 = \omega_0^2 m_0$$

$$k_0 = 100.057$$

Next a physical damage to the structure is introduced by decreasing the stiffness by 50%. Then in order to make the identification procedure more challenging, the noise level (40%) is increased intentionally and a permanent equipment is introduced with a frequency exactly equal to undamaged structure, thus $f=1.5915 \text{ Hz}$ ($w=10 \text{ rad/sec}$).

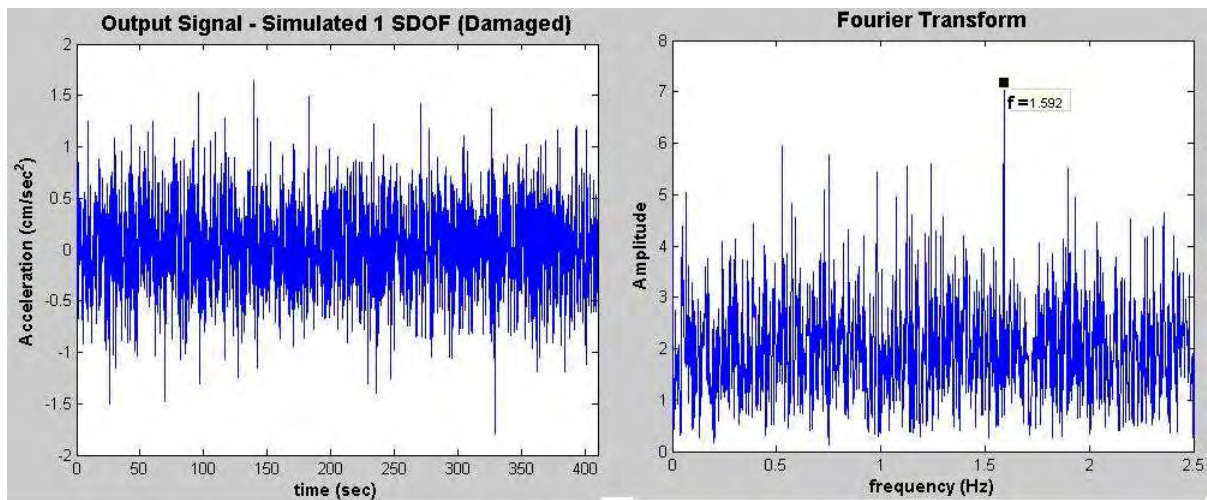


Figure 4-12 Typical output signal and its FFT for SDOF model

From the previous Figure, it can be seen that it is practically impossible to get the system frequencies and only one dominant peak at $f=1.592 \text{ Hz}$ appears (the machine frequency in this case).

Now the MTRF for the set of signals from the damage stage (12 Records) will be evaluated as it is shown in the following graph:

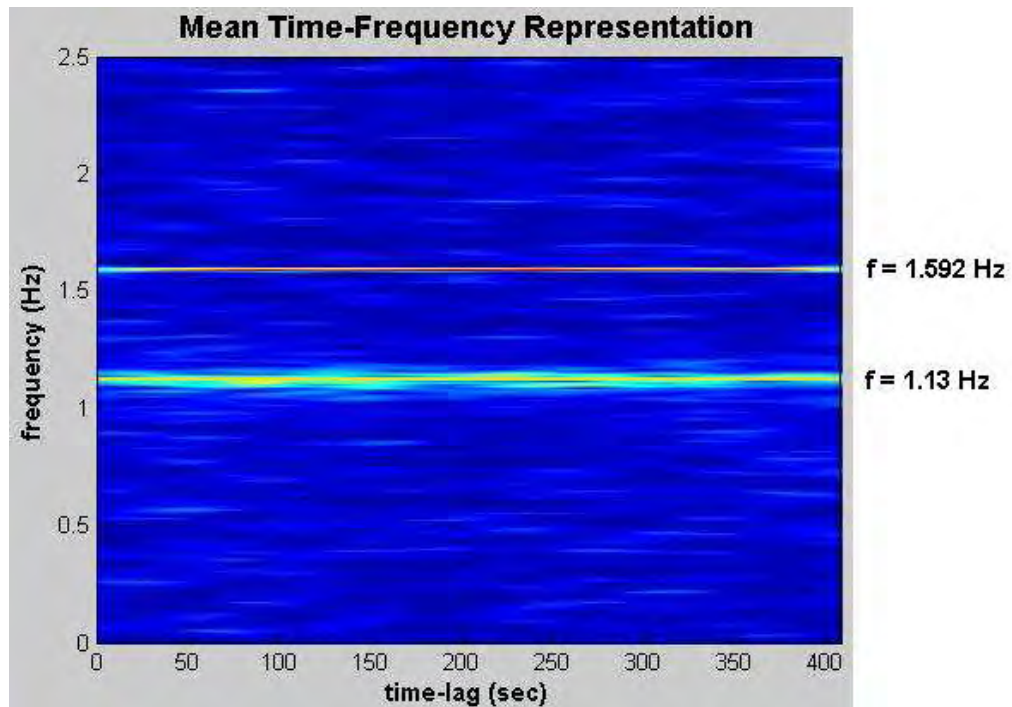


Figure 4-13 Mean Time-Frequency Representation for damaged SDOF model

From the Figure 4-13 two frequencies emerge, a dominant frequency at $f=1.592$ Hz and a second frequency at $f_2=1.13$ Hz.

If there is no information available about the structure, the first frequency can be interpreted wrongly because it is equal to undamaged frequency identified earlier.

Now the second or third method for frequency differentiation that has been proposed in the literal 4.4.3 can be applied in order to extract non-structural frequencies.

It is important to remember that the first method for extraction of non-structural frequencies is not useful here, because the equipment is permanent and does not make any changes in the time-frequency plane.

Evaluating the empirical probabilistic density function (epdf) with the proposed procedure in the Figure 4.5, it is clear that the real structural frequency is identified as $f=1.13$ Hz, see the Gaussian form of the epdf for this frequency and non-gaussian form for the frequency at $f=1.592$ Hz (Machine).

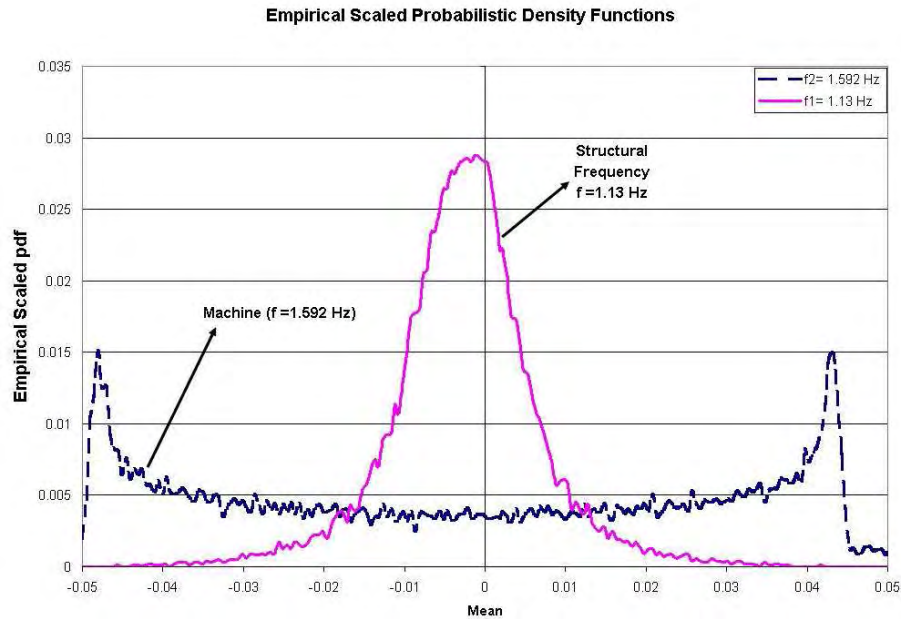


Figure 4-14 Empirical Probabilistic Density Function for damaged SDOF model

The new stiffness value by using the real structural frequency ($f = 1.13$ Hz) and the previous mass value ($m=1$) can be evaluated:

$$f_1 = 1.13 \text{ Hz}$$

$$\omega_1 = 2\pi f_1 = 7.099 \frac{\text{rad}}{\text{sec}}$$

$$\omega_1 = \sqrt{\frac{k_1}{m_1}} \Rightarrow k_1 = \omega_1^2 m_1$$

$$k_1 = 50.41$$

Finally, the damage (stiffness loss) using a simplified version of equation 4.33 is obtained:

$$\Delta k = \frac{|k_0 - k_1|}{k_0}$$

$$\Delta k = \frac{|100.057 - 50.41|}{100.057}$$

$$\Delta k = 49.63\% \text{ Vs Theoretical value (50\%)}$$

For this case the stiffness loss with an error of 0.7% was evaluated. This error is very low, considering that the noise level in the signal has been set for values much higher than the noise in normal conditions.

4.5.2 Multiple Degree of Freedom Models

In the evaluation of MDOF models, three models; a 3 DOFs structure, the benchmark ASCE problem with 12 DOFs [106-112], and a large structure of 30 DOF will be used.

4.5.2.1 A Three DOF Model

A structure with the following matrices is defined (in any consistent units):

$$[M] = \begin{bmatrix} 50 & 20 & 10 \\ 20 & 50 & 5 \\ 10 & 5 & 30 \end{bmatrix}$$

$$[K] = \begin{bmatrix} 1000 & -500 & -200 \\ -500 & 700 & 300 \\ -200 & 300 & 400 \end{bmatrix}$$

By solving the eigenvalue problem, the following frequencies and modal matrix are obtained:

$$\{f\} = \begin{Bmatrix} 0.3298 \\ 0.4742 \\ 1.1748 \end{Bmatrix} (\text{Hz})$$

$$[\Phi] = \begin{bmatrix} 0.0632 & -0.0503 & -0.1363 \\ 0.1067 & 0.0271 & 0.1082 \\ -0.0530 & -0.1605 & 0.0846 \end{bmatrix}$$

Taken the output signals (20 records of 10 minutes each, sampling rate=5Hz, Noise Level 15%), the structural frequencies using the MTFR can be identified:

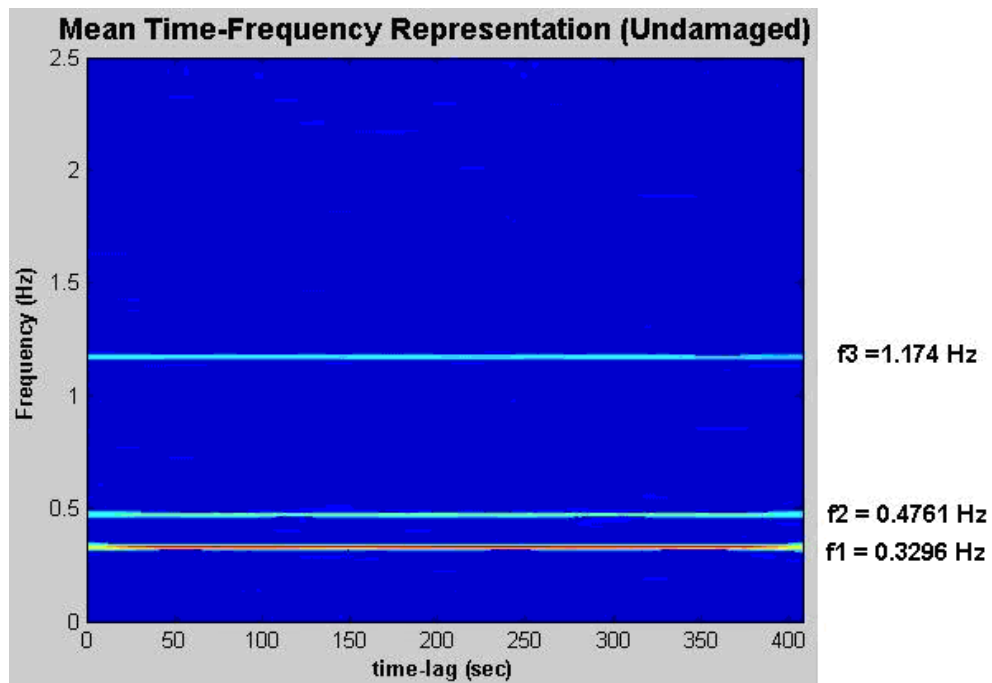


Figure 4-15 Mean Time-Frequency Representation (Undamaged) 3 DOFs model

For this set of signal using the eigenvalues from MTFR and applying FDD the following scale version of stiffness matrix for undamaged stage can be obtained:

$$[K_0] = \begin{bmatrix} 34.5100 & -21.3208 & -8.7114 \\ -21.3208 & 22.8500 & 11.2767 \\ -8.7114 & 11.2767 & 13.0029 \end{bmatrix}$$

Now by generating punctual damage in the DOF number 3 of 30%, the theoretical frequencies and modes are obtained:

$$[M] = \begin{bmatrix} 50 & 20 & 10 \\ 20 & 50 & 5 \\ 10 & 5 & 30 \end{bmatrix}$$

$$[K] = \begin{bmatrix} 1000 & -500 & -200 \\ -500 & 700 & 300 \\ -200 & 300 & \underline{280} \end{bmatrix}$$

$$\{f\} = \begin{Bmatrix} 0.2966 \\ 0.3965 \\ 1.1662 \end{Bmatrix} (Hz)$$

$$[\Phi] = \begin{bmatrix} -0.0396 & 0.0685 & -0.1373 \\ -0.1057 & 0.0229 & 0.1101 \\ 0.1171 & 0.1259 & 0.0786 \end{bmatrix}$$

For this modified structure, a new set of output measurements is simulated by applying random excitation (Noise Level=30%) and with these output signals the new estimative of the structural properties will be obtained. The frequencies (and its eigenvalues) will be obtained using MTFR, the estimative for the modes shapes will be obtained using FDD (equations 4-22 – 4.24) and by applying the equation 4-26 a estimative of the stiffness matrix will be obtained.

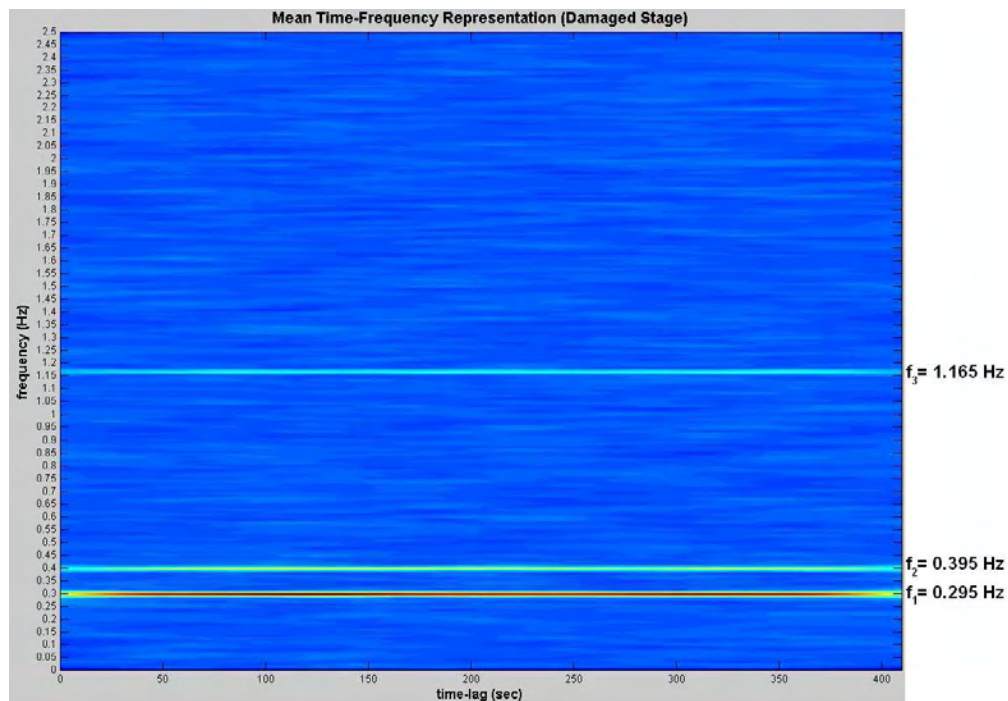


Figure 4-16 Mean Time-Frequency Representation (Damage Stage) 3 DOFs model

$$[K_1] = \begin{bmatrix} 33.4100 & -20.5115 & -8.8023 \\ -20.5115 & 23.4642 & 10.3449 \\ -8.8023 & 10.3449 & 9.3299 \end{bmatrix}$$

Now by comparing the identified stiffness matrix for undamaged and damaged stage and using the equation 4-33, the changes in stiffness matrix term by term can be evaluated thus the damage in the structure.

$$\Delta k_{i,j} = \frac{|k_{0,i,j} - kc_{1,i,j}|}{k_{0,i,j}}$$

$$[\Delta K] = \begin{bmatrix} -3.1875 & -3.7959 & 1.0428 \\ -3.7959 & 2.6882 & -8.2626 \\ 1.0428 & -8.2626 & -28.2479 \end{bmatrix} \text{ (Values in percentage)}$$

The above matrix implies that by using the output signals a stiffness loss in the DOF number 3 equal to 28.25% can be estimated (relative error of 5% in the estimative for this case).

Note that although there were no changes for the other values in the stiffness matrix, from the damage detection algorithm, it appears that others DOF were affected. This is useful because this damage propagation effect can be used to detect the approximate localization of the damage.

In real cases, the damage generally affects several members (one or numerous zones of the structure). Therefore, a number of stiffness matrix elements will be affected. Consequently the estimative matrix will perform in a real-like manner contrary to our punctual matrix assumption.

4.5.3 The Phase I – IASC-ASCE Structural Health Monitoring Benchmark Problem

According to preceding results, by applying this methodology to Phase I of IASC-ASCE Structural Health Monitoring Benchmark Problem and compare the performance of the approach with previous benchmark result reports [41, 106-112].

The Benchmark Problem is a study proposed by IASC-ASCE in 2000 for system identification and damage detection, Phase I consists of two analytical models; the first one with 12 DOFs, and the second one with 120 DOFs, a complete review of the Benchmark problems, its description and structural properties, can be found in the references [106, 107].



Figure 4-17 ASCE Benchmark model in University of British Columbia
(taken from: <http://mase.wustl.edu/wusceel/asce.shm/structure.htm>)

Six damage patterns for this building has been proposed in the Phase I of Benchmark problem[107]:

- (i) No stiffness in the 1st floor braces
- (ii) No stiffness in 1st floor braces and no stiffness in 3rd floor braces
- (iii) No stiffness in one 1st floor brace
- (iv) No stiffness in one 1st floor brace and no stiffness in one 3rd floor brace
- (v) No stiffness in one 1st floor brace and no stiffness in one 3rd floor brace and beam-column connection weakened.
- (vi) 2/3 of the stiffness in one 1st floor brace

For the 12 DOFs model, there are no differences between the cases (iv) and (v) therefore the Benchmark problem is reduced to 5 cases.

The procedure for damaged detection in all patterns is:

- 1) Using the “datagen” program provided by the IASC-ASCE benchmark task group (<http://mase.wustl.edu/wusceel/asce.shm/structure.htm>), noise output data for the undamaged stage and for the six damage cases will be generated.
- 2) Using only the output signals and applying MTRF and FDD, the structural frequencies, modal shapes , mass and matrix for undamaged and damaged stages will be identified.
- 3) The damage will be estimated by comparing the stiffness matrix for undamaged and damaged stages.
- 4) Finally, a comparison between the estimative damage with theoretical damage [107] will be made.

The following Figure was taken directly from reference [107], the general geometry and the aforementioned cases are shown:

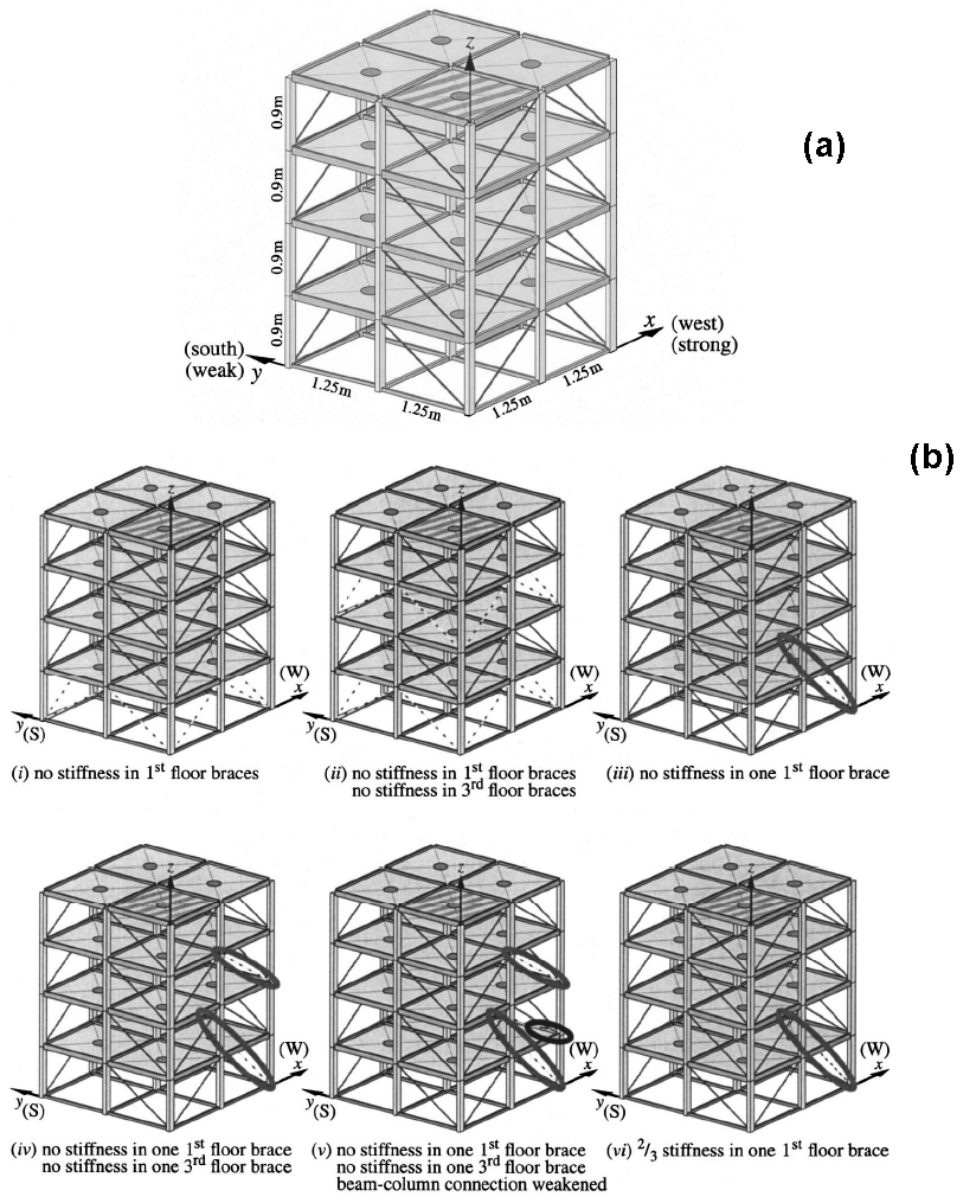


Figure 4-18 ASCE Benchmark problem (a) Geometry (b) Damage patterns (taken from reference [107])

Next, the first damage pattern is shown in detail, for the additional patterns only graph and tables resume result are shown.

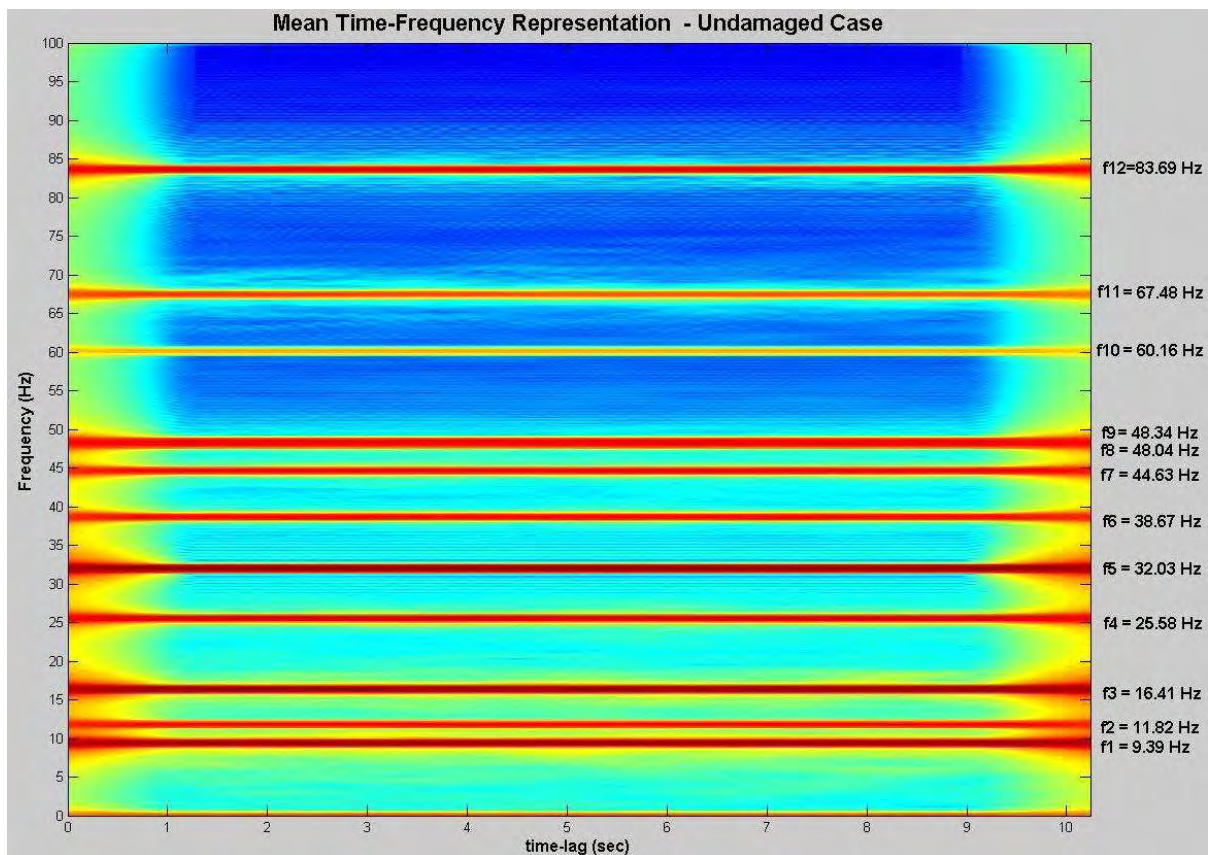


Figure 4-19 Mean Time-Frequency Representation for ASCE Benchmark problem

In Figure 4-19, the fundamental frequencies are estimated using the MTFR of 320 records of 2048 data each one (sampling rate 200 Hz), as can be seen the noise is spread in all time-frequency domain and the fundamental frequencies emerge clearly.

Using FDD with this eigenvalues constraint, an estimative of the structural mode shapes is obtained and by using the equations 4-26 the mass and stiffness matrices for the undamaged case is evaluated:

TABLE 4.1 Estimative for undamaged case – Phase I – ASCE Benchmark problem

K estimative (Undamaged)												K theoretical (Undamaged)											
1	2	3	4	5	6	7	8	9	10	11	12	1	2	3	4	5	6	7	8	9	10	11	12
83130	0	0	-4270	0	0	0	0	0	0	0	0	213.2	0	0	-106.6	0	0	0	0	0	0	0	0
0	52940	0	0	-27200	0	0	0	0	0	0	0	0	135.81	0	0	-67.9	0	0	0	0	0	0	0
0	0	160830	0	0	-82070	0	0	0	0	0	0	0	0	464.04	0	0	-232.02	0	0	0	0	0	0
-4270	0	0	84330	0	0	-42410	0	0	0	0	0	-106.6	0	0	213.2	0	-106.6	0	0	0	0	0	0
0	-27200	0	0	53730	0	0	-27000	0	0	0	0	0	-67.9	0	0	135.81	0	0	-67.9	0	0	0	0
0	0	-82070	0	0	162630	0	0	-84840	0	0	0	0	0	-232.02	0	0	464.04	0	0	-232.02	0	0	0
0	0	0	-42410	0	0	84840	0	0	-42340	0	0	0	0	0	-106.6	0	0	213.2	0	0	-106.6	0	0
0	0	0	0	-27000	0	0	54040	0	0	-26960	0	0	0	0	0	-67.9	0	0	135.81	0	0	-67.9	
0	0	0	0	0	-81840	0	0	163500	0	0	-81520	0	0	0	0	0	-232.02	0	0	464.04	0	-232.02	
0	0	0	0	0	0	-42340	0	0	41950	0	0	0	0	0	0	0	0	-106.6	0	0	106.6	0	
0	0	0	0	0	0	0	-26960	0	0	26730	0	0	0	0	0	0	0	0	0	-67.9	0	67.9	
0	0	0	0	0	0	0	0	-81520	0	0	81040	0	0	0	0	0	0	0	0	-232.02	0	232.02	

Mass estimative (All cases)												M theoretical (Undamaged)											
1	2	3	4	5	6	7	8	9	10	11	12	1	2	3	4	5	6	7	8	9	10	11	12
13445	0	0	0	0	0	0	0	0	0	0	0	3452.4	0	0	0	0	0	0	0	0	0	0	0
0	13441	0	0	0	0	0	0	0	0	0	0	0	3452.4	0	0	0	0	0	0	0	0	0	0
0	0	13245	0	0	0	0	0	0	0	0	0	0	0	3819.4	0	0	0	0	0	0	0	0	0
0	0	0	10593	0	0	0	0	0	0	0	0	0	0	0	2652.4	0	0	0	0	0	0	0	0
0	0	0	0	10594	0	0	0	0	0	0	0	0	0	0	0	2652.4	0	0	0	0	0	0	0
0	0	0	0	0	10582	0	0	0	0	0	0	0	0	0	0	0	2986.1	0	0	0	0	0	0
0	0	0	0	0	0	10796	0	0	0	0	0	0	0	0	0	0	0	2652.4	0	0	0	0	0
0	0	0	0	0	0	0	10796	0	0	0	0	0	0	0	0	0	0	0	2652.4	0	0	0	0
0	0	0	0	0	0	0	0	10774	0	0	0	0	0	0	0	0	0	0	0	2986.1	0	0	0
0	0	0	0	0	0	0	0	0	0.7246	0	0	0	0	0	0	0	0	0	0	0	1809.9	0	0
0	0	0	0	0	0	0	0	0	0	0.7247	0	0	0	0	0	0	0	0	0	0	0	1809.9	0
0	0	0	0	0	0	0	0	0	0	0	0.7313	0	0	0	0	0	0	0	0	0	0	0	2056.3

As can be seen from Table 4.1, the structure of the estimate mass and stiffness matrices are perfect, however the values are not equal (mass differ in a factor of 350~400 depending of the DOF and stiffness in a factor of 2500~2800).

Since the theoretical undamaged matrix is not known, the scale factors can not be evaluated. Therefore for damaged detection cases, the estimative stiffness matrix will be taken from Table 4.1, like the zero reference matrix.

Next the damage patterns 1 to 6 will be introduced and for each one using MTRF-FDD, the following stiffness matrix estimative will be obtained. By comparing each term with the original undamaged stiffness estimative matrix, the location and severity of the structural damage can be evaluated.

TABLE 4.2 Estimative for damage pattern 1 – Phase I – ASCE Benchmark problem

K estimative (Undamaged)												Estimate Stiffness Loss (%)											
1	2	3	4	5	6	7	8	9	10	11	12	1	2	3	4	5	6	7	8	9	10	11	12
83330	0	0	-4270	0	0	0	0	0	0	0	0	21.617	0	0	-2.08382	0	0	0	0	0	0	0	0
0	52940	0	0	-27200	0	0	0	0	0	0	0	0	33.869	0	-2.64706	0	0	0	0	0	0	0	0
0	0	160830	0	0	-82070	0	0	0	0	0	0	0	0	31.027	0	0	-2.71719	0	0	0	0	0	0
-4270	0	0	84330	0	0	-4240	0	0	0	0	0	-2.08382	0	0	1860145	0	-0.02358	0	0	0	0	0	0
0	-27200	0	0	53730	0	0	-2700	0	0	0	0	0	-2.64706	0	2.568398	0	0	-0.07405	0	0	0	0	0
0	0	-82070	0	0	162630	0	0	-81640	0	0	0	0	0	-2.71719	0	0	2.29355	0	0	-0.07349	0	0	0
0	0	0	-4240	0	0	84840	0	0	-42340	0	0	0	0	0	-0.02358	0	0	0.836869	0	0	-1.91308	0	0
0	0	0	0	-2700	0	0	54040	0	0	-26960	0	0	0	0	0	-0.07405	0	0	1.221318	0	0	-2.59644	
0	0	0	0	0	-81640	0	0	163500	0	0	-81520	0	0	0	0	0	-0.07349	0	0	1.131498	0	-2.42889	
0	0	0	0	0	0	-42340	0	0	41950	0	0	0	0	0	0	0	0	0	-1.91308	0	1.573302	0	
0	0	0	0	0	0	0	-26960	0	0	26730	0	0	0	0	0	0	0	0	0	-2.59644	0	2.543958	
0	0	0	0	0	0	0	0	-81520	0	0	81040	0	0	0	0	0	0	0	0	-2.42889	0	2.208788	

K estimative (Damage Pattern 1)												Theoretical Stiffness Loss (%), according to reference [107]											
1	2	3	4	5	6	7	8	9	10	11	12	1	2	3	4	5	6	7	8	9	10	11	12
65160	0	0	-43600	0	0	0	0	0	0	0	0	22.622	0	0	0	0	0	0	0	0	0	0	0
0	35010	0	0	-27320	0	0	0	0	0	0	0	0	35.513	0	0	0	0	0	0	0	0	0	0
0	0	100330	0	0	-84300	0	0	0	0	0	0	0	0	32.48	0	0	0	0	0	0	0	0	0
-43600	0	0	85730	0	0	-42400	0	0	0	0	0	0	0	0	0	0	0	0	0	0	0	0	0
0	-27320	0	0	5510	0	0	-27030	0	0	0	0	0	0	0	0	0	0	0	0	0	0	0	0
0	0	-84300	0	0	166360	0	0	-81700	0	0	0	0	0	0	0	0	0	0	0	0	0	0	0
0	0	0	-42400	0	0	85550	0	0	-43150	0	0	0	0	0	0	0	0	0	0	0	0	0	0
0	0	0	0	-27030	0	0	54700	0	0	-27660	0	0	0	0	0	0	0	0	0	0	0	0	0
0	0	0	0	0	-81700	0	0	165350	0	0	-83500	0	0	0	0	0	0	0	0	0	0	0	0
0	0	0	0	0	0	-43150	0	0	42610	0	0	0	0	0	0	0	0	0	0	0	0	0	0
0	0	0	0	0	0	0	-27660	0	0	27410	0	0	0	0	0	0	0	0	0	0	0	0	0
0	0	0	0	0	0	0	0	-83500	0	0	82830	0	0	0	0	0	0	0	0	0	0	0	0

From Table 4.2 it can be seen that for damage pattern 1 (No stiffness in the 1st floor braces), the MTRF-FDD method performs an excellent estimative of the damage in value and location, another important thing is that the method has errors in estimative for all DOFs around 2%.

For damage pattern 2 (No stiffness in 1st floor braces and no stiffness in 3rd floor braces), from Table 4.3 it can be seen that the method performs a good damage estimative in location and value, with a mean error in damage prediction of 5.8%.

TABLE 4.3 Estimative for damage pattern 2 – Phase I – ASCE Benchmark problem

K estimative (Undamaged)												Estimate Stiffness Loss (%)											
1	2	3	4	5	6	7	8	9	10	11	12	1	2	3	4	5	6	7	8	9	10	11	12
83330	0	0	-4270	0	0	0	0	0	0	0	0	24.347	0	0	-2.2243	0	0	0	0	0	0	0	0
0	52940	0	0	-27200	0	0	0	0	0	0	0	0	40.536	0	-10.6585	0	0	0	0	0	0	0	0
0	0	160830	0	0	-82070	0	0	0	0	0	0	0	0	36.392	0	0	-7.43268	0	0	0	0	0	
-4270	0	0	84330	0	0	-4240	0	0	0	0	0	-2.2243	0	0	23.052	0	0	-37.4912	0	0	0	0	0
0	-27200	0	0	53730	0	0	-2700	0	0	0	0	0	-10.6585	0	0	40.555	0	-63.495	0	0	0	0	0
0	0	-82070	0	0	162630	0	0	-81640	0	0	0	0	0	-7.43268	0	0	35.824	0	-56.5409	0	0	0	
0	0	0	-4240	0	0	84840	0	0	-42340	0	0	0	0	0	-37.4912	0	0	17.61	0	-7.22721	0	0	0
0	0	0	0	-2700	0	0	54040	0	0	-26960	0	0	0	0	0	-63.495	0	26.351	0	-16.135	0	0	
0	0	0	0	0	0	-81640	0	0	163500	0	-81520	0	0	0	0	0	-56.5409	0	24.55	0	4.600715	-13.3587	
0	0	0	0	0	0	0	-42340	0	0	41950	0	0	0	0	0	0	0	-7.22721	0	0	4.600715	0	
0	0	0	0	0	0	0	0	-26960	0	0	26730	0	0	0	0	0	0	0	-16.135	0	0	13.84212	
0	0	0	0	0	0	0	0	0	-81520	0	81040	0	0	0	0	0	0	0	0	-13.3587	0	10.52567	

K estimative (Damage Pattern 2)												Theoretical Stiffness Loss (%), according to reference [107]											
1	2	3	4	5	6	7	8	9	10	11	12	1	2	3	4	5	6	7	8	9	10	11	12
62890	0	0	-41760	0	0	0	0	0	0	0	0	22.622	0	0	0	0	0	0	0	0	0	0	0
0	31480	0	0	-24290	0	0	0	0	0	0	0	0	35.513	0	0	0	0	0	0	0	0	0	0
0	0	102300	0	0	-75970	0	0	0	0	0	0	0	0	32.48	0	0	0	0	0	0	0	0	0
-41760	0	0	84890	0	0	-26510	0	0	0	0	0	0	0	0	22.622	0	0	-45.2439	0	0	0	0	0
0	-24290	0	0	31940	0	0	-9860	0	0	0	0	0	0	0	0	35.513	0	-71.0309	0	0	0	0	0
0	0	-75970	0	0	104370	0	0	-35480	0	0	7690	0	0	0	0	0	32.48	0	-64.9599	0	0	0	0
0	0	0	-26510	0	0	89900	0	0	-45400	0	0	0	0	0	0	0	-45.2439	0	22.622	0	0	0	0
0	0	0	0	-9860	0	0	39800	0	0	-31310	0	0	0	0	0	0	0	-71.0309	0	35.513	0	0	0
0	0	0	0	0	0	-35480	0	0	123380	0	-32410	0	0	0	0	0	0	0	-64.9599	0	32.48	0	0
0	0	0	0	0	0	0	-45400	0	0	43880	0	0	0	0	0	0	0	0	0	0	0	0	0
0	0	0	0	0	0	0	0	-31310	0	0	30430	0	0	0	0	0	0	0	0	0	0	0	0
0	0	0	0	0	0	0	0	0	-32410	0	83570	0	0	0	0	0	0	0	0	0	0	0	0

In the following Table, the performance of the MTFR-FDD for damage pattern 3 (No stiffness in one 1st floor brace) is shown, it is clear that the results are highly precise in location and damage value (less than 1%).

TABLE 4.4 Estimative for damage pattern 3 – Phase I – ASCE Benchmark problem

K estimative (Undamaged)												Estimate Stiffness Loss (%)											
1	2	3	4	5	6	7	8	9	10	11	12	1	2	3	4	5	6	7	8	9	10	11	12
1	83130	0	0	-42710	0	0	0	0	0	0	0	0.024055	0	0	-0.04683	0	0	0	0	0	0	0	0
2	0	52940	0	0	-27200	0	0	0	0	0	0	0	8.6513	0	0	-0.95588	0	0	0	0	0	0	0
3	0	0	160830	0	0	-82070	0	0	0	0	0	0	0	3.768	0	0	-0.46302	0	0	0	0	0	0
4	-42710	0	0	84330	0	0	-42410	0	0	0	0	-0.04683	0	0	0.01958	0	0	0	0	0	0	0	0
5	0	-27200	0	0	53730	0	0	-27010	0	0	0	0	-0.95588	0	0	0.956347	0	0	0	-0.14809	0	0	0
6	0	0	-82070	0	0	162630	0	0	-91640	0	0	0	0	-0.46302	0	0	0.301297	0	0	-0.049	0	0	0
7	0	0	0	-42410	0	0	84840	0	0	-42340	0	0	0	0	0	0	0.023574	0	0.240563	0	0	0	
8	0	0	0	0	-27010	0	0	54040	0	0	-26960	0	0	0	0	-0.14809	0	0	0	0.17737	0	-0.74184	
9	0	0	0	0	0	-91640	0	0	163500	0	-91520	0	0	0	0	-0.049	0	0	0	0.022838	0	-0.33121	
10	0	0	0	0	0	0	-42340	0	0	41950	0	0	0	0	0	0	0	0	0	0	0.523756	0	
11	0	0	0	0	0	0	0	-26960	0	0	26730	0	0	0	0	0	0	0	0	-0.74184	0	0	
12	0	0	0	0	0	0	0	0	-91520	0	0	81040	0	0	0	0	0	0	0	-0.33121	0	0.28381	

K estimative (Damage Pattern 3)												Theoretical Stiffness Loss (%), according to reference [107]											
1	2	3	4	5	6	7	8	9	10	11	12	1	2	3	4	5	6	7	8	9	10	11	12
1	83110	0	0	-42690	0	0	0	0	0	0	0	0	0	0	0	0	0	0	0	0	0	0	0
2	0	49360	0	0	-27460	0	0	0	0	0	0	0	8.8801	0	0	0	0	0	0	0	0	0	0
3	0	0	154770	0	0	-82450	0	0	0	0	0	0	0	4.06	0	0	0	0	0	0	0	0	0
4	-42690	0	0	84320	0	0	-42410	0	0	0	0	0	0	0	0	0	0	0	0	0	0	0	0
5	0	-27460	0	0	54030	0	0	-26370	0	0	0	0	0	0	0	0	0	0	0	0	0	0	0
6	0	0	-82450	0	0	163120	0	0	-91680	0	0	0	0	0	0	0	0	0	0	0	0	0	0
7	0	0	0	-42410	0	0	84860	0	0	-42340	0	0	0	0	0	0	0	0	0	0	0	0	0
8	0	0	0	0	-26370	0	0	54170	0	0	-27160	0	0	0	0	0	0	0	0	0	0	0	0
9	0	0	0	0	0	-91680	0	0	163790	0	-91790	0	0	0	0	0	0	0	0	0	0	0	0
10	0	0	0	0	0	0	-42340	0	0	41960	0	0	0	0	0	0	0	0	0	0	0	0	0
11	0	0	0	0	0	0	0	-27160	0	0	26870	0	0	0	0	0	0	0	0	0	0	0	0
12	0	0	0	0	0	0	0	0	-91790	0	0	81270	0	0	0	0	0	0	0	0	0	0	0

Similar to the previous case, the results obtained for damage pattern 4 (No stiffness in one 1st floor brace and no stiffness in one 3rd floor brace) are quite remarkable, the damage location is almost perfect and the damage severity is predicted with an error of less than 1.5%, it is shown in Table 4.5:

TABLE 4.5 Estimative for damage pattern 4 – Phase I – ASCE Benchmark problem

K estimative (Undamaged)												Estimate Stiffness Loss (%)											
1	2	3	4	5	6	7	8	9	10	11	12	1	2	3	4	5	6	7	8	9	10	11	12
1	83130	0	0	-42710	0	0	0	0	0	0	0	0.541321	0	0	-0.14048	0	0	0	0	0	0	0	0
2	0	52940	0	0	-27200	0	0	0	0	0	0	0	8.6513	0	0	-1.02941	0	0	0	0	0	0	0
3	0	0	160830	0	0	-82070	0	0	0	0	0	0	0	3.7928	0	0	-0.57260	0	0	0	0	0	0
4	-42710	0	0	84330	0	0	-42410	0	0	0	0	-0.14048	0	0	5.7275	0	0	-10.186	0	0	0	0	0
5	0	-27200	0	0	53730	0	0	-27010	0	0	0	0	-1.02941	0	0	0.6142	0	-0.07405	0	0	0	0	0
6	0	0	-82070	0	0	162630	0	0	-91640	0	0	0	0	-0.57268	0	3.6156	0	-7.0799	0	0	0	0	0
7	0	0	0	-42410	0	0	84840	0	0	-42340	0	0	0	0	-10.186	0	5.1744	0	0	-0.44875	0	0	
8	0	0	0	0	-27010	0	0	54040	0	0	-26960	0	0	0	0	-0.07405	0	0.2036	0	0	0	-0.66766	
9	0	0	0	0	0	-91640	0	0	163500	0	-91520	0	0	0	0	0	-7.0799	0	3.4434	0	0.095352	0	
10	0	0	0	0	0	0	-42340	0	0	41950	0	0	0	0	0	0	0	-0.44875	0	0	0.448934	0	
11	0	0	0	0	0	0	0	-26960	0	0	26730	0	0	0	0	0	0	0	-0.66766	0	0	0.444229	
12	0	0	0	0	0	0	0	0	-91520	0	0	81040	0	0	0	0	0	0	0	-0.71146	0	0	

K estimative (Damage Pattern 4)												Theoretical Stiffness Loss (%), according to reference [107]											
1	2	3	4	5	6	7	8	9	10	11	12	1	2	3	4	5	6	7	8	9	10	11	12
1	82680	0	0	-42650	0	0	0	0	0	0	0	0	0	0	0	0	0	0	0	0	0	0	0
2	0	49360	0	0	-27480	0	0	0	0	0	0	0	8.8801	0	0	0	0	0	0	0	0	0	0
3	0	0	154730	0	0	-82540	0	0	0	0	0	0	0	4.06	0	0	0	0	0	0	0	0	0
4	-42650	0	0	79500	0	0	-38090	0	0	0	0	0	0	0	5.6567	0	0	-11.313	0	0	0	0	
5	0	-27480	0	0	54060	0	0	-26390	0	0	0	0	0	0	0	0	0	0	0	0	0	0	0
6	0	0	-82540	0	0	156750	0	0	-75860	0	0	0	0	0	0	4.06	0	0	-8.12	0	0	0	0
7	0	0	0	-38090	0	0	80450	0	0	-42530	0	0	0	0	-11.313	0	5.6567	0	0	0	0	0	
8	0	0	0	0	-26390	0	0	54150	0	0	-27140	0	0	0	0	0	0	0	0	0	0	0	
9	0	0	0	0	0	-75860	0	0	157870	0	-82100	0	0	0	0	0	0	0	-8.12	0	0	4.06	
10	0	0	0	0	0	0	-42530	0	0	41990	0	0	0	0	0	0	0	0	0	0	0	0	
11	0	0	0	0	0	0	0	-27140	0	0	26850	0	0	0	0	0	0	0	0	0	0	0	
12	0	0	0	0	0	0	0	0	-82100	0	0	81400	0	0	0	0	0	0	0	0	0	0	0

Finally, for damage pattern 5 and 6, excellent results with an error less than 0.5% and perfect location of damage is obtained, as shown in Table 4.6:

TABLE 4.6 Estimative for damage pattern 5 – Phase I – ASCE Benchmark problem

K estimative (Undamaged)												Estimate Stiffness Loss (%)											
1	2	3	4	5	6	7	8	9	10	11	12	1	2	3	4	5	6	7	8	9	10	11	12
83130	0	0	-42710	0	0	0	0	0	0	0	0	0.024955	0	0	0	0	0	0	0	0	0	0	0
0	52940	0	0	-27200	0	0	0	0	0	0	0	0	2.8334	0	0	-0.40441	0	0	0	0	0	0	0
0	0	160820	0	0	-82070	0	0	0	0	0	0	0	0	1.2622	0	0	-0.19496	0	0	0	0	0	0
-42710	0	0	84340	0	0	-42410	0	0	0	0	0	0	0	0	0.018959	0	0	0	0	0	0	0	0
0	-27200	0	0	53730	0	0	-27010	0	0	0	0	0	-0.40441	0	0	0.186116	0	0	0	0	0	0	0
0	0	-82070	0	0	162620	0	0	-91640	0	0	0	0	0	-0.19496	0	0	0.104532	0	0	-0.01225	0	0	0
0	0	0	-42410	0	0	84840	0	0	-42340	0	0	0	0	0	0	0	0	0	0	0	0	0	0
0	0	0	0	-27010	0	0	54040	0	0	-26960	0	0	0	0	0	0	0	0	0.129524	0	0	-0.29674	
0	0	0	0	0	0	-91640	0	0	163500	0	0	0	0	0	0	0	-0.01225	0	0	0.055046	0	0	-0.12267
0	0	0	0	0	0	0	-42340	0	0	41950	0	0	0	0	0	0	0	0	0	0	0.023838	0	0
0	0	0	0	0	0	0	0	-26960	0	0	26720	0	0	0	0	0	0	0	0	-0.29674	0	0	0.149645
0	0	0	0	0	0	0	0	0	-91620	0	0	0	0	0	0	0	0	0	0	-0.12267	0	0	0.074039

K estimative (Damage Pattern 5-6)												Theoretical Stiffness Loss (%), according to reference [107]											
1	2	3	4	5	6	7	8	9	10	11	12	1	2	3	4	5	6	7	8	9	10	11	12
83110	0	0	-42710	0	0	0	0	0	0	0	0	0	0	0	0	0	0	0	0	0	0	0	0
0	51440	0	0	-27310	0	0	0	0	0	0	0	0	2.96	0	0	0	0	0	0	0	0	0	0
0	0	159800	0	0	-82220	0	0	0	0	0	0	0	0	1.3533	0	0	0	0	0	0	0	0	0
-42710	0	0	84340	0	0	-42410	0	0	0	0	0	0	0	0	0	0	0	0	0	0	0	0	0
0	-27310	0	0	53830	0	0	-27010	0	0	0	0	0	0	0	0	0	0	0	0	0	0	0	0
0	0	-82220	0	0	162800	0	0	-91650	0	0	0	0	0	0	0	0	0	0	0	0	0	0	0
0	0	0	-42410	0	0	84840	0	0	-42340	0	0	0	0	0	0	0	0	0	0	0	0	0	0
0	0	0	0	-27010	0	0	54100	0	0	-27040	0	0	0	0	0	0	0	0	0	0	0	0	0
0	0	0	0	0	0	-91650	0	0	163590	0	0	0	0	0	0	0	0	0	0	0	0	0	0
0	0	0	0	0	0	0	-42340	0	0	41960	0	0	0	0	0	0	0	0	0	0	0	0	0
0	0	0	0	0	0	0	0	-27040	0	0	26770	0	0	0	0	0	0	0	0	0	0	0	0
0	0	0	0	0	0	0	0	0	-91620	0	0	0	0	0	0	0	0	0	0	0	0	0	0

4.6 Variables Dependence

In the damage detection procedure using MTFRs and FDD only from output signals, several variables have strong importance in the final results. A complete and mathematical study of this topic is out of the scope of this research.

However, some brief comments based exclusively on numerical simulations and real case studies will be mentioned here.

Additional information and some results of the FDD errors for load estimation using output signals can be found in the reference [195].

The amount of installed sensor plays a crucial role in the final result. In general, a big amount of the sensors are desirable, and even redundant information is always welcome (i.e. sensors localized in symmetrical places in plan and elevation). It is so because the real structure is not symmetrical and always the stiffness discontinuities exists.

Although it is not strictly necessary, it is recommended to have the same number of sensor equal to DOF model that will be constructed.

For example, if only 5 sensors are available in a 30 story building, it can reliably identify many structural frequencies (perhaps 10 or more) using MTFR. The matrix model reconstruction beyond 5x5 not only have additional mathematical complications and but also it's reliably decreases because of the lack of cross information to extract the singular values from the scaled epdf.

A strong aspect of damage identification using MTFR-FDD is the fact that the frequency identification using MTFR is quite remarkable and also it is one of the most important things in an output signal identification procedure, since the possible errors decreases considerably.

Regarding the noise effect this method is reliable, even for high noise levels. A 1.53% of mean error in the stiffness prediction for 150 noise levels from 0 to 20% in a 10 DOF models can be seen in the following graphs:

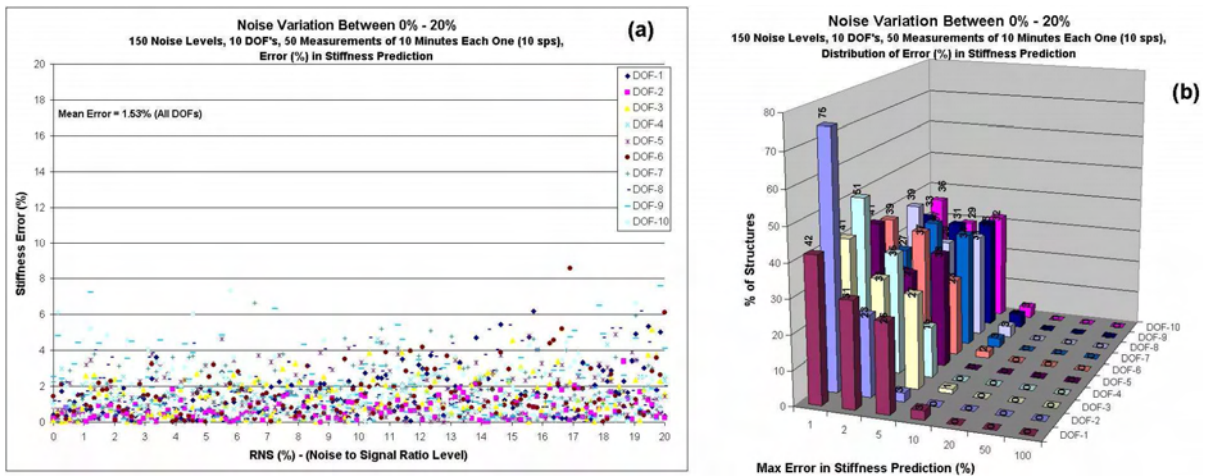


Figure 4-20 Noise effect in stiffness predictions for a 10 DOFs model

It is recommended to take long time duration records but the signal processing stage of these records require computational effort and memory capacity, on the other hand in a temporary field measurement program the allowed time for taking measurements is limited.

Therefore, it is recommended to take record length of minimum 10 – 30 minutes and of course take as many as possible.

For a continuous recording program it is recommended to windowed (with overlapping not less than 20%) the records in 30 minutes – 1 hour of length for computational efforts.

In the next graph, the results of record length variations for 10 DOFs models using 50 measurements of durations between 1 to 120 minutes are shown, for these cases the mean stiffness error is 1.58%.

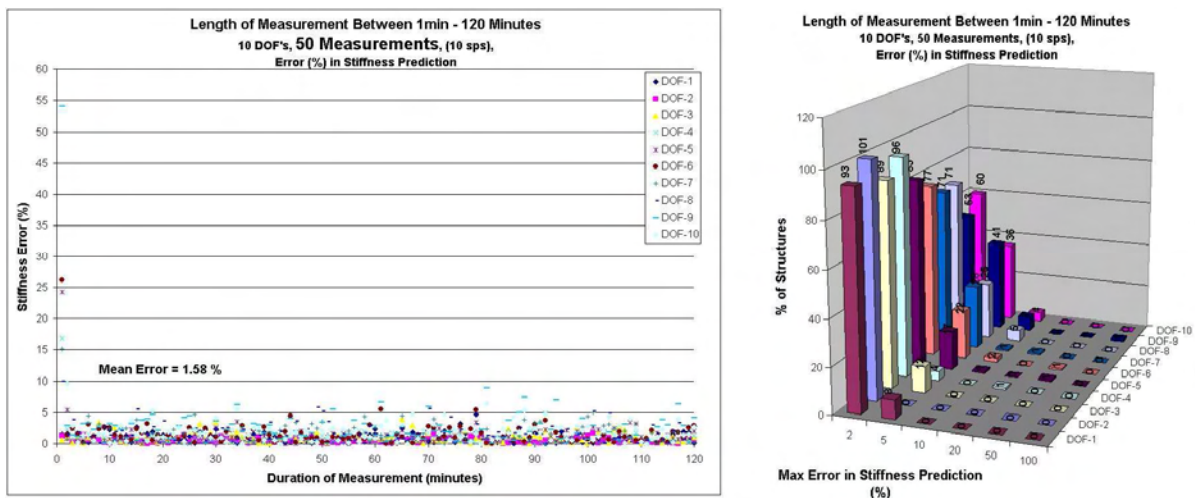


Figure 4-21 Length of measurement effect in stiffness predictions to a 10 DOFs model

According to the above analysis, it has been established that the amount of measurements might be the most important factor, as shown in the Figure 4.22.

It is important to indicate that for less than 5 measurements of 10 minutes, the stiffness errors predictions were between 40% to 160%, not shown in the Figure 4-22 for clarity purposes. Therefore, it is strongly recommended to avoid any structural damaged identification using MTFR-FDD methodology with less than 5 sets of 10 minutes each.

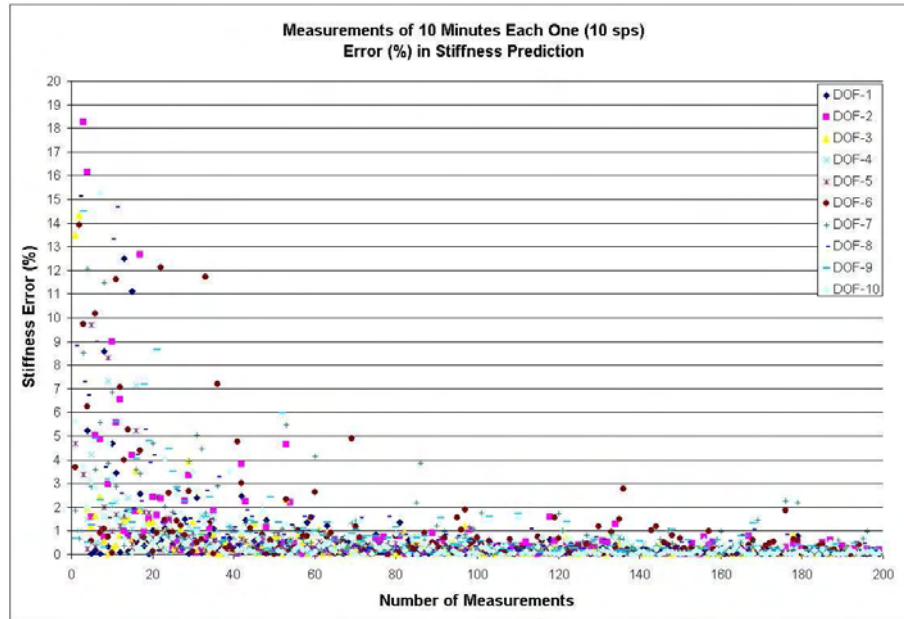


Figure 4-22 Number of measurements effect in stiffness predictions for a 10 DOFs model

By using 1000 structures and simulated 50 measurements of 10 minutes each, it was found that in the 99.98% of the cases, the algorithm have errors of less than 2% in stiffness prediction and when the structures have frequencies that are too close to each other, the error increases.

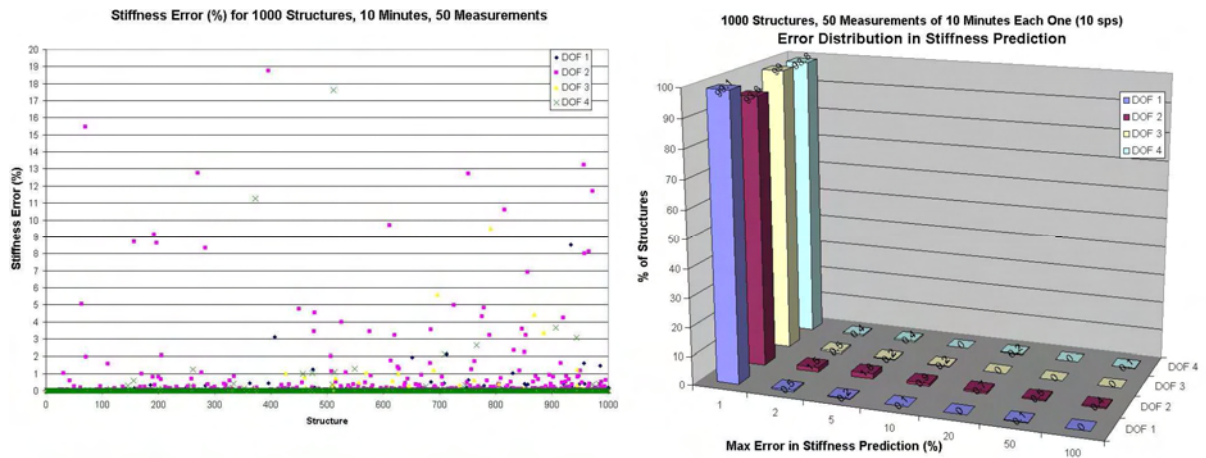


Figure 4-23 Stiffness error for 1000 simulated structures

In order to identify the location and severity of damage in the structure, a test has been done using 80 structures of 30 DOFs, with a random damage (between 5% and 45%) in any DOF (randomly chosen also).

In localization the 96% of the cases have been absolutely successful, and the remaining 4% failed with a maximum error of one DOF. The real and estimate damage localization is presented in the following graph.

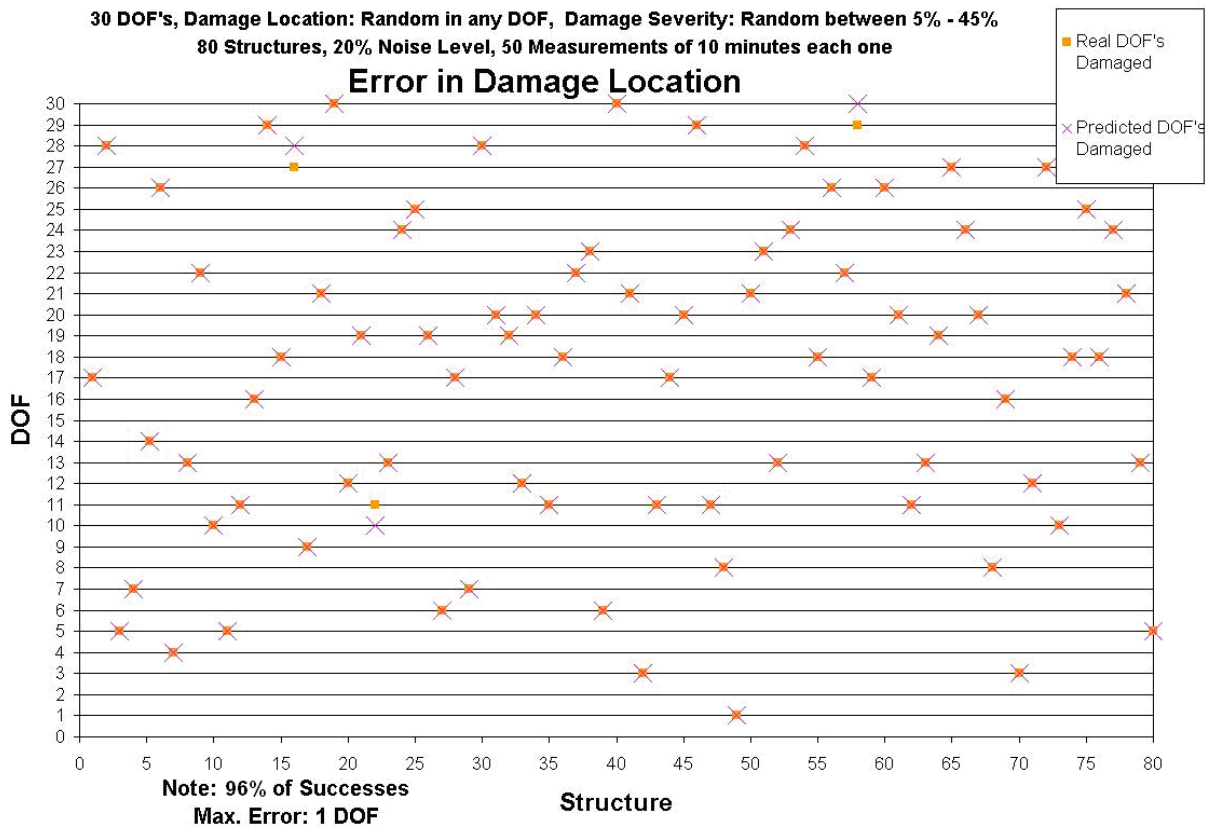


Figure 4-24 Error in damage location predictions for 80 models of 30 DOFs

In the evaluation of the damage severity the results are also quite remarkable, the mean error is less than 2% in all cases, in the following graph, the real and estimate damage severity is presented.

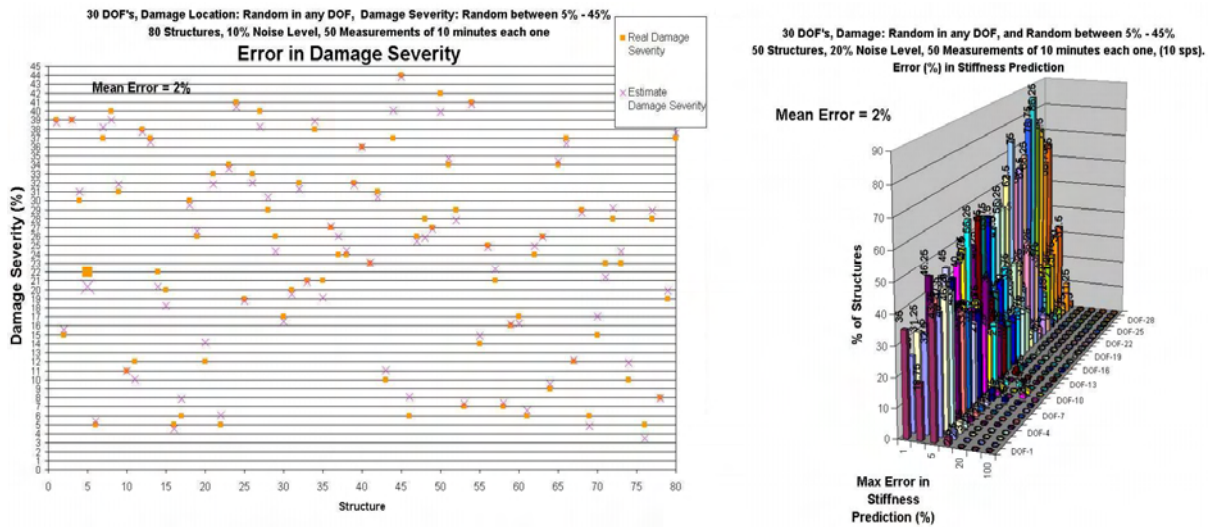


Figure 4-25 Error in location for 80 models of 30 DOFs

In the following tables, the real stiffness matrices and its estimate for the structure number 5 is shown. This structure has been damaged in the DOF #14 with a damage of 22%, the MTFR-FDD algorithm predicted an estimated damage of the 20.31% in the same DOF.

As it can be seen, not models, not material properties, structural geometry, types of elements, supports conditions, cracking level (in the concrete structures cases) or connections stiffness (in the steel structures cases), amount and distribution of dead and live load, damping or stiffness values are used in the estimation.

The 900 terms of the stiffness matrix has been obtained using **only** noisily output signals recorded by equipment in the structure and processed with MTFR-FDD algorithm. Therefore an error of around 2% is considered acceptable.

4.7 Case Studies

In this section an attempt is made to show the results for real structures with seismic instrumentation. The structures that will be shown are:

- El Castillo Building – Mayagüez, Puerto Rico
- Robert Millikan Library – California Institute of Technology at Pasadena, California
- Airport Control Tower – British Virgin Island
- Plaza Inmaculada Building – San Juan, Puerto Rico

For each one of these structures we will show the following:

- A brief description of the structure and its instrumentation
- An identification of the structure using real output signal and MTFR-FDD
- A Finite Element Model (FEM) using a computer structural program
- An identification and calibration of the FEM using the result of the structural properties obtained from the real output signals, thus we attempt to match the model results with real structure results.
- A comparison between real earthquakes recorded in the building (when it is available) and output signal obtained from the FEM and MTFR-FDD models.

4.7.1 *El Castillo Building – Mayagüez, Puerto Rico*

El Castillo Building is a Reinforced Concrete Shear Building, localized in the city of Mayagüez which is at the West of Puerto Rico Island, the general information is:

Name: “El Castillo Building”

Location: Road #2 – Mayagüez, PR.

Construction Date: 1992

Structural Designer: Walter M. Ruiz

Total Levels: 21

Underground levels: 2

Height:

Total absolute: 203.83 ft (top of roof-stairs)

194.4 ft (roof floor)

Over ground height: 174.4 ft (roof floor)

Underground height: 19.66 ft

Earthquake & Wind Resistant System: Reinforced Concrete Shear Wall

Gravitational Load System: Reinforced Concrete Shear Wall

Floor System: Slabs thickness of 4", 5" and 6" (Two way slabs)

Concrete strength (28 days): 4.000 psi (basement to 11th floor)

3.000 psi (12th to roof floor)

Steel strength (reinforcement bar): 60.000 psi

Wall thickness: 10" (Basement to Lobby floor)

8" (Second to Roof)



Figure 4-26 Photo of El Castillo Building in Mayagüez, P.R. (photo by: L. Cano)

A plan and elevation view of the building is shown in the following Figure:

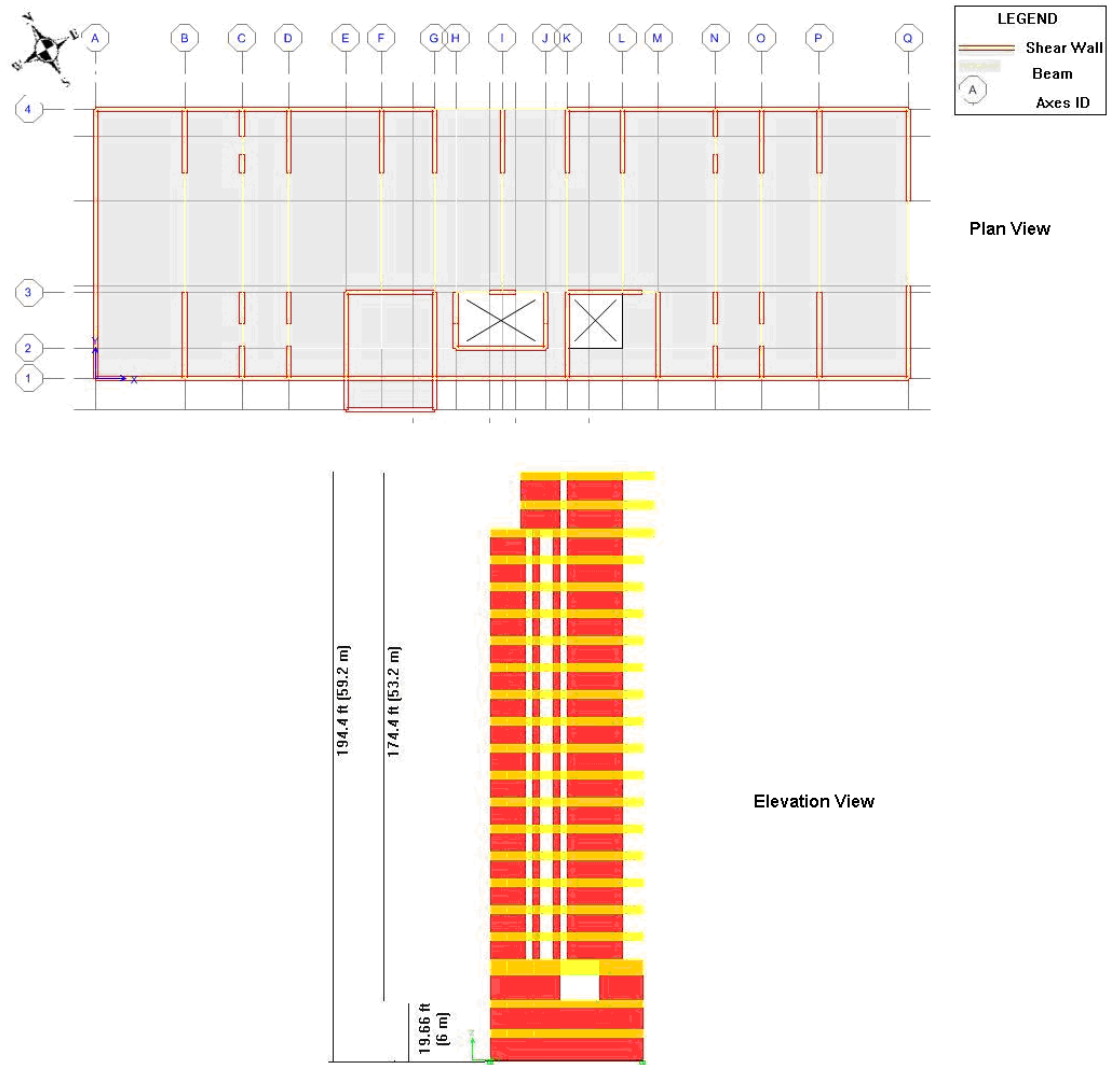


Figure 4-27 Elevation and Plan view of El Castillo Building

An ambient vibration test has been performed during five days (continuous recordings). The typical acceleration recorded for several points in the roof floor in the “X” direction is shown in the next Figure:

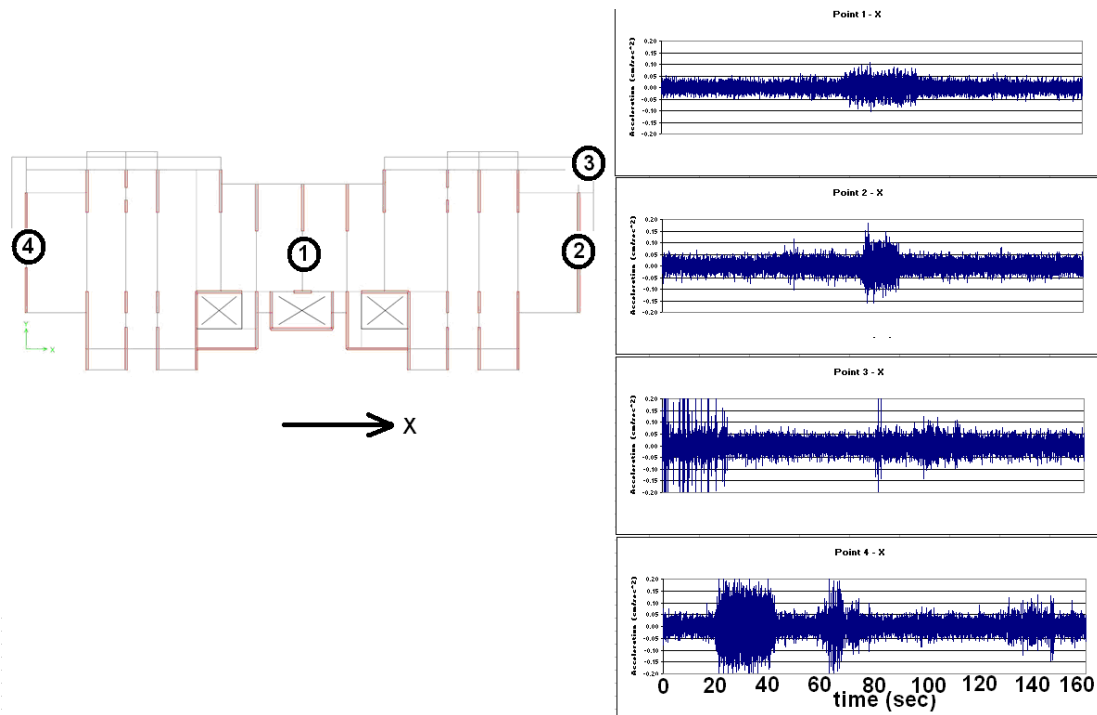


Figure 4-28 Typical acceleration recorded from Ambient Vibration taken in several points of roof floor in El Castillo Building

In the next Figure the continuous acceleration record for channel oriented in the “x” directions is shown. As can be seen from the two small earthquakes recorded during the time lapse

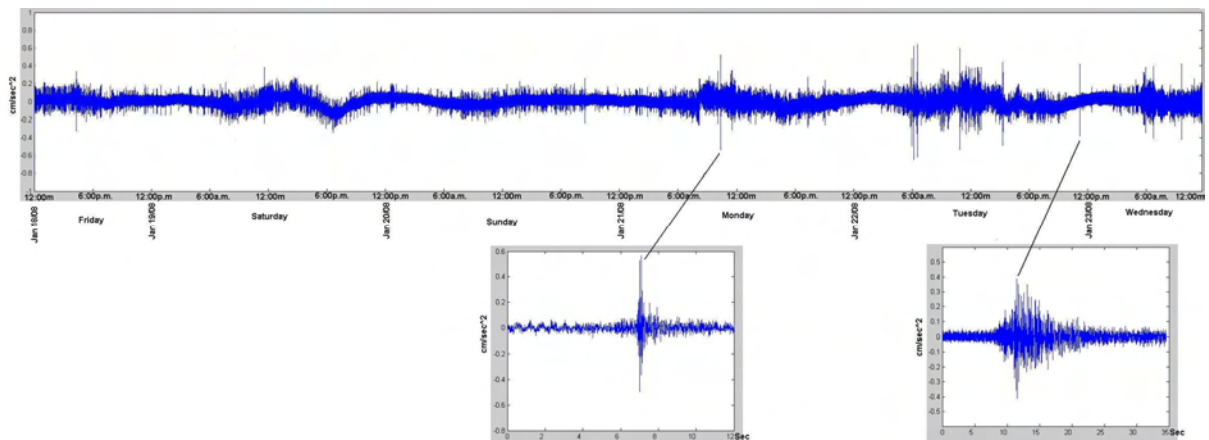


Figure 4-29 Five days of continuous acceleration recorded from Ambient Vibration taken on the roof floor in El Castillo Building

For the first 2.5 days of the record of the Figure 4-29, a 3D time-frequency representation using the STFT is shown in the following graph:

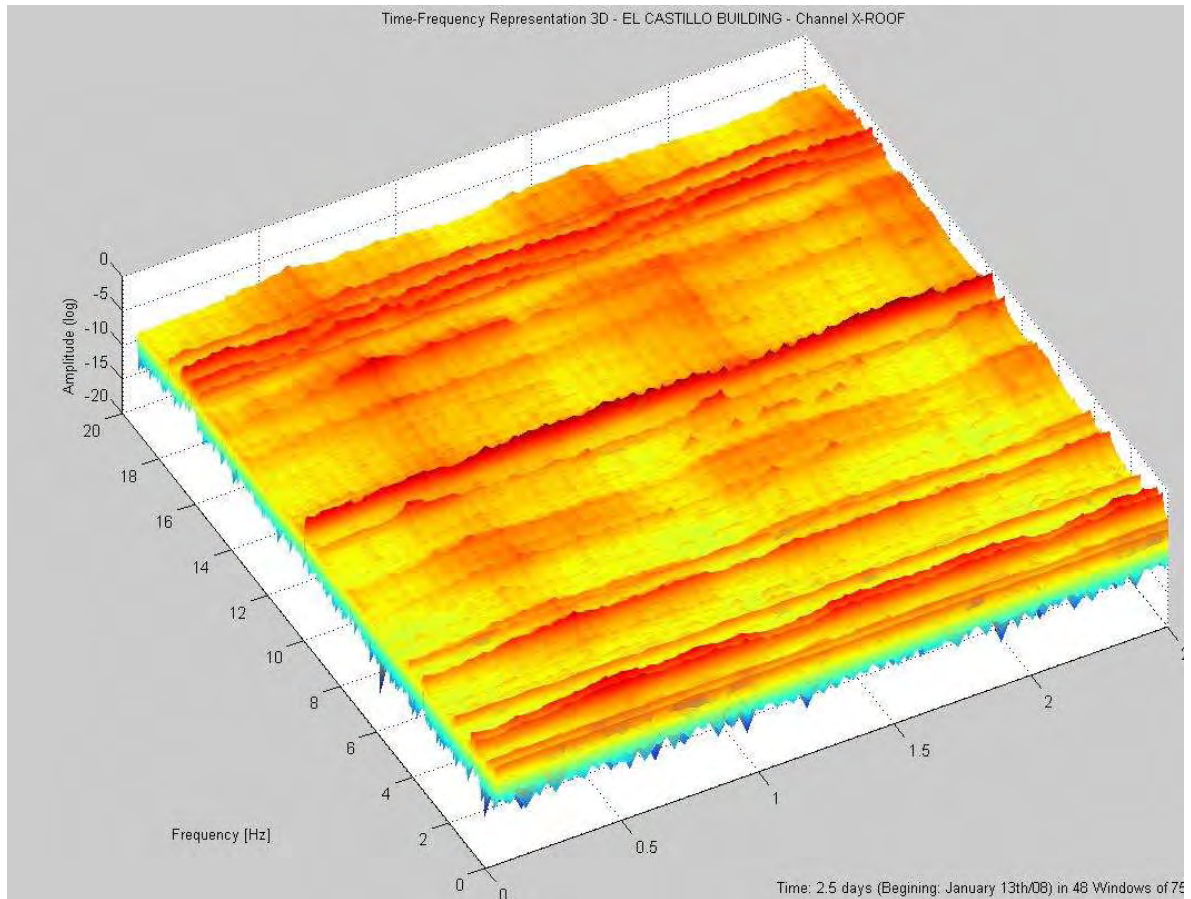


Figure 4-30 Time Frequency Representation for 2.5 days of continuous acceleration recorded from Ambient Vibration taken on the roof floor in El Castillo Building

It is necessary to use the technique developed in chapter 3 of this dissertation, at first the Mean Time Frequency Representation is evaluated, it is shown in Figure 4-31:

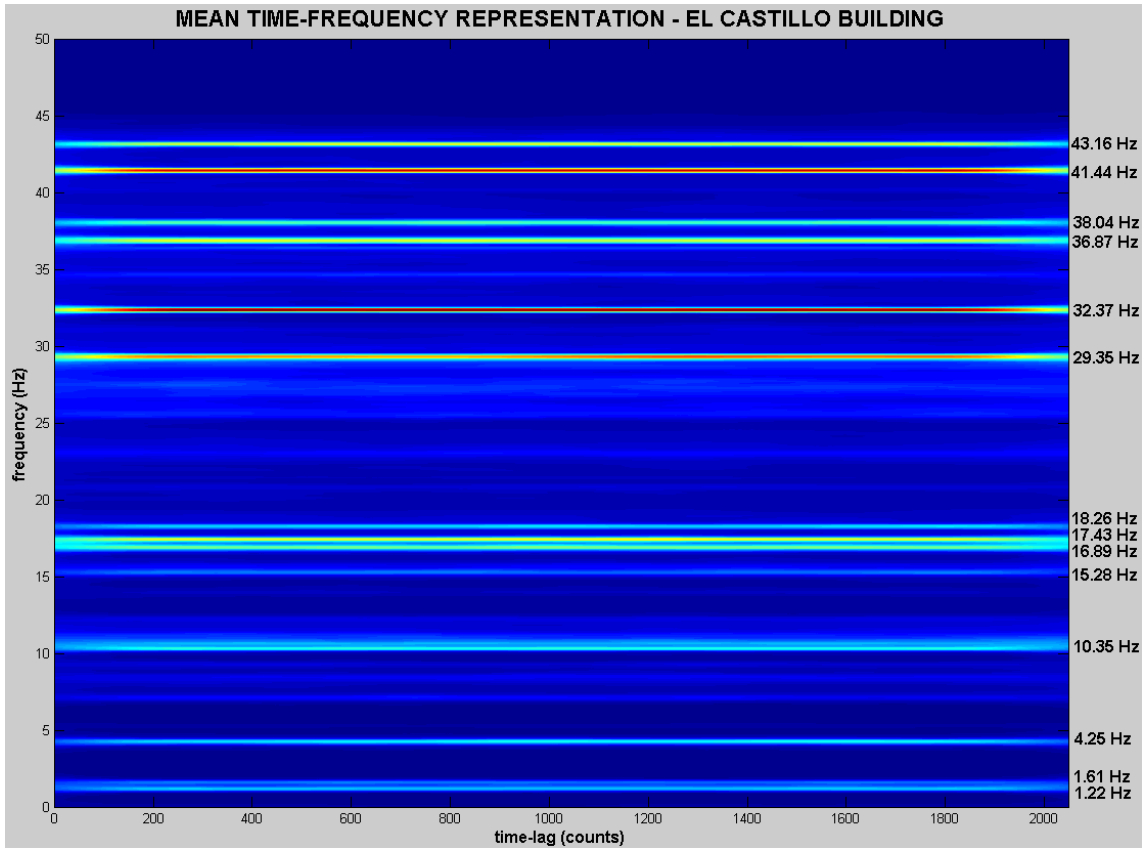


Figure 4-31 Mean Time Frequency Representation for El Castillo Building

From the MTFR of Figure 4-31, all dominant signals frequencies can be extracted, although machines and structural frequencies appear together (i.e. the frequencies in 10.6 Hz and 11.8 Hz).

The next step consists of the differentiation between real structural and external or machines frequencies. In order to do that, the empirical density distribution can be constructed around frequencies and by using the form criteria discussed earlier extract the real structural frequencies.

In the Figure 4-32 the empirical probabilistic density distributions obtained from MTFR are shown:

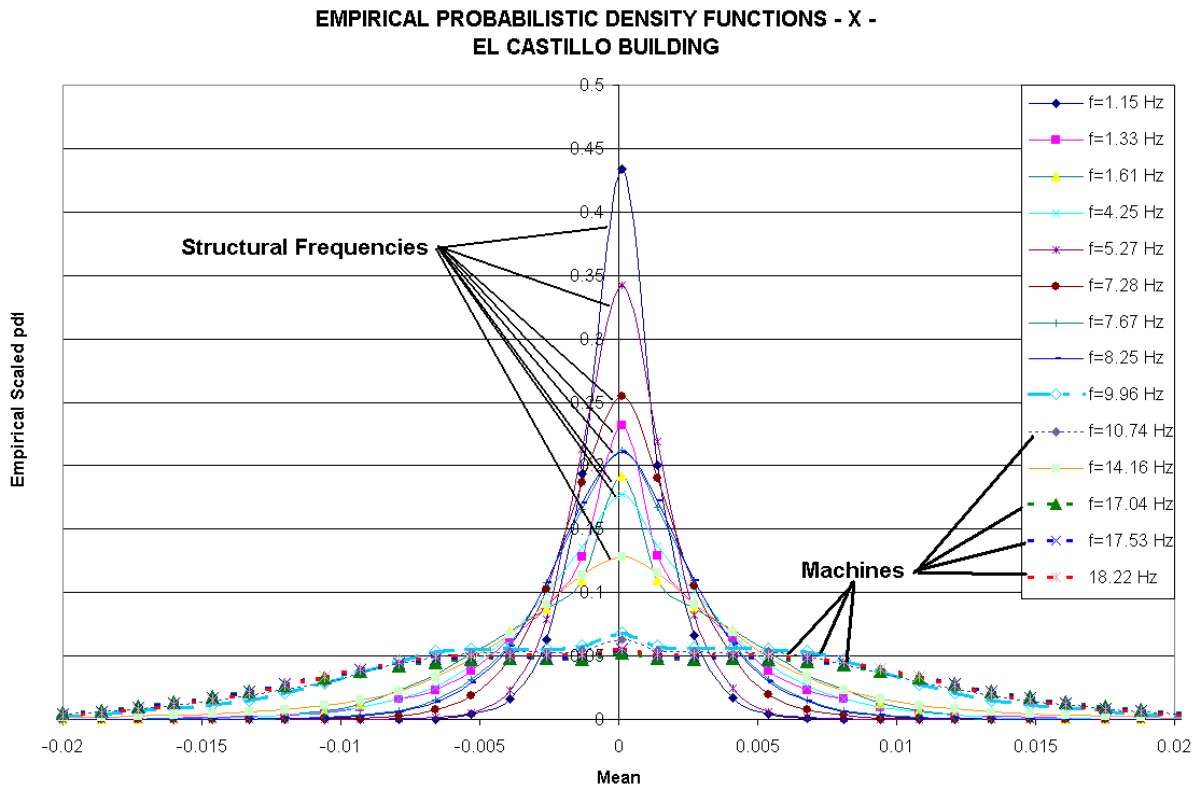


Figure 4-32 Empirical Probabilistic Density Functions from MTFR of ambient vibration test in the El Castillo Building.

Now using MTFR-FDD the relative and stiffness matrix of the structure can be evaluated.

In order to get an independent structural identification result, the continuous record of 5 days has been divided in five parts. By taking the first interval (day 1) and the last interval of record (day 5), thus a three day gap between set has been established.

In the following Table the results of these two different identification process using MTFR-FDD is shown (Note: Mass values divided by 1E6, and Stiffness values divided by 1E8 for both sets):

TABLE 4.8 Estimative for a 3 DOFs Model from El Castillo Building (Uncorrected)

Mass Matrix Estimative (First day)			Stiffness Matrix Estimative (First day)				
	1	2	3		1	2	3
1	0.38396413138143	-0.78303150977644	0.39122537081562	1	0.31295593745373	-0.63748059554801	0.31846287480024
2	-0.78303150977644	1.59693940569779	-0.79788562854860	2	-0.63748059554801	1.29857799555242	-0.64872640737885
3	0.39122537081562	-0.79788562854860	0.39865234882895	3	0.31846287480024	-0.64872640737885	0.32408487482768

Mass Matrix Estimative (Fifth Day)			Stiffness Matrix Estimative (Fifth Day)				
	1	2	3		1	2	3
1	2.15515455648994	-4.36193560673253	2.17725489268950	1	1.75761921106213	-3.55560969174992	1.77468181836639
2	-4.36193560673253	8.82843484845719	-4.40671063739082	2	-3.55560969174992	7.19293964833202	-3.59015646236029
3	2.17725489268950	-4.40671063739082	2.19960966623057	3	1.77468181836639	-3.59015646236029	1.79192781537580

As can be seen from Table 4.8, the mass matrix estimative and stiffness matrix change, since the mass do not have any changes between measurements, the equations 4.29 and 4.31 can be applied. Therefore the corrected stiffness matrix for the two independent measurement sets is:

TABLE 4.9 Stiffness Matrix Estimative for a 3 DOFs Model from El Castillo Building (Corrected)

Stiffness Matrix Estimative (First Day)			Stiffness Matrix Estimative (Fifth Day)				
	1	2	3		1	2	3
1	1.75659224250209	-3.55113334981350	1.77231566258922	1	1.75761921106213	-3.55560969174992	1.77468181836639
2	-3.55113334981350	7.17898950233824	-3.58291749003450	2	-3.55560969174992	7.19293964833202	-3.59015646236029
3	1.77231566258922	-3.58291749003450	1.78817514920995	3	1.77468181836639	-3.59015646236029	1.79192781537580

From Table 4.9 is evident that no changes occur in the structure and according to the damage definition no damage occurred between the first set of measures and the second set.

From the MTFR-FDD by solving the eigenvalue problem the modal matrix is:

TABLE 4.10 Modal Matrix Estimative for a 3 DOFs Model from El Castillo Building

Modal Matrix Estimative			
	1	2	3
1	0.01601236557993	-0.24581489092588	-0.30795239137751
2	0.45282360588480	-0.52759697660068	-0.54218084901480
3	0.89145633224785	-0.81315218060056	-0.78179616665240

Using the traditional dynamic formulation [127], and from the results of MTFR-FDD and tables 4.8 and 4.9, the following dynamic structural model can be constructed:

$$[M]\{\ddot{x}(t)\} + [C]\{\dot{x}(t)\} + [K]\{x(t)\} = \{F(t)\} \quad 4-34$$

Where:

[M]: Mass matrix

[C]: Damping matrix.

[K]: Stiffness Matrix

{x(t)}: Displacement time history vectors (superscript dot represent time derivative)

{F(t)}: Force time history vectors

The coefficient of damping matrix ([C]) can be evaluated using:

$$[\Phi]^T [C][\Phi] = [\tilde{c}_j] \quad 4-35$$

Where:

$$\tilde{c}_j = 2\xi_j \omega_j$$

In order to do that, the damping coefficient was set to 5% of the critical damping for all modes.

Using the frequency values extracted from MTFR (see Figure 4-31):

$$\{f_j\} = \begin{Bmatrix} 1.153564453 \\ 1.330566406 \\ 1.611328125 \end{Bmatrix} \quad (\text{Hz}) \quad 4-36$$

In addition, remembering that:

$$\omega_j = 2\pi f_j$$

$$\{\omega_j\} = \begin{Bmatrix} 7.24743718513091 \\ 8.36019528943606 \\ 10.1242731967199 \end{Bmatrix} \text{ (rad/sec)} \quad 4-37$$

Therefore:

$$\tilde{c}_j = 2\xi_j \omega_j$$

$$\{\tilde{c}_j\} = \begin{Bmatrix} 0.72474371851309 \\ 0.83601952894361 \\ 1.01242731967199 \end{Bmatrix} \quad 4-38$$

$$[\tilde{c}_j] = \begin{bmatrix} 0.72474371851309 & 0 & 0 \\ 0 & 0.83601952894361 & 0 \\ 0 & 0 & 1.01242731967199 \end{bmatrix}$$

From equation 4-35, and solving for [C]:

$$[C] = \left[[\Phi]^T \right]^{-1} [\tilde{c}_j] \left[[\Phi] \right]^{-1} \quad 4-39$$

Using the modal matrix From the Table 4-10, and by replacing the equation 4-38 into 4-39:

$$[C] = \begin{bmatrix} 1.93663707470189 & -3.91870046593497 & 1.95595746351539 \\ -3.91870046593496 & 7.92937992638448 & -3.95783078242975 \\ 1.95595746351539 & -3.95783078242975 & 1.97549272603928 \end{bmatrix} * 1E6 \quad 4-40$$

Finally, by replacing the results from tables 4.8, 4.9 and equation 4-40, into the equation 4-34, the following equivalent dynamic structural system for El Castillo Building is obtained:

$$[M]\{\ddot{x}(t)\} + [C]\{\dot{x}(t)\} + [K]\{x(t)\} = \{F(t)\}$$

Where:

$$[M] = \begin{bmatrix} 2.15515455648894 & -4.36193560673253 & 2.17725489268950 \\ -4.36193560673253 & 8.82843484845719 & -4.40671063739082 \\ 2.17725489268950 & -4.40671063739082 & 2.19960966623057 \end{bmatrix} * 1E6$$

$$[C] = \begin{bmatrix} 1.93663707470189 & -3.91870046593497 & 1.95595746351539 \\ -3.91870046593496 & 7.92937992638448 & -3.95783078242975 \\ 1.95595746351539 & -3.95783078242975 & 1.97549272603928 \end{bmatrix} * 1E6$$

$$[K] = \begin{bmatrix} 1.75761921106213 & -3.55560969174992 & 1.77468181836639 \\ -3.55560969174992 & 7.19293964833202 & -3.59015646236029 \\ 1.77468181836639 & -3.59015646236029 & 1.79192781537580 \end{bmatrix} * 1E8$$

4-41

Using the Extend Tridimensional Analysis of Building Systems (ETABS – V.9.04) computer program [201], a finite element model of the building has been constructed; the schematic view of this model is shown in the next graph:

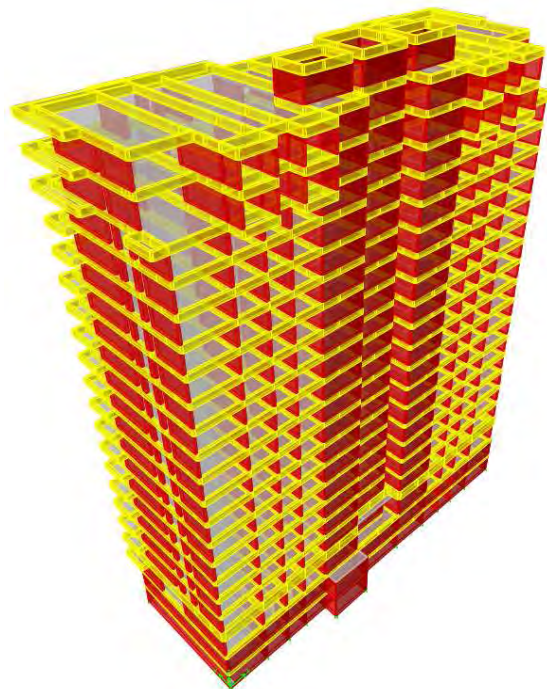


Figure 4-33 Schematic view of the Finite Element structural model for El Castillo Building

A comparison between MTFR apply to ambient vibration and a finite element model of the structure can be seen in the Table 4.11, the results are very consistent, the first three modal frequencies and modal shapes can be obtained using the analytical model acquired through MFTR-FDD:

TABLE 4.11 Comparison between MTFR-FDD and Finite Element Model for El Castillo Building

Mode	Frequency (Hz)	
	MTFR-FDD	ETABS
1	1.154	1.223
2	1.331	1.278
3	1.611	1.564
4	4.248	4.173
5	5.280	4.979
6		5.831
7	7.280	7.963
8	9.980	10.425
9	10.720	11.797
10		12.036
11		16.109
12		16.210
13		17.661
14		20.585
15		22.782
16		24.298
17		25.344
18		30.289
19		30.540
20		31.691
21		35.311

Finally the output result for El Castillo Building from two different models will be shown, the first one is the output signal of the finite element model building (ETABS model) and the second one is the output signal from the 3 DOFs model obtained using MTFR-FDD.

The selected input signal is the EW acceleration record for the earthquake of Tokachi-Oki of 2003, recorded in the Station TKCH11, (Mw=8.3), the acceleration recorded and the Fourier Spectra are shown in the following Figures:

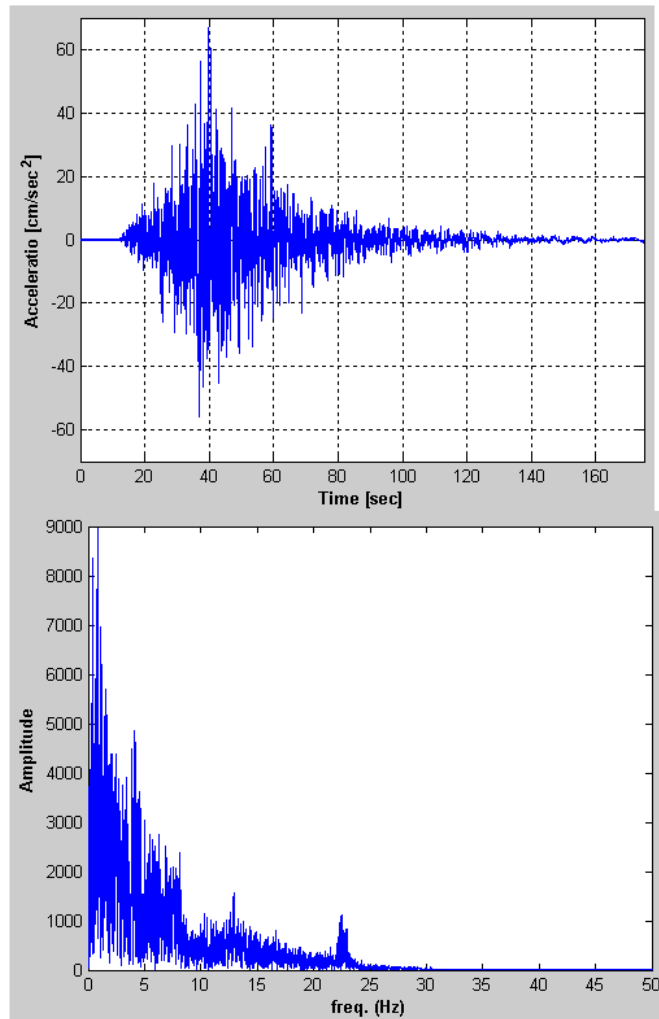


Figure 4-34 Acceleration record and Fourier Spectra for Earthquake of Tokachi-Oki (2003), recorded in the Station TKCH11.

Using the previous record, the two models of the building has been excited at the base and the output signals for this event is shown in Figure 4-35:

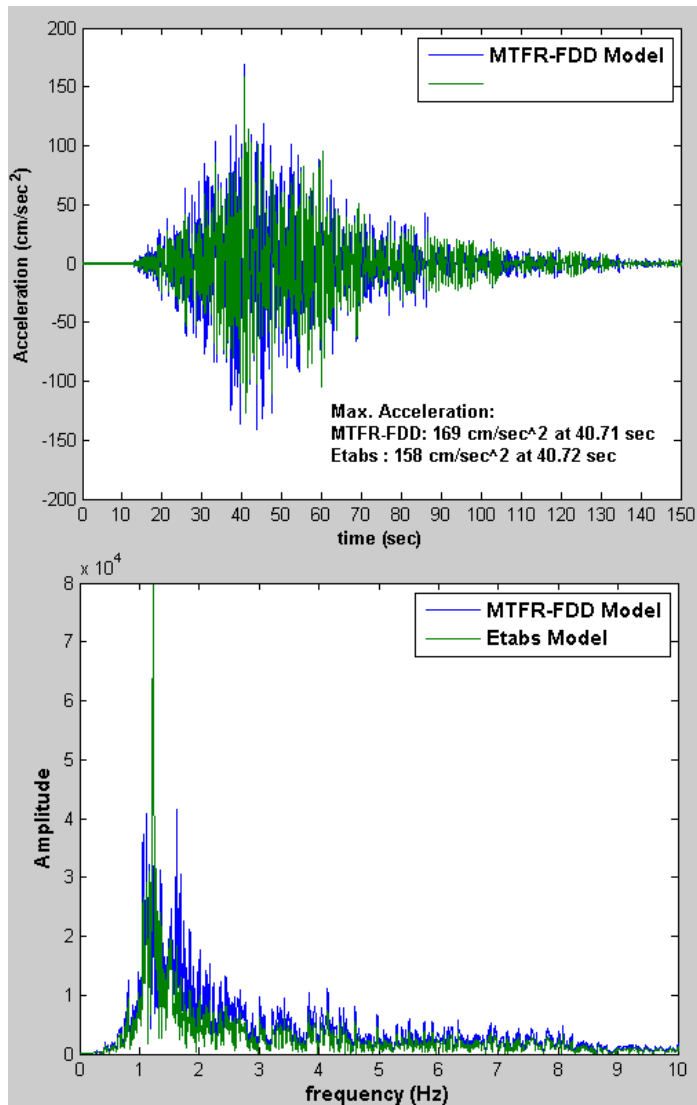


Figure 4-35 Comparison of output signal to El Castillo Building, from Etabs Model and MTFR-FDD Model for Earthquake of Tokachi-Oki of 2003, recorded in the Station TKCH11.

As can be seen, the match between two different models is quite good. In order to evaluate the frequency match, the coherence function can be evaluated using [193]:

$$\gamma_{xy}^2(\omega) = \frac{S_{xy}(\omega) S_{xy}^*(\omega)}{S_{xx}(\omega) S_{yy}(\omega)} \quad 4-42$$

Where:

$S_{xx}(\omega), S_{yy}(\omega)$: Power Spectral Density for signal x and y respectively.

$S_{xy}(\omega)$: Cross-Power Spectra Density Function between signal x and y.

$\gamma_{xy}^2(\omega)$: Coherence function between signal x and y.

For this earthquake the coherence function is shown in the following graph:

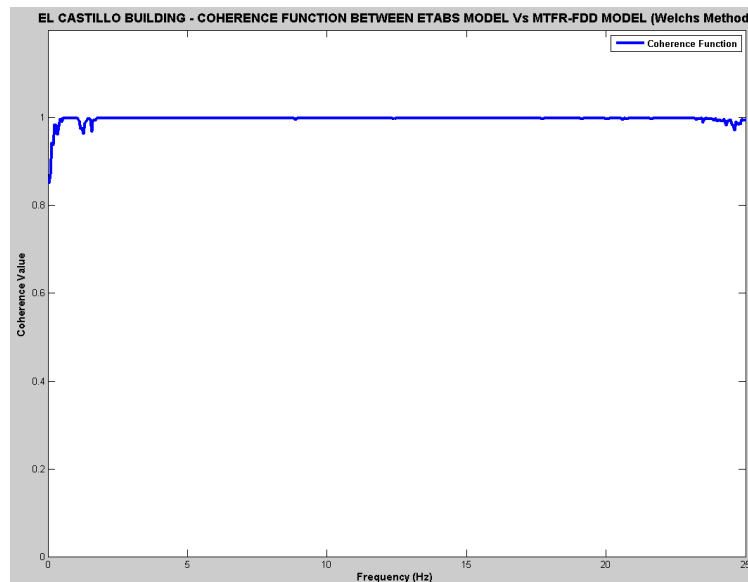


Figure 4-36 Coherence Function for El Castillo Building, from Etabs Model and MTFR-FDD Model for Earthquake of Tokachi-Oki of 2003, recorded in the Station TKCH11.

From the previous graph is evident that the single 3 DOFs model obtained using only output signals from the building has an excellent agreement in frequency with the huge finite element model of the El Castillo Building.

4.7.2 Robert A. Millikan Library - Caltech

The Robert A. Millikan Library is located at the campus of the California Institute of Technology – Caltech at Pasadena California. It is a nine story shear-wall reinforced concrete building.

Millikan Library is perhaps one of the most recognize instrumented building in the world. Many technical reports of this building are available, geometry description and results of several researches for this building can be found in the references [11, 16, 25, 26, 58-60, 90, 91, 113-117, 119, 121].

Some general data for Millikan library are [11]:

Full Name: “Robert A. Millikan Memorial Library”

Location: Campus of the California Institute of Technology at Pasadena (Cal.) USA

Construction Date: 1967

Structural Designer: Flewelling and Moody Inc. using ACI-318-63 and UBC-64

Total Levels: 10 (9 above the ground)

Underground levels: 1

Height:

Total absolute: 48.2 mts (top of roof-Wall lateral cover)

43.3 mts (roof floor)

Over ground height: 39 mts (roof floor)

Underground height: 4.3 mts

Earthquake & Wind Resistant System: Perimetral Concrete Shear Wall (N-S) and Columns (E-W) and an internal Shear Wall Core

Gravitational Load System: Concrete Shear Wall and Concrete Columns

Floor System: Slabs 9” (Two way)

Concrete strength (28 days): 5.000 psi (basement to 5th floor) (Shear Walls and Columns)

4.000 psi (5th to roof floor)

4.000 psi to floor slabs

Steel strength (reinforcement bar): 36.000 psi

Wall thickness: 12" (Basement to Roof) and a few Internal Shear Wall=10"

Column Section: 20"x36"

Beam Sections; 36"x24" and 16"x36"

Total Area per floor = 8.450 ft²

Shear Wall area in NS direction: 234 ft² (2.8% of Total Area)

Shear Wall are in EW direction: 73.8 ft² (0.87% of Total Area)

The building has a permanent monitoring system and on-line records can be obtained trough Internet from the COMET web site at <http://www.comet.caltech.edu> [113], in addition a permanent copy of the data is stored in the Southern California Earthquake Data Center [204] (Station MIK) Internet: <http://www.data.scec.org/index.html>



Figure 4-37 Photo of Robert Millikan Library Caltech (photo by: L. Cano)

A plan and elevation view of the building are shown in the following graph:

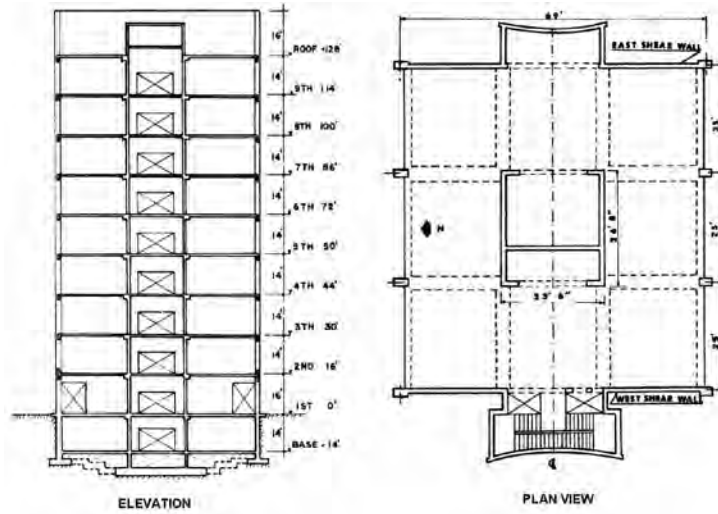


Figure 4-38 Elevation and Plan view of Millikan Library (taken from COMET website [113])

Although the building has an extensive set of permanent instrumentation (above 36 channels), actually only 3 channels localized in the nine floors are available from Internet website. The building instrumentation is shown in the following graph:

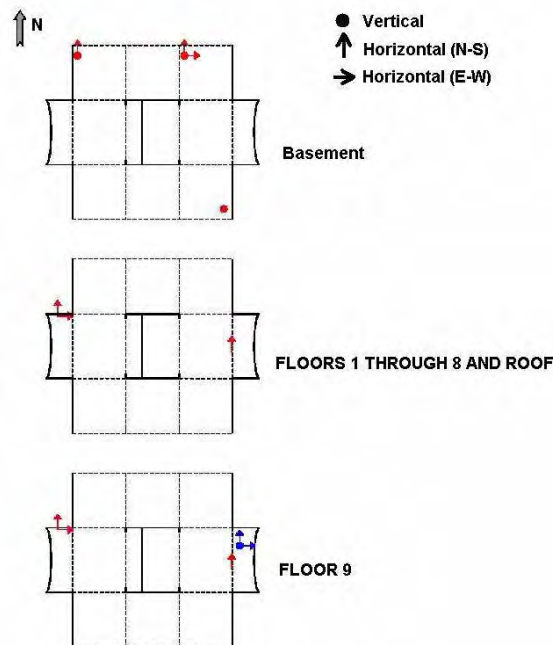


Figure 4-39 Millikan Library Instrumentation (taken from COMET website [113])

In the Figure 4-40 a typical continuous one day of recording (June 16/2005) is shown. The Yucaipa earthquake can be seen in this graph, (Mw=4.9, Depth= 11.8 km., Epicenter distance from Millikan Library ~ 125 Km)

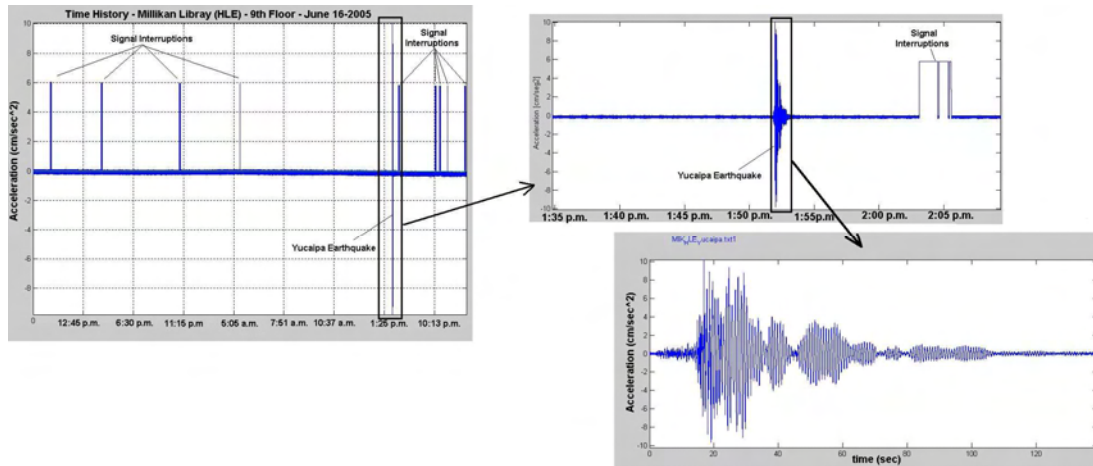


Figure 4-40 Time History of a continuous 24 hours recording in Millikan Library

A linear time-frequency representation for the ambient vibration records from the building can be obtained using ambient vibration real data, it is shown in the next Figure:

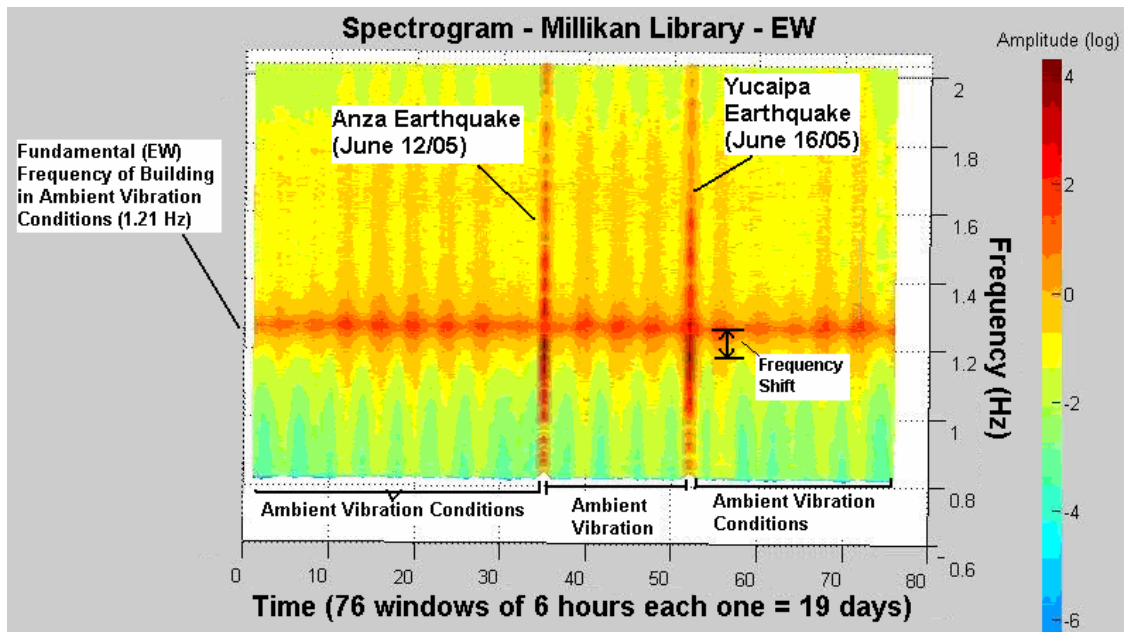


Figure 4-41 Linear Time-Frequency Representation for 19 days of continuous recording in Millikan Library

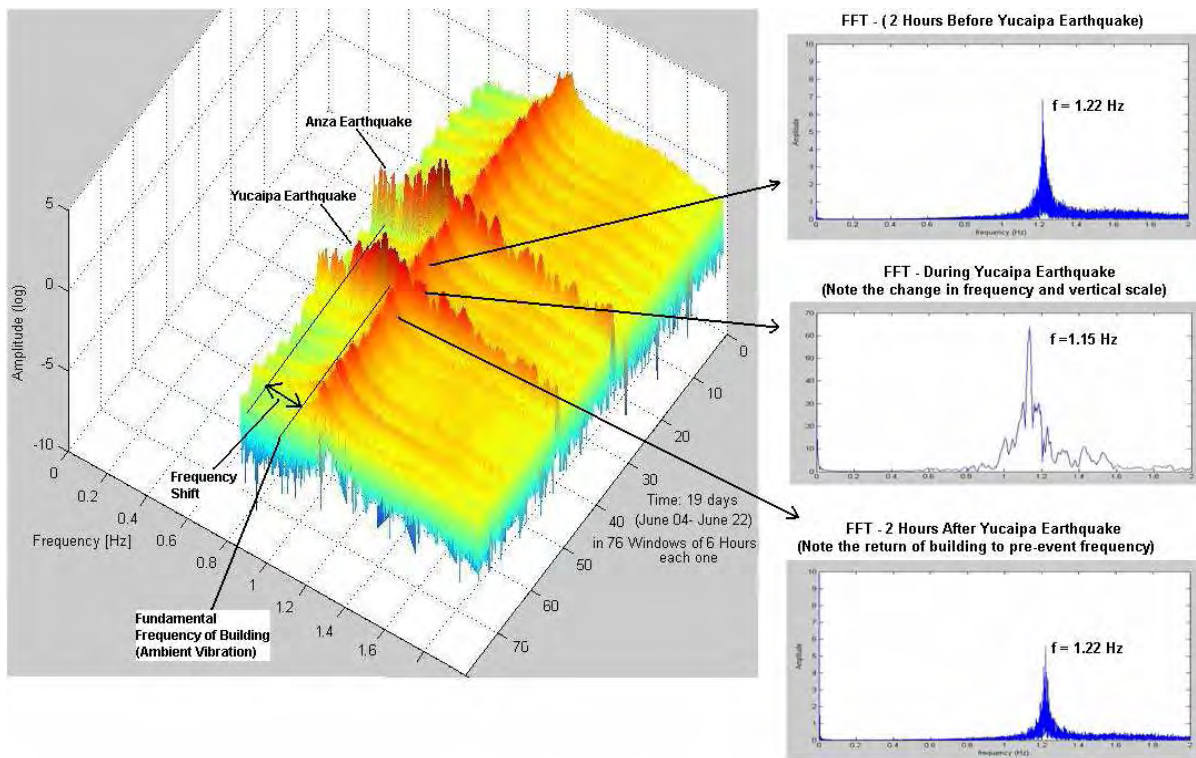


Figure 4-42 Linear 3D Time-Frequency for 19 days of continuous recording in Millikan Library

Figures 4-41 and 4-42 show that the Yucaipa earthquake of June 16/2005 produced a temporary shift in frequency in Millikan Library of 6% (from 1.22 Hz to 1.15 Hz, the frequency returned to its initial value of 1.22 Hz at the end of the excitation).

Long time continuous recording is a good way to understand the behavior of structures; in this case linear time-frequency representation is an excellent tool for the analysis of small frequency changes in the structure. For Millikan Library, for example, recently several researchers [114-116] have demonstrated the correlation between the changes in building frequencies and weather conditions, windstorms, daily temperature, rainfall and small earthquakes.

In order to apply the MTFR-FDD method for Millikan Library a continuous six days record for the three channels available in SCEDC [204] was selected. The records beginning at the 00:00:00 hours of June 12/2005 and ending at 23:59:59 of June 17/2005.

As can be seen from Figure 4-42 the select days include the two earthquakes (Anza and Yucaipa), because of the interest in determining if any of these earthquakes has produced a permanent damage in the building.

In the first stage 500 measurements of 1 min at a sampling frequency of 20 Hz has been processed from 00:00:00 to 08:20:00 of June 12th-2005, prior to Anza Earthquake.

The MTFR for this first set is shown in the next graph:

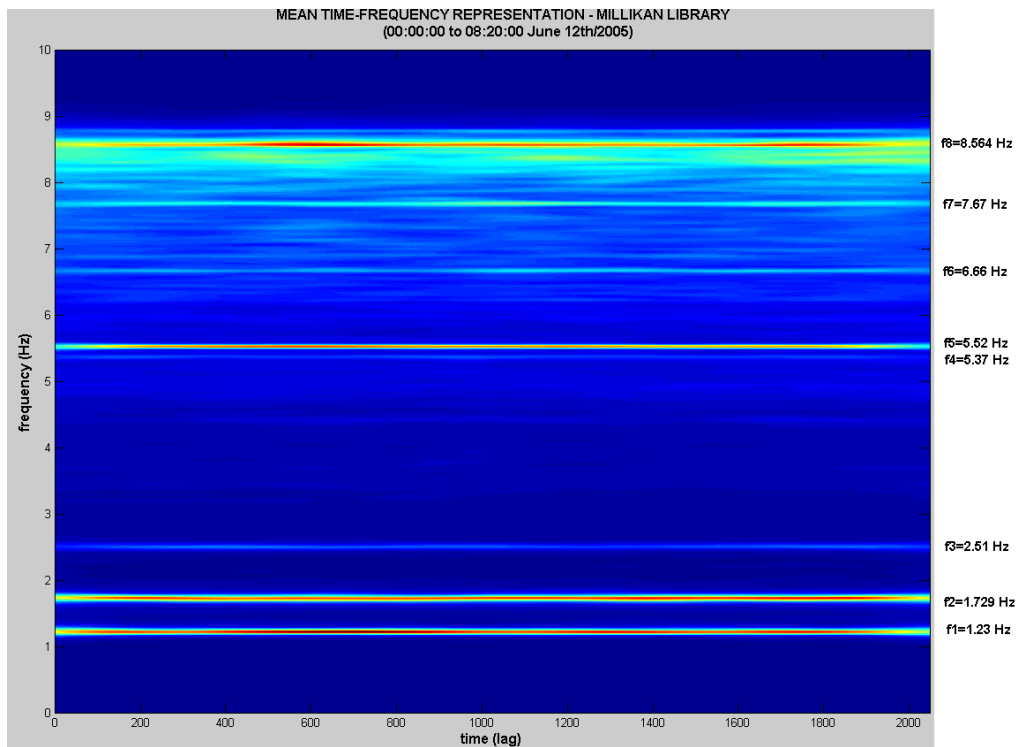


Figure 4-43 MTFR to Millikan Library (00:00:00 to 08:20:00 June 12th/2005)

The next step consists of the differentiation between real structural and external or machines frequencies.

In the Figure 4-44 the empirical probabilistic density distributions obtained from MTFR for Millikan Library are shown:

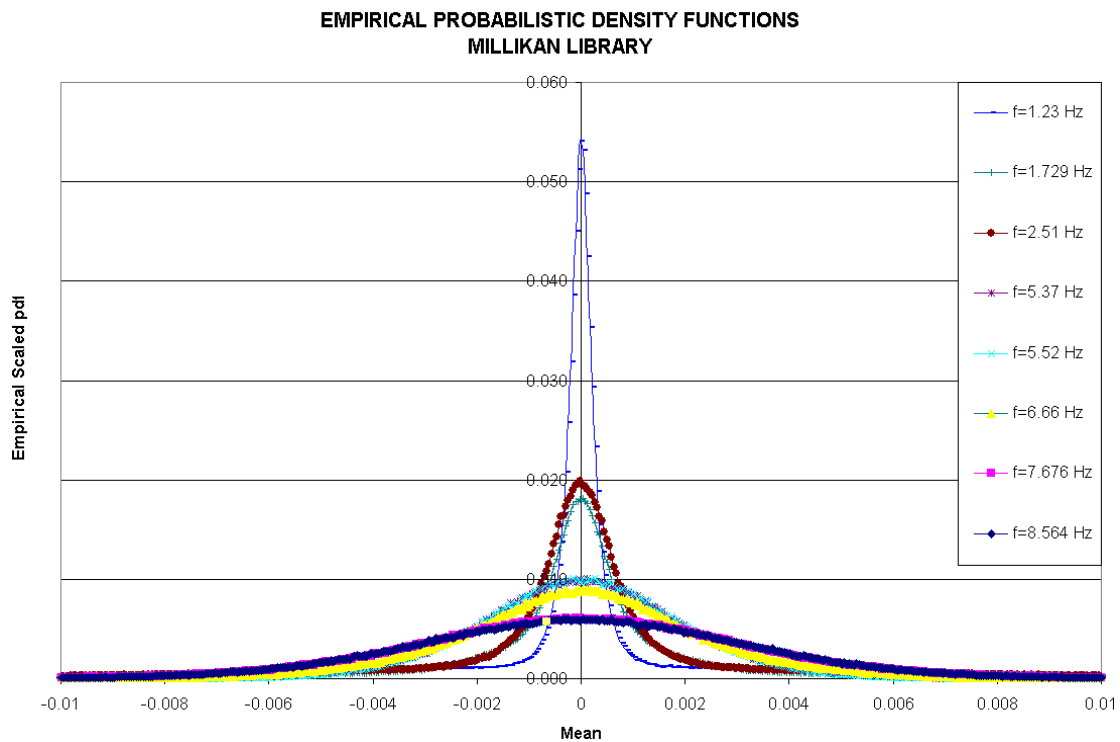


Figure 4-44 Empirical Probabilistic Density Functions from MTFR from ambient vibration for Millikan Library.

From Figure 4.44 and according to Brincker's criteria [192], all frequencies identified from MTFR are structural frequencies.

The procedure to get the MTFR for the second measurements set (June 17th/2005) has been repeated and the obtained frequencies are the eigenvalues of the second identification stage.

Now using MTFR-FDD the relative and stiffness matrices for the structure can be evaluated.

In order to get an independent structural identification result, the continuous record of 6 days has been divided in six parts. the first interval (day 1) and the last interval of record (day 6) has been taken, thus a four day gap between set has been established.

For each of those days 500 measurements of 1 minute each (8:20 hours) was used. In the following Table the results of these two different identification process using MTFR-FDD are shown (Note: Mass values divided by 1E5, and Stiffness values divided by 1E7 for the first set and 1E8 for the second set):

TABLE 4.12 Estimative for a 3 DOFs Model for Millikan Library (Uncorrected)

Mass Matrix Estimative (2005-06-12 - First day)			Stiffness Matrix Estimative (2005-06-12 - First day)				
	1	2	3		1	2	3
1	0.86610022238664	-1.78673813325745	0.91174704877052		1.59189046181392	-3.27596341812187	1.67035032335308
2	-1.78673813325745	3.68662268561622	-1.88124981244445		-3.27596341812187	6.74219040299165	-3.43775298869124
3	0.91174704877052	-1.88124981244445	0.95998954790842		1.67035032335308	-3.43775298869124	1.75287216674734
Mass Matrix Estimative (2005-06-17 - Sixth Day)			Stiffness Matrix Estimative (2005-06-17 - Sixth Day)				
	1	2	3		1	2	3
1	1.65173770262574	-3.40620792606054	1.73795974828419		0.30003569873091	-0.61751082584908	0.31488858624413
2	-3.40620792606054	7.02493679012762	-3.58437623852224		-0.61751082584908	1.27097352392202	-0.64811463297627
3	1.73795974828419	-3.58437623852224	1.82888323843600		0.31488858624413	-0.64811463297627	0.33049753220312

As it can be seen from Table 4.12, the mass matrix estimative and stiffness matrix change, since the mass do not have any changes between measurements, the equations 4.29 and 4.31 can be applied. Therefore, the corrected stiffness matrix for the two independent measurement sets is:

TABLE 4.13 Stiffness Matrix Estimative for a 3 DOFs Model from Millikan Library (Corrected)

Stiffness Matrix Estimative (First Day)			Stiffness Matrix Estimative (Sixth Day)				
	1	2	3		1	2	3
1	0.30358905658548	-0.62452422952140	0.31839899297863		0.30003569873091	-0.61751082584908	0.31488858624413
2	-0.62452422952140	1.28473851128881	-0.65500073648180		-0.61751082584908	1.27097352392202	-0.64811463297627
3	0.31839899297863	-0.65500073648180	0.33394098215651		0.31488858624413	-0.64811463297627	0.33049753220312

From Table 4.13 is evident that no changes occur in the structure and according to the damage definition no damage occurred between the first set of measures and the second set.

From the MTFR-FDD by solving the eigenvalue problem the modal matrix is:

TABLE 4.14 Modal Matrix Estimative for a 3 DOFs Model for Millikan Library

Modal Matrix Estimative			
	1	2	3
1	0.26893585929471	-0.02958653416949	-0.041249386657365
2	0.53757486839289	0.44218879415339	0.43882745710591
3	0.79984905302662	0.89643388342874	0.89762405981245

Using the traditional dynamic formulation [127] and from results of MTFR-FDD and tables 4.8 and 4.9, the following dynamic structural model can be constructed:

$$[M]\{\ddot{x}(t)\} + [C]\{\dot{x}(t)\} + [K]\{x(t)\} = \{F(t)\} \quad 4-43$$

Where:

[M]: Mass matrix

[C]: Damping matrix

[K]: Stiffness Matrix

{x(t)}: Displacement time history vectors (superscript dot represent time derivative)

{F(t)}: Force time history vectors

Using common modal dynamic equations:

$$\{f_j\} = \begin{Bmatrix} 1.23 \\ 1.729 \\ 2.51 \end{Bmatrix} \text{ (Hz)} \quad \{\omega_j\} = \begin{Bmatrix} 7.72831792782450 \\ 10.86362739608425 \\ 15.77079512094639 \end{Bmatrix} \text{ (rad/sec)} \quad 4-44$$

And using 5% of damping:

$$[C] = \begin{bmatrix} 1.15480555465352 & -2.37931217422767 & 1.21363063741182 \\ -2.37931217422767 & 4.90281781536189 & -2.50084048574906 \\ 1.21363063741182 & -2.50084048574906 & 1.27564071224913 \end{bmatrix} * 1E5 \quad 4-45$$

Finally, replacing the results of tables 4.12, 4.13 and equation 4-45, into the equation 4-34, the following equivalent dynamic structural system for Millikan Library is obtained only from the output signals:

$$[M]\{\ddot{x}(t)\} + [C]\{\dot{x}(t)\} + [K]\{x(t)\} = \{F(t)\}$$

Where:

$$[M] = \begin{bmatrix} 1.65173770262574 & -3.40620792606054 & 1.73795974828419 \\ -3.40620792606054 & 7.02493679012762 & -3.58437623852224 \\ 1.73795974828419 & -3.58437623852224 & 1.82888323843600 \end{bmatrix} * 1E5$$

$$[C] = \begin{bmatrix} 1.15480555465352 & -2.37931217422767 & 1.21363063741182 \\ -2.37931217422767 & 4.90281781536189 & -2.50084048574906 \\ 1.21363063741182 & -2.50084048574906 & 1.27564071224913 \end{bmatrix} * 1E5$$

$$[K] = \begin{bmatrix} 0.30003569873091 & -0.61751082584908 & 0.31488858624413 \\ -0.61751082584908 & 1.27097352392202 & -0.64811463297627 \\ 0.31488858624413 & -0.64811463297627 & 0.33049753220312 \end{bmatrix} * 1E8 \quad 4-46$$

Using the Extend Tridimensional Analysis of Building Systems (ETABS – V.9.04) computer program [201], a finite element model of the building from the “As built” drawings has been constructed, the schematic view of this model is shown in the next graph:

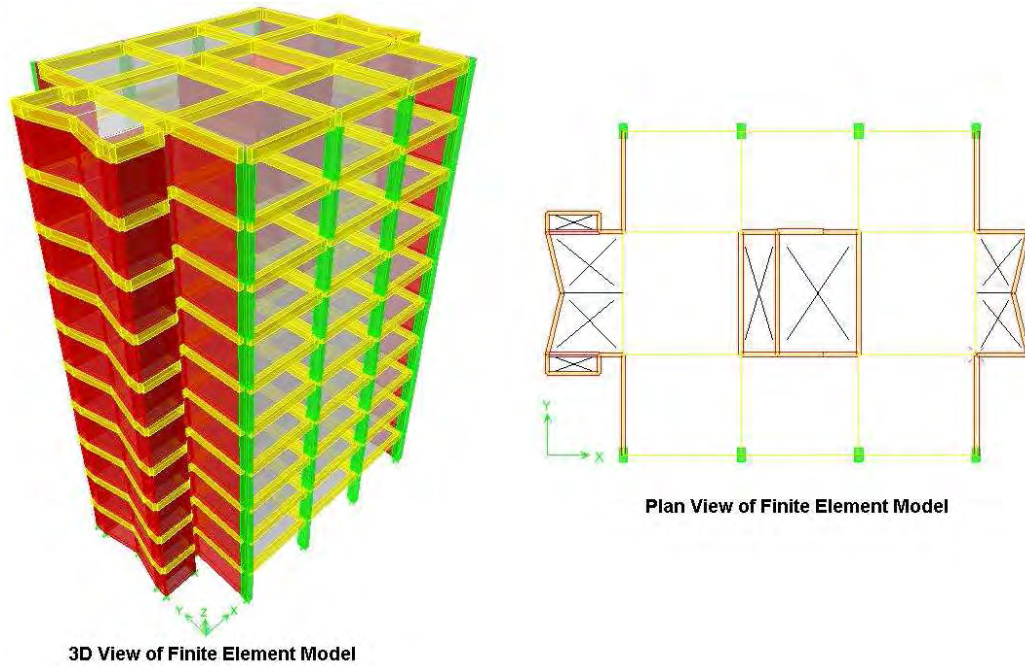


Figure 4-45 Finite Element Model of the Millikan Library

A comparison between MTRF apply to ambient vibration and a finite element model of the structure is shown in the Table 4.15, the results are very consistent, the first three modal frequencies and modal shapes can be obtained using the analytical model acquired through MFTR-FDD:

TABLE 4.15 Comparison between MTRF-FDD and Finite Element Model to Millikan Library

Mode	Freq. ETABS (Hz)	Freq. MTRF-FDD (Hz)	Modal Participation Mass Ratios			Cumulative Modal Participation		
			UX	UY	RZ	SumUX	SumUY	SumRX
1	1.17121802	1.23	70.1629	0.022	0.0748	70.1629	0.022	0.0337
2	1.815478406	1.73	0.0321	69.2128	0.0282	70.195	69.2348	97.4232
3	2.228635741	2.51	0.11	0.0876	72.7828	70.305	69.3224	97.57
4	4.574565416	5.37	17.6725	0.0205	0.0321	87.9774	69.3429	97.5745
5	4.800837266	5.52	0.0065	1.019	1.9463	87.9839	70.3619	98.8686
6	6.444627758	6.66	0.0046	2.9961	10.0607	87.9885	73.358	98.9943
7	6.525540967	7.67	0.0072	14.2869	2.445	87.9956	87.6448	99.6443
8	6.855795204		0.0558	0	0	88.0515	87.6448	99.6444
9	6.982362552		0.0003	0.1944	0.2522	88.0518	87.8392	99.8224
10	7.323432053		0.1538	0.004	0.0001	88.2056	87.8432	99.8229
11	7.652163267		0.0457	0	0	88.2512	87.8432	99.8229
12	8.171536903	8.564	1.5756	0.0018	0	88.8269	87.845	99.823
13	8.632075065		0.1516	0.0005	0	89.9785	87.8456	99.823
14	9.621768289		2.4088	0.0018	0	92.3872	87.8473	99.8231
15	10.76797174		0.2572	0.0001	0.0001	92.6445	87.8474	99.8231
16	11.35537791		1.856	0.0029	0.2721	94.5004	87.8503	99.8232
17	11.3918571		0.1116	0.0083	5.1181	94.6121	87.8586	99.8236
18	12.25535253		0.0002	1.5974	0.8422	94.6122	89.456	99.8444
19	12.70825655		0.0063	1.4605	0.8192	94.6185	90.9165	99.8774
20	13.07548477		0.5019	0.0006	0.0005	95.1204	90.917	99.8774

Finally the output result for Millikan Library for two different models and the real record will be shown, the first one is the output signal of the finite element model building (ETABS model) and the second one is the output signal from the 3 DOFs model obtained using MTFR-FDD and the final is the real record obtained from the Millikan Library.

The selected input signal is the NE270 acceleration record of San Simeon Earthquake (December 22 - 2003, Mw=6.5), recorded in the basement of Millikan Library (PGA=3.4 cm/sec²), Hipocentral Distance=322 Km.

For this earthquake recorded output signal in the building roof are available. Therefore it is possible to make a complete comparison between the two analytical models (damping ratio 5%) and the real record. The time histories for the real record and the output signals from MTFR-FDD and ETABS model are shown in the Figure 4-46.

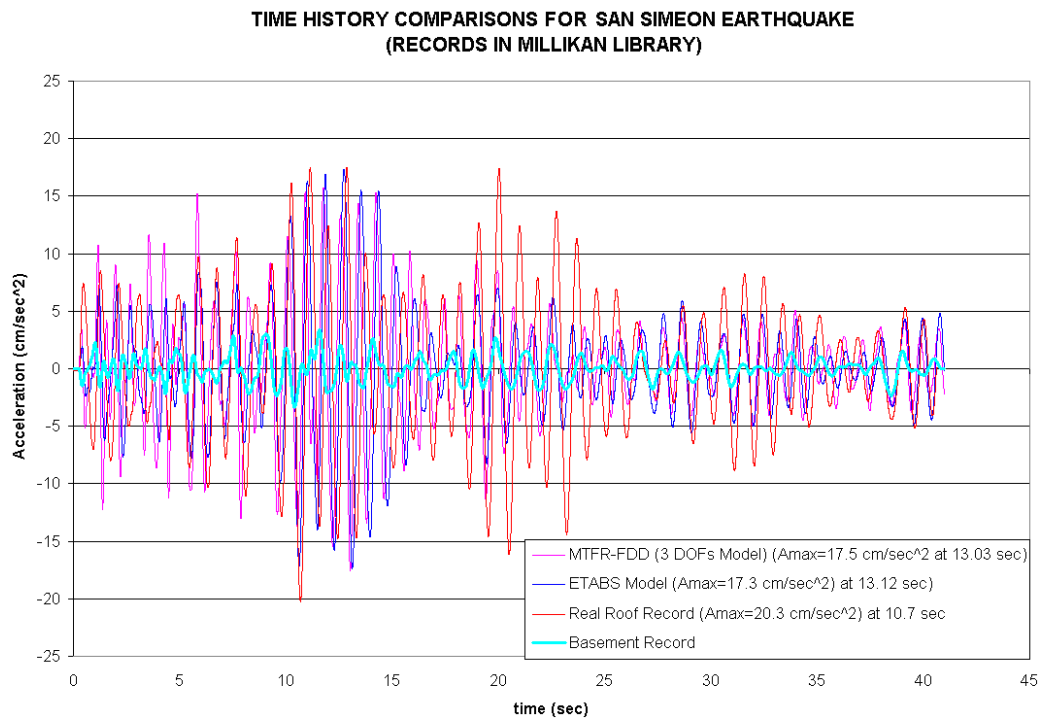


Figure 4-46 Time History Comparisons for San Simeon Earthquake recorded in Millikan Library

From the previous Figure is evident that there is an excellent correlation between the three records, although in the lapse between 20 and 25 seconds the real record have a significantly higher level than the two analytical models.

However, the results for the simple 3 DOFs model obtained from MTFR-FDD method have a remarkable behavior, since the maximum acceleration predicted is only 15% less than the real record (17.3 cm/sec² vs 20.3 cm/sec²).

Regarding to frequency behavior, in the Figure 4-47 we can see a good correlation also between real and numerical models.

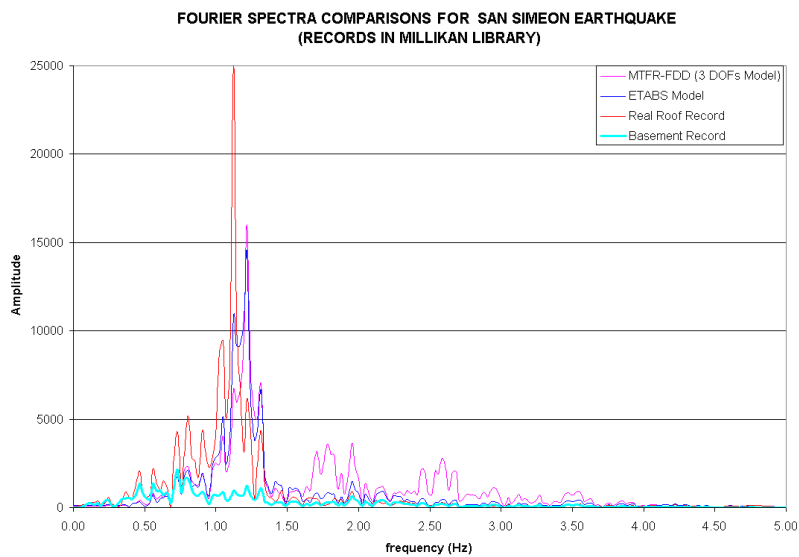


Figure 4-47 Fourier Spectra Comparisons for San Simeon Earthquake recorded in Millikan Library

Finally, the coherence function (Equation 4.42) has been evaluated and is shown in the Figure 4-48. From this graph it is evident that a non-uniform good coherence is presented in the whole frequency range. Therefore, it is recommended to take information from the other sensors in order to enhance the models results.

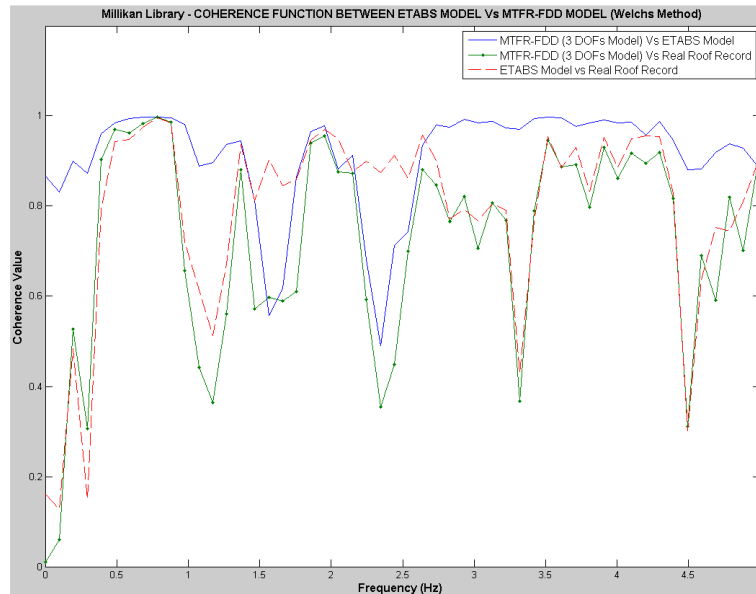


Figure 4-48 Coherence Function for Millikan Library, from Etabs Model and MTFR-FDD Model for San Simeon Earthquake of 2003, recorded in the MIK Station.

4.7.3 Airport Control Tower – Beef Island (British Virgin Islands)

The Airport control tower of the British Virgin Island is in Beef Island, in the central zone of Caribbean Sea.

The general information of Airport Control Tower is [202]:

Full Name: “Airport Control Tower – Beef Island (British Virgin Islands)”

Location: Beef Island – (64° 32’ 18”W, 18° 26’ 38”N)

Construction Date: 2001. Structural Designer: No data available

Total Levels: 7. Underground levels: 0

Height: Total absolute: 25.73 mts (top of roof-Wall lateral cover)

Earthquake & Wind Resistant System: Concrete Shear Wall (thickness: 10” and 12”)

Gravitational Load System: Concrete Shear Wall

Floor System: Slabs 8” (One way)

Concrete strength (28 days): 3.000 psi. Steel yield strength (reinforcement bar): 60.000 psi



Figure 4-49 Photo of Airport Control Tower of British Virgin Island. (Photo by: J. Martinez-Cruzado)

In the next Figure a plan and elevation view of the Airport Control Tower are shown:

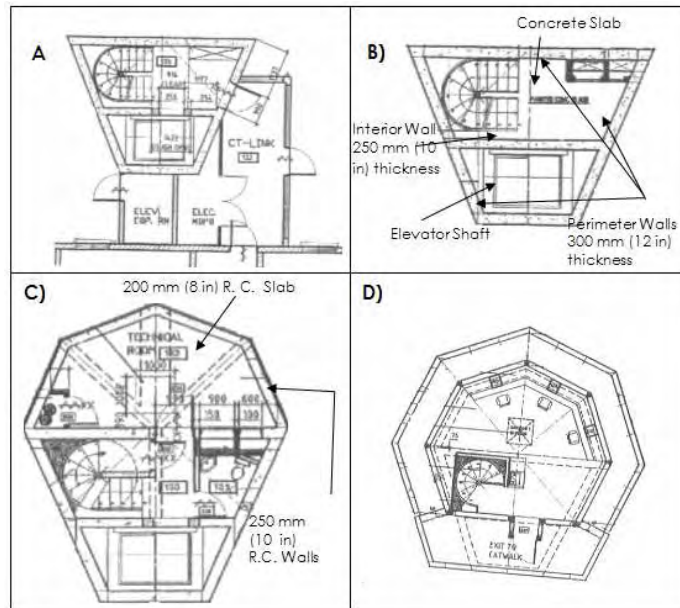


Figure 4-50 Plan view of Airport Control Tower of British Virgin Island. A) Base B) One to 4th floor C) 5th Floor D) 6th floor (Taken from reference [202])

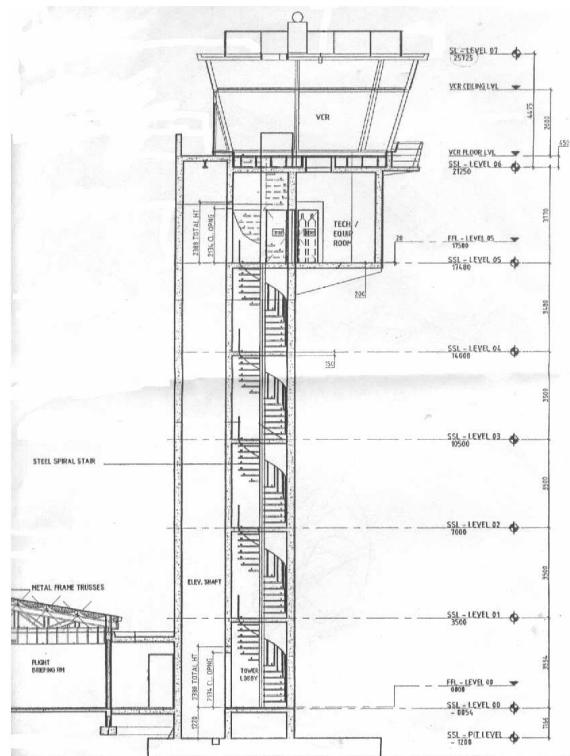


Figure 4-51 Elevation view of Airport Control Tower of British Virgin Island. (Taken from reference [202])

An ambient vibration monitoring test has been done during 22 continuous hours, the general data of the ambient vibration test is:

Duration: 22 hours, 1 min, 23 seconds (79274 seconds)

Number of Channels: 3

Sampling rate: 100 sps

Start time: 7/30/2007 - 22:08:58.000 (10:08 p.m.) End time: 7/31/2007 - 20:10:21 (8:10 p.m.)

The acceleration record of longitudinal sensor placed on the 6th floor of the building is shown in Figure 4-38:

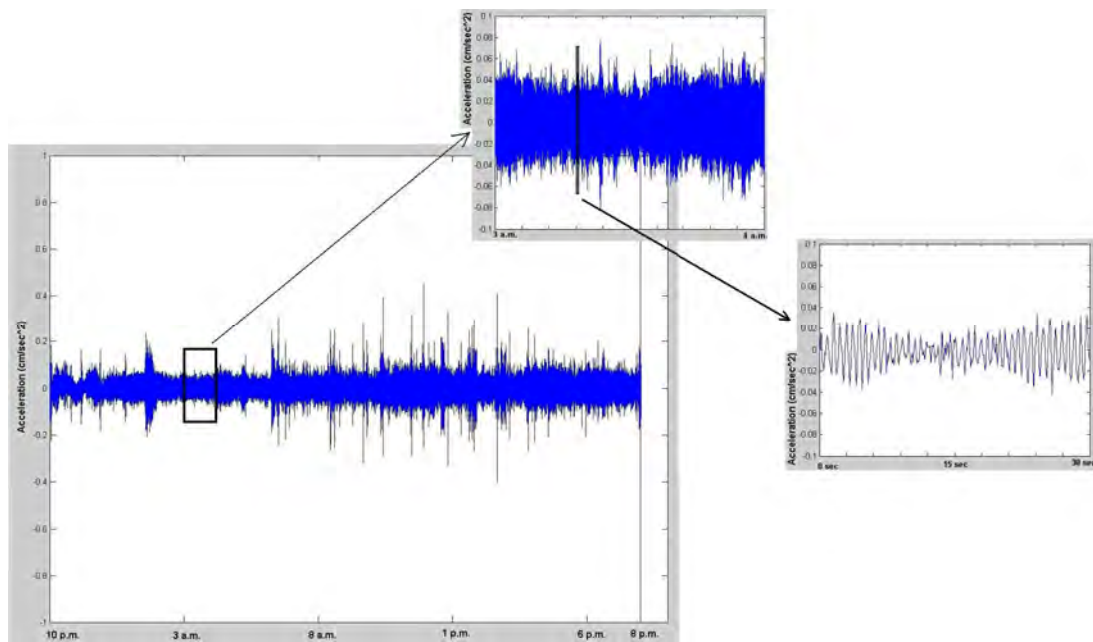


Figure 4-52 Acceleration record of ambient vibration test in the Airport Control Tower of British Virgin Island.

From the traditional direct analysis of the ambient vibration (such as Fourier analysis) is not straightforward to extract the fundamental frequencies of the system without the use of additional building information. As it is evident in the next Figure:

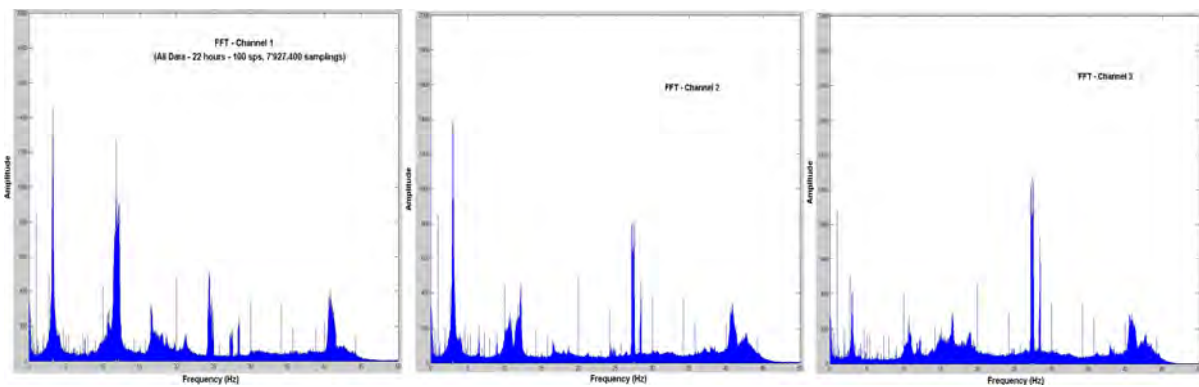


Figure 4-53 Fourier spectra of ambient vibration test in the Airport Control Tower of British Virgin Island (Horizontal Channels: 1 and 2, Vertical Channel: 3).

Using a simple time-frequency representation such as a spectrogram, some useful information about the system emerges, thus it is evident from the Figure 4-54:

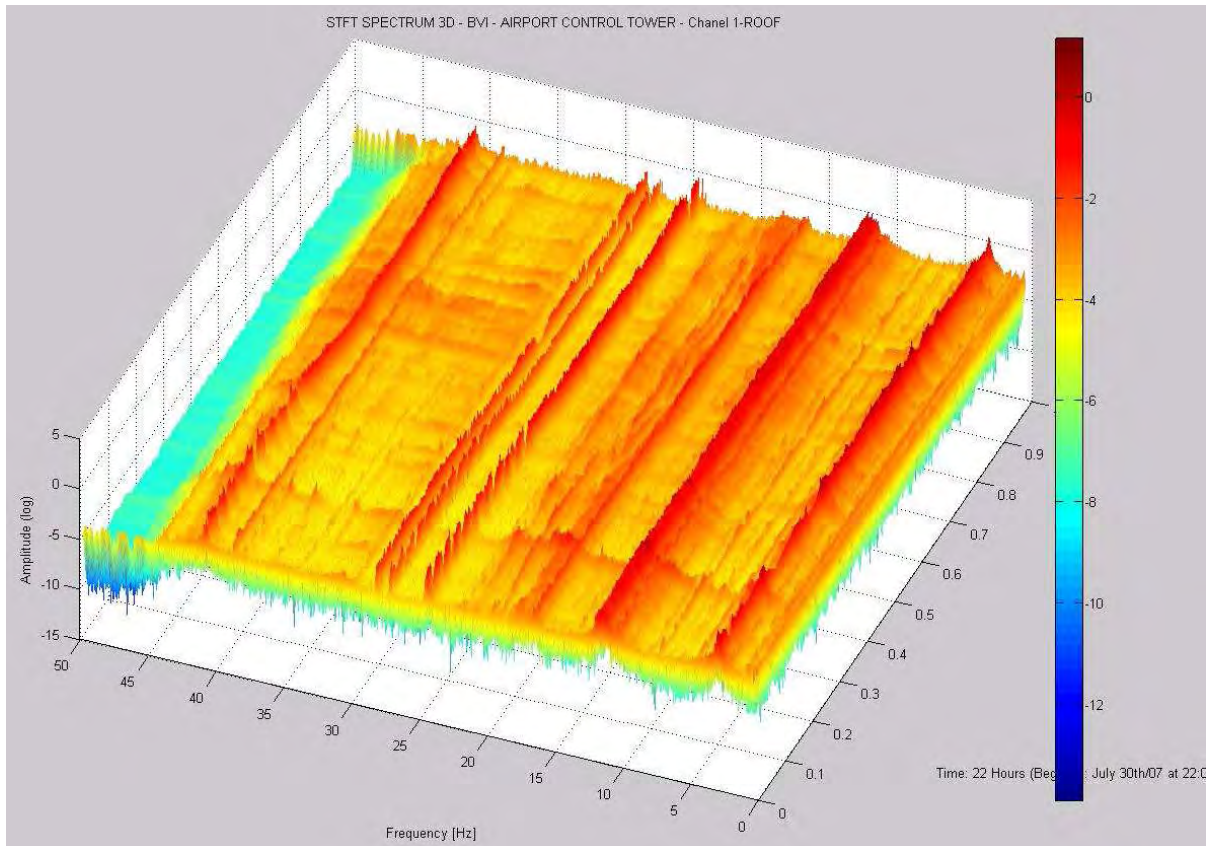


Figure 4-54 STFT Spectrum for ambient vibration test in the Airport Control Tower of British Virgin Island.

Observing the Figures 4.53 and 4-54, some frequencies can be seen that look like machines (close to 40 Hz and between 25 to 30 Hz), and frequencies that seem to be from the structure (i.e. near to 5 Hz), but this visual inspection is not absolute.

It is necessary to use the technique developed in this Chapter, first the Mean Time Frequency Representation will be evaluated, as shown in the Figure 4-55:

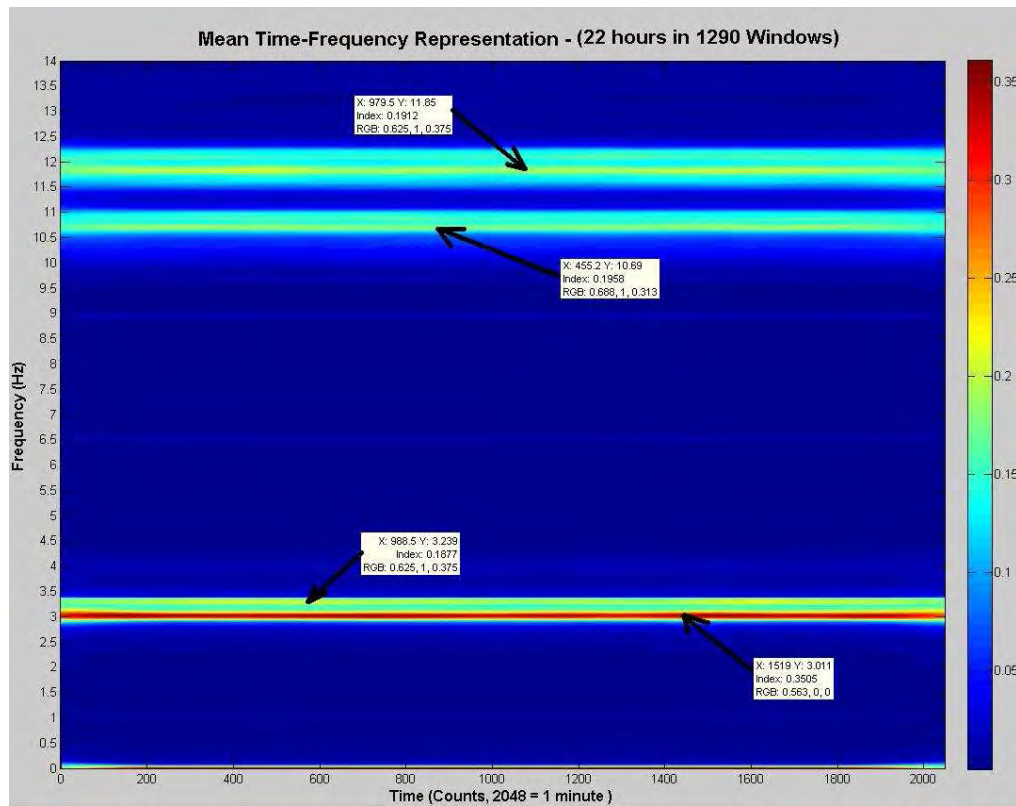


Figure 4-55 Mean Time Frequency Representation of ambient vibration test in the Airport Control Tower of British Virgin Island.

From the MTFR of Figure 4-55, all dominant signals frequencies can be extracted, although machines and structural frequencies appear together (i.e. the frequencies in 10.69 Hz and 11.85 Hz).

The next step consists in the differentiation between real structural and external or machines frequencies from MTFR.

In the Figure 4-56 the empirical probabilistic density distributions obtained from MTFR is shown, and from this Figure it is clear which frequencies are or which are not structural frequencies.

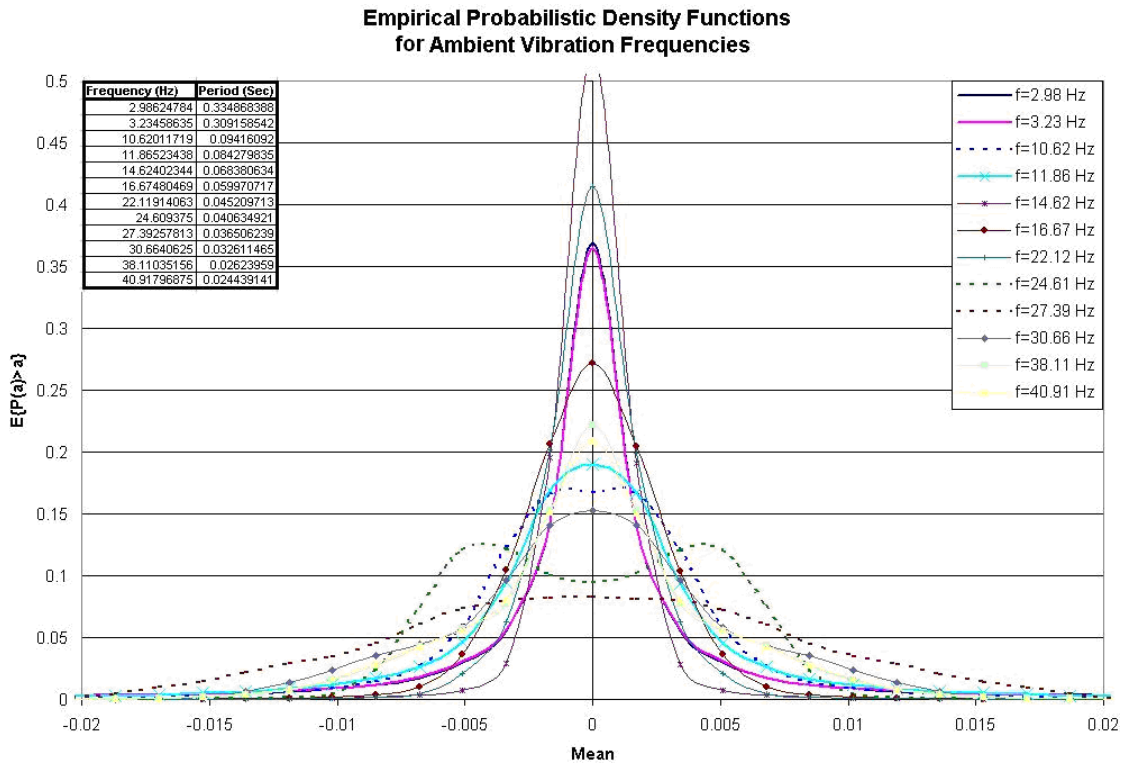


Figure 4-56 Empirical Probabilistic Density Functions from MTFR of ambient vibration test in the Airport Control Tower of British Virgin Island.

Now using MTFR-FDD the relative mass and stiffness matrices of the structure can be evaluated.

In order to get an independent structural identification result, the continuous record of 22 hours has been divided in two parts, the first interval between zero time to 10 hours (10:00 p.m. to 8:00 a.m.), and the second part between 12 hours and the final of record (10:00 a.m. to 8:00 pm.), thus a two hours gap between set has established..

In the following Table the results of these two identification process is shown (Note: Mass values divided by 1E5 and Stiffness values divided by 1E9) :

TABLE 4.16 Estimative for a 3 DOFs Model from Airport Control Tower (Uncorrected)

Mass Matrix Estimative (First 10 Hours)			Stiffness Matrix Estimative (First 10 Hours)				
	1	2	3		1	2	3
1	0.67347717481820	-2.38383415401125	1.39121254831664	1	0.16556652295403	-0.57932412692466	0.33792597911578
2	-2.38383415401125	8.44025215222022	-4.92593530566408	2	-0.57932412692466	2.02722405699632	-1.18250924979239
3	1.39121254831664	-4.92593530566408	2.87491322566494	3	0.33792597911578	-1.18250924979239	0.68977550666141

Mass Matrix Estimative (Second 10 Hours)			Stiffness Matrix Estimative (Second 10 Hours)				
	1	2	3		1	2	3
1	0.45991850682484	-1.66964296968441	0.97847183279040	1	0.11352335306900	-0.40554956939741	0.23742960312546
2	-1.66964296968442	6.06479938501595	-3.55446326568957	2	-0.40554956939741	1.44898536970795	-0.84832303752715
3	0.97847183279041	-3.55446326568957	2.08322898858133	3	0.23742960312546	-0.84832303752715	0.496660263595635

As can be seen from Table 4.16, the mass matrix estimation and stiffness matrix change, since the mass do not have any changes between measurements, the equations 4.29 and 4.31 can be applied. Therefore, the corrected stiffness matrix for the two independent measurement sets is:

TABLE 4.17 Stiffness Matrix Estimative for a 3 DOFs Model from Millikan Library (Corrected)

Stiffness Matrix Estimative (First Day)			Stiffness Matrix Estimative (Sixth Day)				
	1	2	3		1	2	3
1	0.30358905658548	-0.62452422952140	0.31839889297863	1	0.30003569873091	-0.61751082584908	0.31488858624413
2	-0.62452422952140	1.28473851128881	-0.65500073648180	2	-0.61751082584908	1.27097352392202	-0.64811463297627
3	0.31839889297863	-0.65500073648180	0.33384098215651	3	0.31488858624413	-0.64811463297627	0.33049753220312

The comparison between MTFR-FDD apply to ambient vibration and a finite element model of the structure is shown, the FE model has been elaborated by N. Rojas and Martinez-Cruzado [202], using ETABS[201] software.

As can be seen from Table 4.18, the results of the FE model [202] are very consistent with the ambient vibration and MTFR-FDD results of this study:



Figure 4-57 Finite Element Model for the Airport Control Tower of British Virgin Island [202].

TABLE 4.18 Comparison between MTFR-FDD and Finite Element Model [202] for Airport Control Tower

Mode	Frequency (Hz)	
	MTFR-FDD	ETABS
1	2.986	3.020
2	3.234	3.533
3	11.862	9.811
4	14.620	14.982
5	16.667	19.045
6	22.124	22.163
7	30.675	33.952
8	38.168	35.573
9	40.984	43.800

Finally the output result for the Control Tower for the two different models is shown. The first one is the output signal of the finite element model building (ETABS model) and the second one is the output signal from the 3 DOFs model obtained using MTFR-FDD.

The selected input signal is the acceleration record for the earthquake of November 29th of 2007, recorded in the basement of the Airport Control Tower, (Mw=7.4, Depth= 140 Km, Hipocentral Distance= 543 Km), the acceleration record and the Fourier Spectra are shown in the following Figure:

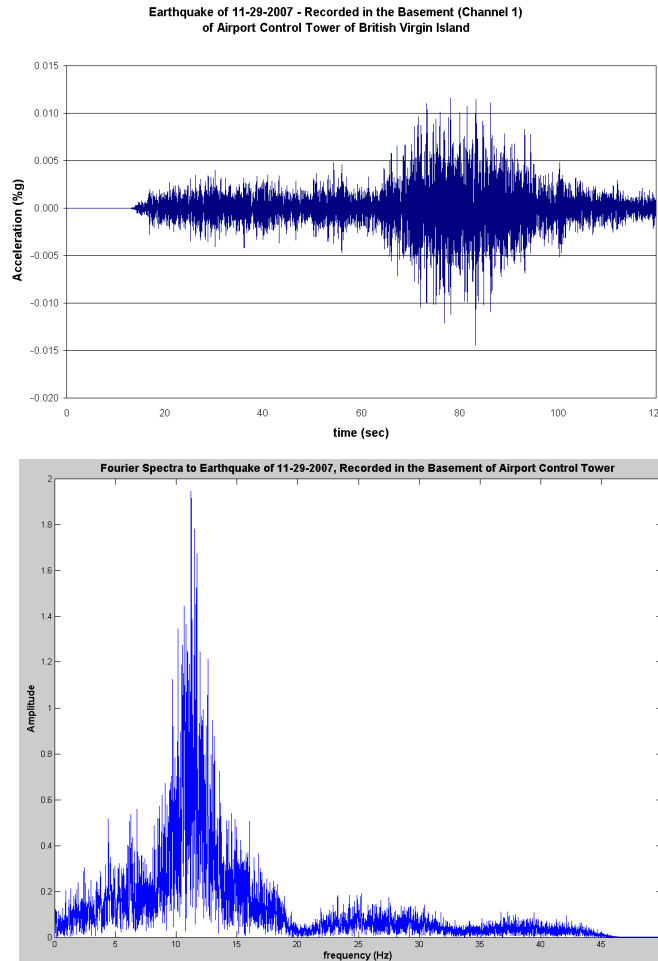


Figure 4-58 Horizontal Acceleration record and Fourier Spectra for Earthquake from 11-29-2007, recorded in the Basement of Airport Control Tower of British Virgin Islands.

Using the previous record, the two models of the building has been excited in the base and the output signals for this event is shown in Figure 4-59. From this Figure is evident that the single model obtained using MTFR-FDD can predict the real output signal better:

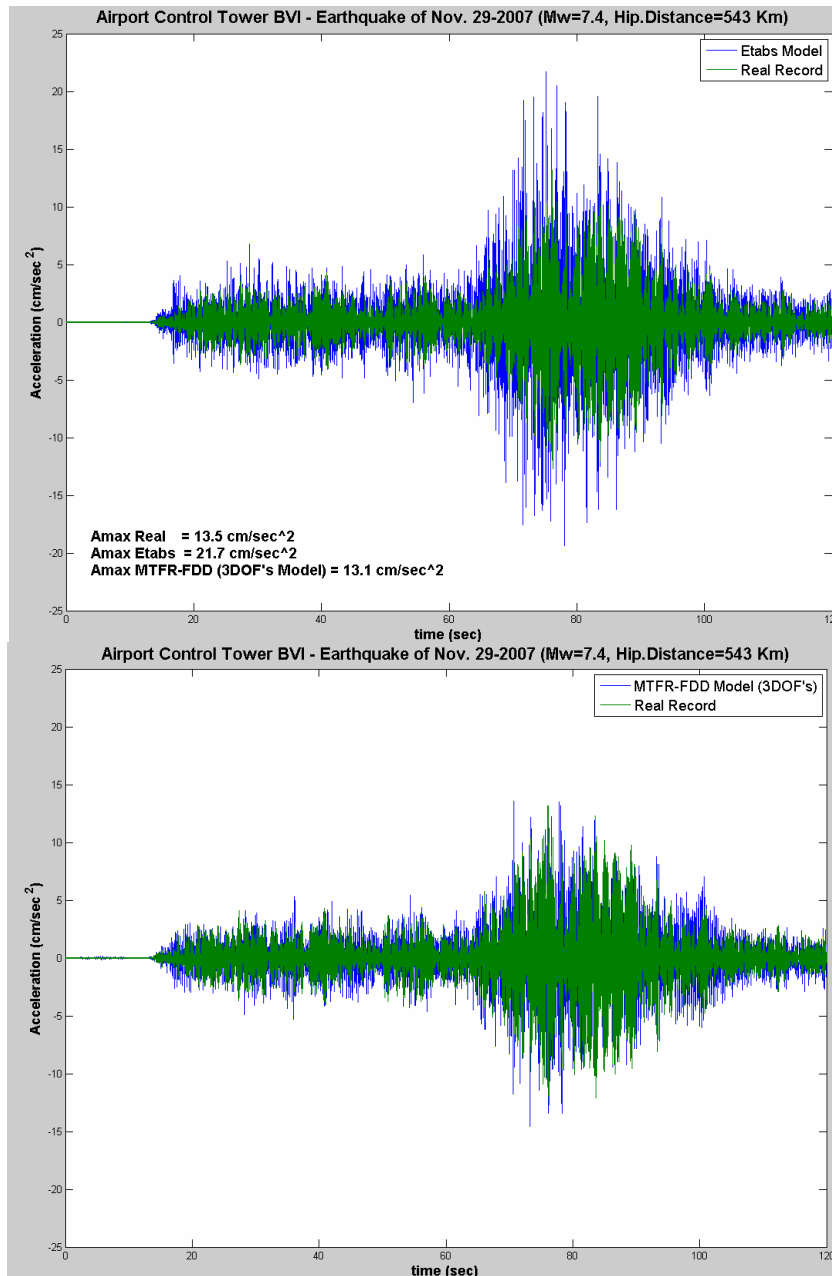


Figure 4-59 Comparison of output signal for Etabs Model, MTFR-FDD Model and Real record for Earthquake from 11-29-2007, recorded in the roof of Airport Control Tower of British Virgin Islands.

4.7.4 Plaza Inmaculada Building – San Juan, Puerto Rico

For the first case, a complete system identification and damage detection evaluation of the structure has been done using the MTFR-FDD technique. The second stage is the development of a complete FEM for the Building and a comparison of the model results with the MTFR-FDD.

The Plaza Inmaculada Building is located in the Santurce area in the city of San Juan Puerto Rico. It is a 27 story shear-wall reinforced concrete building. The complex is conformed by two slender twin buildings, and only the Torre Norte (or Plaza Inmaculada II) has been instrumented. A view of the complex is shown in the Figure 4-60. In this Figure the slender instrumented building can be seen. They are the most slender towers in Puerto Rico [120].



Figure 4-60 View of Plaza Inmaculada Building (Photo by: L. Cano).

Some general data for Plaza Inmaculada Building are [120]:

Full Name: "Plaza Inmaculada II"

Location: Santurce, San Juan, Puerto Rico, (Building is at: 18.44282 N, 66.06153 W)

Design Date: 1987

Final Construction Date: 1992

Design Code: Puerto Rican Building Code (1987) and ACI-318-83

Total Levels: 27

Height: 253 ft

Mean Interstory height: 8.5 ft

Earthquake & Wind Resistant System: Reinforced Concrete Shear Walls

Gravitational Load System: Reinforced Concrete Shear Wall

Floor System: Slabs 5.5" (One way)

Concrete strength (28 days): 5.000 psi (basement to 9th floor) (Shear Walls and Columns), 4.000 psi (10th to roof floor), 4.000 psi to floor slabs

Steel yield strength (reinforcement bar): 60.000 psi

Wall thickness: 8", 10" and 12" (First Floor) and 8" and 10" (Second to roof floor)

Beam Sections: b=8" to 14", Depth: 14" to 36"

Total Area per floor = 5.400 ft², Shear Wall area in NS direction: 256.5 ft² (4.75% of Total Area), Shear Wall area in EW direction: 129.6 ft² (2.4% of Total Area)

A plan and elevation view of the building and the installed instrumentation is shown in the following Figure:

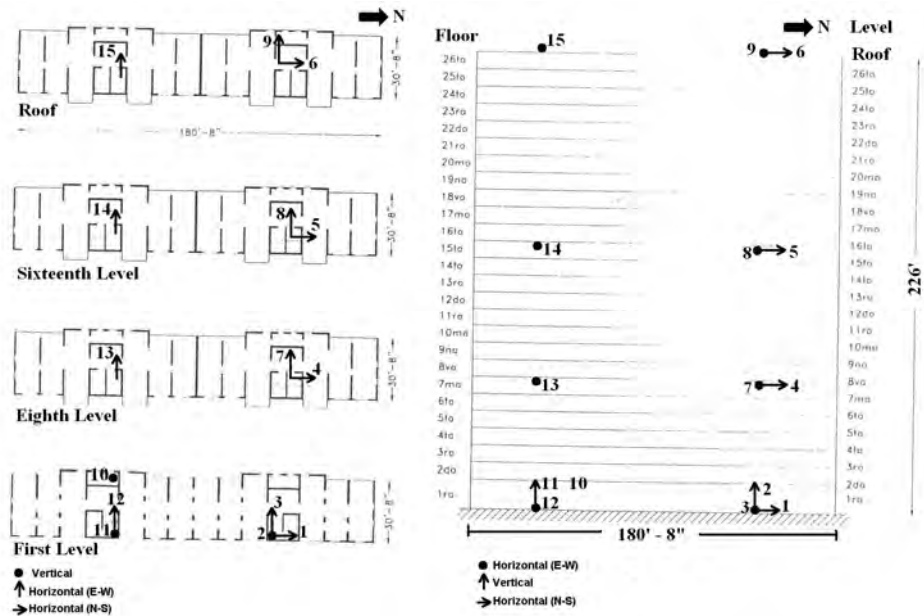


Figure 4-61 Plan, Elevation and Installed Instrumentation view of Plaza Inmaculada Building (Adapted from [120])

In the Figure 4-62 a typical continuous 15 hours of recording (December 26/2005) is shown.

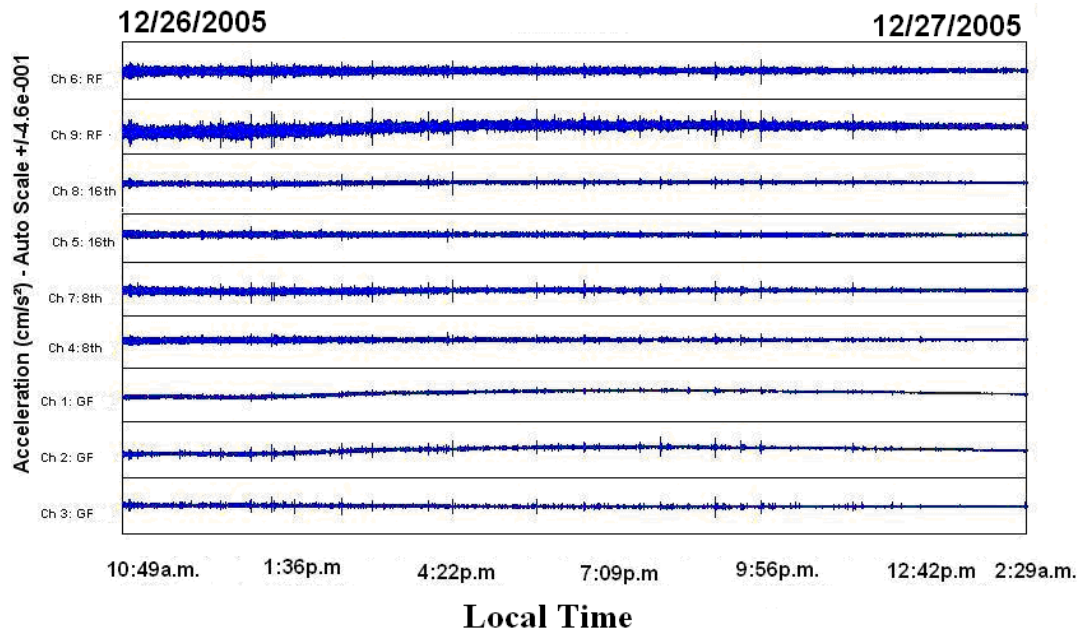


Figure 4-62 Time History of a continuous 15 hours recording in Plaza Inmaculada

As it can be seen from Figure 4-62, the amplitudes increase for higher stories and the movements in the N-S direction (Channels 4, 5 and 6) are significantly less than the movements in E-W direction for the same stories (Channels 7, 8 and 9). This is a clear indicative of the stiffness differences between the strong (N-S direction) and weak (E-W direction) axis of the structure. In Figure 4-63, a continuous recording of twenty days for the Channel 9 is shown, in this graph the two small earthquakes can be noted which appear in a spike fashion can be seen.

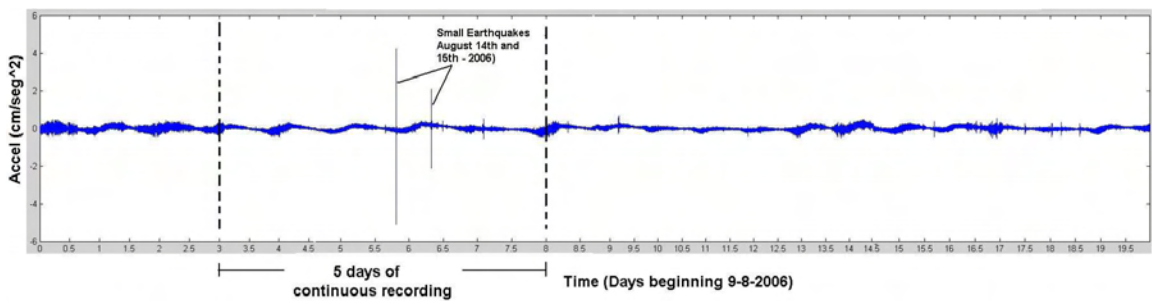


Figure 4-63 Time History of a continuous 20 days (Channel 9) recording in Plaza Inmaculada

Using ambient vibration real data a linear time-frequency representation for the five days of ambient vibration record windows (Figure 4-63) from the building can be obtained, it is shown in the Figures 4-64 and 4-65:

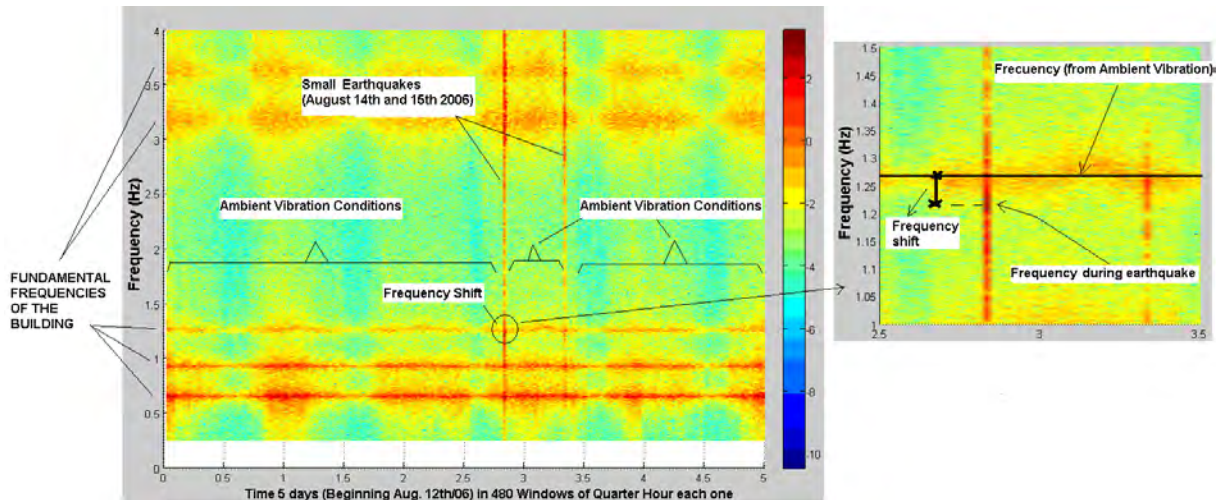


Figure 4-64 Linear Time-Frequency Representation for a 5 days of continuous recording in Plaza Inmaculada

A 3D view of this linear time-frequency representation can be seen in Figure 4-65:

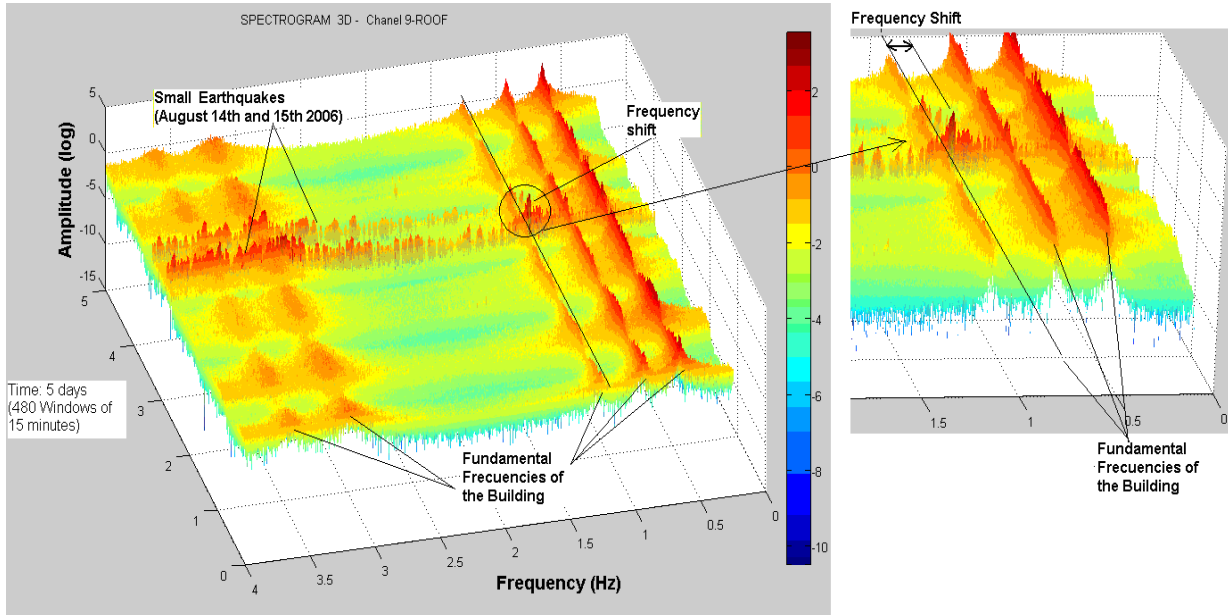


Figure 4-65 Linear 3D Time-Frequency for a 5 days of continuous recording in Plaza Inmaculada Building

Figures 4-64 and 4-65 show that the small earthquakes of August 14th and 15th /2006 produced a temporary shift in the third frequency in Plaza Inmaculada of 4% (from 1.28 Hz to 1.22 Hz, the frequency returned to its initial value of 1.28 Hz at the end of the excitation). The previous temporary frequency shift is not due to damage. For this building the third frequency is the fundamental translational mode in the strong direction (N-S) of the building and it will be discussed in detail furthermore.

In order to apply the MTFR-FDD method for Plaza Inmaculada, two years of available data were selected, the previous continuous 20 days record for nine of the fifteen channels available in Plaza Inmaculada (the six input channels in the building basement are not used due to the philosophy of this research).

As can be seen in the Figure 4-63 the selected days include the two small earthquakes of August 14th and 15th of 2006, because of the interest in determining if any of these earthquakes had produced a permanent damage in the building.

For the first stage 500 measurements of 1 min at a sampling frequency of 200 Hz has been processed from 00:00:00 to 08:20:00 of August 11th-2006, prior to August 14th and 15th Earthquakes. The MTFR for the first set is shown in the next two graphs:

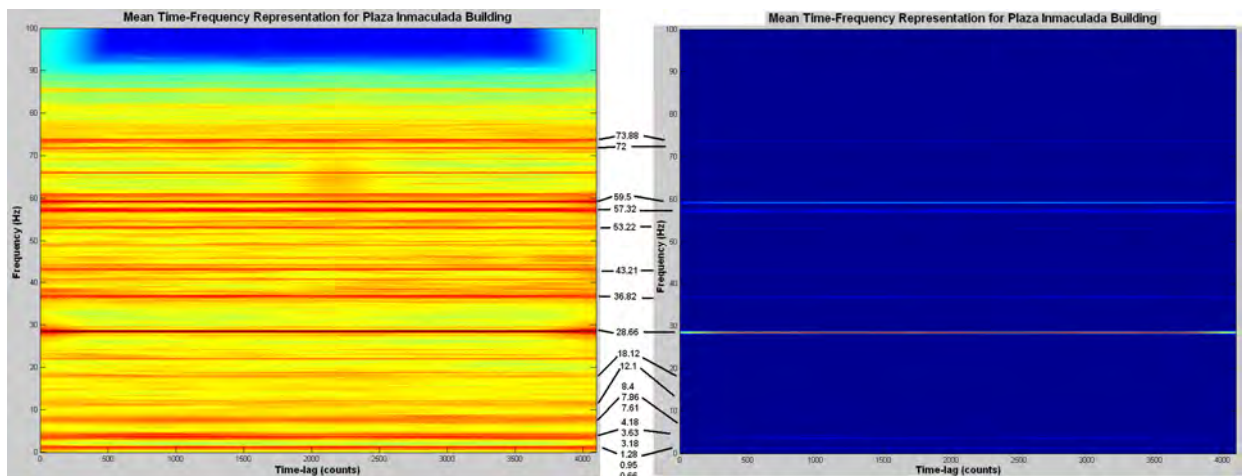


Figure 4-66 MTFR from DC to 100 Hz for Plaza Inmaculada Building (00:00:00 to 08:20:00 August 11th/2006) (Left: Linear Scale, Right: Logarithmic Scale)

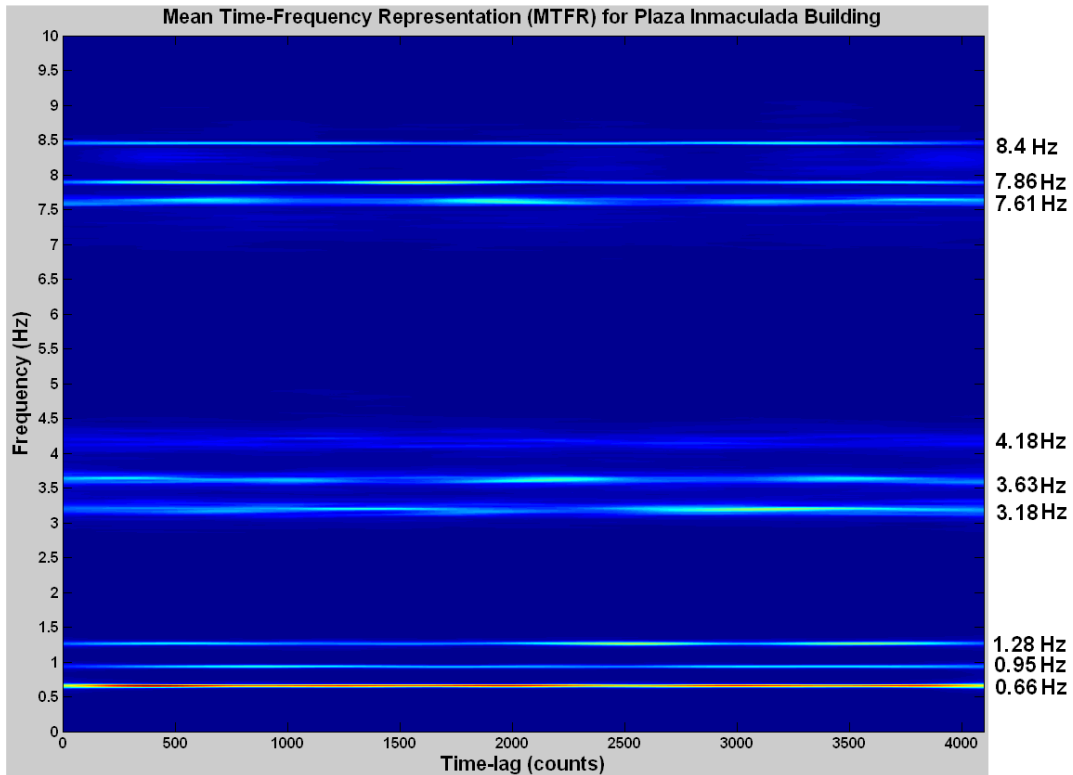


Figure 4-67 MTRF from DC to 10 Hz for Plaza Inmaculada Building (00:00:00 to 08:20:00 August 11th/2006)

From the Figures 4-66 and 4-67 it is evident that there exist a lot of frequencies that should be structural frequencies. If one knows what type of structure is the records from, one can perform a direct elimination of several frequencies (i.e. in this case frequencies more than 20 Hz), on the other hand the frequencies due to electric and electronic noise [206] can also be eliminated, for instance frequencies at 28.66 and 59.5 Hz [206].

For other frequencies from non-evident source, it is necessary to perform a detail separation using for example the empirical probabilistic density procedure.

In the Figure 4-68 the empirical probabilistic density distributions obtained from MTRF for Plaza Inmaculada is shown :

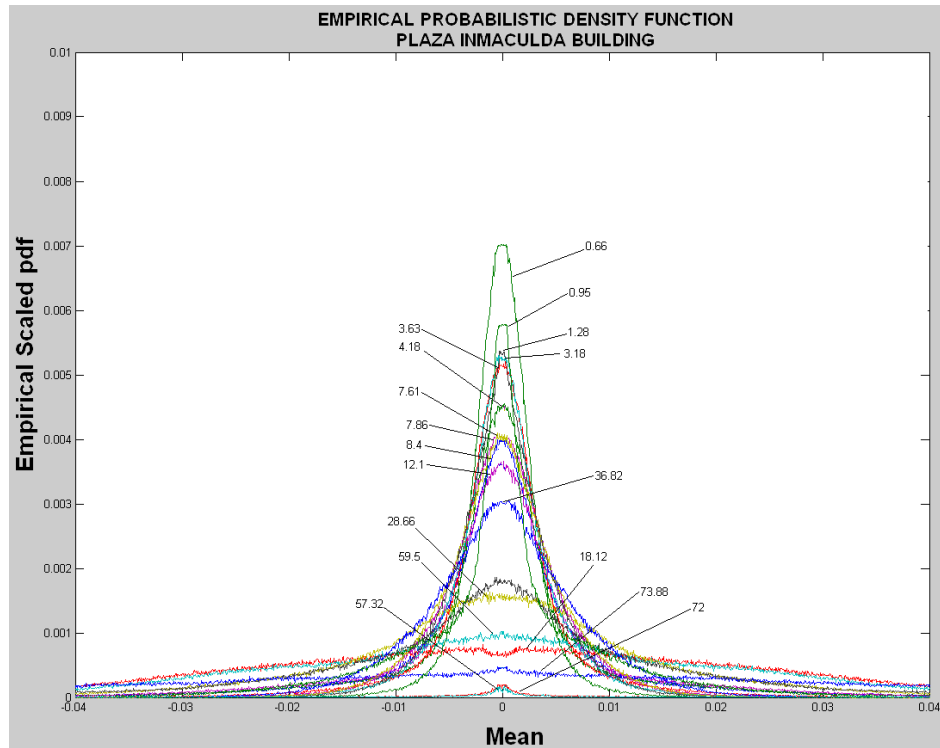


Figure 4-68 Empirical Probabilistic Density Functions from MTFR of ambient vibration for Plaza Inmaculada Building.

From Figure 4.68 and according to Brincker’s criteria [192] all frequencies below 10 Hz identified from MTFR are structural frequencies.

The procedure to get the MTFR for the second measurements set (August 16th/2006) has been repeated and the frequencies obtained are the eigenvalues for the second identification stage.

Now using MTFR-FDD the relative stiffness matrix for the structure can be evaluated. In order to get an independent structural identification result, the continuous record of 20 days has been divided in twenty parts. The first interval is corresponding to the record of August 11th (day 1), and the second interval corresponds to August 17th, thus a five day gap between sets has been established and this gap includes the two small earthquakes from August 14th

and 15th. For each of those days we have used 500 measurements of 1 minute each (8:20 hours).

In the following Table the results for these two different identification process using MTRF-FDD are shown (Note: Mass values divided by 1E6, and Stiffness values divided by 1E8):

TABLE 4.19 Estimative for a 9 DOFs Model for Plaza Inmaculada Building (Uncorrected)

Mass Matrix Estimative (2006-08-11)									Mass Matrix Estimative (2006-08-17)								
1	2	3	4	5	6	7	8	9	1	2	3	4	5	6	7	8	9
0.015180	-0.009890	-0.003980	0.011880	-0.009070	0.055260	-0.068500	-0.013450	0.030200	0.020920	-0.006980	-0.018570	0.028420	-0.009540	0.018000	-0.025630	-0.013630	0.018630
-0.009890	0.006930	0.001820	-0.007150	0.005990	-0.038290	0.047300	0.009090	-0.020670	-0.006980	0.006340	-0.004660	0.002260	0.000480	-0.018640	0.023280	0.004890	-0.010510
-0.003980	0.001820	0.003010	-0.005180	0.002640	-0.011300	0.014360	0.003320	-0.006780	-0.018570	-0.004660	0.052050	-0.066570	0.019990	0.009170	-0.005170	0.014960	-0.011500
0.011880	-0.007150	-0.005180	0.011890	-0.007650	0.041070	-0.051280	-0.010600	0.023080	0.028420	0.002260	-0.066570	0.088110	-0.027410	0.001250	-0.010010	-0.023470	0.022980
-0.009070	0.005990	0.002640	-0.007650	0.005990	-0.034460	0.042580	0.008210	-0.018650	-0.009540	0.000480	0.019890	-0.027410	0.012180	-0.015970	0.020050	0.005810	-0.010560
0.055260	-0.038290	-0.011300	0.041070	-0.034460	0.218010	-0.269030	-0.051050	0.117050	0.018000	-0.018640	0.009170	0.001250	-0.015970	0.120190	-0.142730	-0.015660	0.052410
-0.068500	0.047300	0.014360	-0.051280	0.042580	-0.269030	0.332240	0.063220	-0.144720	-0.025630	0.023280	-0.005170	-0.010010	0.020050	-0.142730	0.172110	0.023970	-0.067610
-0.013450	0.009090	0.003320	-0.010600	0.008210	-0.051050	0.063220	0.012630	-0.028020	-0.013630	0.004890	0.014960	-0.023470	0.005810	-0.015660	0.023970	0.016660	-0.020590
0.030200	-0.020670	-0.006780	0.023080	-0.018650	0.117050	-0.144720	-0.028020	0.063440	0.018630	-0.010510	-0.011500	0.022990	-0.010560	0.052410	-0.067610	-0.020590	0.035970

Stiffnes Matrix Estimative (2006-08-11)									Stiffnes Matrix Estimative (2006-08-17)								
1	2	3	4	5	6	7	8	9	1	2	3	4	5	6	7	8	9
0.190200	-0.119100	-0.049300	0.146600	-0.113600	0.687700	-0.851500	-0.165700	0.377000	0.261500	-0.083000	-0.230400	0.354300	-0.119700	0.224500	-0.318900	-0.168300	0.234100
-0.120100	0.087700	0.022200	-0.088200	0.074700	-0.481100	0.590400	0.117600	-0.266800	-0.084900	0.080700	-0.056900	0.029000	0.006000	-0.233000	0.289200	0.063300	-0.136100
-0.050400	0.022800	0.037000	-0.064200	0.032100	-0.140200	0.177800	0.043000	-0.086000	-0.234000	-0.058700	0.641300	-0.839600	0.242800	0.113000	-0.064200	0.194300	-0.145600
0.148700	-0.088900	-0.064900	0.149800	-0.099900	0.516700	-0.651800	-0.134300	0.291600	4	0.356800	0.028100	-0.834700	1.122600	-0.154100	0.015800	-0.125400	-0.298300
-0.115600	0.076800	0.033000	-0.095000	0.073900	-0.439300	0.545200	0.101600	-0.237300	5	-0.121800	0.006200	0.250400	-0.343700	0.154400	-0.205100	0.254400	0.071500
0.688400	-0.475500	-0.142700	0.522900	-0.425800	2.643400	-3.359500	-0.645200	1.465600	6	0.223200	-0.230900	0.116500	0.015900	-0.198900	1.447000	-1.789900	-0.196200
-0.883300	0.587400	0.182400	-0.630700	0.518800	-3.407700	4.037300	0.769700	-1.787100	7	-0.331500	0.289100	-0.065200	-0.123100	0.243700	-1.800100	2.097300	0.289500
-0.163100	0.114900	0.041300	-0.129100	0.100900	-0.625600	0.789100	0.150200	-0.345400	8	-0.163400	0.062100	0.186500	-0.267500	0.071100	-0.193000	0.297600	0.199500
0.367000	-0.260100	-0.085800	0.289300	-0.232600	1.386000	-1.810000	-0.344200	0.788800	9	0.227000	-0.131800	-0.145000	0.289900	-0.131600	0.625100	-0.846100	-0.254600

As can be seen from Table 4.19, the mass matrix estimation and stiffness matrix change. Since the mass does not have any changes between measurements, the equations 4.29 and 4.31 can be applied. Therefore, the corrected stiffness matrix for the two independent measure sets are:

TABLE 4.20 Stiffness Matrix Estimative for a 9 DOFs Model from Plaza Inmaculada Building (Corrected)

Final Stiffnes Matrix Estimative (2006-08-11)									Final Stiffnes Matrix Estimative (2006-08-17)								
1	2	3	4	5	6	7	8	9	1	2	3	4	5	6	7	8	9
0.190200	-0.119100	-0.049300	0.146600	-0.113600	0.687700	-0.851500	-0.165700	0.377000	0.189750	-0.117603	-0.049380	0.148103	-0.113803	0.689215	-0.852308	-0.165979	0.379486
-0.120100	0.087700	0.022200	-0.088200	0.074700	-0.481100	0.590400	0.117600	-0.266800	-0.120295	0.086210	0.022223	-0.088584	0.074675	-0.478625	0.587593	0.117668	-0.267688
-0.050400	0.022800	0.037000	-0.064200	0.032100	-0.140200	0.177800	0.043000	-0.086000	-0.050152	0.022626	0.037086	-0.065332	0.032200	-0.139248	0.175320	0.043120	-0.085841
0.148700	-0.088900	-0.064900	0.149800	-0.099900	0.516700	-0.651800	-0.134300	0.291600	4	0.149064	-0.086800	-0.084950	0.150343	-0.100781	0.519125	-0.642158	-0.134724
-0.115600	0.076800	0.033000	-0.095000	0.073900	-0.439300	0.545200	0.101600	-0.237300	5	-0.115799	0.077371	0.033236	-0.095925	0.074665	-0.442564	0.540267	0.101035
0.688400	-0.475500	-0.142700	0.522900	-0.425800	2.643400	-3.359500	-0.645200	1.465600	6	0.685224	-0.474311	-0.143561	0.522410	-0.429186	2.624682	-3.373760	-0.639592
-0.883300	0.587400	0.182400	-0.630700	0.518800	-3.407700	4.037300	0.769700	-1.787100	7	-0.885983	0.587390	0.181097	-0.630380	0.517543	-3.392986	4.048614	0.763546
-0.163100	0.114900	0.041300	-0.129100	0.100900	-0.625600	0.789100	0.150200	-0.345400	8	-0.161242	0.115437	0.041389	-0.129847	0.100470	-0.629160	0.784909	0.151242
0.367000	-0.260100	-0.085800	0.289300	-0.232600	1.386000	-1.810000	-0.344200	0.788800	9	0.367976	-0.259211	-0.085487	0.290031	-0.232419	1.396069	-1.811087	-0.346746

From Table 4.20 it is evident that no changes occur in the structure and according to the damage definition no damage occurred between the first and second sets of measurements.

From the MTFR-FDD by solving the eigenvalue problem the modal matrix is:

TABLE 4.21 Modal Matrix Estimative for a 9 DOFs Model from Plaza Inmaculada Building

Modal Matrix Estimative									
	1	2	3	4	5	6	7	8	9
1	0.000600	-0.022200	0.009900	-0.007600	0.071100	0.079800	0.061200	0.052100	-0.023600
2	0.002100	-0.092600	0.040000	-0.019200	0.202400	0.215400	0.072200	0.068100	-0.023100
3	0.005700	-0.237400	0.102700	-0.021300	0.256300	0.248400	0.166900	0.149200	-0.062200
4	-0.013100	-0.356900	0.170400	-0.108200	0.251300	0.322100	0.225100	0.230100	-0.135400
5	-0.059000	-0.444600	0.242000	-0.242100	0.215200	0.407600	0.308300	0.307600	-0.193200
6	-0.219300	-0.423000	0.330300	-0.262900	0.256300	0.436200	0.339600	0.386700	-0.308900
7	-0.380300	-0.403800	0.418000	-0.369300	0.351000	0.417500	0.412500	0.426400	-0.417600
8	-0.543600	-0.378700	0.506700	-0.559000	0.502300	0.346300	0.481400	0.494000	-0.526900
9	-0.712800	-0.352200	0.599600	-0.641000	0.581100	0.362100	0.547900	0.497400	-0.626000

Using the traditional dynamic formulation [127] and from results of MTFR-FDD and tables 4.20 and 4.21, the following dynamic structural model can be constructed:

$$[M]\{\ddot{x}(t)\} + [C]\{\dot{x}(t)\} + [K]\{x(t)\} = \{F(t)\} \quad 4-47$$

Where:

$[M]$: Mass matrix

$[C]$: Damping matrix

$[K]$: Stiffness Matrix

$\{x(t)\}$: Displacement time history vectors (superscript dot represent time derivative)

$\{F(t)\}$: Force time history vectors

Using data from MTFR-FDD:

$$\{f_j\} = \begin{Bmatrix} 0.660 \\ 0.952 \\ 1.280 \\ 3.180 \\ 3.630 \\ 4.180 \\ 7.610 \\ 7.860 \\ 8.400 \end{Bmatrix} \text{ (Hz)} \quad \{\omega_j\} = \begin{Bmatrix} 4.1469 \\ 5.9816 \\ 8.0425 \\ 19.9805 \\ 22.8080 \\ 26.2637 \\ 47.8150 \\ 49.3858 \\ 52.7788 \end{Bmatrix} \text{ (rad/sec)} \quad 4-48$$

And using 5% of damping:

$$[C] = \begin{bmatrix} 0.1216 & -0.0703 & -0.0504 & 0.1128 & -0.0680 & 0.3533 & -0.4423 & -0.1018 & 0.2076 \\ -0.0703 & 0.0537 & 0.0001 & -0.0367 & 0.0367 & -0.2636 & 0.3253 & 0.0634 & -0.1428 \\ -0.0504 & 0.0001 & 0.1047 & -0.1398 & 0.0470 & -0.0402 & 0.0622 & 0.0423 & -0.0534 \\ 0.1128 & -0.0367 & -0.1398 & 0.2141 & -0.0899 & 0.2366 & -0.3089 & -0.1002 & 0.1705 \\ -0.0680 & 0.0367 & 0.0470 & -0.0899 & 0.0560 & -0.2338 & 0.2883 & 0.0585 & -0.1289 \\ 0.3533 & -0.2636 & -0.0402 & 0.2366 & -0.2338 & 1.5247 & -1.8670 & -0.3342 & 0.7950 \\ -0.4423 & 0.3253 & 0.0622 & -0.3089 & 0.2883 & -1.8670 & 2.2932 & 0.4204 & -0.9853 \\ -0.1018 & 0.0634 & 0.0423 & -0.1002 & 0.0585 & -0.3342 & 0.4204 & 0.1052 & -0.2040 \\ 0.2076 & -0.1428 & -0.0534 & 0.1705 & -0.1289 & 0.7950 & -0.9853 & -0.2040 & 0.4429 \end{bmatrix} *1E5 \quad 4-49$$

Finally, by replacing the results from tables 4.19, 4.20 and equation 4-49 into the equation 4-34, the following equivalent dynamic structural system for Plaza Inmaculada Building is obtained only from the output signals:

$$[M]\{\ddot{x}(t)\} + [C]\{\dot{x}(t)\} + [K]\{x(t)\} = \{F(t)\}$$

Where:

$$[M] = \begin{bmatrix} 0.1518 & -0.0989 & -0.0398 & 0.1188 & -0.0907 & 0.5526 & -0.6850 & -0.1345 & 0.3020 \\ -0.0989 & 0.0693 & 0.0182 & -0.0715 & 0.0599 & -0.3829 & 0.4730 & 0.0909 & -0.2067 \\ -0.0398 & 0.0182 & 0.0301 & -0.0518 & 0.0264 & -0.1130 & 0.1436 & 0.0332 & -0.0678 \\ 0.1188 & -0.0715 & -0.0518 & 0.1180 & -0.0765 & 0.4107 & -0.5126 & -0.1060 & 0.2308 \\ -0.0907 & 0.0599 & 0.0264 & -0.0765 & 0.0589 & -0.3446 & 0.4258 & 0.0821 & -0.1865 \\ 0.5526 & -0.3829 & -0.1130 & 0.4107 & -0.3446 & 2.1801 & -2.6903 & -0.5105 & 1.1705 \\ -0.6850 & 0.4730 & 0.1436 & -0.5126 & 0.4258 & -2.6903 & 3.3224 & 0.6322 & -1.4472 \\ -0.1345 & 0.0909 & 0.0332 & -0.1060 & 0.0821 & -0.5105 & 0.6322 & 0.1263 & -0.2802 \\ 0.3020 & -0.2067 & -0.0678 & 0.2308 & -0.1865 & 1.1705 & -1.4472 & -0.2802 & 0.6344 \end{bmatrix} *1E5$$

$$[C] = \begin{bmatrix} 0.1216 & -0.0703 & -0.0504 & 0.1128 & -0.0680 & 0.3533 & -0.4423 & -0.1018 & 0.2076 \\ -0.0703 & 0.0537 & 0.0001 & -0.0367 & 0.0367 & -0.2636 & 0.3253 & 0.0634 & -0.1428 \\ -0.0504 & 0.0001 & 0.1047 & -0.1398 & 0.0470 & -0.0402 & 0.0622 & 0.0423 & -0.0534 \\ 0.1128 & -0.0367 & -0.1398 & 0.2141 & -0.0899 & 0.2366 & -0.3089 & -0.1002 & 0.1705 \\ -0.0680 & 0.0367 & 0.0470 & -0.0899 & 0.0560 & -0.2338 & 0.2883 & 0.0585 & -0.1289 \\ 0.3533 & -0.2636 & -0.0402 & 0.2366 & -0.2338 & 1.5247 & -1.8670 & -0.3342 & 0.7950 \\ -0.4423 & 0.3253 & 0.0622 & -0.3089 & 0.2883 & -1.8670 & 2.2932 & 0.4204 & -0.9853 \\ -0.1018 & 0.0634 & 0.0423 & -0.1002 & 0.0585 & -0.3342 & 0.4204 & 0.1052 & -0.2040 \\ 0.2076 & -0.1428 & -0.0534 & 0.1705 & -0.1289 & 0.7950 & -0.9853 & -0.2040 & 0.4429 \end{bmatrix} *1E5$$

$$[K] = \begin{bmatrix} 0.1902 & -0.1191 & -0.0493 & 0.1466 & -0.1136 & 0.6877 & -0.8515 & -0.1657 & 0.3770 \\ -0.1201 & 0.0877 & 0.0222 & -0.0882 & 0.0747 & -0.4811 & 0.5904 & 0.1176 & -0.2668 \\ -0.0504 & 0.0228 & 0.0370 & -0.0642 & 0.0321 & -0.1402 & 0.1778 & 0.0430 & -0.0860 \\ 0.1487 & -0.0889 & -0.0649 & 0.1498 & -0.0999 & 0.5167 & -0.6518 & -0.1343 & 0.2916 \\ -0.1156 & 0.0768 & 0.0330 & -0.0950 & 0.0739 & -0.4393 & 0.5452 & 0.1016 & -0.2373 \\ 0.6884 & -0.4755 & -0.1427 & 0.5229 & -0.4258 & 2.6434 & -3.3595 & -0.6452 & 1.4656 \\ -0.8833 & 0.5874 & 0.1824 & -0.6307 & 0.5188 & -3.4077 & 4.0373 & 0.7697 & -1.7871 \\ -0.1631 & 0.1149 & 0.0413 & -0.1291 & 0.1009 & -0.6256 & 0.7891 & 0.1502 & -0.3454 \\ 0.3670 & -0.2601 & -0.0858 & 0.2893 & -0.2326 & 1.3860 & -1.8100 & -0.3442 & 0.7888 \end{bmatrix} *1E7$$

4-50

Using the Extended Tridimensional Analysis of Building Systems (ETABS – V.9.04) computer program [201], a finite element model of the building from the “As built” drawings has been constructed, the schematic view of this model is shown in the next graph:

Nine modal frequencies and modal shapes can be obtained using the analytical model through MFTR-FDD.

TABLE 4.22 Comparison between MTFR-FDD and Finite Element Model for Plaza Inmaculada Building

Mode	Frequency (Hz)		Modal Participation			Cumulative Modal Participation		
	MTFR-FDD	ETABS	UX (N-S)	UY (E-W)	RZ	SumUX (N-S)	SumUY (E-W)	SumRZ
1	0.680	0.739	0.0247	66.8114	0.0034	0.0247	66.8114	0.0034
2	0.952	0.839	0.9007	0.0051	68.32	0.9254	66.8165	68.3234
3	1.280	0.934	70.6545	0.022	0.8008	71.5799	66.8385	69.1243
4	3.180	3.073	0.012	17.6136	0.0207	71.592	84.4521	69.1449
5	3.630	3.174	0.6858	0.0325	15.0911	72.2778	84.4846	84.2361
6	4.180	3.315	14.1458	0.0064	0.8627	86.4236	84.491	85.0987
7		6.657	4.1489	0.0057	1.1524	90.5725	84.4967	86.2511
8		6.794	1.2197	0.0026	3.8537	91.7921	84.4993	90.1048
9		6.933	0.0014	5.4269	0.0061	91.7936	89.9262	90.1109
10	7.610	7.880	0	0.0002	0	91.7936	89.9263	90.1109
11	7.860	8.163	0.0437	0	0	91.8373	89.9264	90.1109
12	8.400	8.717	0.0001	0.0002	0.0001	91.8374	89.9266	90.1109

Finally the output result for Plaza Inmaculada Building for different models and the real record is shown. The first one is the output signal of the finite element model building (ETABS model) and the second one is the 9 DOFs model obtained using MTFR-FDD. The final comparison is made between the two analytical models and the real record obtained in the Plaza Inmaculada Building for a small earthquake.

The selected input signal is the acceleration record for Earthquake of January 13th – 2006 (Origin time: 04:10:17 UTC, Mw=4.0, Depth: 54.5 Km, Epicentral Distance: 116 Km), recorded in the basement of Plaza Inmaculada Building (PGA=2.29 cm/sec², at 21.14 sec).

For this earthquake the output signal on the roof of the building was recorded. Therefore, it is possible to make a complete comparison between the two analytical models and the real record. The time histories for the real record and the output signals from MTFR-FDD and ETABS model are shown in the Figure 4-70.

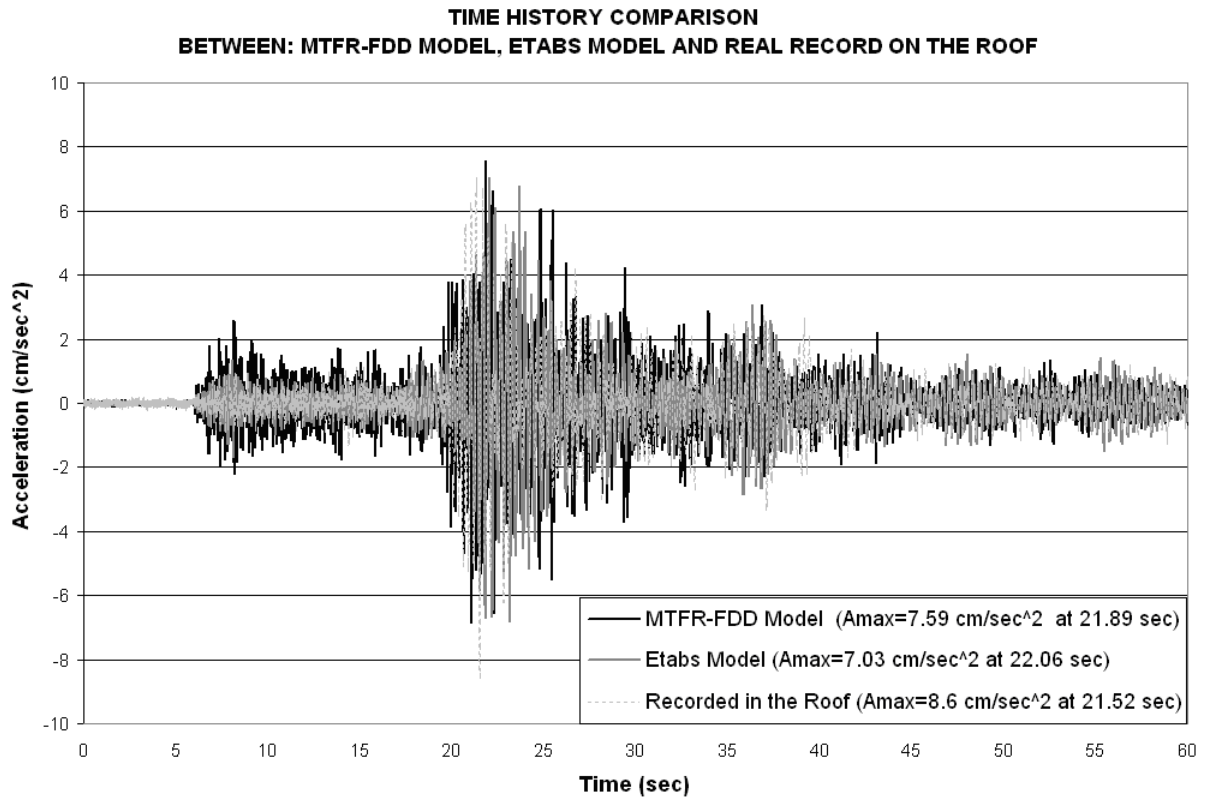


Figure 4-70 Time History Comparisons for Earthquake recorded in Plaza Inmaculada Building

From the previous Figure is evident that there is an excellent match between the three records. The results of the 9 DOFs model obtained from MTFR-FDD method have a remarkable behavior, since the maximum predicted acceleration is only 1.3% more than the real record (21.89 cm/sec² vs 21.52 cm/sec²), and the predicted time of occurrence for this peak is less than 0.17 sec the real record.

As can be seen in Figure 4-71, there is a good correlation between the real record and numerical models frequencies.

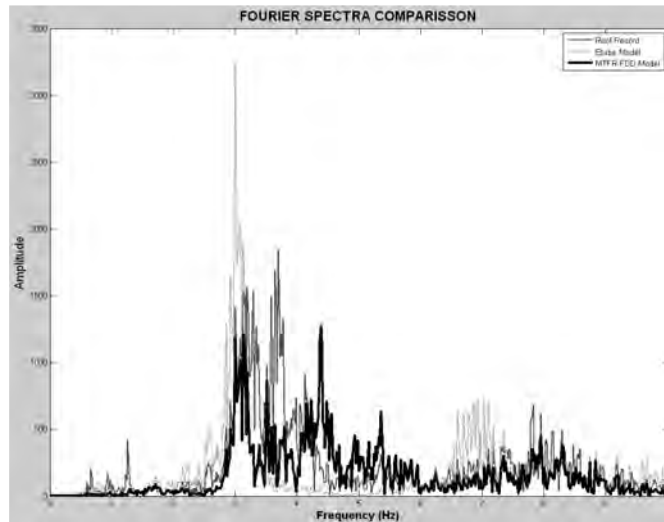


Figure 4-71 Fourier Spectra Comparisons for Earthquake recorded in Plaza Inmaculada Building

Finally, the coherence function has been evaluated and is shown in Figure 4-72. From this graph it is clear that a good coherence exists in the whole frequency range.

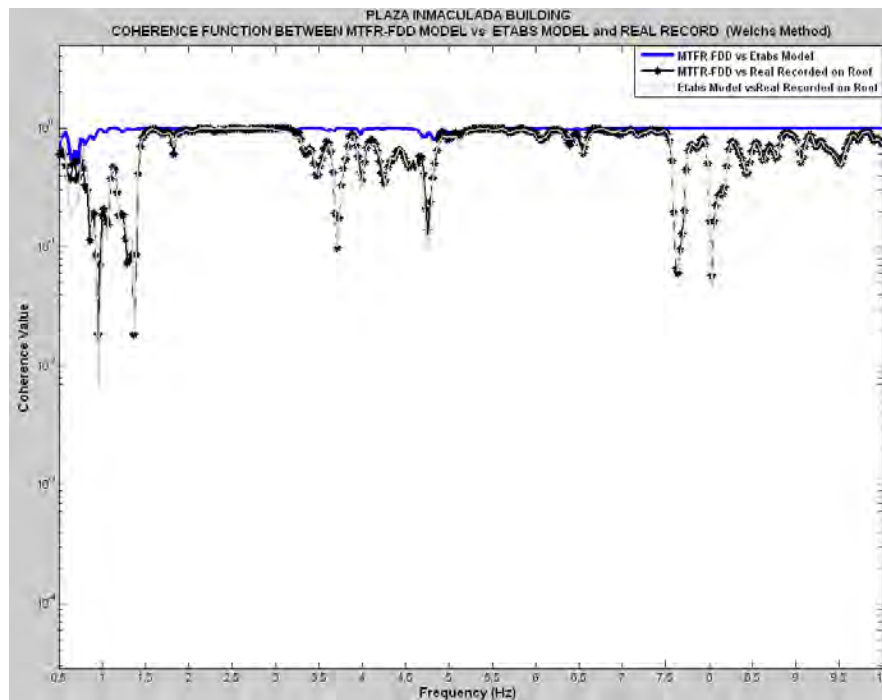


Figure 4-72 Coherence Function for Plaza Inmaculada Building, (Etabs Model, MTR-FDD Model and Real Record for Earthquake of January 13th -2006 recorded on the roof of the building).

5 DAMAGE DETECTION USING TIME-FREQUENCY ANALYSIS OF STRONG EVENTS OUTPUT SIGNALS

A new method namely Time-Frequency Structural Damage Method (TFSDM) for tracking the damage in instrumented structures during strong events will be proposed in this chapter. One of the most remarkable characteristic of this method is that it uses only output signals from the system and no additional structural information is required.

The method is based mainly on the direct association of system frequency changes during the event with changes in stiffness and damping. Due to a very precise tracking of time-frequency behavior of the system in association with the damping history, it is possible to make an estimative of when, where and how much the damage is.

Initially, the methodological approach is shown and then, the basic equations for damaged tracking are developed completely.

Numerical applications of methodology for nonlinear SDOF and MDOF are shown.

5.1 Time-Frequency for Structural Damage Detection Method from Strong Events (TFSDDM)

A new method for damage detection using only output signals from the structure for strong events like earthquakes, hurricanes, blast and explosion will be proposed in this section.

The difference between TFSDDM and the damage detection using ambient vibration of the structure is that the TFSDM method does not attempt to use a complete matrix system identification reconstruction.

For the proposed method no previous knowledge of the system is necessary and only a rigorous frequency and damping tracking is required, in order to determine the answer to the When, Where and How much the damage is (WWH)?

Obviously the exact answer to WWH is absolutely depended to how many sensors are available and where they are located. Theoretically, if we have infinite number of sensors, we can answer WWH with certainty.

The basic idea of the TFSDM is to evaluate the damage of the structure using the tracking of frequency in the time-frequency plane for signals from the structural modes.

In order to do that, the original multicomponent signal is decomposed into single modes (monocomponent signals) using the Empirical Mode Decomposition (EMD) proposed by Huang [73], with the frequencies band limits (buffer zones) extracted from an initial TFR analysis as it will be proposed in this Chapter.

Once the signal is decomposed into its monocomponents, for each modal component a time-frequency transformation was applied (using TFR with fixed kernels like WVD, CWD or RID or adaptive kernels like Kernel Adaptive Distribution or Adaptive Optimal Kernel) and using this TFR we will track the frequency of this monocomponent signal in each time instant, thus we evaluate the instantaneous signal frequency for each mode.

Because for strong event the frequency changes are not only function of stiffness changes but due to the changes in damping also, it is necessary to obtain the time history damping variations. In order to obtain these damping variations, the Random Decrement Signature Method (RDM) proposed by Cole [203] is used for each modal monocomponent signal, previously extracted using EMD. The algorithm developed by Bejarano [222] has been enhanced through a three step method proposed in this thesis. The proposed method for damping tracking is namely the Improvement Random Decrement Method (IRDM).

Finally, the damage is evaluated from frequency and damping changes of the system instant by instant, using the equation developed in the next section.

A schematic representation of this process for a 3 DOFs is shown in the Figure 5.1. Regarding this Figure it can be seen that 3 different records have been taken from the structure, for each one of these records a TFR is calculated using a bilinear time-frequency representation or an adaptive time-frequency distribution. Using this TFR plane we can generate several buffers zones around its main values, it is the constraint for the EMD method. Next the modes are separated in each channel using the EMD and for these separate signals a TFR-IRDM is applied in order to get the damping time-history. Finally the damage detection for each independent modal signal for each channel using the tracking of the frequency history is obtained from its TFR according to the procedure that will be explained in this Chapter.

The proposed method for damage detection is straightforward and does not require any human intervention or previous knowledge of the structural properties. Only the output signals from the structure are required. For this reason this method is a perfect candidate to be implemented in an on-line algorithm for real-time damage detection or a continuous structural health monitoring program. However, this topic is out of the scope to this research.

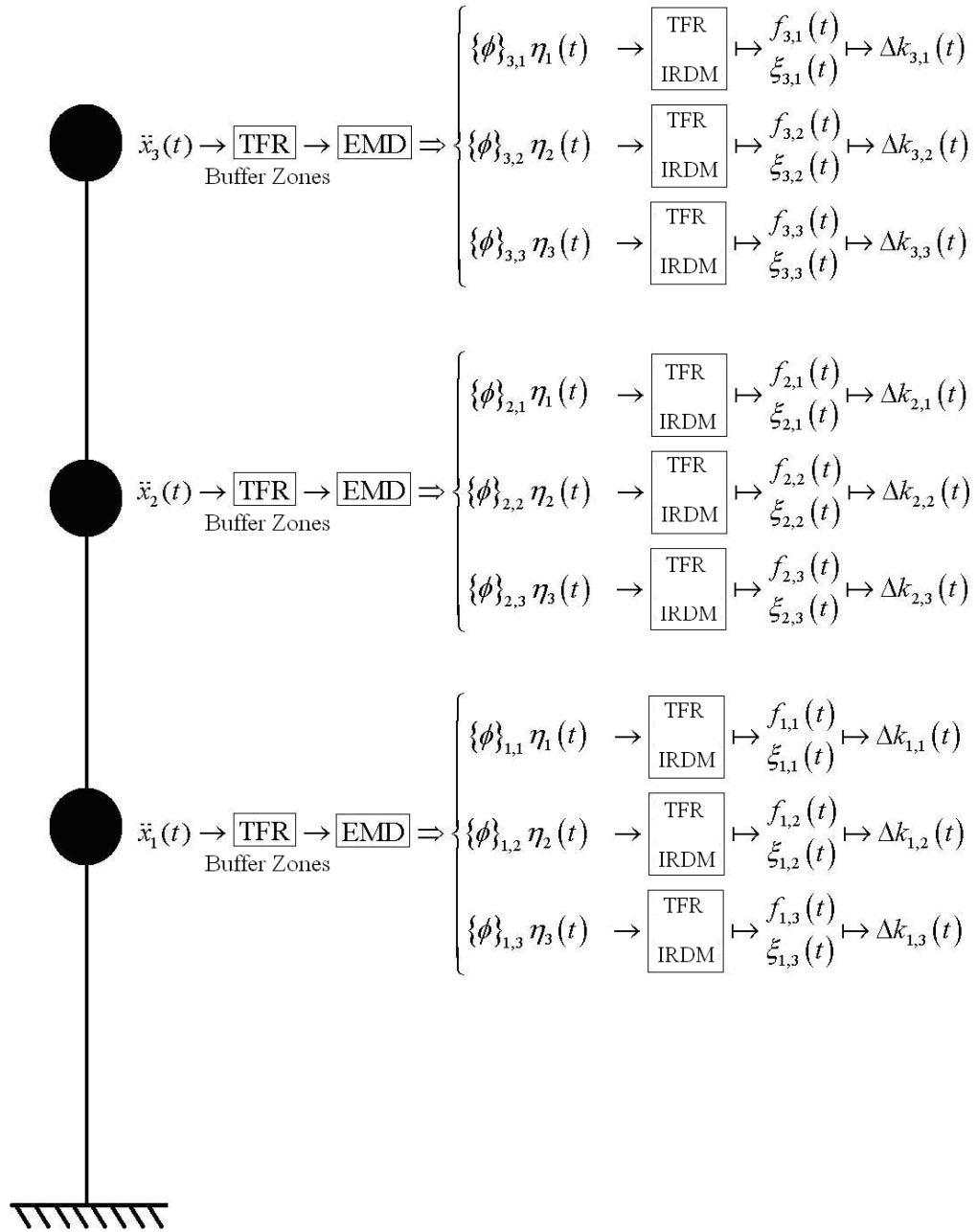


Figure 5-1 Schematic Process of Time Frequency Structural Damage Detection Method (TFSDM) for a MDOF system.

5.1.1 Mathematical Formulation for TFSDM

For a MDOF with external force the classical movement equation in matricial form can be written as [127]:

$$[M]\{\ddot{x}(t)\} + [C]\{\dot{x}(t)\} + [K]\{x(t)\} = \{F(t)\} \quad 5-1$$

Where:

$[M]$: Mass matrix, defined, positive

$[C]$: Damping matrix

$[K]$: Stiffness Matrix

$\{x(t)\}$: Displacement time history vectors (superscript dot represent time derivative)

$\{F(t)\}$: Force time history vectors

Using modal analysis and assuming classical damping, it can be proved [127] that the coupled system of differential equation represented by equation (5-1) can be resolved as an uncoupled system using a matrix transformation:

$$\{x(t)\} = [\Phi]\{\eta(t)\}$$

Where:

$[\Phi]$: Modal Matrix

5-2

$\{\eta(t)\}$: Displacement time history vector in modal coordinates

Replacing the equation 5-2 into equation 5-1, and pre-multiplying by the transpose of modal matrix:

$$[\Phi]^T [M] [\Phi] \{\ddot{\eta}(t)\} + [\Phi]^T [C] [\Phi] \{\dot{\eta}(t)\} + [\Phi]^T [K] [\Phi] \{\eta(t)\} = [\Phi]^T \{F(t)\}$$

And using the orthogonal properties of the modal matrix the following uncoupled system is obtained:

$$[I]\{\ddot{\eta}(t)\} + [\tilde{C}]\{\dot{\eta}(t)\} + [\Lambda]\{\eta(t)\} = [N(t)]$$

Where:

$[I]$: Identity matrix

$[\tilde{C}]$: Diagonal Modal Damping Matrix ($\tilde{c}_j = 2\xi_j\omega_j$) 5-3

$[\Lambda]$: Diagonal Eigenfrequency Matrix ($\lambda_j = \omega_j^2$)

$[N(t)]$: Modal Forces ($[N(t)] = [\Phi]^T \{F(t)\}$)

$\eta(t)$: Displacement in modal coordinates (superscript dot imply time differentiation)

Any single equations of the (5-3) system have the following form:

$$\ddot{\eta}_j(t) + 2\xi_j\omega_j\dot{\eta}_j(t) + \omega_j^2\eta_j(t) = N_j(t) \quad 5-4$$

And its solution can be obtained using the Duhamel's integral [127]:

$$\eta_j(t) = \frac{1}{\omega_{dj}} \int_0^t N_j(\tau) e^{-\xi_j\omega_j(t-\tau)} \sin \omega_{dj}(t-\tau) d\tau \quad 5-5$$

Thus the whole response of a MDOF can be evaluated by summation of individual responses of SDOFs. The behavior of this single modal component can be evaluated by decomposing the output signal into a single response of modal components.

The previous equation is only valid in linear range; in the case of non-linear range the linear approximations between intervals can be used. A popular method for these types of approximation is known as the incremental method.

Therefore by knowing the correct values of damping and frequency in a time interval for any SDOF, its impulse response can be evaluated. Therefore, the only difference between

linear or non-linear response is that these values are constant for the first case and varies in the second case.

Lets consider one of these SDOFs systems with constant mass and nonlinear behavior at two different instants (t_i and t_{i+1}). The systems will have the following frequencies:

$$\begin{aligned}\omega_{d_i} &= \omega_{n_i} \sqrt{1 - \xi^2(t_i)} \quad ; \quad \omega_{n_i} = \sqrt{\frac{k_i}{m}} \quad \text{para } t = t_i \\ \omega_{d_{i+1}} &= \omega_{n_{i+1}} \sqrt{1 - \xi^2(t_{i+1})} \quad ; \quad \omega_{n_{i+1}} = \sqrt{\frac{k_{i+1}}{m}} \quad \text{para } t = t_{i+1}\end{aligned}\tag{5-6}$$

As it can be seen the instantaneous system frequencies are functions of stiffness and damping at this time (constant mass). Therefore, by knowing the instantaneous damping and system frequency, the system stiffness as a function of mass can be evaluated. If the mass does not change then the change in frequency is due to damping and/or stiffness changes.

The subscripts ‘ i ’, and ‘ $i+1$ ’ indicate the values at instants t_i and t_{i+1} , where ($t_i < t_{i+1}$). From equation 5-6 it is evident that:

$$\omega_{d_i} - \omega_{d_{i+1}} = \omega_{n_i} \sqrt{1 - \xi_i^2} - \omega_{n_{i+1}} \sqrt{1 - \xi_{i+1}^2}\tag{5-7}$$

And remembering that:

$$\begin{aligned}\omega_n &= 2\pi f \\ \omega_{d_i} - \omega_{d_{i+1}} &= 2\pi \left(f_i \sqrt{1 - \xi_i^2} - f_{i+1} \sqrt{1 - \xi_{i+1}^2} \right)\end{aligned}\tag{5-8}$$

Therefore:

$$\sqrt{\frac{k_i}{m}} \sqrt{1 - \xi_i^2} - \sqrt{\frac{k_{i+1}}{m}} \sqrt{1 - \xi_{i+1}^2} = 2\pi \left(f_i \sqrt{1 - \xi_i^2} - f_{i+1} \sqrt{1 - \xi_{i+1}^2} \right)\tag{5-9}$$

Solving for k_{i+1} from equation 5-9:

$$k_{i+1} = m \left(\frac{\sqrt{1-\xi_i^2} \sqrt{\frac{k_i}{m}} - 2\pi \left(f_i \sqrt{1-\xi_i^2} - f_{i+1} \sqrt{1-\xi_{i+1}^2} \right)}{\sqrt{1-\xi_{i+1}^2}} \right)^2 \quad 5-10$$

A relative stiffness change (damage) between the two time instants can be defined as:

$$\Delta k = \frac{k_i - k_{i+1}}{k_i} = 1 - \frac{k_{i+1}}{k_i} \quad 5-11$$

Substituting the equation 5-10 into equation 5-11 the stiffness changes between instant t_i and t_{i+1} can be express as:

$$\Delta k = 1 - \frac{m}{k_i} \left(\frac{\sqrt{1-\xi_i^2} \sqrt{\frac{k_i}{m}} - 2\pi \left(f_i \sqrt{1-\xi_i^2} - f_{i+1} \sqrt{1-\xi_{i+1}^2} \right)}{\sqrt{1-\xi_{i+1}^2}} \right)^2 \quad 5-12$$

The equation 5-12 is a powerful tool for damage detection using time-frequency analysis, because the damage can be tracked instant by instant for a SDOF system from the direct interpretation of instantaneous frequency changes obtained from its time-frequency plane.

Note that in the equation 5-12, if no frequency and damping changes occur between the two instants then f_i and f_{i+1} becomes equal and the damping factor will cancel each other. Therefore, the stiffness change (Δk) becomes equal to zero and no damage is produced as expected for this situation.

The subscripts ' i ', and ' $i+1$ ' indicate the values at instants t_i and t_{i+1} , where ($t_i < t_{i+1}$), the damage can be tracked during whole event as:

$$\Delta k(t) = 1 - \frac{m}{k_{t_i}} \left(\frac{\sqrt{1-\xi_{t_i}^2} \sqrt{\frac{k_{t_i}}{m}} - 2\pi \left(f_{t_i} \sqrt{1-\xi_{t_i}^2} - f_{t_{i+1}} \sqrt{1-\xi_{t_{i+1}}^2} \right)}{\sqrt{1-\xi_{t_{i+1}}^2}} \right)^2 \quad 5-13$$

At this point it is important to remember that according to the philosophy of this thesis (only using the output signal information and not using any structural information), since there are no available information about mass and initial system stiffness. But this is not a problem, since there is no attempt in evaluating the “real” stiffness value and the goal is only to evaluate the damage (the stiffness changes through time). Therefore, the prediction of damage is in percentage of stiffness loss at a particular instant, and the total percentage of stiffness loss at the final of strong event. Therefore, any value for the mass can be assumed, the only condition is that this assumption does not change through the time, a good selection is to set the mass value equal to one.

In fact when a nonlinear finite element model of the structure is used, the information will only have meaning if the initial structural properties are compared with the final properties. Therefore a percentage scale in all cases is always used.

For example, if we were to tell you that during a strong event the moment capacity of one column is decreased by 300 KN.m, practically you would not have any idea about how much the damage is. But if we were to tell you that the moment capacity of the column has been reduced by 80%, you will immediately know that a severe damage has happened.

It is the approach of the TFSDM using only output signals that we can evaluate the percentage losses of the stiffness for any MDOF.

5.1.2 Algorithm for Instantaneous Frequency Tracking Estimation for Quasi-Monocomponent Structural Signals

The evaluation of equation 5-13 for structural damage detection requires instant by instant estimation of the damping and frequency.

As aforementioned in the literal 2.3, for a perfect monocomponent signal the Instantaneous Frequency (IF) can be evaluated using the first derivative of the phase (Equation 2-36) and for multicomponent signals a weighted average of the instantaneous frequency is evaluated rather than the instantaneous frequency itself (Equation 2-37).

However in real cases, direct application of Equation 2-36 is limited for some types of machinery or perfect controlled systems, because it produces unacceptable high spurious oscillations in frequency. The signal from the structures is not monocomponent, even if the structure is a SDOF because the noise and external forces induced additional frequencies in the system. Obviously, the signal for MDOFs is multicomponent. Therefore a direct application of equations 2-36 and 2-37 is not adequate for signals from civil engineering structures.

It is necessary to evaluate the (IF) from the TFR map; in order to do this a specifically structural oriented algorithm is proposed. This algorithm deals with quasi-monocomponent signals of SDOF structures. Since the output signal from MDOFs systems can be decomposed in SDOF responses using the EMD. Only a frequency tracking algorithm for SDOF is required.

The term quasi-monocomponent signals (namely here monocomponent signals) refer to signals from SDOFs that are close to have only one main frequency at any time instant. In fact, the signal is not a pure tone, because noise and imperfections in the EMD extraction algorithm introduce non system additional frequencies.

In the technical literature there exist methods for frequency estimation from TFR, because this problem is common in other fields like communications, wireless, imaging processing, medical signal analysis, radar, speech and others. The frequency estimation is strongly linked to the optimal kernel design and optimal filter theory used to noise reduction [206]. By using the optimal kernel design, it is possible to obtain free interference time-frequency distributions [97, 129, 131-138, 144, 225].

Fundamental concepts of the IF estimation can be reviewed in the classical papers of Boashash [226, 227]. A common method for IF from TFR is based on determination of TFR maxima [227, 228, 229], in the same way the method proposed is based on tracking of the TFR maxima with the restrictions according to the structural source of signal.

The proposed algorithm is based on the principle that the IF is usually a slow varying function. In a short interval, this function varies quickly for uncommon higher stiffness losses. Therefore it is possible to limit the frequency tracking area in the time-frequency map to the areas closer to the fundamental structural frequency (i.e. initial frequency of the system).

Very often the time history contains a pre-event time interval that is useful in order to set a pre-event system frequency. However, if no pre-event record is available, we can setup the structural system frequency to the main value in the time-frequency map for a short window length taken at initial instants record.

Next, the proposed algorithm for IF tracking of signal from civil engineering structures is described:

- 1) For a real signal $x_r(t)$ (Obtained from a SDOF or an empirical mode obtained from a MDOFs), evaluate the associated analytical signal by using:

$$x(t) = x_r(t) + jHT(x_r(t))$$

Where:

$jHT(x_r(t))$: Hilbert Transform

- 2) If a short pre-event record interval is available (from 0 to t_0), the initial frequency of the system is evaluated using $f(t_0)$:

$$f(t_0) = \arg \max |FT(x(t) * w(t))|$$

Where:

$$w(t) = \begin{cases} 1 & \text{if } 0 \leq t \leq t_0 \\ 0 & t_0 < t \end{cases}$$

Where:

FT : Fourier Transform

If the pre-event record interval is not available, then evaluate the initial system frequency of the system using:

$$f(t_0) = \arg \max |P_w(t, f)|$$

Where:

$P_w(t, f)$: Is the time-frequency distribution of the analytical signal at an initial short time length window.

- 3) Optional : Evaluate a direct mean instantaneous frequency (IF_{dm}) for the signal, (Note: Some times the instable IF_{dm} show trends that can be used for a final general frequency trend comparison), using:

$$IF_{dm}(t) = \frac{d\phi(t)}{dt} = \frac{x_r(t)d \frac{HT(x_r(t))}{dt} - d \frac{x_r(t)}{dt} HT(x_r(t))}{x_r^2(t) + HT^2(t)}$$

where:

$x(t)$: Real Signal

$\phi(t)$: Phase of signal

$HT(x(t))$: Hilbert transform of $x_r(t)$

- 4) Using the maximum value of spectrogram, evaluate the mean time instantaneous frequency $IF_m(t)$ using :

$$IF_m(t) = \arg \max \left| \frac{1}{\sqrt{2\pi}} \int_{-\infty}^{+\infty} x(\tau) h(\tau - t) e^{-jf\tau} d\tau \right|_{t=0..t_{\max}}^2$$

Recommendation: Select a good set of windows ($h(t)$) (lots of numerical simulations shown in this research that 100 Hamming windows with 30% of overlap conducted to a stable mean instantaneous frequency).

- 5) Evaluate the most common frequency (f_c) from the frequency history which has been obtained in the step 4, this frequency is taken from a frequency histogram using:

$$f_c = \arg \max \{ hist(IF_m(t)) \}$$

- 6) Perform a bandpass filter around the (f_c) obtained in the step 5. The lower and upper limits will be set at $0.25*(f_c)$ and $2*(f_c)$ respectively.

- 7) Calculate a time-frequency transform for the filter signal obtained in the step 6.

- 8) Evaluate the final Instantaneous Frequency ($IF(t)$) history using the maximum values of the TFR obtained in the step 7, using:

$$IF(t) = \arg \max |P(t_i, f)|_{t_i=0..t_{\max}}$$

- 9) Smooth the $IF(t)$ (Optional): Using the information content in the TFR and the concept of energy (like Arias Intensity) it is possible to evaluate the time intervals when the energy have been introduced into the system. The smoothing process consists of taking the frequency values of the tracking between the time interval when $E_N(t)=0.05$ and $E_N(t_k)=0.97$, these limits agree with common engineering practice for Energy Methods and Arias Intensity. For frequencies outer of these limits the frequency can be taken equal to f_0 and $f=IF(t_k)$. The $E_N(t)$ can be evaluated using the normalized time marginal of the TFR:

$$E_N(t) = \frac{\int P_x(t, f) df}{2\pi \arg \max \left(\int P_x(t, f) df \right)}$$

It is important to point out two aspects regarding the precedent algorithm. The first one is the frequency limits for the bandpass filter of the step 6. It has the justification in the structural response of any SDOF, thus it is physically impossible that any common structure can have variations in its fundamental frequency beyond this limit. In the Figure 5-2 we can see the frequency value in function of remanent stiffness (i.e. available stiffness) for any SDOF (the mass value does not have any influence):

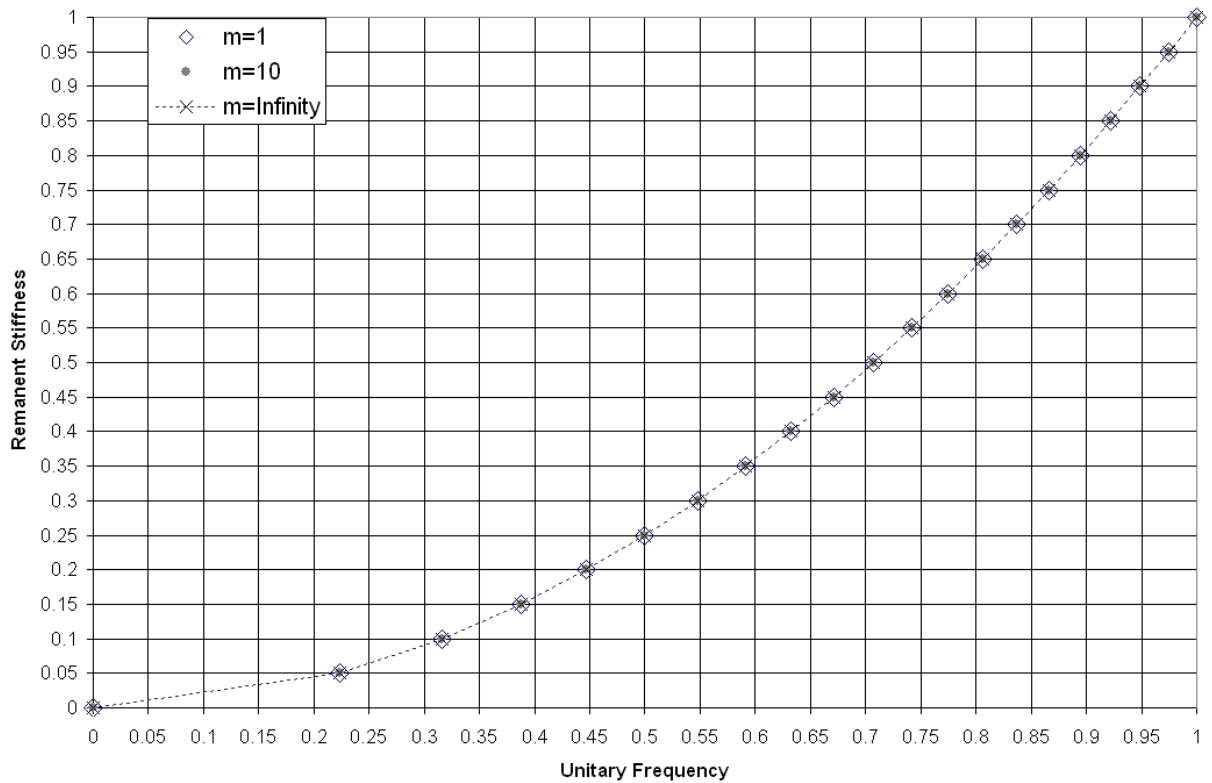


Figure 5-2 Remanent Stiffness vs Unitary Frequency for a SDOF system

Although theoretically the Wigner-Ville have the major energy concentration around fundamental frequency, there exist other bilinear TFR that is concentrated near to the IF [49, 56, 220, 224]. Therefore, a WVD or smoothed family can be used (i.e. a Cohen's Class) for IF estimation, if a fixed kernel type of TFR is selected. However other types of TFRs, such as adaptive or optimal time varying kernels, can be used without requiring any modification to the algorithm proposed. The algorithm is an off-line procedure working in a TFR map regardless the procedure used in the TFR map construction.

5.1.3 Empirical Mode Decomposition (EMD) with Time-Frequency Bandwidths

The equation 5-13 is valid only for a SDOF, as it will be seen further on for these types of systems (i.e. inverted pendulum, elevated tanks and others) its direct application is possible.

In general, the structures are more complex than SDOF models, the response of any MDOF can be obtained as a summation of SDOF systems. This approach is valid in the linear range and is acceptable in intervals of the non-linear range when the structural properties do not change during these intervals.

In order to apply the equation 5-13 for a MDOF, it is necessary to perform signal decomposition to extract from the signal, the modal components individually. Then the proposed algorithm of the 5.1.2 can be applied to get the time history frequency variation. This frequency variation jointly with the damping history are used in equation 5-13 to obtain the stiffness loss time history.

There is not a unique way to perform this modal decomposition and in the technical literature, several methods can be found as was mentioned earlier in Chapter 1.

Signal decomposition methods based on time-frequency and cross-time-frequency techniques can be found in references [71, 72]. Decomposition methods based on Phase Ratio Estimation from TFR can be reviewed in De Stefano et. al. [77] and Ceravolo et. al. [78]. An interesting method using Smoothed Pseudo Wigner-Ville distribution can be found in the reference [92].

Based on Gabor expansion, Zhang et. al.. [83], proposed a modal parameter identification method. It can decompose each signal into uncoupled responses.

Renyi entropy can also be used in order to extract the basic components of a signal [177, 180, 183], as was discussed in chapter 3. It is a good criteria for time-frequency separation and distribution performance.

In this research, the Empirical Mode Decomposition (EMD) will be used in order to get the individual signals corresponding to each mode component.

The main reasons for selecting EMD is that there exist a lot of experimental and analytical studies that support this method. It may be one of the most powerful methods actually available for signal decomposition of non-stationary signals. This method is fully data-driven and data-adaptive [209].

Another important issue is that EMD consider oscillation in signals at very local level and it can be used for extraction of modes with nonlinear trends in time [214].

The EMD has its beginnings in 1998, when Huang et. al. [73] showed a powerful approach for system identification of dynamic systems based mainly on empirical mode decomposition and Hilbert transform. This method today is known as Hilbert-Huang Transform (HHT). Huang proved that any real signal could be decomposed into n-empirical modes and one residue such as:

$$x(t) = \sum_{i=1}^n c_i(t) + r_n(t) \quad 5-14$$

Where :

$x(t)$: Original signal

$c_i(t)$: component

$r_n(t)$: residue after sifting process.

The extraction procedure has been explained in the original paper of Huang et.. al. [73], additional explanation and algorithms can be found in reference [209], improvements of this technique can be found in the references [89, 209-212], sampling effects and limits for EMD can be reviewed in the references [210, 213].

Unfortunately, the EMD does not have a pure mathematical prove and it is based only on an algorithm [73, 214, 217]. There were several attempts to link the EMD with the filter bank theory and adaptive time filters to give a mathematical base to EMD [214, 215], but the results had not been satisfactory.

Due to the fact that the mathematical base for the EMD is lacking, the general algorithm description for performing EMD based on the references [73, 209] is sketched and a numerical example of its operation will be shown.

According to [73, 209], the EMD process for a signal can be summarizing as:

- 1) Identify the positive and negative extremes of $x(t)$
- 2) Interpolate between minimum and maximum extremes to obtain $e_{min}(t)$ and $e_{max}(t)$
- 3) Compute the mean $m(t)$ between $e_{min}(t)$ and $e_{max}(t)$
- 4) Extract the detail from the original signal, thus $d(t)=x(t) - m(t)$
- 5) Take $x(t)=d(t)$ and repeat steps 1 to 4 until $d(t)$ can be considered as a zero-mean signal according to a stop criteria (this iteration process is namely sifting process)
- 6) Once the stopping criteria is achieved, $d(t)$ is considered an Intrinsic Mode Function (*IMF*).
- 7) Evaluate the residual like $m(t)=x(t)-IMF(t)$, and take a new $x_{new}(t)=x_{original}(t)-IMF(t)$
- 8) Repeat all the process for this new $x(t)$. The process end when no new IMFs can be obtained from residuals or when the residue becomes small.

In the following graph a step-by-step representation of the EMD procedure is shown, this graph has been adapted from Flandrin work [216] :

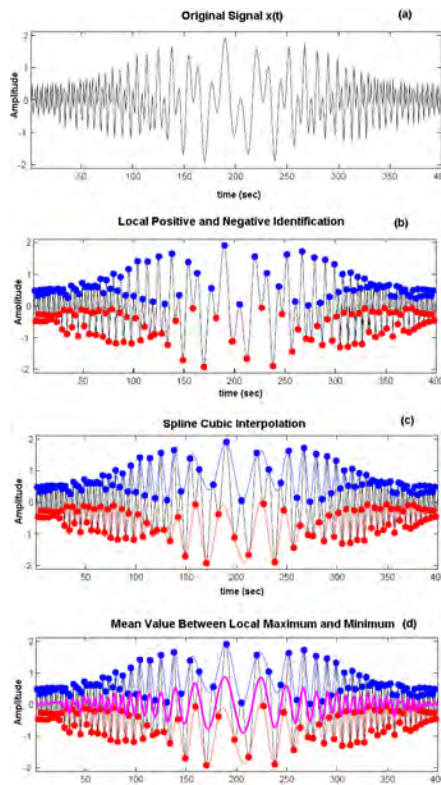


Figure 5-3 Schematic Empirical Mode Decomposition procedure (adapted from Flandrin [216]).

As it can be seen in Figure 5-3 the procedure for EMD starts with the evaluation of the mean value between the local maximum and minimum of the original signal.

Next the first Intrinsic Mode Function candidate (IMF) can be evaluated by subtracting the mean value (see picture (d) in the previous Figure) from the original signal, thus is shown in the next Figure:

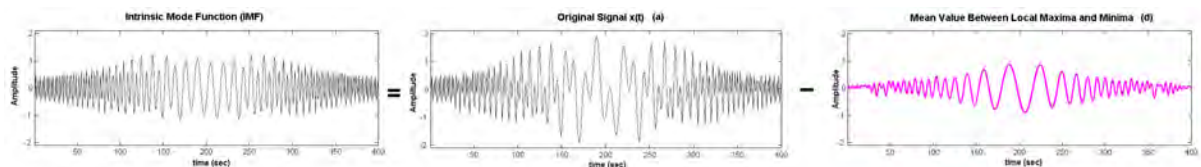


Figure 5-4 Evaluation of the Intrinsic Mode Function (IMF) (adapted from Flandrin [216]).

The IMF obtained in Figure 5-4 is the first mode contained in the signal. However, according to references [73, 209-213] this IMF is not a pure mono-component signal, and it is necessary to perform an iterative process namely sifting [73, 209] to remove spurious spikes from this mode.

The sifting process is similar to the main algorithm but in this case the IMF is evaluated in the Figure 5-4 like the original signal.

Therefore, the local maximum and minimum of this IMF is obtained, next spline cubic interpolation performed and evaluate a new mean value signal, and finally it is subtracted from the original IMF the mean value. This depurate IMF is submitted again to sifting process and the procedure will be finished when the stopping criteria is reached.

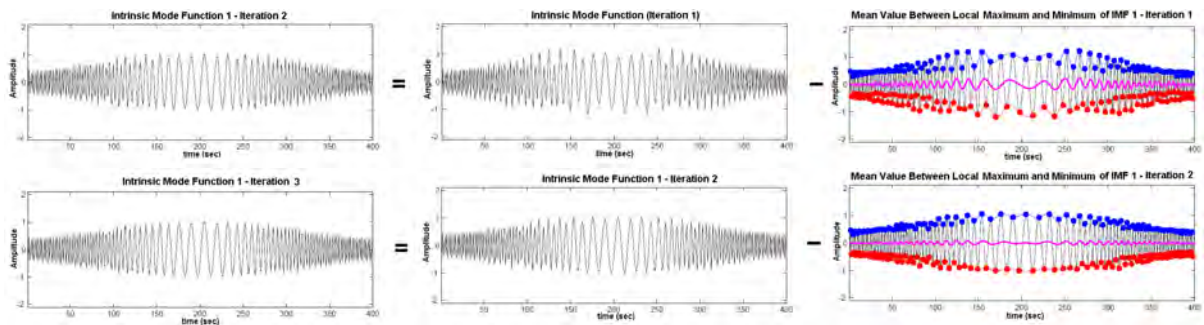


Figure 5-5 Sifting Process (adapted from Flandrin [216]).

As it can be seen in Figure 5-5, the mean value becomes a flat signal (zero amplitude) in the sifting process iteration.

Huang et. al. [73] has established stopping criteria as standard deviation (S.D.) values between 0.2 – 0.3, when the SD is evaluated using the equation 5-15. Other authors have suggested different stopping criteria for sifting process [209, 218, 219].

$$SD = \sum_{t=0}^T \left[\frac{|h_{1(k-1)}(t) - h_{1k}(t)|^2}{h_{1(k-1)}^2(t)} \right] \quad \mathbf{5-15}$$

Where: SD: Standard Deviation from the two consecutive sifting results

$h_{1(k-1)}(t)$: Time history of precedent sifting operation

$h_{1k}(t)$: Time history of actual sifting operation

Once the sifting process has ended for the first IMF, this deperated IMF is extracted from the original signal (signal (a) of Figure 5-2) and the residue is submitted to a new sifting process in order to get a new IMF (second empirical mode), this new IMF is subtracted from the previous residue and the process will continue. In the next Figure the results of EMD process for the original signal (Figure 5-2 (a)) can be see.

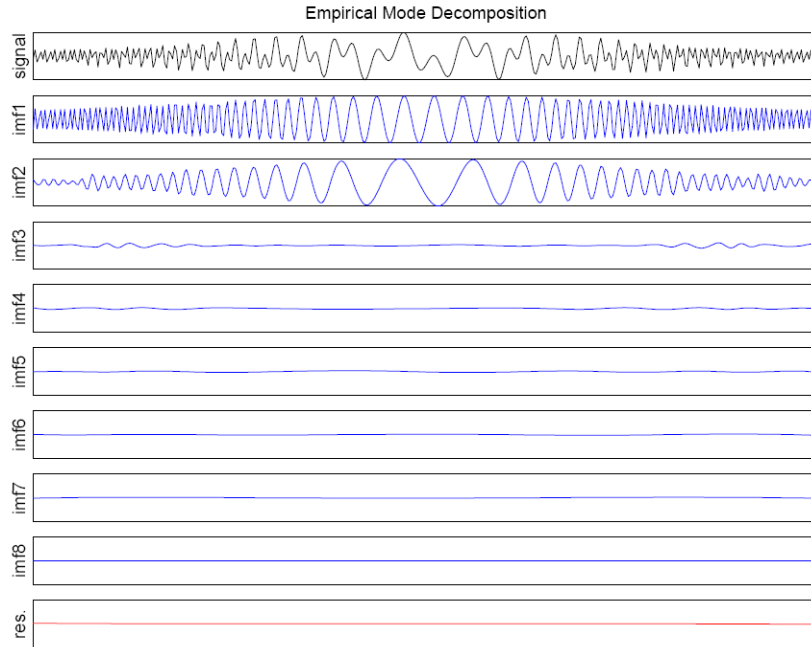


Figure 5-6 Final results of EMD applied to an original signal of Fig. 5-2 (Taken from Flandrin [216]).

Although the EMD procedure is quite simple, there are many evidence that show the final IMFs are not necessarily mono-component, regardless of how many iterations were made during the sifting process. Thus the empirical modes are not exactly isolated specially when its frequencies are close [218], the energy component is low [89]. Also EMD performs poorly when the frequency content of the signal approaches the sampling frequency [210] and when high noise is present in the original signal [219].

Although theoretically the Instantaneous Frequency (IF) of a monocomponent signal is its phase derivative [49, 123, 127] (see the section 2.3), a direct evaluation of this mathematical IF only produces good results if the signal is absolutely monocomponent.

The Hilbert-Huang method [73] applies reiteratively the evaluation of IF of IMFs obtained from an EMD in order to get a time-frequency signal representation, this TFR is known as Hilbert-Huang Transform. For structural applications, Huang in a recent paper proposed a preprocessing method prior to EMD evaluation [112] and other authors have also proposed alternative methods for improving the EMD results [209, 219].

A preprocessing procedure was adopted in order to get a more reliable performance from EMD. This process consists of applying a Time-Frequency transformation and decomposing the original signal into narrow band signals. This approach has been proposed by Peng et. al. [89] but by using wavelet transforms instead of the time-frequency representations. The advantages of preprocessing the signal with time-frequency analysis is that, if the frequency bandwidth of the signal submitted to EMD is not wide, then the output of IMFs becomes almost monocomponent.

Suppose that there is an output signal corresponding to a two single degree of freedom system. As a result of stiffness softening of the structure its frequencies will decrease. The time history and Fourier Transform for this behavior are shown in the following Figure:

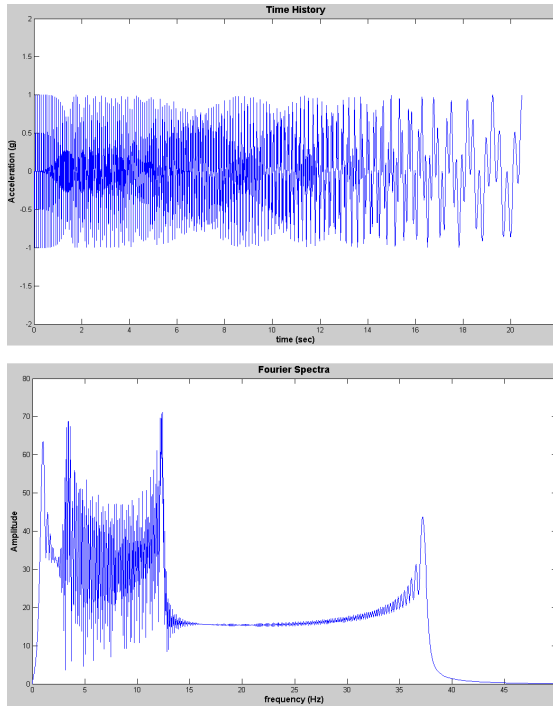


Figure 5-7 Time History and Fourier Spectra for a 2 DOFs with stiffness softening

As it can be seen from Figure 5-7 there is no useful information using time or frequency domain analysis.

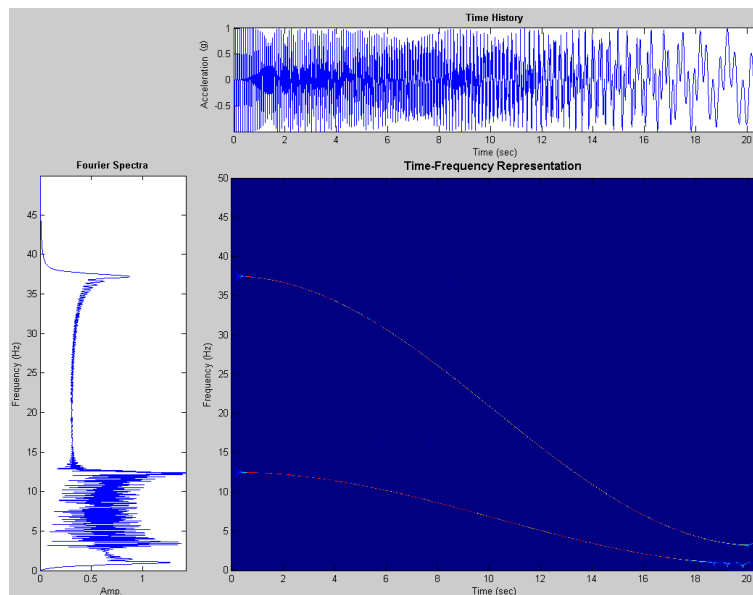


Figure 5-8 Time History and Fourier Spectra for a 2 DOFs with stiffness softening

From the Figure 5-8 it is clear that two non-constant frequencies are presented in the signal, and the information obtained from TFR can be used to establish two buffer zones around principal frequencies of the system.

Thus the frequency evolution can be obtained directly from the TFR of the original signal and by predefining two frequencies zones to perform the EMD algorithm. In fact this type of pre-constrained has been mentioned by Huang et. al. in the EMD original paper [73] and proposed to use a wavelet approach in the reference [89].

By proposing a $\pm 0.3 \cdot f$ (30%) in transition zones around frequencies and using these parameters the buffer zones for TFR are:

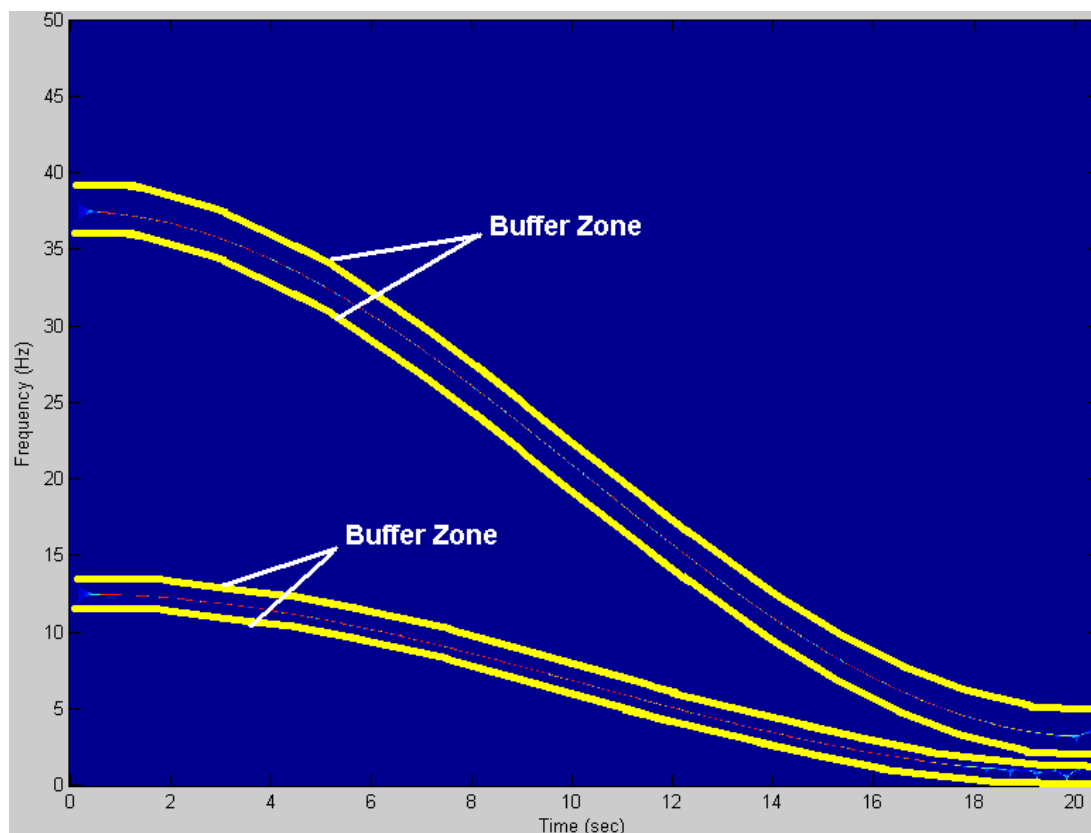


Figure 5-9 Frequency Constrained Buffer Zones from TFR to use in EMD algorithm.

Finally by applying the EMD algorithm in order to obtain the two empirical modes for this structure. In this research the algorithms developed in the references [209, 216] is used.

The two IMFs (modes) are shown in Figure 5-10. It is important to note that only 2 IMFs (empirical modes) are significant in Figure 5-10, and the other IMFs obtained can be ignored by using correlation criteria as has been proposed in the reference [89].

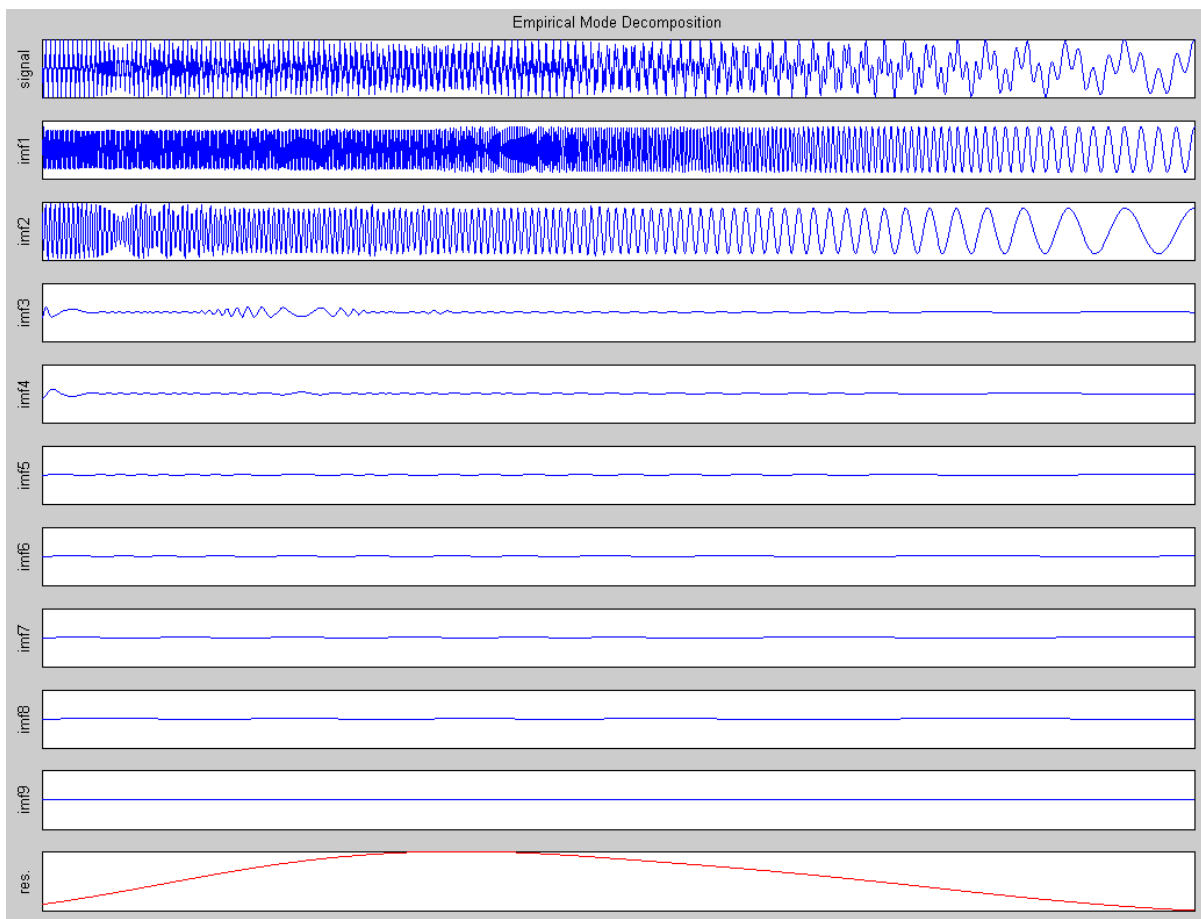


Figure 5-10 EMD result of a signal from Figure 5-7

5.1.4 Improving Random Decrement Technique with a Windowed Scheme Obtained From Time-Frequency Bandwidths (IRDM)

Once the multicomponent signal has been decomposed in its intrinsic mode functions (modes) using the procedure described in the section 5.1.3, the next step is to get the instantaneous damping of the system.

Before describing the methodology for damping assessment, first let us show relative influence of the damping in the system frequency change.

According to equation 5-13, if the mass and stiffness do not change, any frequency changes is due to the damping change. Therefore, the frequency changes can be evaluated as a function of damping changes. It is shown in Figure 5-11:

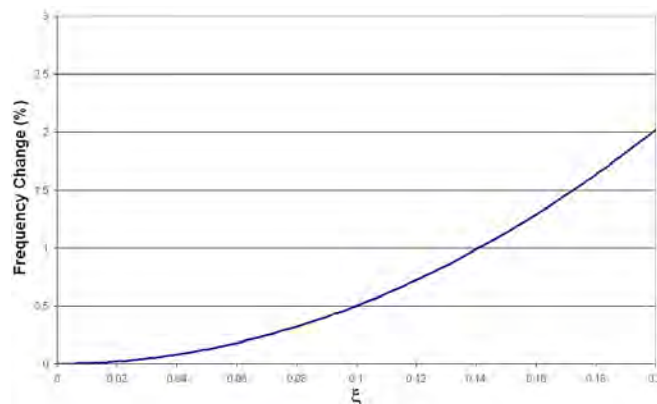


Figure 5-11 Damping vs Frequency Changes

From the previous Figure is clear that a strong damping by itself is incapable of producing a significant frequency change (i.e. an enormous damping factor of 20% only produces a 2% of frequency changes). Therefore damping is a secondary factor in frequency changes, although high damping values can be indicative of inelastic damage, the primary key in frequency changes is the stiffness. This theme has been controversial and at this time is the subject of several studies.

From the point of view of this research the mean instantaneous damping for each separate mode will be evaluated separately and then by introducing this damping in equation 5-13 in order to take into account the damping effect in the frequency change.

Several methods have been proposed for damping assessment, specifically using time-frequency methodologies in the references [66, 69, 71, 72, 74-78, 87, 93].

On the other hand, the Random Decrement Method (RDM) proposed by Cole [203] has been used successfully as a powerful and computational efficient method to achieve a damping estimation for structural systems submitted to random excitations.

The RDM is basically an empirical procedure for obtaining a pseudo free vibration damped curve namely decay curve. This method has been proposed by Cole [203] using the following expression:

$$\delta(\tau) = \frac{\sum_{m=1}^M x(t_m + \tau)}{M} \quad \mathbf{5-16}$$

where:

$x(t)$: Time History

t_m : Time at the threshold (y_0) value is exceed by a sub-time history array (segments)

τ : Time index varying between zero to preset value.

M : Number of segments satisfying the threshold and time length.

The segments that satisfy the amplitude threshold and time length are superimposed into a new time-lag axes and its mean value are evaluated using the equation 5-16. The result is a pseudo free vibration damped curve that is a candidate for extracting the damping value and the system frequency.

In the next Figure, a schematic procedure for obtaining the pseudo free vibration damped curve is shown. The selected signal is the NE270 acceleration record of San Simeon Earthquake (December 22 - 2003, $M_w=6.5$), recorded on the roof of Millikan Library.

The threshold amplitude value is set to $Y_0=12.5 \text{ cm/sec}^2$ and the length of segment (τ) is set to 8 sec. Ten segments have been obtained as shown in the following Figure:

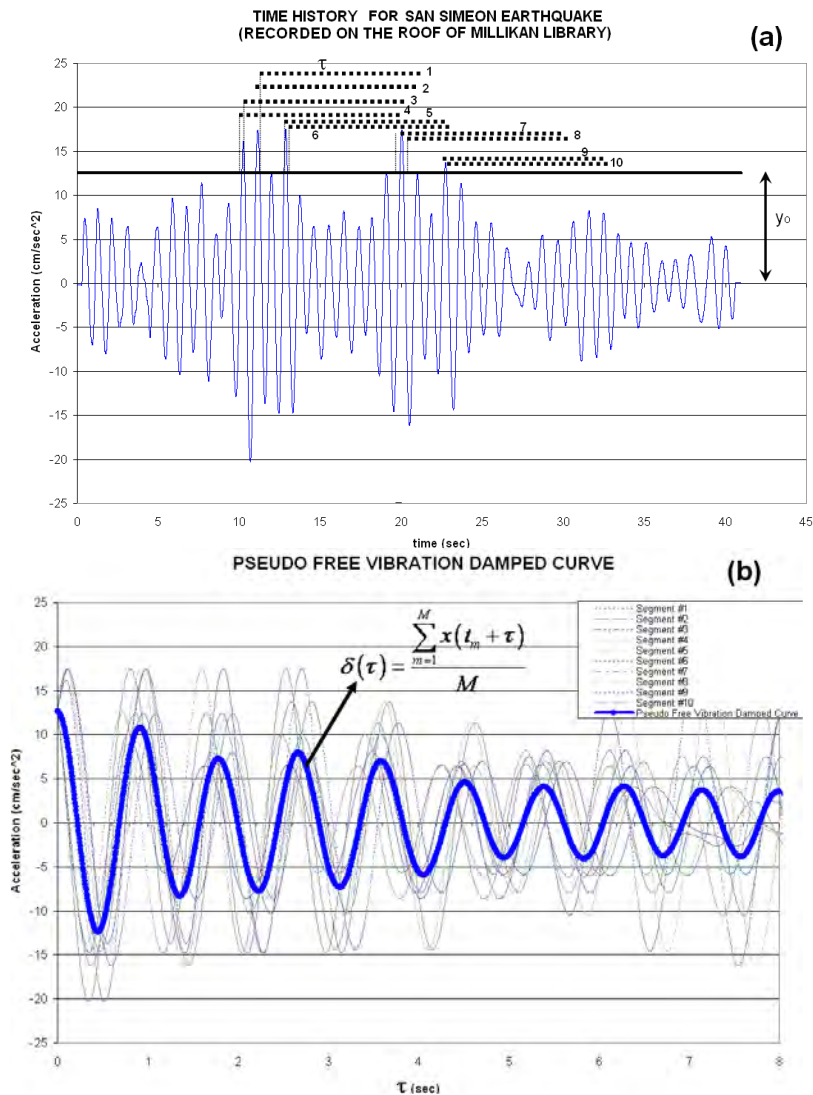


Figure 5-12 Pseudo Vibration Damped Curve (PVDC) for Millikan Library: (a) San Simeon Earthquake. (b) Segments and SVDC

From the Figure 5-12(b), it is easy to apply the classical equation of logarithmic decrement in order to get the damping [127]:

$$\delta = \frac{1}{j} \ln \left(\frac{x_1}{x_{j+1}} \right) = \frac{2\pi\xi}{\sqrt{1-\xi^2}}$$

$$\xi = \frac{\delta}{\sqrt{(2\pi)^2 + \delta^2}}$$
5-17

Where:

ξ : Damping

δ : Logarithmic decrement

x_1, x_{j+1} : Amplitude measurement corresponding to times t_1 and t_1+jT (T: Period)

In this particular case the damping obtained is ξ : 2.6%

Although the RDM procedure appears to be easy and straightforward, there exist many tricks and traps that can not be solved without an expertise intervention. To mention some of the major problems:

- a) For a whole record the damping obtained (if there is possible any) is a mean damping, thus time history evolution of the damping is not extracted.
- b) For multicomponent signals the damping is a mean damping of the system or the corresponding damping of the system dominant mode.
- c) The obtained damping is strongly depends on the amplitude threshold and segments length, thus a unique solution is not guaranteed.

Unfortunately the RDM lacks a rigorous mathematical support, and it is not possible to constrain an analytical solution for the aforementioned problems.

In a recent research Bejarano [222] proposed two indicators in order to minimize the uncertainty of a unique solution in the damping estimation (literal (c)). In the first one the Pearson correlation coefficient. It is evaluated for a least square regression of the PVDC maximums in a semi-log scale. The second indicator is the test of the null hypothesis. Additional informations can be found in Bejarano's thesis [222].

However the aforementioned problems related to time-history damping evolution (literal a) and modal damping discrimination (literal b) have not been resolved in the Bejarano's work.

For this reason in this research it was proposed to use the Bejarano's algorithms [222] with the following improvements:

- 1) For a multicomponent, given signal to perform the EMD with buffers using the procedure shown in the section 5.1.3 in order to get single mode responses (quasi-monocomponent signals).
- 2) For each quasi-monocomponent signal obtained in the previous step, establish a scheme based on the selection of time windows according to frequency laws obtained from TFR.
- 3) For each selected windows apply the Bejarano's algorithms to obtain the mean damping values for this window, thus the time-history evolution of damping for each mode can be extracted with this approach.

The previous enhanced procedure is namely the Improvement Random Decrement Method (IRDM), numerical applications of the IRDM will be shown in the section 5.2 for SDOF models and 5.3 for MDOF models.

5.2 Numerical Simulations for Time-Frequency Structural Damage Detection Method (TFSDDM)

5.2.1 *Single Degree of Freedom Models*

In this literal the application of the TFSDDM for SDOF models will be shown, in order to do that, the model of known properties is set and at several time instants its known properties will be changed, the goal is to predict when and how much is the damage using TFSDDM.

For the evaluation of the output time-history of each structure a MatLab [125] program has been developed. The main assumption of the program is that the dynamic non-linear response of the structure can be evaluated using linear variation between time instants of samples and set the new structural properties according to damaged values. Thus the structural variations (if any exist) are supposed to be linear between two sample instants. The response takes into account the initial conditions of the equilibrium equations at each time intervals.

The use of any theoretical hysteretic behavior (i.e. bilinear, tri-linear, pinching) is avoided, because in fact there is no information about the structural properties, thus not even the material type which the structure has been made of, and only the output signals from the response will be used.

Let consider a SDOF with constant mass equal to 1, initial stiffness equal to one (1), and initial ratio of 3% with respect to critical damping.

For this system the following characteristics has been assumed:

- Random number of the damage occurrences (between 2 to 15) and random time instants when these damages happened.

- Random number of the amount of damages between 0% to 95% (stiffness loss)
- Random number of the damping changes and random number of the damping values between (3% to 12%) and random time instants when these damping changes are happening.
- Random input excitation with an earthquake like shape.
- For each time history of random output signal, a random white Gaussian noise is added.

One thousand of these structures have been created and submitted to random external excitation and the output signal has been analyzed using the proposed TFSDDM method, the theoretical values have been compared with the predicted values.

In Figure 5-13, the procedure for generating these models is shown. Note that in the proposed methodology only the output time-history is known. Therefore, the reliability of damage estimative only can be evaluated in a probabilistic sense, as will be shown later on.

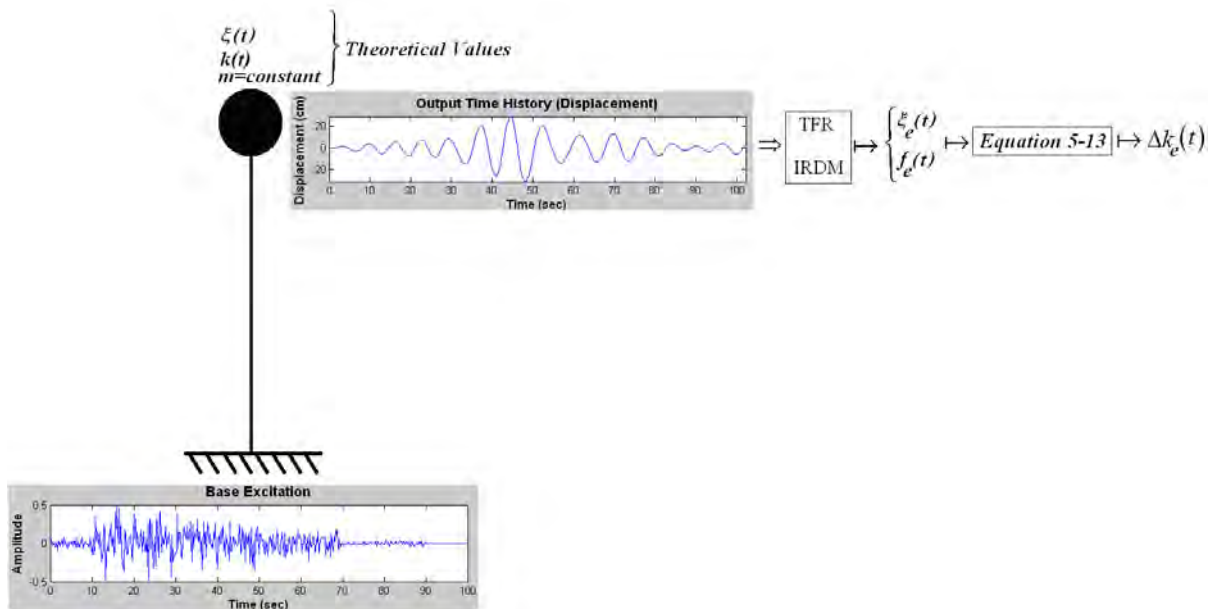


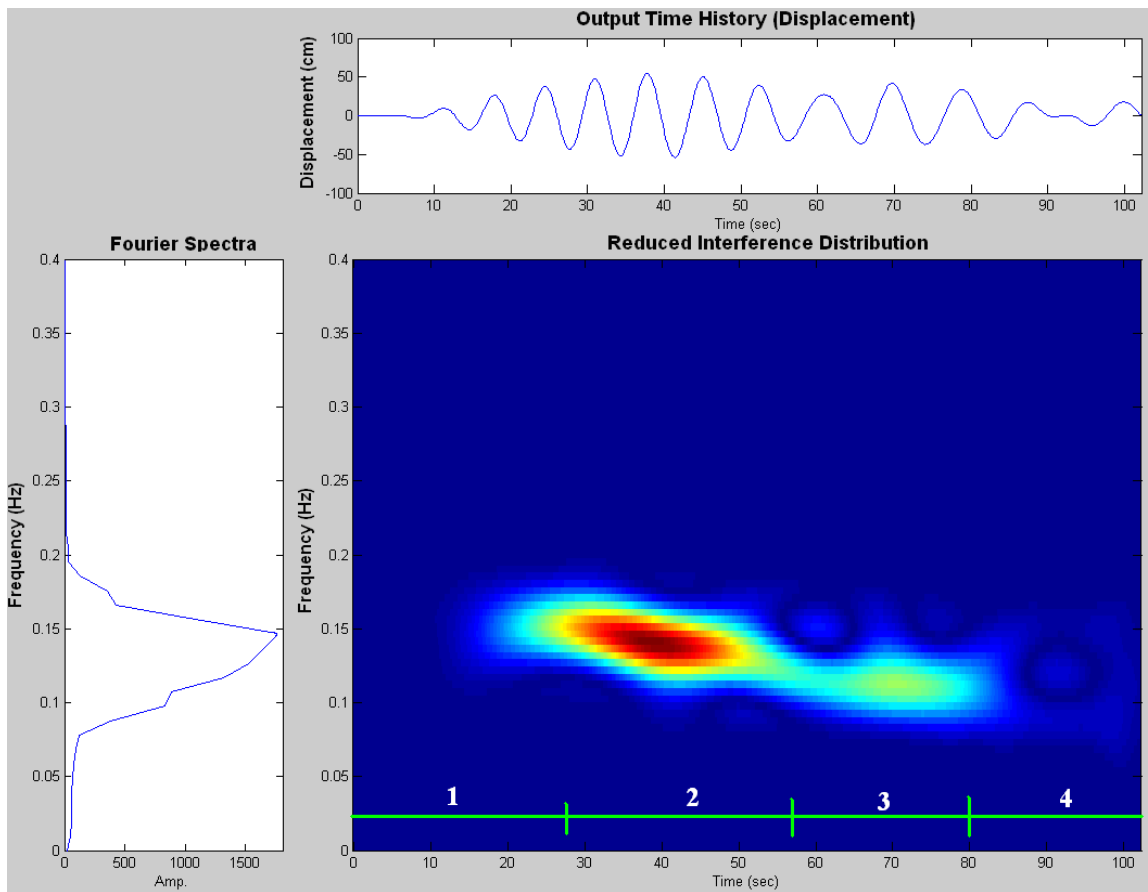
Figure 5-13 Schematic procedure to obtain the Estimation damage for SDOFs

In the next section a completed damage evaluation for one of these 1000 structures will be shown:

- *Step One: Time history of the structural damping*

The RDM has the limitation that the damping evaluation is an average damping of the whole record. A Reduced Interference Distribution of the output signal is used in order to get the time intervals when the frequency changes. By using these intervals, the original output time series is divided and applied to the RDM method.

In the next Figure this procedure for the selected case study is shown:



7

Figure 5-14 Time intervals obtained from TFR-RID to apply the Random Decrement Method

In Figure 5-14, four time intervals are clearly identified from time-frequency plane. Although for explanation purposes, the procedure has been made visually and the Gaussian noise has been removed, the algorithm was developed to do this procedure automatically (without any human intervention).

Using these four time zones, the output signal has been divided in the following intervals (0-27 sec, 27-57 sec, 57-80 sec, 80-102 sec). For each one of these intervals the RDM algorithms proposed by Bejarano [222] has been applied. In the next Figure the results of the IRDM algorithms is shown.

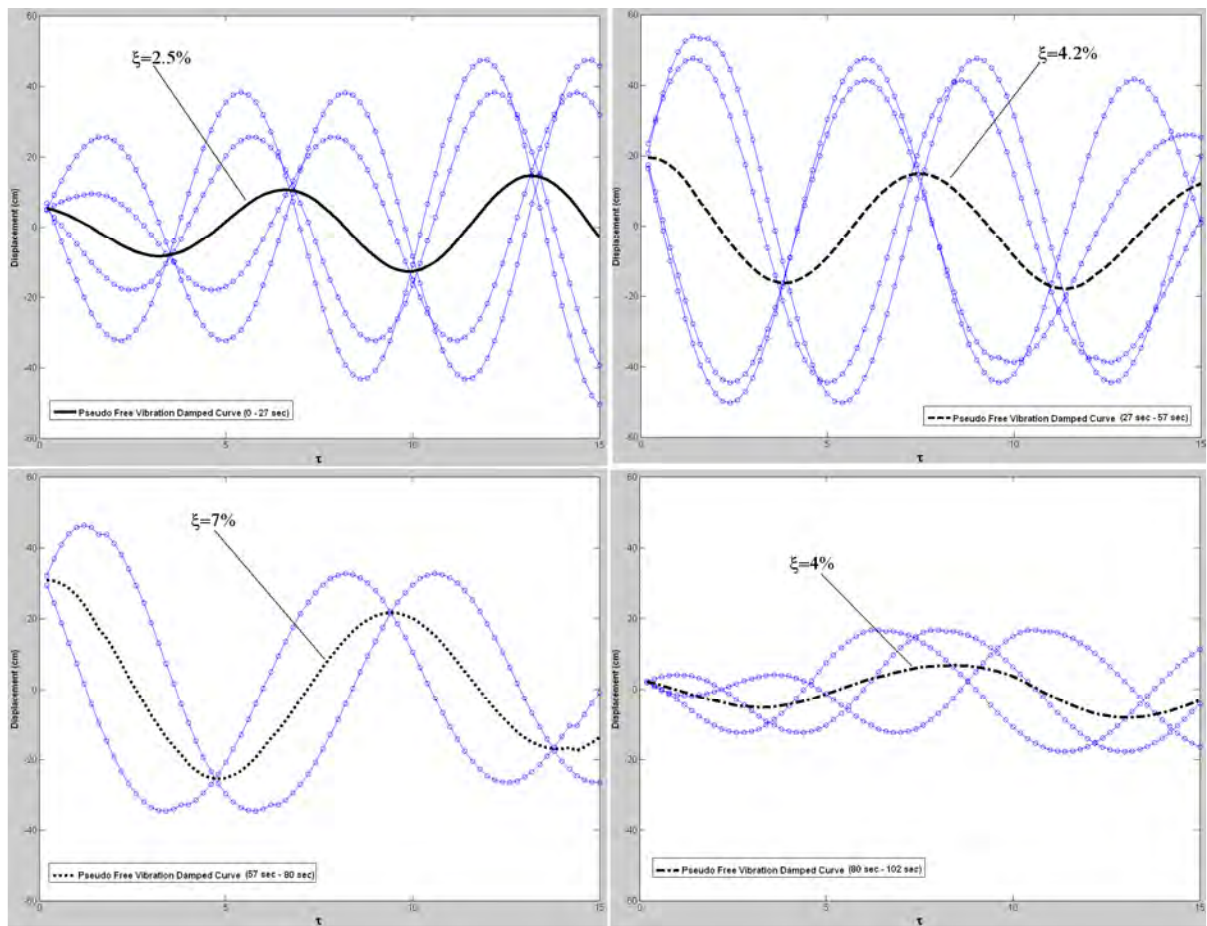


Figure 5-15 Pseudo Vibration Damped Curves for each time intervals obtained from TFR-RID

Using the information of Figures 5-14 and 5-15, the estimate structural damping time-history is extracted; it is shown in Figure 5-16. From this Figure an excellent agreement between theoretical and estimate damping can be observed. A complete study of the prediction quality of the RDM can be found in the reference [222], and this topic is omitted in this thesis. It is only mentioned so if the whole signal is used for RDM, the estimative damping is 6% (a constant time history damping to the Equation 5-13).

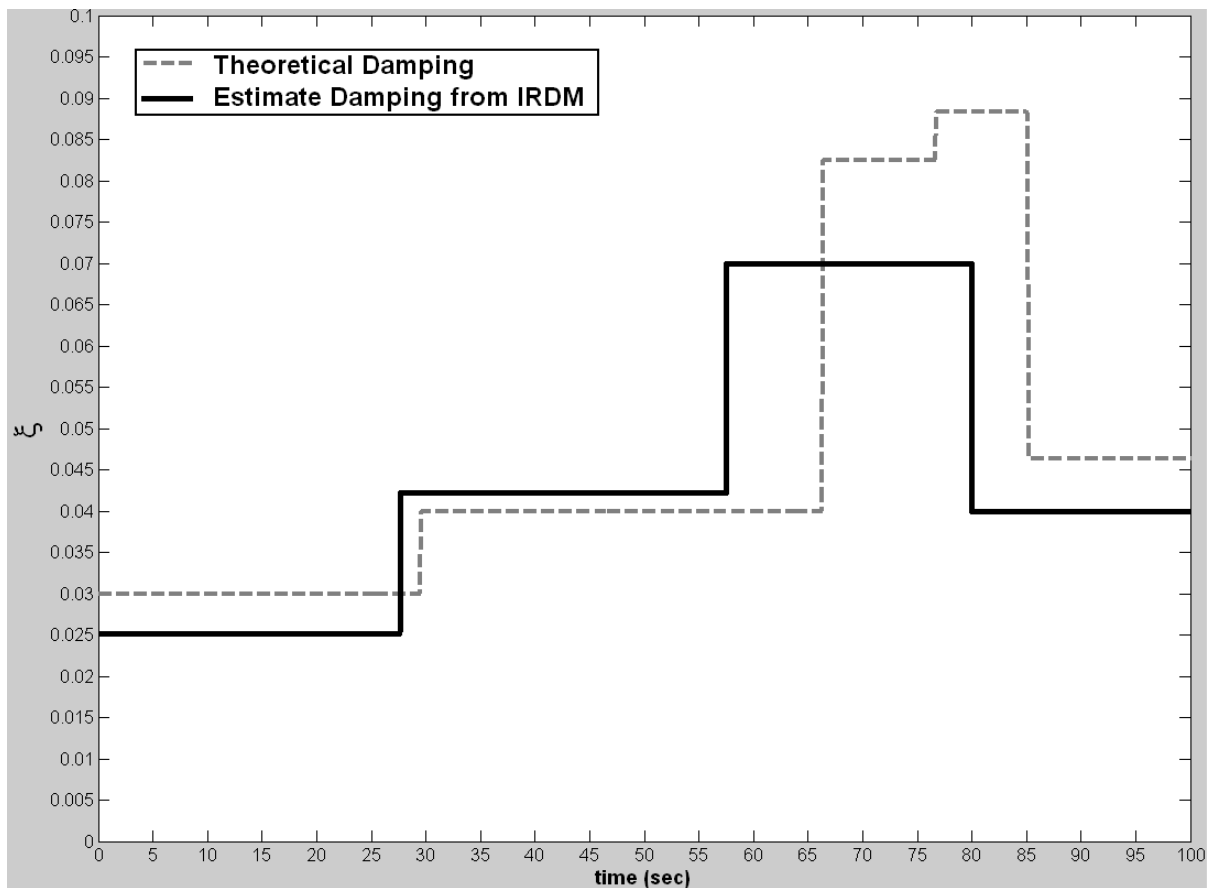


Figure 5-16 Estimate structural damping time history and Theoretical damping time history

- **Step Two: Time History of Instantaneous Frequency:**

The next step is the evaluation of the instantaneous time history frequency using the algorithm proposed in 5.1.2. :

- The complex analytical signal is evaluated using the Hilbert transform.
- Using the maximum value of a time-frequency representation $P_w(t,f)$ for a short window time (the first 10 seconds) an initial frequency equal to 0.156 Hz can be calculated, the theoretical value is 0.1592 Hz (Unitary mass and stiffness) .
- The exact mathematical instantaneous frequency (time derivative of the phase) do not produced any useful information in this case, as can be seen in the Figure 5-17.

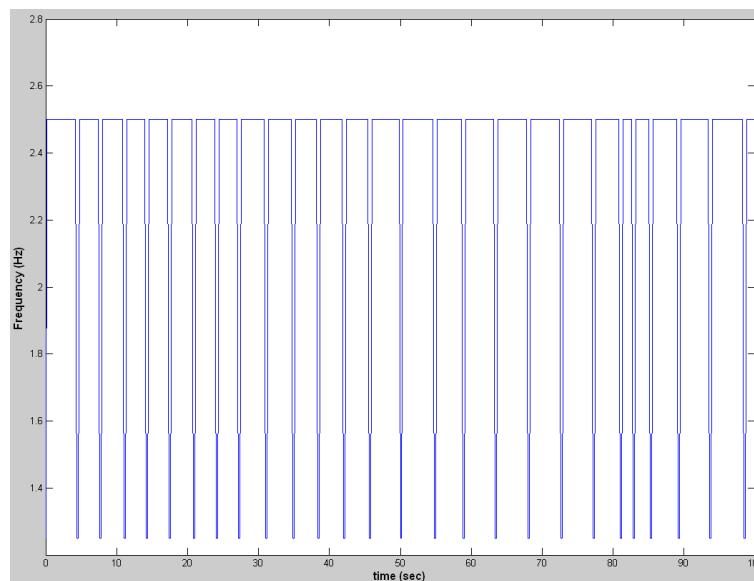


Figure 5-17 Instantaneous Frequency (IF) evaluated from Phase time derivative.

- Using the maximum value of spectrogram, evaluate the mean time instantaneous frequency $IF_m(t)$ using:

$$IF_m(t) = \arg \max \left| \frac{1}{\sqrt{2\pi}} \int_{-\infty}^{+\infty} x(\tau) h(\tau - t) e^{-jf\tau} d\tau \right|^2_{t=0..t_{\max}}$$

Thus is shown in the Figure 5-18, using 100 Hamming windows with 50% of overlap:

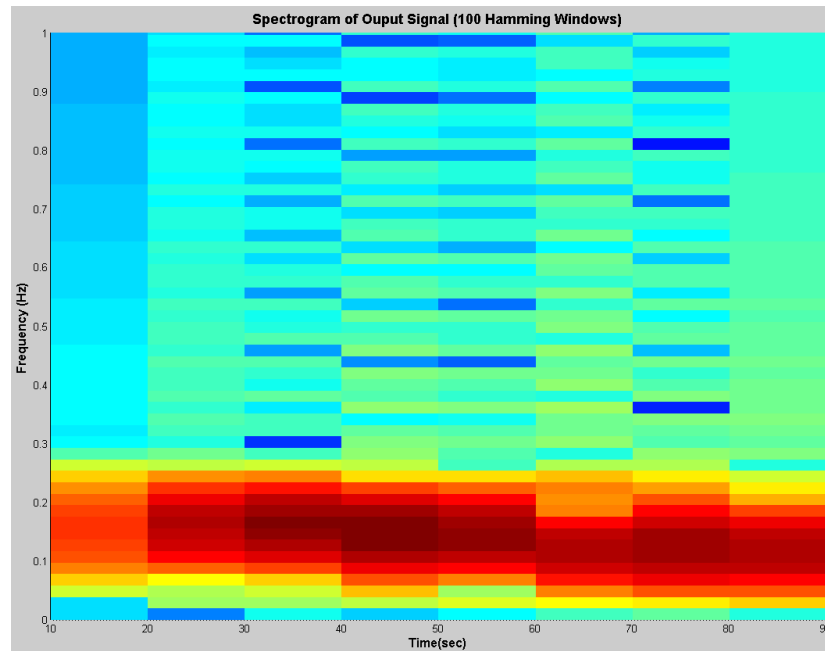


Figure 5-18 Spectrogram using 100 Hamming windows (50% overlap)

As it can be seen from Figure 5-18 the resolution of the spectrogram is not good. However, it is useful for a frequency bandwidth limitation of the problem.

- The most common frequency (f_c) in the frequency history from spectrogram is $f_c=0.1172$.

- Next a bandpass filter around the (f_c) is made, the filter limits have been taken as 0.03 Hz and 0.23 Hz for lower and upper limits, respectively.

- Next a Reduced Interference Distribution of the filter signal obtained in step 6 has been made, it is shown in Figure 5-19:

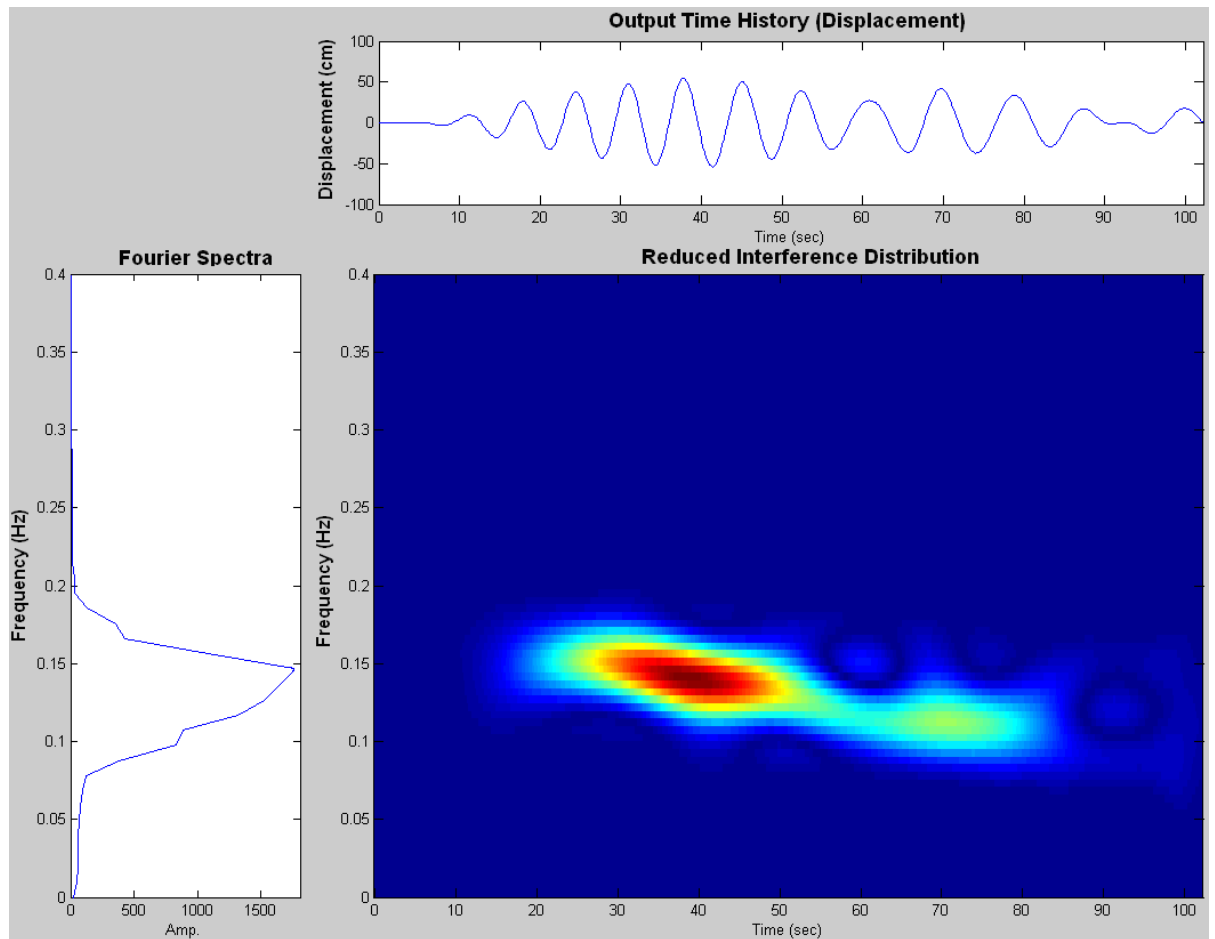


Figure 5-19 Reduced Interference Distribution for Output Signal

The final stage is the evaluation of the final Instantaneous Frequency ($IF(t)$) history using the maximum values of the TFR obtained in the step 7, using:

$$IF(t) = \arg \max |P(t_i, f)|_{t_i=0..t_{\max}}$$

In the Figure 5-20 the tracking of the IF(t) is shown:

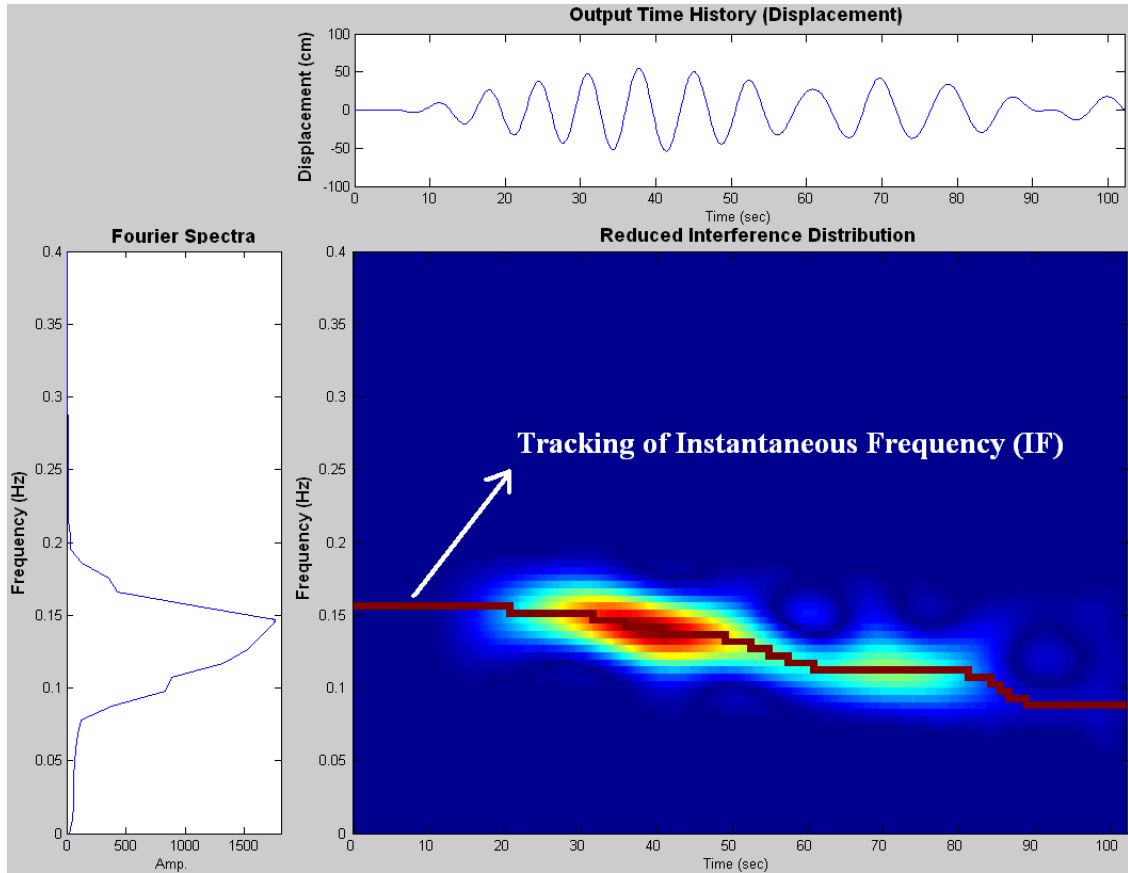


Figure 5-20 Reduced Interference Distribution for Output Signal

The previous IF(t) has been smoothed using the information of the time energy by using the time marginal of the TFR, it is shown in Figure 5-21. Note that the energy axis appears at the right side of the plot and it can be read in unitary normalized scale using:

$$E_N(t) = \frac{\int P_x(t, f) df}{2\pi \arg \max \left(\int P_x(t, f) df \right)}$$

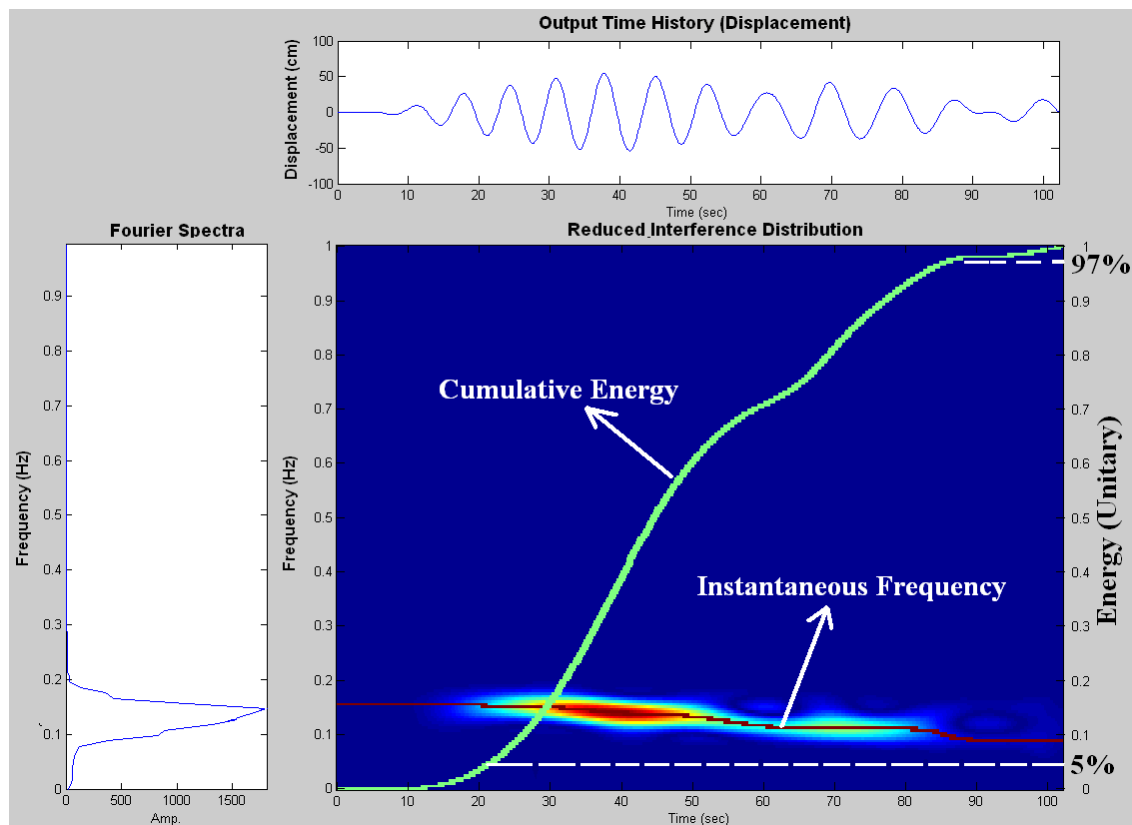


Figure 5-21 Reduced Interference Distribution for Output Signal

Using the limits from normalized cumulative energy, the initial value of the frequency can be taken from zero to time when the cumulative energy is equal to 5% (0.05) and the final value equals to the instantaneous frequency at the time when the cumulative energy is equal to 97% (0.97).

Finally the time history stiffness loss is evaluated from the damping time history and the Instantaneous Frequency time history by applying the equation 5-13.

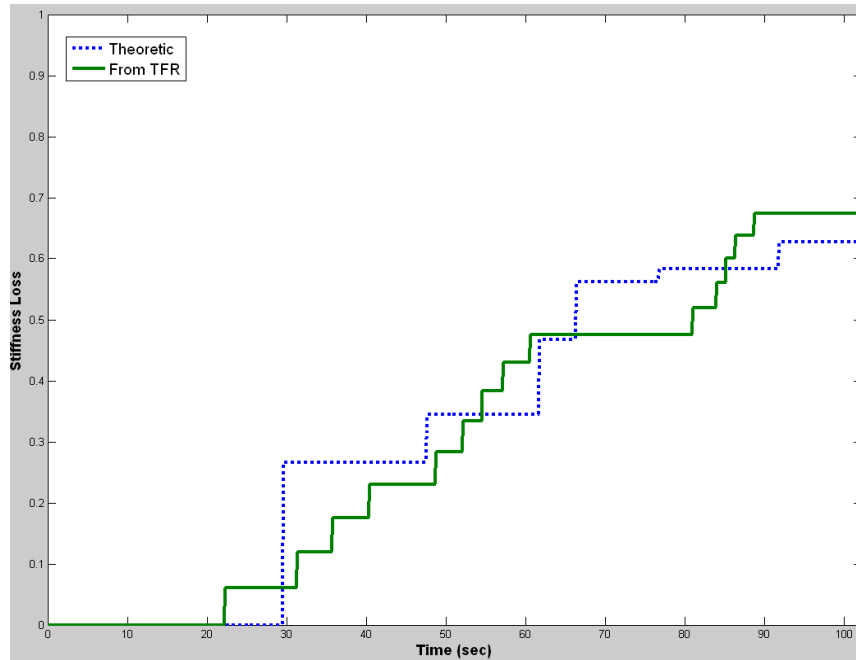


Figure 5-22 Comparative time history Stiffness Loss between theoretical and stiffness loss from TFSDDM

As can be seen in the Figure 5-22, the stiffness loss prediction perform well correlate at time (instant of occurrence) and value (stiffness loss). In this particular case the final stiffness loss from the TFDDSM algorithm is 67%, the exact value of the random model is at 63%, thus a relative error of the 6% ($1-0.63/0.67=0.06$).

One thousand of damage random cases have been made, a comparison between predicted against theoretical damage is shown in Figure 5-23 for 100 of these cases. As can be seen in this Figure the method appears to perform very well, However, the final question is how much is the relative error for any particular prediction of the stiffness loss?

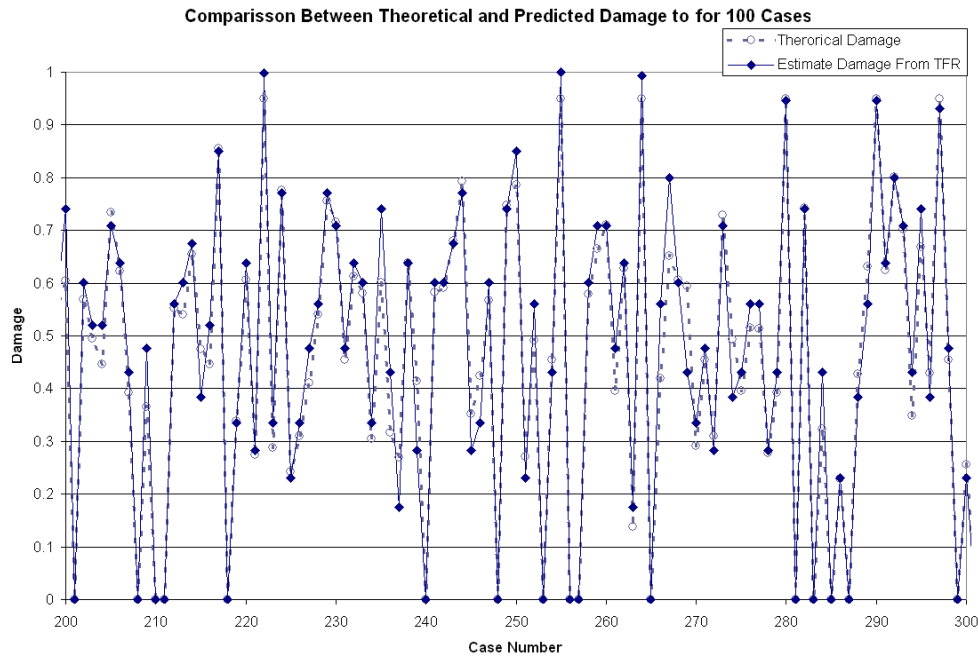


Figure 5-23 Theoretical and Predicted Damaged Comparisons (Note: Connecting lines are only for viewing purposes).

The answer to the aforementioned question is absolutely probabilistic, due to the fact that there is not a close solution for the problem. This is true even if a sophisticated finite element model of structure with millions of DOFs is used. There are enormous uncertainties associated with the problem (i.e. materials, base conditions, external loads etc.). At this time the structural engineering does not have the capacity for a collapse prediction [148] and the response of structural models can be too different of the real responses even in the linear regime [27].

Therefore, in this research a probabilistic evaluation of the performance prediction has been developed using the random database of the numerical simulations. Because in this work we do not appeal for any pre-established damaged pattern and all variables such as the input signals, the number, level and time instants of the damage, the noise added has been obtained in a random manner. Considering that the results are general and its validity can be expanded for any damage pattern of SDOF models.

First a distribution of the maximum relative error against occurrence probability is shown in the Figure 5-24. From this Figure it is clear that relative errors above 10% have very low probability of occurrence (i.e. below to 0.02).

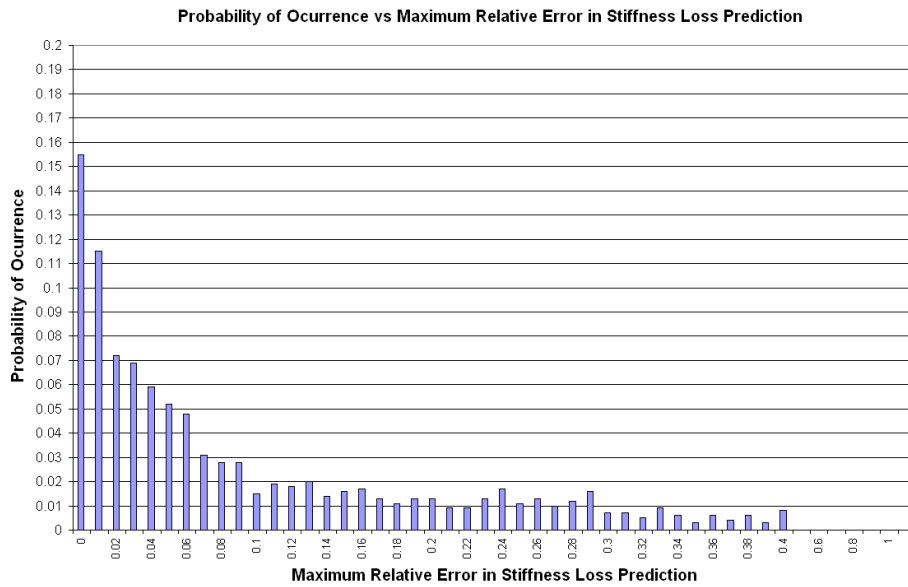


Figure 5-24 Probability of Occurrence of Relative Error in Stiffness Loss Predictions.

The absolute exceedence probability of any particular threshold error value is one minus its cumulative occurrence probability and for the test database the following equation has been obtained:

$$P_e(x_i) = 155.06x_i^4 - 151.09x_i^3 + 53.39x_i^2 - 9.19x + 0.84 \quad 5-18$$

where:

x_i : Maximum Relative Error

P_e : Exceedence Probability

A graphical representation of the equation 5-18 is shown in Figure 5-25:

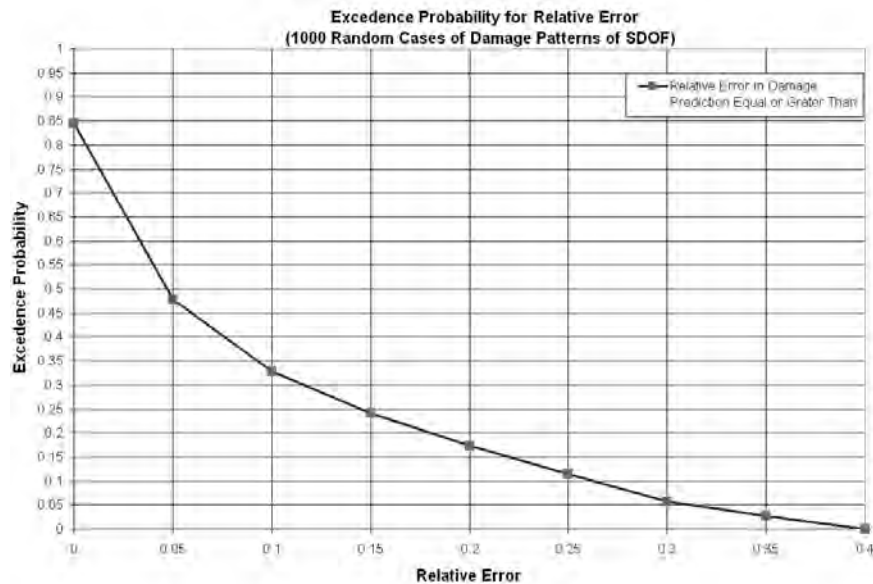


Figure 5-25 Excedence Probability for Relative Error in Stiffness Loss Predictions

If the equation 5-18 (or Figure 5-25) is taken as a representative of an ergodic process, it is valid for establishing the following general observations for the damage method proposed in this research:

- The mean value of relative error in stiffness loss prediction is around 5%
- Only 16% of the predictions have a zero error in its prediction
- Errors in prediction above 25% have a minimum excedence probability (Less than 5%).
- Error in prediction above 40% will never happen

For example if a threshold value of 25% in relative error prediction is taken, the reliability of the method is 90%. In other word if a damage level of 30% is predicted, the real damage level is in the interval ($22.5\% < 30\% < 37.5\%$) with a 90% of probability that it is true. This performance is quite remarkable if we consider that it has been obtained only using the very short-length time series of structural output signals for strong events and no additional structural information has been required.

5.2.2 Multiple Degree of Freedom Models

In this literal the application of the TFSDDM for MDOF models is shown.

For testing the proposed methodology in this work the numerical example number 8 developed by Filippou and Constantinides [231] has been selected. The structure is a two story steel frame submitted to the recorded motion of Erzican (Turkey) earthquake of 1992. For nonlinear analysis of the model which include elements with “*distributed inelasticity with 5 integration points along the span and discretization of each section in layers with uniaxial material response*” [231]. Additional information of the model and computational capabilities of the FEDEASLab software can be found in the reference [231]. Geometry, section types and vertical and horizontal additional loads are shown in the figure 5-26:

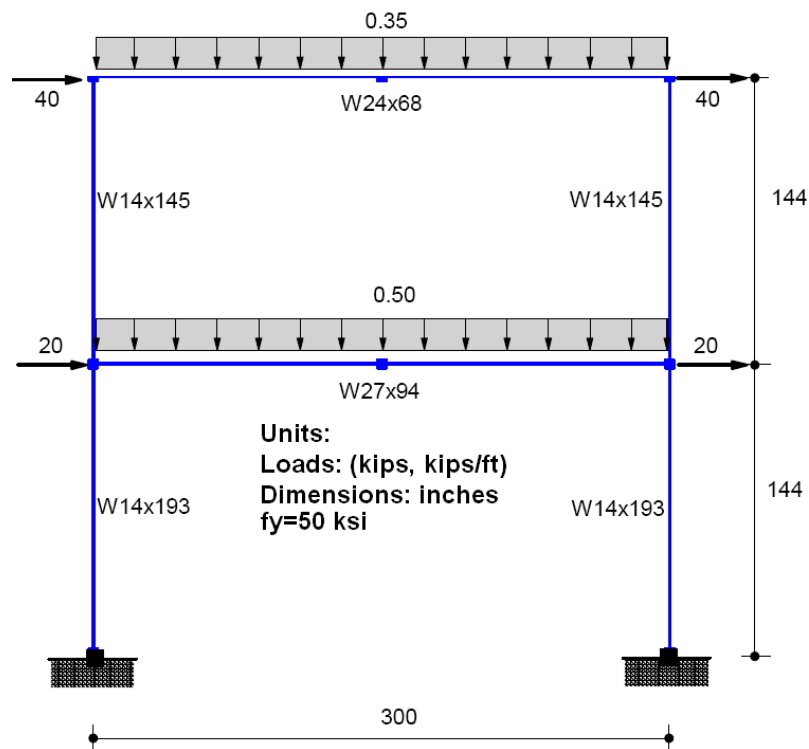


Figure 5-26 Two story steel frame used for MDOFs testing (Taken from reference [231])

It is assumed that two horizontal accelerometers have been installed in the structure in the floor of first level and the roof. According to the philosophy only the output signals of these instruments are available and no other additional structural information is on hand. The acceleration records obtained using FEDEASLab are shown in the next figure:

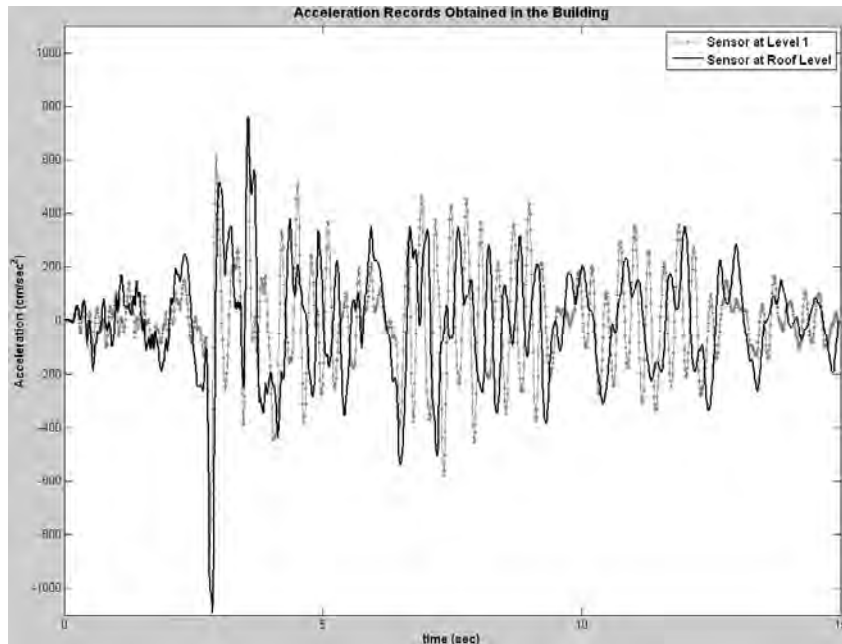


Figure 5-27 Acceleration records obtained in the building

The displacement records are obtained by using numerical integration and it is shown in the Figure 5-28. From this figure a permanent displacement of 0.748cm at the level 1 and 3.1cm at the roof can be obtained, thus it is evident that the structure has a permanent damage.

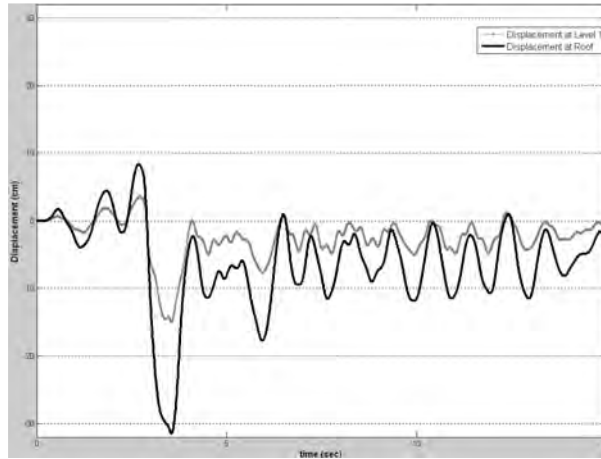


Figure 5-28 Displacement records obtained in the building

A comparison between the linear and nonlinear response of the structure at the roof level is shown in the Figure 5-29. It is clear that at the beginning of the record the two models have the same response, but at the 3.12 sec the system have an important incursion in the inelastic range and a permanent damage happened. In the real cases for strong motion events the complete time-history of the linear response of the structure is not measurable and only the real signal is obtainable (Nonlinear for this example).

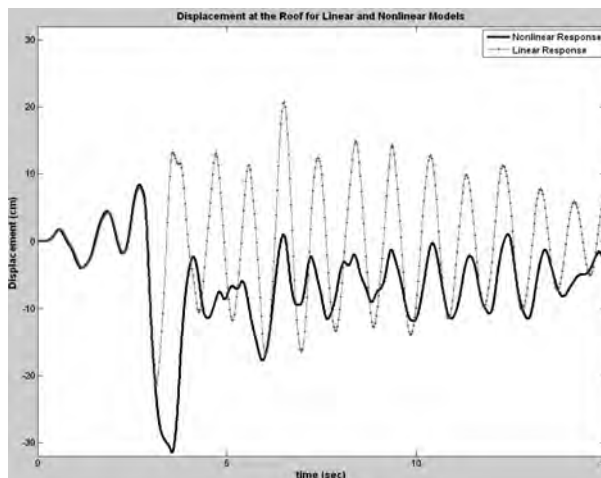


Figure 5-29 Linear and Nonlinear Displacement Records obtained at the Roof

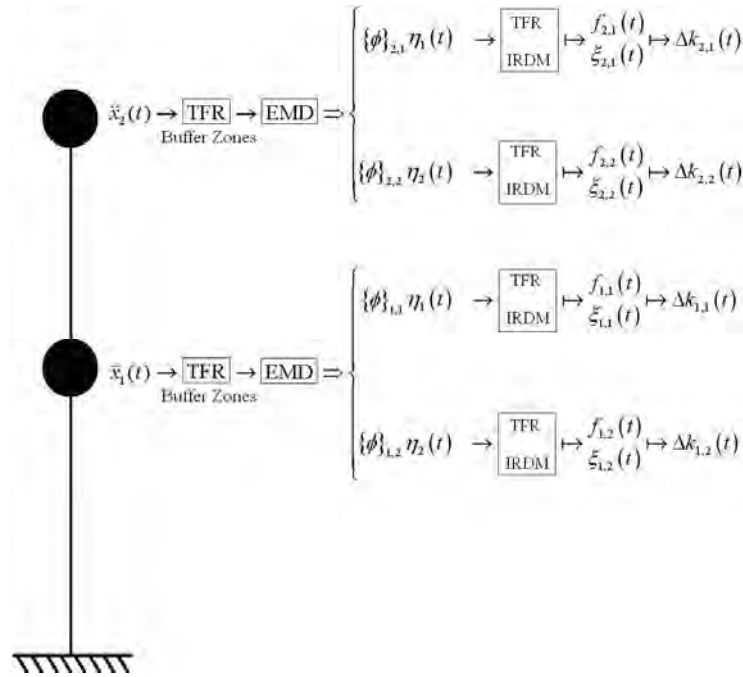


Figure 5-30 Schematic Process of Time Frequency Structural Damage Detection Method (TFSDDM) for a the FEDEASLab example 8 [231].

The system can be interpreted as a two degree of freedom system as shown in the Figure 5-30. Regarding to the schematic procedure for damage detection of Figure 5-30 it is important to point out that the damping in the example 8 of reference [231] has been set to 2%. For this reason it is not necessary to apply the IRDM method and the equation 5-13 becomes:

$$\Delta k(t) = 1 - \frac{m}{k_{t_i}} \left(\sqrt{\frac{k_{t_i}}{m}} - 2\pi(f_{t_i} - f_{t_{i+1}}) \right)^2 \quad 5-19$$

Therefore the procedure for damage detection starts with an evaluation of TFR for each recorded signal. It is shown in Figures 5-31 and 5-32, that the buffer zones have been established in the time-frequency plane.

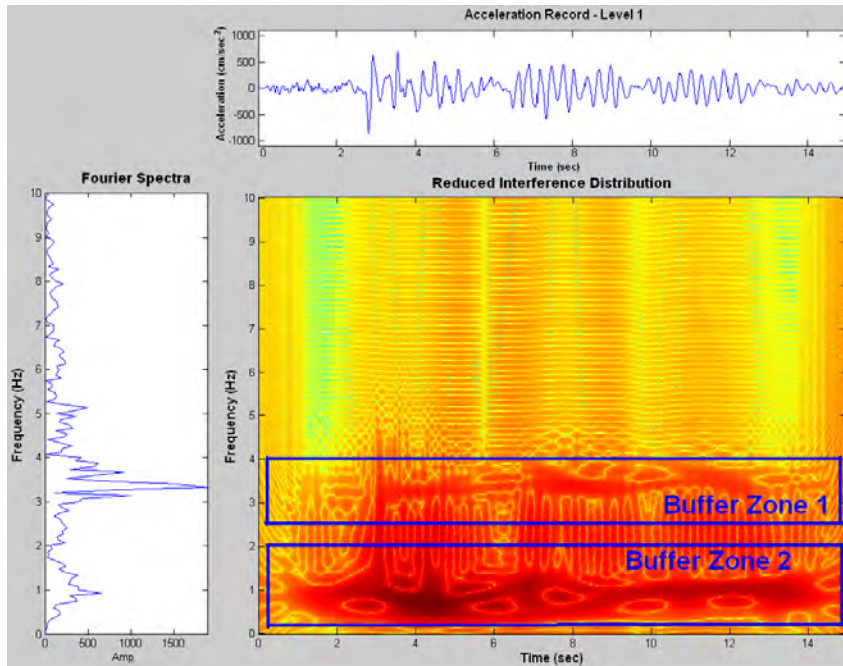


Figure 5-31 Buffer Zones for Acceleration Record from Sensor 1 (Level 1).

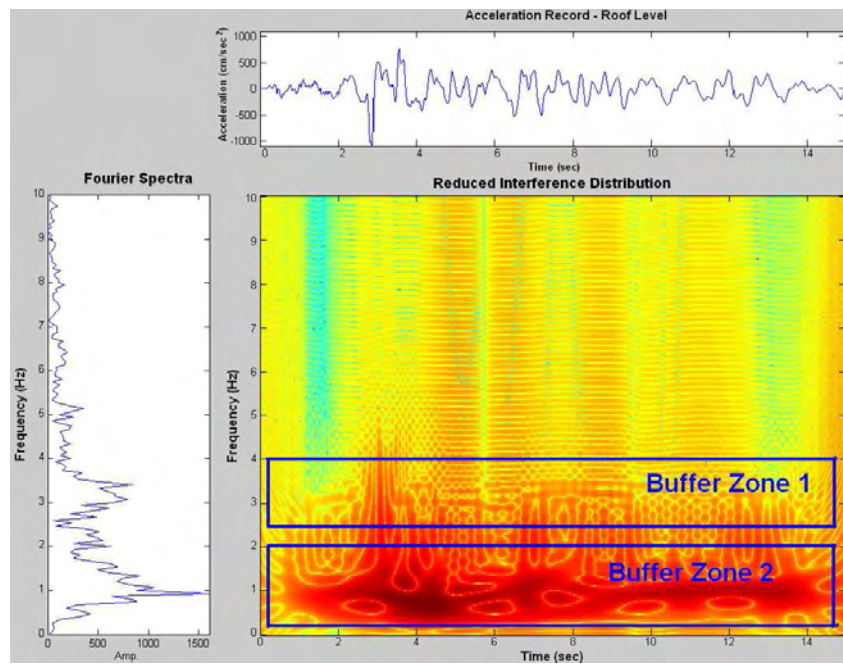


Figure 5-32 Buffer Zones for Acceleration Record from Sensor 2 (Roof Level).

From Figures 5-31, 5-32 it is evident that the two buffer zones can be limited from TFR maps. It represents the time-frequency zone where the structural response of the two component modes is concentrated. The initial system frequencies have set at 1.08 Hz and 3.49 Hz respectively. These values have been obtained using the first 2 seconds of the TFR maps of Figures 5-31 and 5-32.

Using the buffer as constraints of the EMD algorithms [209, 216] it is possible to extract the empirical mode functions for each output signal. The application of the EMD algorithm produces several empirical functions for each independent signal (i.e. it is assumed that the first two empirical functions of each signal with the buffer zones are the modes for each recorded output signal). In Figure 5-33 the extracted empirical mode functions are shown:

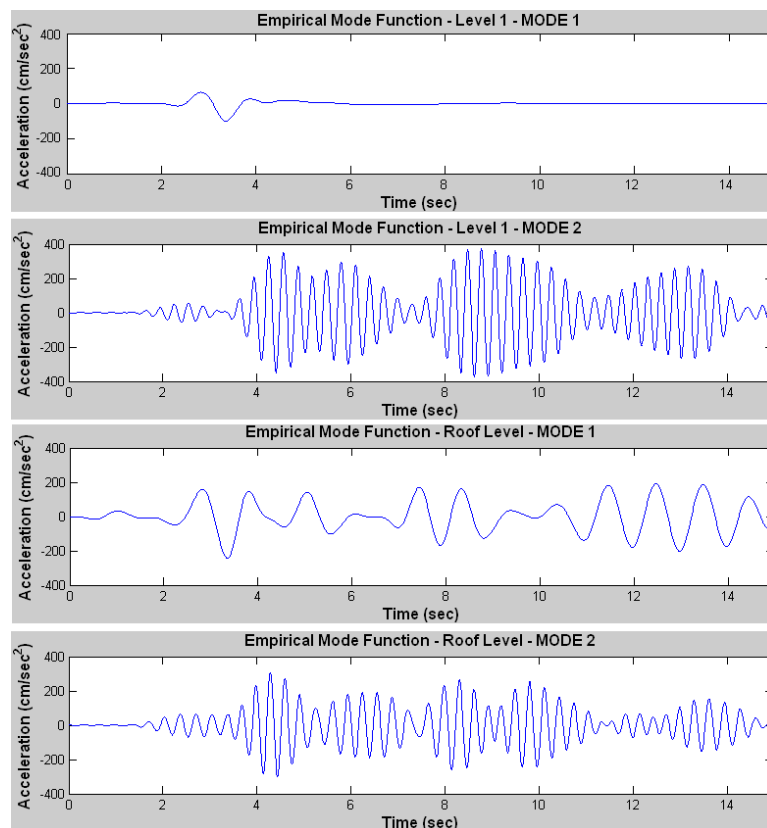


Figure 5-33 Empirical Mode Functions Extracted using the Buffer Zones of TFR maps.

Regarding to Figure 5-33, it is important to point out that the most non-linear response is for the mode 1 of the each recorded signal. Because the extracted empirical mode signals are quasi-monocomponent, it is possible to apply the algorithm used for SDOF output signals (see literal 5.2.1), in order to obtain the frequency tracking from the TFR maps and with this link the frequency changes with the damage.

In Figures 5-34 to 5-37 the frequency tracking (red lines) for each empirical mode functions are shown. In the same Figures the evolution of the energy (blue line) evaluated from the TFR marginal can be read using the right lateral scale

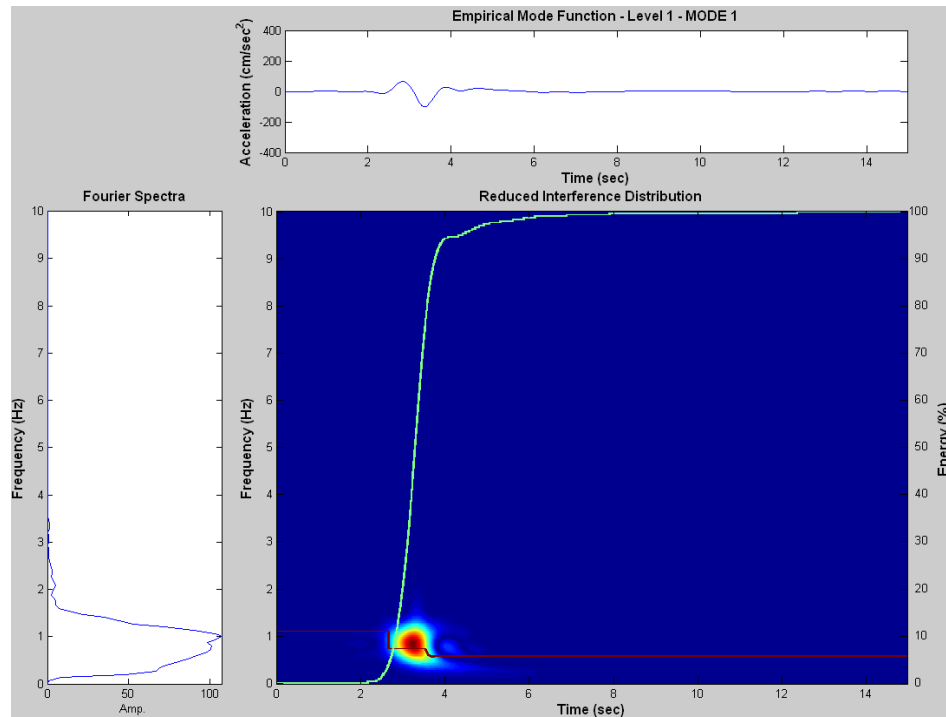


Figure 5-34 TFR for Empirical Mode Functions – Level 1 – Mode 1.

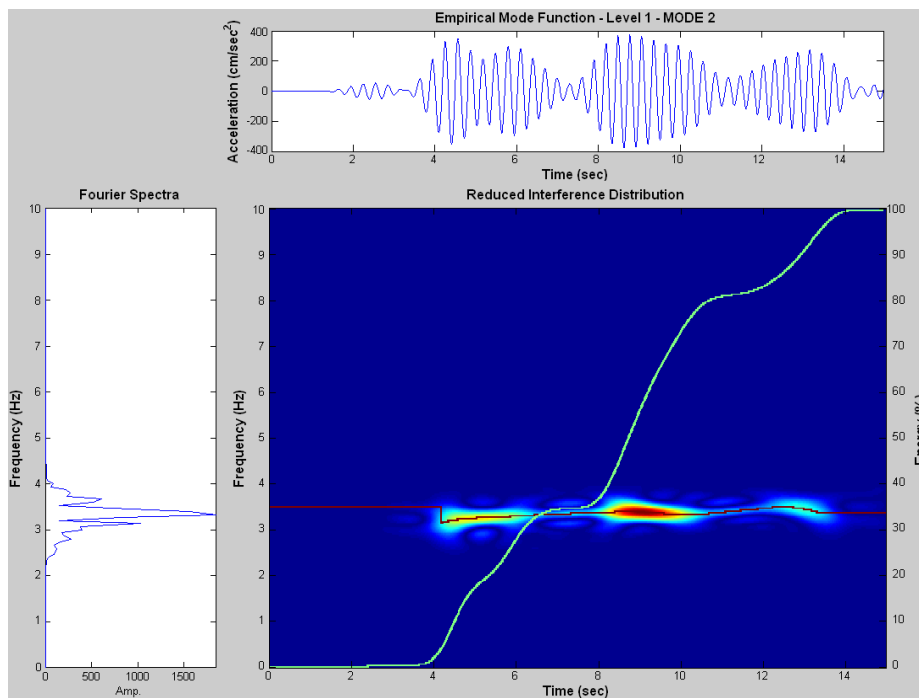


Figure 5-35 TFR for Empirical Mode Functions – Level 1 – Mode 2

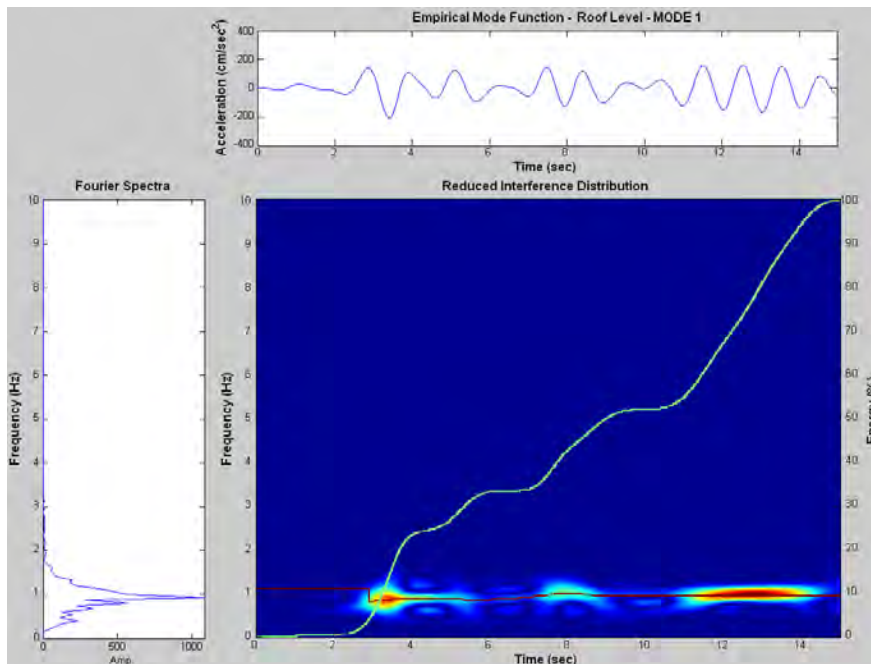


Figure 5-36 TFR for Empirical Mode Functions – Roof Level – Mode 1

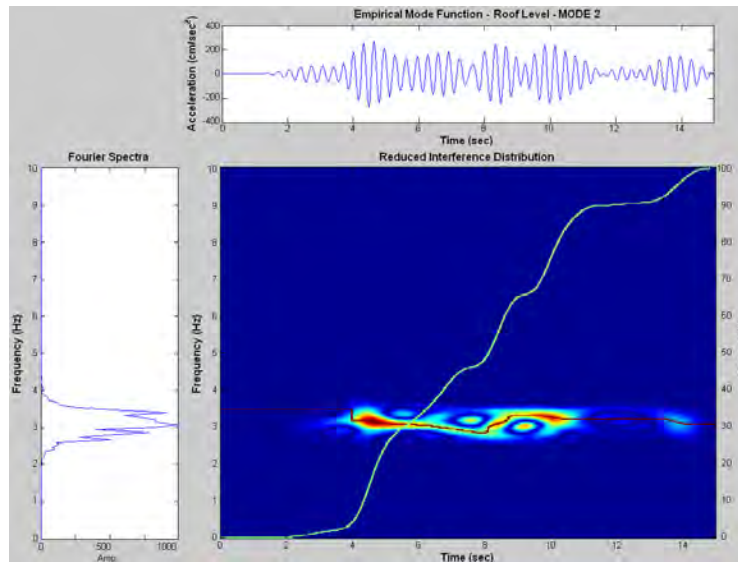


Figure 5-37 TFR for Empirical Mode Functions – Roof Level – Mode 2

Finally by using the Equation 5-13 or its simplified version Equation 5-19 when the damping is constant or neglected, it is possible to obtain the damage sequence (stiffness loss) as it is shown in Figure 5-38:

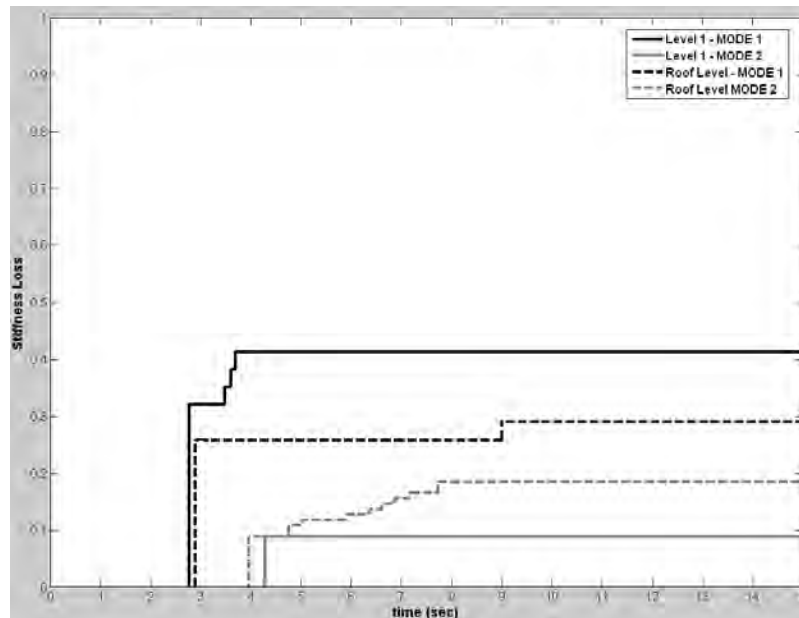


Figure 5-38 Predicted Damage for a MDOF model

6 TIME-FREQUENCY DAMAGE DETECTION PROGRAM – TFDDP: A Graphical User Interface (GUI)

In this chapter the main characteristics of a Graphical User Interface program (GUI) which has been developed in order to help in the process of damage detection using the methodologies proposed in this research will be shown briefly.

The program named “Time-Frequency Damage Detection Program - TFDDP” has been developed using MatLab®[125] language and the current version can be downloaded free of charge in the web site of the Puerto Rico Strong Motion Program at the internet site: <http://prsmpr.uprm.edu/> or by contacting the author of this research on the e-mail: leocanos@hotmail.com.

The current complete documentation and the Open File Archives can be downloaded directly from the internet, due to the fact that the software is being updated continuously, not many details are given here.

6.1 Software Requirements of TFDDP Program

The program developed is not a stand alone program in the sense that it is supported on the MatLab base platform and some MatLab Toolbox and other Open File Programs developed by others.

The main software requirements for the TFDDP are:

- MatLab Program Version 7.14 [125] or higher for Windows.
- Signal Processing Toolbox [122]
- Time-Frequency Toolbox [123]
- Empirical Mode Decomposition Algorithms for MatLab developed by Flandrin et. al. [209, 216].
- Random Decrement Technique Algorithms for MatLab developed by Bejarano [222]

At the Puerto Rico Strong Motion Program website, **ONLY** the open file algorithms developed in this research can be obtained, the other software requirements can be purchased or acquired directly from the other developers. Internet Links for doing that can be found in the Puerto Rico Strong Motion Program website.

6.2 General Description of TFDDP Program

The program does not have a strict sequence of operation, but obviously for doing some task is necessary to make some preceding steps.

Basic knowledge in signal processing and time-frequency analysis is required to operate the program. The bibliographic references have been provided in the previous chapters.

To start the program, it is necessary to install the software requirements mentioned in 6.1 and type “tfddp” in the MatLab prompt window.

Once the TFDDP has been initialized, a welcome window will be displayed in the screen as is shown in the figure 6-1:



Figure 6-1 Initial Screen of Time-Frequency Damage Detection Program - TFDDP

The program has been divided into independent modules:

- File
- Ambient Vibration
- Strong Motion Events
- Tools
- About

Next a brief description of each module is presented

6.2.1 File Module

In this module the following procedures will be done:

- Load the data previously saved in MatLab format (extension .mat)
- Save the data in MatLab format.

- Print the current graphic available
- Finish the tfddp program

A view of the screen when the Sub-Menu File is active can be seen in the figure 6-2:

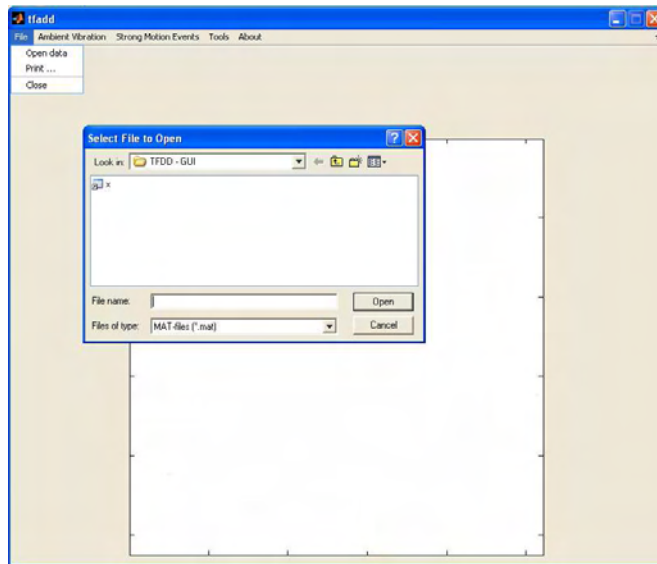


Figure 6-2 Sub-Menu File

6.2.2 Ambient Vibration Module

In this module the following procedures will be done:

- Perform a Mean Time Frequency Representation for Ambient Vibration Signals using any type of fixed kernel TFR included in the Time-Frequency Toolbox [123].
- Perform a structural system identification procedure using the MTFR results and applying FDD methodology [124].
- Evaluate the matrix stiffness loss according to the procedure proposed in the Chapter 4 of this research.

A view of the screen when the Sub-Menu Ambient Vibration is active can be seen in the figure 6-3:

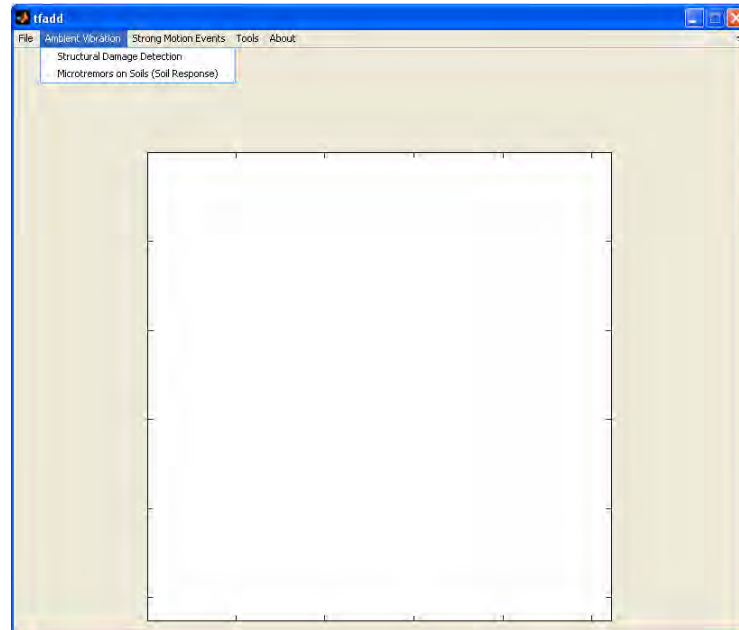


Figure 6-3 Sub-Menu Ambient Vibration

6.2.3 Strong Motion Events Module

For any SDOF signal using this module the following procedures will be done:

- Using a signal of a strong motion event recorded in a single channel one can evaluate a Time Frequency Representation by using any type of fixed kernel TFR included in the Time-Frequency Toolbox [123].
- From the precedent TFR plane the macro-windows where the frequency change can be selected.
- Using the pre-selected windows of the previous step it is possible to apply the RDM algorithms [222] in order to get the time history damping.
- Using the completed TFR information plane the tracking of the frequency can be evaluated in an automatic procedure.
- For the previous time history frequency and damping changes, the stiffness loss is evaluated in an automatic form.

For any MDOF signal using this module the following procedures will be done:

- Select particular skeletons curves for constructing buffer zones center in the skeleton to constrain the EMD results.
- Apply the EMD algorithms [209, 216] to get the quasi-monocomponent signals corresponding to each SDOF modal component.
- Once the SDOF quasi-monocomponent signal has obtained it is possible to apply the procedure developed in the SDOF module to evaluate the damage for each one SDOF.

A view of the screen when the Sub-Menu Strong Event is active is shown in the figure 6-4:

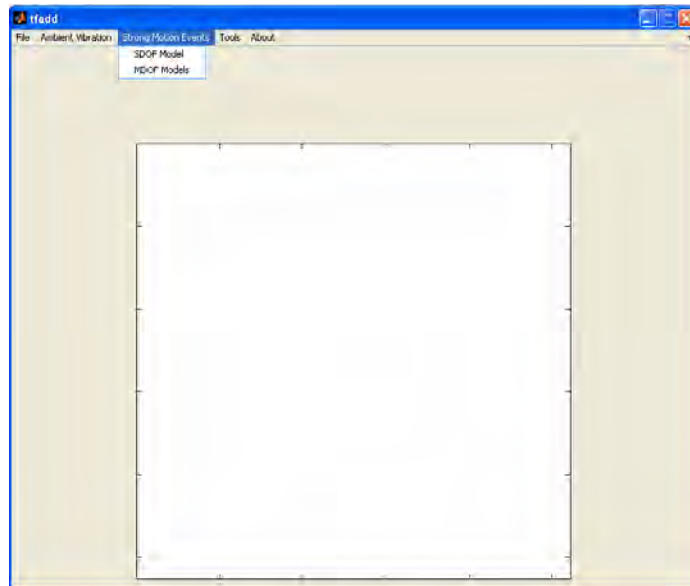


Figure 6-4 Sub-Menu Strong Motion Events

6.2.4 Tools Module

In this module, several tools for signal analysis and pre-processing can be found.

For any single signal using this module the following procedures will be done:

- Perform a Baseline Correction using a Linear or Polynomial trend.

- Evaluate Low Pass, High Pass and Band Pass Filters, using several windows functions like Butter, Hanning, Hamming, Rectangular and Gaussian.
- Add Gaussian random noise.
- Perform a single Fourier Transform for a signal in the time domain or a Inverse Fourier Transform for a complex signal in the frequency domain.
- Evaluate the Elastic Response Spectra to any damping coefficient between 0 and 0.7.
- Evaluate the signal differentiation or signal integration in the time domain.
- Perform a Cepstrum Analysis.
- Convert K2 and ETNA digital records into TFDDP format (MatLab format).
- Convert a single text file (in columns format) into TFDDP format.

A view of the screen when the Sub-Menu Strong Event is active is shown in the figure 6-5:

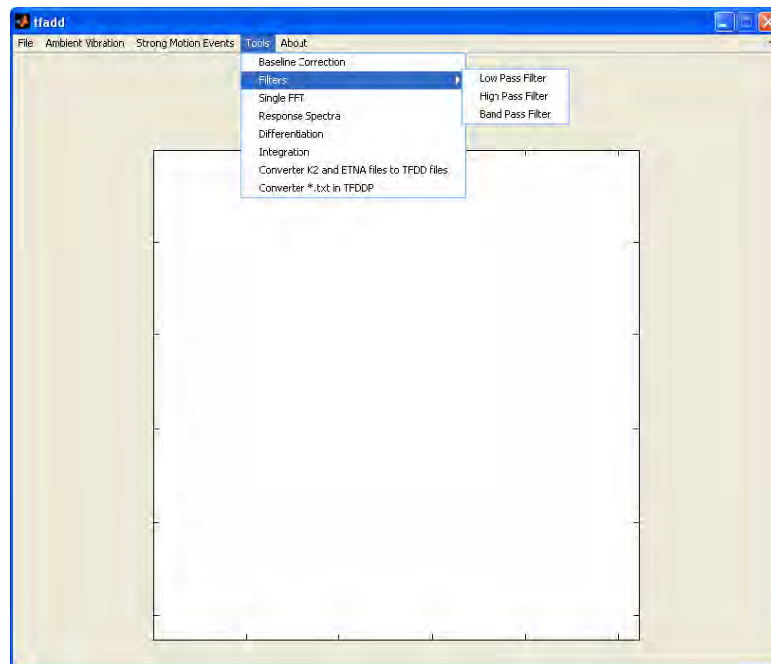


Figure 6-5 Sub-Menu Tools

6.2.5 About Module

In this module, two options can be activated:

- A topic help with link describing the main characteristics of the TFDDP
- An About window with the author information and the program version

It is shown in the Figure 6-6:

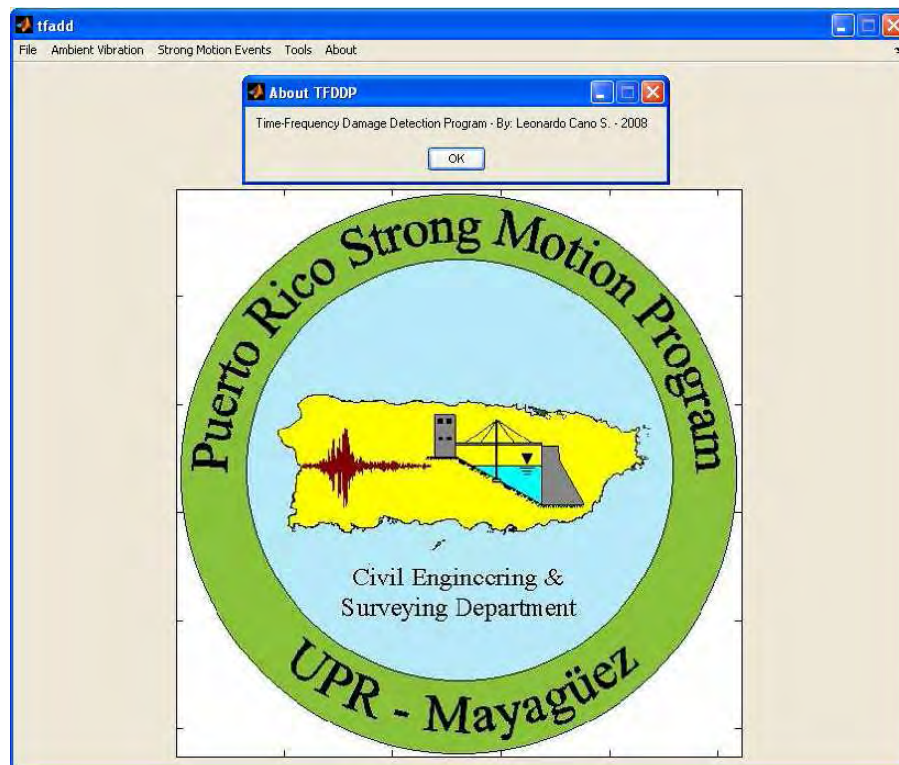


Figure 6-6 Sub-Menu Help

7 CONCLUSIONS

In this work the capacity of the Time-Frequency Analysis together with other techniques of signal analysis and system identification for structural damage detection using only output data has been investigated.

According to the philosophy of this research only the output signal from structures has been used. The damage has been defined as permanent changes of one or more structural properties and it will be estimated from analysis of the output signals. It has been determined that permanent changes in structural frequency can be associated with stiffness losses and hence, damage.

Regarding the Time-Frequency Analysis, one of the first problems to use these methodologies is the selection of a TFRs useful in dealing with signals from civil engineering structures. In order to solve this problem a new objective methodology has been developed. The methodology is based on four aspects, the first two directly associate with earthquake and civil engineering application and the last two based on resolution and information measure. Using the methodology proposed in this research it has been shown that from a group of Cohen Class TFRs, the Reduced Interference Distribution have the best performance dealing with signal from civil engineering structures.

The problems of damage detection using ambient vibration signal has been studied in detail. The mathematical formulation of a Mean Time-Frequency Representation has been developed and the remarkable and stable frequency detection of this representation has been introduced as eigenvalues constraint in the Frequency Domain Decomposition algorithm proposed by Brincker [124] for system identification.

For structural and non-structural frequency separation, the direct observation of Time-Frequency plane has been suggested and the shape method of scale Empirical Probabilistic Density form has been adopted. An additional equation for the exceedance coefficient based on Time-Frequency information has also been proposed.

Regarding frequency separation of very close and coupled modes, the Cepstrum analysis has been used and complemented with the evaluation of time marginals of the Time-Frequency Representation. For the simulated data this proposed methodology showed a good behavior. For coupled modes, the identification or separation between real structural frequencies and non-structural frequencies for a narrow frequency bandwidth around natural frequencies is not possible without using any additional structural information or information about the external sources.

Using exhaustively simulated and real signals of ambient vibration, it has been proved that the methodology proposed here is valuable for damage detection using output signal in a dual scheme that require the data acquisition and system identification before and after the event. The resolution of the MTFR-FDD method is remarkable but depends strongly on the amount and location of sensors. A variable sensibility study has been made and it was shown that the other important variable in the methodology is the amount of available records. Mean errors in damage detection predictions have been established close to 2% and the predictions in location have been quite remarkable.

Damage detection using output signals from strong event has been investigated. For SDOF systems a mathematical relation that links the frequency and damping changes with the stiffness loss has been developed. A complete scheme based on the frequency tracking from Time-Frequency plane has been established and proved using numerical data. A complete algorithm for the aforementioned frequency tracking has been proposed and proved. A probabilistic study has shown that the reliability of the predictions of amount damage is around 90%. The damping tracking has been made using the Random Decrement Method

[222] with an improvement based on a windowed scheme obtained directly from the TFR plane. For MDOF systems a mode separation has been proposed using the Empirical Mode Decomposition (EMD) algorithms [79] enhanced with time-frequency buffers around the main frequencies, once the MDOFs system is reduced to modal SDOFs, its TFRs are evaluated and the developed algorithm for these cases is applied again.

A computer program has been developed and published as an open file in the internet website of Puerto Rico Strong Motion Program. The program named “Time-Frequency Damage Detection Program - TFDDP” has been developed using MatLab@[125] and the current version can be downloaded free of charge in the web site of the Puerto Rico Strong Motion Program at the internet site: <http://prsmg.uprm.edu/> or by contacting the author of this research on the e-mail: leocano-s@hotmail.com.

REFERENCES

- [1] E.P. Carden, P. Fanning, *Vibration Based Condition Monitoring: A Review*, Structural Health Monitoring, Vol 3(4), pp.355-377, 2004
- [2] H. Sohn, C. Farrar, F. Hemez, D. Shunk, D. Stinemat, B. Nadler, *A Review of Structural Health Monitoring Literature*, LA-13976-MS, Los Alamos National Laboratory, 2003
- [3] S. Doebling, C. Farrar, M. Prime, D. Shevitz, *Damage Identification and Health Monitoring of Structural and Mechanical Systems from Changes in Their Vibration Characteristics: A Literature Review*, LA-13070-MS, Los Alamos National Laboratory, 1996.
- [4] S. Doebling, C. Farrar, M. Prime, *A Summary Review of Vibration-Based Damage Identification Methods*, The Shock and Vibration Digest, Vol 30(2), pp. 91-105, 1998
- [5] A. Alvandi, C. Cremona. *Assessment of Vibration-Based Damage Identification Techniques*, Journal of Sound and Vibration, Vol(292), pp. 179-202, 2006.
- [6] P. Chang, A. Flatau, C. Liu, *Review Paper: Health Monitoring of Civil Infrastructure*, Structural Health Monitoring, Vol(2) No. 3, pp. 257-267, 2003.
- [7] P. Laura, S. La Malfa, D. Bambill, *Monitoring Structural Health Through Changes in Frequency*, Journal of Sound and Vibration, Vol 212(5), pp. 909-911, 1998
- [8] H. Wenzel, D. Pichler, *Ambient Vibration Monitoring*, Wiley & Sons Ltd, West Sussex, England, 2005.
- [9] O. Salawu, *Detection of Structural Damage Through Changes in Frequency: A Review*, Engineering Structures, Vol. 19 (9) pp. 718-723, 1997
- [10] M. Giberson, *The Response of Non-Linear Multi-Story Structures Subject to Earthquake Excitation*, Ph.D. Thesis, California Institute of Technology, 1967.
- [11] J. Kuroiwa, *Vibration Test of a Multistory Building*, Report EERL-01-67, Earthquake Engineering Research Laboratory, California Institute of Technology, 1967
- [12] J.N., Distefano, A. Rath, *Modeling and Identification in Nonlinear Structural Dynamics*, Report UBC-EERC-74-15, Earthquake Engineering Research Center, University of California at Berkeley, 1974
- [13] J. Beck, *Determining Models of Structures from Earthquake Records*, Ph.D. Thesis, California Institute of Technology, 1978
- [14] P. Carydis, H. Mouzakis, *Small Amplitude Vibration Measurements of Buildings Undamaged, Damaged, and Repaired After Earthquakes*, Earthquake Spectra, Vol(2) No. 3. pp. 515-534, 1986

- [15] R. Beck, J. Beck, *Comparison Between Transfer Function and Modal Minimization Methods for System Identification*, Report EERL-85-06, Earthquake Engineering Research Laboratory, California Institute of Technology, 1967
- [16] C. Loh, Y. Tsaur, *Time Domain Estimation of Structural Parameters*, Engineering Structural, Vol(10), pp. 95-105, 1988
- [17] R. Beck, *Fundamental Problems in the Application of Structural Identification Procedures to Damage Detection*, Ph.D. Thesis, California Institute of Technology, 1991.
- [18] Y. Li, J. Jirsa, *Nonlinear Analyses of an Instrumented Structure Damage in 1994 Northridge Earthquake*, Earthquake Spectra, Vol(14) No. 2, pp. 265-283, 1998
- [19] C. Yang, *Statistical System Identification and Applications to Seismic Response of Structures*, Report EERL-96-02, Earthquake Engineering Research Laboratory, California Institute of Technology, 1996
- [20] R. Goel., A. Chopra, *Vibration Properties of Buildings Determined From Recorded Earthquake Motions*, Report UBC-EERC-97-14, Earthquake Engineering Research Center, University of California at Berkeley, 1997
- [21] J. De la Llera, A. Chopra, J. Almazan, *Three-Dimensional Inelastic Response of an RC Building During the Northridge Earthquake*, Journal of Structural Engineering, Vol(127) No. 5, pp. 482-489, 2001
- [22] J. Ching, M. Muto, J. BeckH., *Structural Model Updating and Health Monitorign with Incomplete Modal Data Using Gibbs Sampler*, Computer-Aided Civil and Infrastructure Engineering. Vol(210), pp. 242-257, 2006.
- [23] N.A. Haskell, *The Dispersion of Surface Waves in Layered Media*, Bulletin of Seismological Society of America, Vol(43), pp. 17-34, 1953
- [24] D. Hudson., *A Comparison of Theoretical and Experimental Determinations of Building Response to Earthquakes*, Proceedings Second World Conference on Earthquake Engineering, Vol(2), pp. 1105-1120, 1960
- [25] G. McVerry, *Frequency Domain Identification of Structural Models From Earthquake Records*, Report EERL-79-02, Earthquake Engineering Research Laboratory, California Institute of Technology, 1979
- [26] J. Luco, M. Trifunac, H. Wong, *On the Apparent Change in Dynamic Behavior of a Nine-Story Reinforced Concrete Building*, Bulletin of Seismological Society of America, Vol(77) No. 6, pp. 1961-1983, 1987
- [27] R. Boroschek, F. Yañez, *Experimental Verification of Basic Analytical Assumptions used in the Analysis of Structural Wall Buildings*, Engineering Structures, Vol(22), pp.657- 669, 2000
- [28] H. Melhem, H. Kim, *Damage Detection in Concrete by Fourier and Wavelets Analysis*, Journal of Engineering Mechanics, Vol(129) No. 5, pp. 571-577, 2003

- [29] S. Bisht, *Methods for Structural Health Monitoring and Damage Detection of Civil and Mechanical Systems*, MSc. Thesis, Virginia Polytechnic Institute and State University, 2005.
- [30] K. Hong, C. Yun, *Improved Method for Frequency Domain Identifications of Structures*, Engineering Structures, Vol(15) No. 3, pp. 179-188, 1993
- [31] M. Trifunac, S. Ivanovic, M. Todorovska, *Apparent Period of a Building I: Fourier Analysis*, Journal of Structural Engineering, Vol(127) No. 5, pp. 517-526
- [32] B. Hubbard, *The World According to Wavelets: The story of an mathematical technique in the making*, A.K. Peters editions, 1996.
- [33] M. R. Taha, A. Noureldin, J. Lucero, T. Baca, *Wavelet Transform for Structural Health Monitoring: An Compendium of Uses and Features*, Structural Health Monitoring, Vol(5) No. 3, pp. 267-295, 2006.
- [34] Q. Wang, X. Deng, *Damage Detection with Spatial Wavelets*, International Journal of Solids and Structures, Vol(36), pp. 3443-3468, 1999.
- [35] B. Kim, T. Park, G. Voyiadjis, *Damage Estimation on Beam-Like Structures Using Multi-Resolution Analysis*, International Journal of Solids and Structures, Vol(43), pp. 4238-4257, 2006.
- [36] I. Kim, Y. Kim, *Damage Size Estimation by the Continuous Wavelet Ridge Analysis of Dispersive Bending Waves in a Beam*, Journal of Sound and Vibration, Vol(287), pp. 707-722, 2005.
- [37] P. Moyo, J. Brownjohn, *Detection of Anomalous Structural Behavior Using Wavelet Analysis*, Mechanical Systems and Signal Processing, Vol(16) Issue 2-3, pp. 429-445, 2002.
- [38] C. Huang, S. Hung, C. Lin, W. Su, *A Wavelet-Based Approach to Identifying Structural Modal Parameters from Seismic Response and Free Vibration Data*, Computer-Aided Civil and Infrastructure Engineering, Vol(20), pp. 408-423, 2005.
- [39] Z. Sun, C. Chang, *Structural Damage Assessment Based on Wavelet Packet Transform*, Journal of Structural Engineering, Vol(128) No. 10, pp. 1354-1361, 2002.
- [40] J. Lin, M. Zuo, K. Fyfe, *Mechanical Fault Detection Based on the Wavelet De-Noising Technique*, Journal of Vibration and Accoustic, Vol(126), pp. 9-16, 2004
- [41] A. Hera, Z. Hou, *Application of Wavelet Approach for ASCE Structural Health Monitoring Benchmark Studies*, Journal of Engineering Mechanics, Vol(130) No. 1, pp. 96-104, 2004.
- [42] Z. Sun, C. Chang, *Statistical Wavelet-Based Method for Structural Health Monitoring*, Journal of Structural Engineering, Vol(130) No. 7, pp. 1055-1062, 2004.

- [43] M. R. Taha, A. Noureldin, A. Osman, N. El-Sheimy, *Introduction to the use of wavelet multiresolution analysis for intelligent structural health monitoring*, Canadian Journal of Civil Engineering, Vol (31), pp. 719-731, 2004.
- [44] A. Ovanesoza, L. Suarez, *Applications of Wavelet Transforms to Damage Detection in Frame Structures*, Engineering Structures, Vol(26), pp. 39-49, 2004.
- [45] Z. Hou, A. Hera, A. Shinde, *Wavelet-Based Structural Health Monitoring of Earthquake Excited Structures*, Computer-Aided Civil and Infrastructure Engineering, Vol(21), pp. 268-279, 2006.
- [46] H. Adeli, X. Jiang, *Dynamic Fuzzy Wavelet Neural Network Model for Structural System Identification*, Journal of Structural Engineering, Vol(132) No. 1, pp. 102-111, 2006.
- [47] H. Kim, H. Melhem, *Damage Detection of Structures by Wavelet Analysis*, Engineering Structures, Vol(26), pp. 347-362, 2004.
- [48] M. Todorovska, *Estimation of Instantaneous Frequency of Signals Using The Continuous Wavelet Transform*, Report CE-01-07, Civil Engineering Department, University of Southern California, Revised 2004.
- [49] S. Qian, D. Chen, *Joint Time-Frequency Analysis*, Prentice Hall, 1996.
- [50] M.D. Trifunac, T.Y. Hao, M.I. Todorovska, *On Energy Flow in Earthquake Response*, Report CE-01-03, University of Southern California, 2001.
- [51] C.M. Uang, V. Bertero, *Use of Energy as a Design Criterion in Earthquake-Resistant Design*, Report UCB/EERC-88-18, University of California at Berkeley, 1988
- [52] E. Kalkan, *Predictions of Seismic Demands in Building Structures*, PhD thesis, University of California at Davis, 2006.
- [53] E. Wigner, *On the Quantum Correction for Thermodynamic Equilibrium*, Physical Review, Vol. 40, 1932.
- [54] J. Ville, *Theorie et Applications de la Notion de Signal Analytique. Cables et Transmissions*. Vol (2A) No. 1, pp. 61-74, 1948. Translate to English by I. Selin, *Theory and Applications of the Notions of Complex Signals*, RAND Corporation Technical Report T-92, 1958.
- [55] L. Cohen, *Generalized Phase-Space Distribution Functions*, Journal of Mathematical Physics, Vol(7) No. 5, 1966
- [56] L. Cohen. *Time-frequency Distribution – A Review*, Proc. IEEE, Vol. 77-7 1989.
- [57] F. Hlawatsch, G.F. Boudreaux-Bartels, *Linear and Quadratic Time-Frequency Signal Representations*, IEEE Signal Processing Magazine, Vol(9) Issue 2, pp. 21-67, 1992.
- [58] F. Udawadia, M. Trifunac, *Time and Amplitude Dependent Response of Structures*, Earthquake Engineering and Structural Dynamics, Vol(20), pp. 359-378, 1974.

- [59] F. Udwadia, P. Marmarelis, *The Identification of Building Structures Systems I: The Linear Case*, Bulletin of Seismological Society of America, Vol(66) No. 1, pp. 125-151, 1976.
- [60] F. Udwadia, P. Marmarelis, *The Identification of Building Structures Systems II: The Nonlinear Case*, Bulletin of Seismological Society of America, Vol(66) No. 1, pp. 153-171, 1976.
- [61] C. Pinnegar, L. Mansinha, *A Method of Time-Time Analysis: The TT-Transform*, Digital Signal Processing, Vol(13), pp. 588-603, 2003.
- [62] C. Pinnegar, *Time-Frequency and Time-Time Filtering with the S-Transform and TT-Transform*, Digital Signal Processing, Vol(15), pp. 604-620, 2005.
- [63] Y. Arici, K. Mosalam, *Modal Identification and Health Monitoring of Bridges Using Seismic Acceleration Records*, Report UBC-EERC-2006-02, Earthquake Engineering Research Center, University of California at Berkeley, 2006.
- [64] P. Robin, B. Jansen, X. Cheng, R. Finch, *Acoustic Monitoring of Beams by Time-Frequency Analysis*, Journal of Acoustical Society of America, Vol(91) No. 4, Pt 2, pp.2359, 1992.
- [65] J. Hammond, P. White, *The Analysis of Non-Stationary Signals Using Time-Frequency Methods*, Journal of Sound and Vibration, Vol(193) No. 3, pp. 419-447, 1996.
- [66] P. Bonato, R. Ceravolo, A. De Stefano, M. Knaflitz, *Bilinear Time-Frequency Transformations in the Analysis of Damage Structures*, Mechanical Systems and Signal Processing, Vol(11) No. 4, pp. 509-527, 1997.
- [67] W. Staszewski, K. Worden, G. Tomlinson, *Time-Frequency Analysis in Gearbox Fault Detection Using Wigner-Ville Distribution and Pattern Recognition*, Mechanical Systems and Signal Processing, Vol(11) No. 5, pp. 673-692, 1997.
- [68] R. Olivito, L. Surace, *The Damage Assessment of Concrete Structures by Time-Frequency Distributions*, Experimental Mechanics An International Journal, Vol(37) No. 3, pp. 355-359, 1997.
- [69] P. Bonato, R. Ceravolo, A. De Stefano, *Time-Frequency and Ambiguity Function Approaches in Structural Identification*, Journal of Engineering Mechanics, Vol(123) No. 12, pp. 1260-1267, 1997
- [70] J. De la LLera, A. Chopra, *Evaluation of Seismic Code Provisions Using Strong-Motion Building Records from the 1994 Northridge Earthquake*, Report No. UCB/EERC-97/16, Earthquake Engineering Research Center, University of California at Berkeley, 1998.
- [71] P. Bonato, R. Ceravolo, A. De Stefano, F. Molinari, *Time-Frequency and Cross-Time-Frequency Based Techniques for Structural Identification of Systems*, Proceedings of the IEEE International Symposium on Time-Frequency and Time-Scale Analysis, Pittsburg, Pennsylvania, 1998.

- [72] P. Bonato, R. Ceravolo, A. De Stefano, F. Molinari, *Modal Identification by Cross-Time-Frequency Estimators*, Key Engineering Materials, Vols(167-168), pp. 363-372, 1999.
- [73] N. Huang, Z. Shen, S. Long, M. Wu, H. Shih, Q. Zheng, N. Yen, C. Tung, H. Liu, *The Empirical Mode Decomposition and Hilbert Spectrum for Nonlinear and Non-Stationary Time Series Analysis*, Proceedings of Royal Society London, Vol(454), pp. 903-995, 1998.
- [74] P. Bonato, R. Ceravolo, A. De Stefano, F. Molinari, *Use of Cross-Time-Frequency Estimators for Structural Identification in Non-Stationary Conditions and Under Unknown Excitation*, Journal of Sound and Vibration, Vol(237) No. 5, pp. 779-791, 2000.
- [75] P. Bonato, R. Ceravolo, A. De Stefano, F. Molinari, *Cross-Time-Frequency Techniques for Identification of Masonry Buildings*, Mechanical Systems and Signal Processing, Vol(14) No. 1, pp. 91-109, 2000.
- [76] M. Trifunac, S. Ivanovic, M. Todorovska, *Apparent Periods of A Building II: Time-Frequency Analysis*, Journal of Structural Engineering, Vol(127) No. 5, pp. 527-537, 2001.
- [77] A. De Stefano, R. Ceravolo, D. Sabia, *Output Only Dynamic Identification in Time-Frequency Domain*, proceedings of the American Control Conference, pp. 447-449, Arlington, VA, 2001.
- [78] R. Ceravolo, A. De Stefano, F. Molinari, *Developments and Comparisons on the Definition of an Instantaneous Damping Estimator for Structures under Natural Excitation*, Key Engineering Materials, Vol(204-205), pp. 231-240, 2001.
- [79] L. Cohen, L. Galleani, R. Hedges, D. Hughes, P. Loughlin, B. Suter, *Time-Frequency Analysis of a Variable Stiffness Model for Fault Development*, Digital Signal Processing, Vol(12), pp. 429-440, 2002.
- [80] S. Neild, M. Williams, P. McFadden, *Nonlinear Vibration Characteristics of Damaged Concrete Beams*, Journal of Structural Engineering, Vol(129) No. 2, pp. 260-268, 2003.
- [81] S. Neild, P. McFadden, M. Williams, *A Review the Time-Frequency Methods for Structural Vibration Analysis*, Engineering Structures, Vol. 25, pp. 713-728, 2003.
- [82] Y. Yan, L. Cheng, Z. Wu, L. Yam, *Development in Vibration-Based Structural Damage Detection Technique*, Mechanical Systems and Signal Processing, Vol(21), pp.2198-2211, 2007.
- [83] Z. Zhang, H. Hua, X. Xu, Z. Huang, *Modal Parameter Identification Through Gabor Expansion of Response Signals*, Journal of Sound and Vibration, Vol. 266, pp. 943-955, 2003.
- [84] X.T. Zhou, *Vibration-Based Damage Detection of Tall Building Structures*, PhD thesis, The Hong Kong Polytechnic University, 2004.

- [85] M. Mucciarelli, A. Masi, M. R. Gallipoli, P. Harabaglia, M. Vona, F. Ponzio, M. Dolce, *Analysis of RC Building Dynamic Response and Soil-Building Resonance Based on Data Recorded during a Damaging Earthquake (Molise, Italy, 2002)*, Bulletin of Seismological Society of America, Vol. 94 No. 5, pp. 1943-1953, 2004.
- [86] J. Zou, J. Chen, *A Comparative Study on Time-Frequency Feature of Cracked Rotor by Wigner-Ville Distribution and Wavelet Transform*, Journal of Sound and Vibration, Vol 276, pp. 1-11, 2004.
- [87] R. Ceravolo, *Use of Instantaneous Estimators for the Evaluation of Structural Damping*, Journal of Sound and Vibration, Vol 274, pp. 385-401, 2004.
- [88] N.P. Politis, *Wavelets Based Time-Frequency Analysis Techniques in Structural Engineering*, PhD thesis, Rice University, Houston Texas, 2005.
- [89] Z. Peng, P. Tse, F. Chu, *An Improved Hilbert-Huang Transform and its Application in Vibration Signal Analysis*, Journal of Sound and Vibration, Vol. 286, pp. 187-205, 2005.
- [90] S.C. Bradford, *Time-Frequency Analysis of Systems with Changing Dynamic Properties*, PhD thesis, California Institute of Technology, 2006.
- [91] S.C. Bradford, J. Yang, T. Heaton, *Variations in the Dynamic Properties of Structures: The Wigner-Ville Distribution*, T49: Experimental and Analytical Simulation of Structures, 1906 San Francisco Earthquake 100th Anniversary Conference, 2006
- [92] A. Roshan-Ghias, M. Shamsollahi, M. Mobed, M. Behzad, *Estimation of Modal Parameters using Bilinear Joint Time-Frequency Distributions*, Mechanical Systems and Signal Processing, Vol. 21, pp. 2125-2136, 2007.
- [93] R. Ceravolo, G. Demaire, S. Erlicher, *Instantaneous Identification of Bouc-Wen-Type Hysteretic Systems from Seismic Response Data*, Key Engineering Materials, Vol. 347, pp. 331-338, 2007.
- [94] M. Todorovska, M. Trifunac, *Earthquake Damage Detection in the Imperial County Services Building I: The data and Time-Frequency Analysis*, Soil Dynamics and Earthquake Engineering, Vol. 27, pp. 564-576, 2007.
- [95] T-H Sang, W. Williams, *Renyi Information and Signal-Dependent Optimal Kernel Design*, International Conference on Acoustic, Speech and Signal Processing, ICASSP-95, Vol. 2, pp. 997-1000, 1995
- [96] P. Honeine, C. Richard, P. Fladrin, J. Pothin, *Optimal Selection of Time-Frequency Representations for Signal Classification: A Kernel-Target Alignment Approach*, Proceedings of International Conference on Acoustic, Speech and Signal Processing, ICASSP-2006, Vol III, pp.476-479, 2006
- [97] J. O'Neill, P. Fladrin, *Virtudes and Vices of Quartic Time-Frequency Distributions*, IEEE Transactions on Signal Processing, Vol. 48, No. 9, pp. 2641-2650, 2000.

- [98] L. Stankovic, *A Measure of Some Time-Frequency Distributions Concentrations*, Signal Processing, Vol. 81, pp. 621-631, 2001.
- [99] Y. Park, Y. Kim, *Bias Error due to Windows for Wigner-Ville Distribution Estimation*, Mechanical Systems and Signal Processing, Vol. 9(6), pp. 675-684, 1995.
- [100] S. Kadambe, F. Boudreaux-Bartels, *A Comparison of the Existence of "Cross Terms" in the Wigner Distribution and the Squared Magnitude of the Wavelet Transform and the Short Time Fourier Transform*, IEEE Transactions on Signal Processing, Vol. 40, No. 10, pp. 2498-2517, 1992
- [101] A. Costa, F. Boudreaux-Bartels, *An Overview of Aliasing Errors in Discrete-Time Formulations of Time-Frequency Representations*, IEEE Transactions on Signal Processing, Vol. 47, Issue 5, pp. 1463-1474, 1999
- [102] P. Flandrin, *Some Features of Time-Frequency Representations of Multicomponent Signals*, Proceedings of International Conference on Acoustic, Speech and Signal Processing, ICASSP-84, Vol. 9, Part 1, pp. 266-269, 1984.
- [103] M. Roemer, D. Mook, *Mass, Stiffness and Damping Matrix Identification: An Integrated Approach*, Journal of Vibration and Acoustics, Vol. 114, pp. 358-363, 1992.
- [104] C. Fritzen, *Identification of Mass, Damping, and Stiffness Matrices of Mechanical Systems*, Journal of Vibration, Acoustic, Stress, and Reliability in Design, Vol. 108, pp. 9-16, 1986.
- [105] S. Chen, M. Ju, Y. Tsuei, *Estimation of Mass, Stiffness and Damping Matrices from Frequency Response Functions*, Journal of Vibration and Acoustics, Vol. 118, pp. 78-82, 1996.
- [106] D. Bernal, J. Beck, *Preface to the Special Issue on Phase I of the IASC-ASCE Structural Health Monitoring Benchmark*, Journal of Engineering Mechanics, Vol. 130, No. 1, pp. 1-2, 2004.
- [107] E. Johnson, H. Lam, L. Katafygiotis, J. Beck, *Phase I IASCE-ASCE Structural Health Monitoring Benchmark Problem Using Simulated Data*, Journal of Engineering Mechanics, Vol. 130, No. 1, pp. 3-15, 2004.
- [108] H. Lam, L. Katafygiotis, N. Mickleborough, *Application of a Statistical Model Updating Approach on Phase I of the IASC-ASCE Structural Health Monitoring Benchmark Study*, Journal of Engineering Mechanics, Vol. 130, No. 1, pp. 34-48, 2004.
- [109] J. Caicedo, S. Dyke, E. Johnson, *Natural Excitation Technique and Eigensystem Realization Algorithm for Phase I of the IASC-ASCE Benchmark Problem: Simulated Data*, Journal of Engineering Mechanics, Vol. 130, No. 1, pp. 49-60, 2004.
- [110] D. Bernal, B. Gunes, *Flexibility Based Approach for Damage Characterization-Benchmark Application*, Journal of Engineering Mechanics, Vol. 130, No. 1, pp. 61-70, 2004.

- [111] H. Lus, R. Betti, J. Yu, M. De Angelis, *Investigation of a System Identification Methodology in the Context of the ASCE Benchmark Problem*, Journal of Engineering Mechanics, Vol. 130, No. 1, pp. 71-84, 2004.
- [112] J. Yang, Y. Lei, S. Lin, N. Huang, *Hilbert-Huang Approach for Structural Damage Detection*, Journal of Engineering Mechanics, Vol. 130, No. 1, pp. 85-95, 2004.
- [113] Caltech Online Monitoring and Evaluation Testbeds (COMET), California Integrated Seismic Network, CEDC. Internet: <http://www.comet.caltech.edu>, 2006.
- [114] J.F. Clinton, S.C. Bradford, T. Heaton, J. Favela, *The Observed Wander of the Natural Frequencies in a Structure*, Bulletin of Seismological Society of America, Vol 96 No. 1, pp. 237-257, 2006.
- [115] S.C. Bradford, J.F. Clinton, J. Favela, T.H. Heaton, *Results of Millikan Library Forced Vibration Testing*, Technical Report EERL-2004-03, California Institute of Technology, 2004.
- [116] J.F. Clinton, *Modern Digital Seismology – Instrumentation, and Small Amplitude Studies in the Engineering World*, PhD thesis, California Institute of Technology, 2004.
- [117] R. Sneider, E. Safak, *Extracting the Building Response Using Seismic Interferometry: Theory and Application to the Millikan Library in Pasadena, California*, Bulletin of Seismological Society of America, Vol. 96 No. 2, pp. 586-598, 2006.
- [118] G. Calvi, R. Pinho, H. Crowley, *State-of-the Knowledge on the Period Elongation of RC Buildings During Strong Ground Shaking*, Paper Number: 1535, First European Conference on Earthquake Engineering and Seismology, Switzerland, 2006.
- [119] F. Dunand, P. Gueguen, P. Bard, J. Rodgers, M. Celebi, *Comparison of the Dynamic Parameters Extracted from Weak, Moderate and Strong Motion Recorded in Buildings*, Paper Number: 1021, First European Conference on Earthquake Engineering and Seismology, Switzerland, 2006.
- [120] F. Cabrera, *Evaluation of Seismic Performance of Plaza Inmaculada Building in San Juan, Puerto Rico*, MSc. Thesis, Civil Engineering Department, University of Puerto Rico at Mayaguez, 1998. (In Spanish).
- [121] L. Cano, J. Martinez-Cruzado, *Damage Identification of Structures Using Instantaneous Frequency Changes*, paper: 1086, Proceedings of International Conference on Computational Methods in Structural Dynamics and Earthquake Engineering, Greece, Vol. 1, 2007.
- [122] T. Krauss, L. Shure, J. Little, *Signal Processing Toolbox for Use with MatLab*, The Math Works Inc., 1995
- [123] F. Auger, P. Flandrin, P. Goncalve, O. Lemoine, *Time-Frequency Toolbox – CNR-France*. 2005.

- [124] R. Brincker, L. Zhang, P. Andersen, *Modal Identification from Ambient Responses using Frequency Domain Decomposition*, Proceedings of 18th International Modal Analysis Conference: A Conference on Structural Dynamics, Vol 1, pp. 625-630, 2000.
- [125] The Math Works Inc., *MATLAB The Language of Technical Computing Version 7.1(R14)*, 2005.
- [126] FEMA 356, *Prestandard and Commentary for the Seismic Rehabilitation of Buildings*, prepared by the American Society of Civil Engineers and Federal Emergency Management Agency, 2000.
- [127] L. Meirovitch, *Elements of Vibration Analysis*, Second Edition, McGraw-Hill Publishing Company, 1986.
- [128] P. Overschee, B.L. De Moor, *Subspace Identification for Linear Systems: Theory – Implementation – Applications*, First Edition, Springer Publishers, 1996.
- [129] H-I. Choi, W.J. Williams, *Improved Time-Frequency Representation of Multicomponent Signals Using Exponential Kernels*, IEEE Transactions on Acoustic, Speech and Signal Processing, Vol. 37, No. 6, pp. 862-871, 1989
- [130] R. Baraniuk, D. Jones, *A Signal-Dependent Time-Frequency Representation: Optimal Kernel Design*, IEEE Transactions on Signal Processing, Vol. 41 No. 4, pp. 1589-1601, 1993.
- [131] R. Baraniuk, D. Jones, *A Signal-Dependent Time-Frequency Representation: Fast Algorithm for Optimal Kernel Design*, IEEE Transactions on Signal Processing, Vol. 42 No. 1, pp. 134-146, 1994.
- [132] F. Auger, P. Flandrin, *Improving the Readability of Time-Frequency and Time-Scale Representation by the Reassignment Method*, Signal Processing, Vol. 43, No. 5, pp. 1068-1089, 1995.
- [133] Y.-K. Park, Y.-H. Kim, *A Method to Minimise the Cross-Talk of Wigner-Ville Distribution*, Mechanical System and Signal Processing, Vol. 11, No. 4, pp. 547-559, 1997.
- [134] J-H. Lee, J. Kim, *Development of Enhanced Wigner-Ville Distribution Function*, Mechanical System and Signal Processing, Vol. 15, No. 2, pp. 367-398, 2001.
- [135] S. K. Lee, *A New Method for Smoothing Non-Oscillation Cross-Terms in Sliced Wigner Fourth-Order Moment Spectra*, Mechanical System and Signal Processing, Vol. 15, No. 5, pp. 1023-1029, 2001.
- [136] P. G. Baum, *A Time-Filtered Wigner Transformation for Use in Signal Analysis*, Mechanical System and Signal Processing, Vol. 16, No. 6, pp. 955-966, 2002.
- [137] D. Nelson, D. Smith, *Adaptive Interference Removal Based on Concentration of the STFT*, Digital Signal Processing, Vol 16, pp. 597-606, 2006.

- [138] R.B. Pachori, P. Sircar, *A New Technique to Reduce Cross Terms in the Wigner-Ville Distribution*, Digital Signal Processing, Vol 17, pp. 466-474, 2007.
- [139] L. Cohen, T. Posch, *Positive Time-Frequency Distributions Functions*, IEEE Transactions on Acoustic, Speech and Signal Processing, Vol. 33, No. 1, pp. 31-38, 1985.
- [140] L. Cohen, *Properties of the Positive Time-Frequency Distributions Functions*, Proceedings of International Conference on Acoustic, Speech and Signal Processing, Vol. 10, pp. 548-551, 1985
- [141] H. Zou, D. Wang, X. Zhang, Y. Li, *Nonnegative Time-Frequency Distributions for Parametric Time-Frequency Respresentations using Semi-Affine transformation group*, Signal Processing, Vol. 85, pp. 1813-1826, 2005
- [142] A.J. Janssen, T. A. Claasen, *On Positivity of Time-Frequency Distributions*, IEEE Transactions on Acoustic, Speech and Signal Processing, Vol. 33, No. 4, pp. 1029-1032, 1985.
- [143] C. Huerta, *Determination of Soil Properties From Earthquake Data*, PhD thesis, University of Texas at Austin, 2002.
- [144] P. Loughlin, J. Pitton, L. Atlas, *Construction of Positive Time-Frequency Distributions*, IEEE Transactions on Signal Processing, Vol. 42 No. 10, pp. 2697-2705, 1994.
- [145] B. Boashash, B. Ristich, *Polynomial Wigner-Ville Distributions and Time-Varying Higher-Order Spectra*, Proceedings of the International Symposium on Time-Frequency and Time-Scale Analysis, pp. 31-34, 1992.
- [146] D. Kammler, *A First Course in Fourier Analysis*, First Edition, Prentice Hall Publisher Inc., 2000.
- [147] J-T. Kim, Y-S. Ryu, H-M. Cho, N. Stubbs, *Damage Identification in Beam-Type Structures: Frequency-Based Method vs Mode-Shape-Based Method*, Engineering Structures, Vol. 25, pp. 57-67, 2003.
- [148] R. Villaverde, *Methods to Assess the Seismic Collapse Capacity of Building Structures: State of the Art*, Journal of the Structural Engineering, Vol. 133, No. 1, pp. 57-66, 2007.
- [149] J. Demmel, *Applied Numerical Linear Algebra*, First Edition, Society for Industrial and Applied Mathematics Publisher, 1997.
- [150] S. Choi, S. Park, R. Bolton, N. Stubbs, C. Sikorsky, *Periodic Monitoring of Physical Property Changes in a Concrete Borx-Girder Bridge*, Journal of Sound and Vibration, Vol. 278, pp. 365-381, 2004.
- [151] Z. Zembaty, M. Kowalski, S. Pospisil, *Dynamic Identification of a Reinforced Concrete Frame in Progressive States of Damage*, Engineering Structures, Vol. 28, pp. 668-681, 2006.

- [152] E. Safak, *Detection and Identification of Soil-Structure Interaction in Buildings from Vibration Recordings*, Journal of Structural Engineering, Vol. 121, No. 5, pp. 899-906, 1995.
- [153] C. Huerta, Y-J. Shin, E. Powers, J. Roesset, *Time-Frequency Analysis of Earthquake Records*, paper 1724, 12th World Conference on Earthquake Engineering, Auckland, New Zealand, 2000.
- [154] P. Steeghs, G. Drijkoningen, *Time-Frequency Analysis of Seismic Sequences*, Proceeding of the 65th Annual Meeting, Society of Exploration Geophysicists, 1995.
- [155] M. Hedlin, *A Global Test of a Time-Frequency Small-Event Discriminant*, Bulletin of Seismological Society of America, Vol. 88, No. 4, pp. 973-988, 1998.
- [156] P. Flandrin, *Time-Frequency and Time-Scale*, Proceedings of Fourth Annual ASSP Workshop on Spectrum Estimation and Modeling, pp. 77-80, 1988.
- [157] D. Jones, R. Baraniuk, *A Simple Scheme for Adapting Time-Frequency Representations*, IEEE Transactions on Signal Processing, Vol 42, No. 12, pp. 3530-3535, 1994.
- [158] V. Sucic, B. Barkat, B. Boashash, *Performance Evaluation of B-Distribution*, Proceedings of the 5th International Symposium on Signal Processing and its Applications, Vol. 1, pp. 22-25, 1999.
- [159] B. Boashash, V. Sucic, *An Resolution Performance Measure for Quadratic Time-Frequency Distributions*, Proceedings of 10th IEEE Workshop on Statistical Signals and Array Processing, pp. 584-588, 2000.
- [160] V. Sucic, B. Boashash, *Parameter Selection for Optimizing Time-Frequency Distributions and Measurements of Time-Frequency Characteristics of Non-Stationary Signals*, Proceedings of International Conference on Acoustic, Speech and Signal Processing, Vol. 6, pp. 3357-3560, 2001.
- [161] V. Sucic, B. Boashash, *Optimization Algorithm for Selecting Quadratic Time-Frequency Distributions: Performance Results and Calibration*, Proceedings of the 6th International Symposium on Signal Processing and its Applications, pp. 331-334, 2001.
- [162] B. Boashash, V. Sucic, *Resolution Measure Criteria for the Objective Assessment of the Performance of Quadratic Time-Frequency Distributions*, IEEE Transactions on Signal Processing, Vol. 51, No.5, 2003.
- [163] V. Sucic, B. Boashash, *An Approach for Selecting a Real-Life Signal Best-Performing Time-Frequency Distribution*, Proceedings of 7th International Symposium on Signal Processing and its Applications, Vol 1, pp. 125-128, 2003.
- [164] J. O'Neill, W. Williams, *Distributions in the Discrete Cohen's Classes*, Proceedings of the International Conference on Acoustics, Speech, and Signal Analysis, Vol. 3, pp. 1581-1584, 1998.
- [165] J. O'Neill, W. Williams, *On the Existence of Discrete Wigner Distributions*, Signal Processing Letters, Vol. 6, No. 12, pp. 304-306, 1999.

- [166] R. Murray, A. Papandreou-Suppappola, G. Boudreaux-Bartels, *New Time-Frequency Representations: Higher Order Warped Wigner Distributions*, Proceedings of the 31th Conference on Signals, Systems and Computers, Vol. 1, pp. 488-492, 1998.
- [167] R. Murray, A. Papandreou-Suppappola, G. Boudreaux-Bartels, *A New Class of Affine Higher Order Time-Frequency Representations*, Proceedings of the International Conference on Acoustic, Speech and Signal Processing, Vol. 3, pp. 1613-1616, 1999.
- [168] K. Le, *Time-Frequency Distributions for Crack Detection in Rotors – A Fundamental Note*, Journal of Sound and Vibration, Vol. 294, pp. 397-409, 2006.
- [169] L. Cohen, *The Frequency and Scale Content of Biological Signals*, Proceedings of the 28th Conference on Signals, Systems and Computers, Vol 2, pp. 1541-1545, 1994.
- [170] P. Flandrin, *Maximum Signal Concentration in a Time-Frequency Domain*, Proceedings of International Conference on Acoustic, Speech and Signal Processing ICASPP-88, Vol. 4, pp. 2176-2179, 1988.
- [171] F. Hlawatsch, T. G. Manickam, R. L. Urbanke, W. Jones, *Smoothed Pseudo-Wigner Distribution, and Cone-Kernel Representation: Ambiguity-Domain Analysis and Experimental Comparison*, Signal Processing, Vol. 43, pp. 149-168, 1995.
- [172] P. J. Boles, B. Boashash, *The Cross Wigner-Ville Distribution – A Two Dimensional Analysis Method for the Processing of Vibroseis Seismic Signals*, Proceedings of the International Conference on Acoustic, Speech and Signal Processing ICASSP-88, Vol. 2, pp. 904-907, 1988.
- [173] O. Rioul, P. Flandrin, *Time-Scale Energy Distributions: A General Class Extending Wavelet Transform*, IEEE Transactions on Signal Processing, Vol. 40, No. 7, pp. 1746-1757, 1992.
- [174] M. D. Licker (Publisher), *McGraw-Hill Dictionary of Electric and Computer Engineering*, First Edition, McGraw-Hill Publishing Company, 2004.
- [175] P. Flandrin, R. Baraniuk, O. Michel, *Time-Frequency Complexity and Information*, Proceedings of the International Conference on Acoustics, Speech and Signal Processing ICASSP-94, Vol. 3, pp. 329-332, 1994.
- [176] S. Aviyente, *Information Processing on the Time-Frequency Plane*, Proceedings of the International Conference on Acoustic, Speech and Signal Processing ICASSP-04, Vol. 2, pp. 617-620, 2004.
- [177] R. Baraniuk, P. Flandrin, O. Michel, *Measuring Time-Frequency Information and Complexity using Renyi Entropies*, Proceedings of the International Symposium on Information Theory, pp. 426, 1995.
- [178] W. Williams, T. Sang, *Adaptive RID Kernels Which Minimize Time-Frequency Uncertainty*, Proceedings of the International Symposium on Time-Frequency and Time-Scale Analysis, pp. 96-99, 1994.
- [179] A. Renyi, *Probability Theory*, First Edition, North-Holland Publishing Company, 1970.

- [180] S. Aviyente, W. Williams, *Entropy Based Detection on the Time-Frequency Plane*, Proceedings of the International Conference on Acoustic, Speech and Signal Processing ICASSP-03, Vol. 6, pp. 441-444, 2003.
- [181] C. Cachin, *Hashing a Source With an Unknown Probability Distribution*, Proceedings of the International Symposium on Information Theory, pp. 269, 1998.
- [182] Z. Shan, S. Aviyente, *Source Separation in the Time-Frequency Domain by Maximizing an Information-Theoretic Criterion*, Proceedings of the International Conference on Electro/Information Technology, pp. 43-48, 2006.
- [183] S. Aviyente, W. Williams, *Information Bounds for Random Signals in Time-Frequency Plane*, Proceedings of the International Conference on Acoustics, Speech and Signal Processing ICASSP-01, Vol. 6, pp. 3549-3552, 2001.
- [184] P. Jennings, *Engineering features of the San Fernando Earthquake of February 9-1971*, Report EERL-02-71, Earthquake Engineering Research Laboratory, California Institute of Technology, 1971.
- [185] J. Jeong, W. Williams, *Kernel Design for Reduced Interference Distributions*, IEEE Transactions on Signal Processing, Vol. 40, No. 2, pp. 402-412, 1992.
- [186] J. Brandon, *A Critique of Location Criteria in Modal Methods for Structural Damage Identification*, Journal of Sound and Vibration, Vol 203, No. 4, pp. 728-729, 1997.
- [187] O. Skjaerbaek, S. Nielsen, *Identification of Damage in Reinforced Concrete Structures from Earthquake Records – Optimal Location of Sensors*, Soil Dynamics and Earthquake Engineering, Vol 15, pp. 347-358, 1996.
- [188] Y. Xia, H. Hao, *Measurements Selection for Vibration-Based Structural Damage Identification*, Journal of Sound and Vibration, Vol 236, No. 1, pp. 89-104, 2000.
- [189] K. McGill, L. Dorfman, *High-Resolution Alignment of Sampled Waveforms*, IEEE Transactions on Biomedical Engineering, Vol. BME-31, No. 6, pp. 462-468, 1984.
- [190] F. Udawadia, *Structural Identification and Damage Detection from Noisy Modal Data*, Journal of Aerospace Engineering, Vol. 18, No. 3, pp. 179-187, 2005.
- [191] W. Woyczynski, *A First Course in Statistics for Signal Analysis*, First Edition, Birkhauser Boston Publishing Company, 2006.
- [192] R. Brincker, P. Andersen, N. Moller, *An Indicator for Separation of Structural and Harmonic Modes in Output-Only Modal Testing*, Proceedings of 18th International Modal Analysis Conference: An Conference on Structural Dynamics, Vol 2, pp. 1649-1654, 2000.
- [193] D. Ewins, S. Rao, S. Braun, *Encyclopedia of Vibration*, First Edition, Academic Press, 2001.

- [194] I. Berg, S. Mosegaard, R. Brincker, M. Lopez, *Load Estimation by Frequency Domain Decomposition*, paper: 129, Proceedings of 3rd International Operational Modal Analysis Conference, IOMAC-07, Copenhagen, 2007.
- [195] I. Berg, S. Mosegaard, *Load Estimation by Frequency Domain Decomposition*, Report-B203, Aalborg University, 2007.
- [196] A-P. Cherng, *Formulating Hankel Singular Values of Closely-Spaced Modes in Time Domain*, Proceedings of the 17th International Modal Analysis Conferences, pp. 1916-1922, Orlando Fl., 1999.
- [197] J. Zhang, B. Gottin, A. Papandreou-Suppappola, C. Ioana, *Time-Frequency Modeling of Shallow Water Enviroments: Rigid Vs. Fluid Seabed*, Proceedings of the 14th of Workshop on Statistical Signal Processing, pp. 740-744, 2007.
- [198] D. Childers, D. Skinner, R. Kemerait, *The Cepstrum: A Guide to Processing*, Proceedings of the IEEE Signals Analysis, Vol. 65, No. 10, pp. 1428-1443, 1977.
- [199] C-H. Chen, *Digital Processing of the Marine Seismic Data*, Oceans, Vol. 4, pp. 346-350, 1972.
- [200] Y. Ito, Y. Kawamura, K. Muzutani, S. Kuraoka, *Cepstrum Analysis Applied to Ultrasonic Reflection Wave Detection Wave Method to Investigate the Depth and the Damage of the Pile*, Proceedings of the SICE-ICASE International Joint Conference, pp. 3404-3407, 2006.
- [201] Computers and Structures Inc., *Extended Tridimensional Analysis of Building Systems – ETABS, Version 9.0.4*, Computers and Structures Inc, Berkeley C.A. 2006
- [202] N. Rojas, J. Martinez-Cruzado, *Instrumentación de la Torre de Control del Aeropuerto de las Islas Virgenes Britanicas en Beef Island*, Report of Puerto Rico Strong Motion Program, 2007 (In Spanish).
- [203] H. Cole, *On-line Failure Detection and Damping Measurements of Aerospace Structures by Random Decrement Signature*, Ames Research Center National Aeronautics and Space Administration, Nasa Contractor Report – 2205.
- [204] Southern California Earthquake Data Center (SCEDC) , Southern California Earthquake Center (SCEC). Internet: <http://www.data.scec.org/index.html>, 2008.
- [205] D. E. Newland, *Random Vibrations, Spectral & Wavelet Analysis*, Third Edition (Reprinted), John Wiley & Sons, Inc, 1994.
- [206] S. Vaseghi, *Advanced Digital Signal Processing and Noise Reduction*, Third Edition, John Wiley & Sons Ltd, West Sussex, England, 2006
- [207] V. Gusella, A.L. Materazzi, *Non-Gaussian Along-Wind Response Analysis in the Time and Frequency Domains*, Engineering Structures, Vol (22), pp. 49-57, 2000.

- [208] Q.S. Li, J.R. Wu, S.G. Liang, Y.Q. Xiao, C.K. Wong, *Full-Scale Measurements and Numerical Evaluation of Wind-Induced Vibration of a 63-Story Reinforced Concrete Tall Building*, Engineering Structures, Vol (26), pp. 1779-1794, 2004.
- [209] G. Rilling, P. Flandrin, P. Goncalves, *On Empirical Mode Decomposition and Its Algorithms*, Proceedings of Workshop on Non-Linear Signal and Imaging Processing, IEEE-EURASIP, NSIP-03- Grade I, 2003.
- [210] N. Stevenson, M. Mesbah, B. Boashash, *A Sampling Limit for the Empirical Mode Decomposition*, Proceedings of the Eighth International Symposium on Signal Processing and its Applications, Vol. (2), pp. 647-650, 2005.
- [211] G. Rilling, P. Flandrin, P. Goncalves, J.M. Lilly, *Bivariate Empirical Mode Decomposition*, Signal Processing Letters, Vol. (14), No. 12, pp. 936-939, 2007.
- [212] R. Deering, J. Kaiser, *The Use of a Masking Signal to Improve Empirical Mode Decomposition*, Proceedings of the International Conference on Acoustics, Speech and Signal Processing – ICASSP-2005, Vol. (4), pp. iv-485 – iv-488, 2005.
- [213] G. Rilling, P. Flandrin, *Sampling Effects on the Empirical Mode Decomposition*, Proceedings of the First International Workshop on the Advances of Hilbert-Huang Transform and its Applications, pp. 1-14, 2007.
- [214] P. Flandrin, P. Goncalves, G. Rilling, *EMD Equivalent Filter Banks, From Interpretation to Applications*, Book Chapter 3, on: *The Hilbert-Huang Transform and Its Applications*, Interdisciplinary Mathematical Science Vol 5, Norden Huang and Samuel Shen Editors, World Scientific Publishing co, 2005.
- [215] P. Flandrin, G. Rilling, P. Goncalves, *Empirical Mode Decomposition as a Filter Bank*, Signal Processing Letters, Vol (11), No. 2, pp. 112-114, 2004.
- [216] P. Flandrin, *Elements of Signal Decomposition*, Transparent Slides from Internet web-page: <http://perso.ens-lyon.fr/patrick.flandrin/publis.html#Transparents>.
- [217] P.D. Spanos, A. Giaralis, N.P. Politis, *Time-Frequency Representation of Earthquake Accelerograms and Inelastic Structural Response Records Using The Adaptive Chirplet Decomposition and Empirical Mode Decomposition*, Soil Dynamics and Earthquake Engineering, Vol. 27, pp. 675-689, 2007.
- [218] G. Rilling, P. Flandrin, *One or Two Frequencies? The Empirical Mode Decomposition Answers*, IEEE Transactions on Signal Processing, Vol. 56, No. 1, pp. 85-95, 2008.
- [219] B. Yan, A. Miyamoto, *A Comparative Study of Modal Parameter Identification Based on Wavelet and Hilbert-Huang Transforms*, Computer-Aided Civil and Infrastructure Engineering, Vol. 21, pp. 9-23, 2006.
- [220] L. Cano, J. Martinez-Cruzado, *Multicriteria Method for An Objective Selection of Time-Frequency Representations of Signal From Civil Engineering Structures*, Proceedings of the 14th World Conference on Earthquake Engineering, paper: 05-01-0387, Beijing China, 2008

- [221] M. Pando, L. Cano, L. Suarez, R. Ritta, L. Montejo, *Comparison of Site Fundamental Period Estimates Using Weak-Motion Earthquakes and Microtremors*, Proceedings of the 14th World Conference on Earthquake Engineering, paper: 02-0142, Beijing China, 2008.
- [222] A. Bejarano, *Study of the Random Decrement Method for In-Situ Soil Properties Estimation (In Spanish)*, Master of Sciences Thesis, Centro de Investigación Científica y de Educación Superior de Ensenada, Baja California, Mexico, 2006.
- [223] S. Hassiotis, G. Jeong, *Identification of Stiffness Reductions Using Natural Frequencies*, Journal of Engineering Mechanics, Vol (121), No. 10, pp. 1106-113, 1995.
- [224] Gröchening K. *Foundation of Time-Frequency Analysis*, Birkhäuser, Boston, USA, 2001
- [225] B. Barkat, B. Boashash, *A High Resolution Quadratic Time-Frequency Distribution for Multicomponent Signals Analysis*, IEEE Transactions on Signal Processing, Vol. 49, No. 10, pp. 2232-2239, 2001.
- [226] B. Boashash, *Estimating and Interpreting The Instantaneous Frequency of a Signal – Part 1: Fundamentals*, Proceedings of the IEEE, Vol. 80, No. 4, pp. 520-538, 1992.
- [227] B. Boashash, *Estimating and Interpreting The Instantaneous Frequency of a Signal – Part 2: Algorithms and Applications*, Proceedings of the IEEE, Vol. 80, No. 4, pp. 540-568, 1992.
- [228] I. Djurovic, L. Stankovic, *An algorithm for the Wigner distribution based instantaneous frequency estimation in a high noise environment*, Signal Processing, Vol. 84, pp. 631-643, 2004.
- [229] L. Rankine, M. Mesbah, B. Boashash, *IF estimation for multicomponent signals using image processing techniques in the time-frequency domain*, Signal Processing, Vol. 87, pp. 1234-1250, 2007.
- [230] D. Walnut, *An Introduction to Wavelet Analysis*, Birkhäuser, Boston, USA, 2002
- [231] F. Filippou, M. Constantinides, FEDEASLab Getting Started Guide and Simulation Examples, Report UCB-SEMM 2004-05, Structural Engineering Mechanics and Materials, Department of Civil and Environmental Engineering, University of California at Berkeley, 2004
- [232] G. Rossini, *IL Barbiere Di Siviglia (The Barber of Seville)*, Opera in Three Acts, English Version by Ruth and Thomas Martin, G. Schirmer Inc, New York, USA, 1962